THE IMPACT OF PERINATAL IRON DEFICIENCY ON RENAL DEVELOPMENT AND LONG-TERM CARDIOVASCULAR FUNCTION IN RATS

by

Andrew Gordon Woodman

A thesis submitted in partial fulfillment of the requirements for the degree of

Doctor of Philosophy

Department of Pharmacology
University of Alberta

Abstract

Stressors that occur in early development can affect long-term health and resilience. Iron deficiency (ID) is one of the most common nutritional deficiencies worldwide, and is an epidemic among pregnant women and young children. Perinatal ID is associated with neonatal morbidity and mortality, but may also predisposing offspring for cardiovascular dysfunction in later life. However, the mechanisms through which this long-term programming of cardiovascular dysfunction occurs have not been fully elucidated. Here, we interrogated the mechanisms through which perinatal ID affects offspring cardiovascular development, and in turn affects long-term cardiovascular health.

Female Sprague Dawley rats were fed either an iron restricted (3 or 10 mg/kg ferric citrate) or iron replete (37 mg/kg ferric citrate) purified diet prior to and throughout gestation; dams were fed an iron-replete diet at birth. Offspring were studied either at the end of gestation, in the neonatal period (postnatal days 1-28), or in adulthood.

At gestational day 21, maternal iron restriction resulted in fetal anemia and asymmetric growth restriction, as well as organ-specific patterns of hypoxia, such that kidneys and livers were affected, whereas the brains and placentae of offspring remained normoxic. Prenatal ID caused mitochondrial dysfunction and increased reactive oxygen species generation in the livers and kidneys, albeit the effects were much more pronounced in the kidneys of male offspring, whereas females were largely spared.

In neonates, perinatal ID reduced nephron endowment of male but not female offspring. Perinatal ID caused dysregulated vitamin A metabolism, especially in male offspring, along with other nephrogenic signaling pathways. Additionally, perinatal ID resulted in alterations in cellular senescence, apoptosis, autophagy, and oxidative stress, implicating these as potential mechanisms for impaired nephrogenesis.

In adult offspring, males exposed to perinatal ID exhibited salt sensitive hypertension and vascular dysfunction, characterized by deficiencies in nitric oxide bioavailability, likely secondary to enhanced oxidative stress. Indeed, adult male perinatal ID offspring exhibit increased renal reactive oxygen species generation concomitant with impaired mitochondrial respiration. A high salt diet in adulthood exacerbated renal injury in male perinatal ID offspring, resulting in glomerular hypertrophy and injury; these effects were not observed in adult females.

In summary, the studies herein provide mechanistic insights into how perinatal ID affects long-term cardiovascular function. Given the high incidence of ID in pregnant women, the developmental programming effects stemming from ID could have substantial implications on the global burden of cardiovascular and kidney disease.

Preface and Co-Authorship

This thesis is an original work by Andrew Gordon Woodman. Ethics approval for the following research was received from the University of Alberta Animal Use and Care Committee, under Animal Use Protocol #974.

Chapter 2 has been published: Woodman AG, Care AS, Mansour Y, Cherak SJ, Panahi S, Gragasin FS, Bourque SL. Modest and severe maternal iron deficiency in pregnancy are associated with fetal anemia and organ-specific hypoxia in rats. ***Scientific Reports***. 2017; 7: 46573.

Authors contributed to experimental design/conception (A.G.W., F.S.G., S.L.B.), data collection (A.G.W., A.S.C., M.Y., S.J.C., S.P.), data analysis (A.G.W., A.S.C., M.Y.), manuscript composition (A.G.W., S.L.B.), and manuscript editing (A.G.W., F.S.G., S.L.B.).

Chapter 3 has been published: Woodman AG, Mah RL, Keddie DL, Noble RMN, Panahi S, Gragasin FS, Lemieux H, Bourque SL. Prenatal iron-deficiency causes sex-dependent mitochondrial dysfunction and oxidative stress in fetal rat kidneys and liver. ***FASEB Journal***. 2018; 32(6):3254-63.

Authors contributed to experimental design/conception (A.G.W., F.S.G., H.L., S.L.B.), data collection (A.G.W., R.L.M., D.L.K., R.M.N.N., S.P.), data analysis (A.G.W., R.L.M., D.L.K.), manuscript composition (A.G.W., S.L.B.), and manuscript editing (A.G.W., F.S.G., H.L., S.L.B.). A.G.W. directly supervised undergraduate summer students for their contributions to this project (R.L.M., D.L.K., R.M.N.N.).

Chapter 4 is under preparation for publication: Woodman AG*, Mah RL*, Holody CD, Noble RMN, Clugston RD, Bourque SL. Perinatal iron deficiency causes sex -dependent changes in kidney oxidative stress, cellular senescence, and apoptosis during development. *Denotes equal contribution.

Authors contributed to experimental design/conception (A.G.W., R.D.C., S.L.B.), data collection (A.G.W., R.L.M., C.D.H, R.M.N.N.), data analysis (A.G.W., R.L.M.), manuscript composition (A.G.W., S.L.B.), and manuscript editing (A.G.W., R.D.C., S.L.B.). A.G.W. directly supervised R.L.M. as an undergraduate summer student for their contributions to this project.

Chapter 5 is under preparation for publication: Woodman AG*, Mah RL*, Kinney S, Holody CD, Noble RMN, Clugston RD, Bourque SL. Perinatal iron deficiency causes sex-dependent alterations in renal retinoic acid signaling and nephrogenesis. *Denotes equal contribution.

Authors contributed to experimental design/conception (A.G.W., R.D.C., S.L.B.), data collection (A.G.W., R.L.M., S.K., C.D.H, R.M.N.N., R.D.C.), data analysis (A.G.W., R.L.M., S.K., R.D.C.), manuscript composition (A.G.W., R.L.M., S.L.B.), and manuscript editing (A.G.W., R.D.C., S.L.B.). A.G.W. directly supervised R.L.M. as an undergraduate summer student and BSc. honours thesis student for their contributions to this project.

Chapter 6 has been published: Woodman AG, Mah RL, Keddie DL, Noble RMN, Holody C, Panahi S, Gragasin FS, Lemieux H, Bourque SL. Perinatal iron deficiency and a high salt diet cause long-term kidney mitochondrial dysfunction and oxidative stress. ***Cardiovascular Research***. 2020; 116(1):183-92. (First appeared as E-Pub in January 2019)

Authors contributed to experimental design/conception (A.G.W., F.S.G., H.L., S.L.B.), data collection (A.G.W., R.L.M., D.L.K., R.M.N.N. C.H., S.P.), data analysis (A.G.W., R.L.M., D.L.K.), manuscript composition (A.G.W., S.L.B.), and manuscript editing (A.G.W., F.S.G., H.L., S.L.B.). A.G.W. directly supervised undergraduate summer students for their contributions to this project (R.L.M., D.L.K., R.M.N.N., C.D.).

Chapter 7 has been published: Woodman AG, Noble RMN, Panahi S, Gragasin FS, Bourque SL. Perinatal iron deficiency combined with a high salt diet in adulthood causes sex-dependent vascular dysfunction. ***Journal of Physiology.*** 2019; 597(18):4715-28; also selected for the September 2019 *Editor's Choice Edition* of ***Journal of Physiology***.

Authors contributed to experimental design/conception (A.G.W., F.S.G., S.L.B.), data collection (A.G.W., R.M.N.N., S.P.), data analysis (A.G.W.), manuscript composition (A.G.W., S.L.B.), and manuscript editing (A.G.W., F.S.G., S.L.B.). A.G.W. directly supervised R.M.N.N. as an undergraduate summer student for their contributions to this project.

Chapter 8 of this thesis contains excerpts from the following publication: Woodman AG & Bourque SL. Developmental programming of renal function: nephron endowment and beyond. ***Journal of Physiology.*** 2018; 596(23):5495-5496.

Authors contributed manuscript composition and editing (A.G.W., S.L.B.).

Acknowledgements

I am truly grateful to Stephane for his mentorship, patience, support, and enthusiasm throughout my graduate studies. It is an honour to be the first PhD graduate (hopefully) from the Bourque lab, and any student would be lucky to have you as a mentor, given your level of investment in their success. I am also incredibly grateful to Ferrante for his excellent advice, support, and mentorship throughout my program.

Next, I would like to thank the indispensable members of the Bourque lab, to whom I owe much of my progress. First, I would not be where I am today without the help of Richard and Ronan, whose hard work was only outshone by the great times we had outside of the lab. Additionally, I would like to thank Claudia, Danae, Alyssa and all other Bourque lab students for their hard work and making the lab a place we could look forward to going (well, maybe not quite). I would also like to thank Sareh, our 'lab mom' who was always so thoughtful and helpful to every student that came through our doors.

I also owe a debt of gratitude to our collaborators. Drs. Lemieux and Clugston have been instrumental for the projects conducted herein, and I will always be grateful for their help and expertise that made this work possible.

Thank-you to all members of our informal 'perinatal research group' from the Davidge, Hemmings, Riddell, and Ospina labs; your feedback on presentations, help with troubleshooting experiments, and friendship have made graduate school more bearable.

Last but certainly not least, I can't thank my parents enough for always believing in me and supporting my dreams, even if it meant moving away to Deadmonton.

Finally, I am grateful to the following agencies for providing financial support: Canadian Institutes of Health Research, Alberta Innovates, University of Alberta Women and Children's Health Research Institute, Heart and Stroke Foundation of Canada, University of Alberta Faculty of Agricultural, Life and Environmental Sciences Vitamin Research Fund, University of Alberta Faculty of Graduate Studies and Research, University of Alberta Faculty of Medicine and Dentistry, University of Alberta Department of Pharmacology, Society of Reproductive Investigation, University of Alberta Graduate Students' Association, and Hypertension Canada.

Table of Contents

List of Tables

List of Figures

Chapter 1

Introduction

1.1 Iron Status and Metabolism

1.1.1 Iron Metabolism & Markers of Iron Status

Iron is a trace element which is essential to several biological processes, including oxygen transport, oxidation-reduction reactions, energy metabolism, and DNA synthesis [1]. While iron is necessary to sustain all life, too much iron can be toxic to cells, necessitating complex regulatory mechanisms that ensure homeostasis is maintained. Whole-body iron distribution is summarized in **Figure 1.1**. Briefly, the majority of body iron (i.e. >2 grams) is contained within hemoglobin (Hb) molecules in erythrocytes and erythrocyte precursors in the bone marrow. Approximately 600mg is contained in the reticuloendothelial system (e.g. macrophages), 300mg in myoglobin within muscle tissues, and the remaining iron (~1g) is stored in the liver [2]. Although virtually all tissues within the body contain iron, their quantities are comparatively small in comparison to those mentioned above. Notably, iron status is regulated at the level of uptake, meaning that tight control of iron absorption is critical, as the body does not have regulated mechanisms to actively expel excess iron when needed. Approximately 1-2mg of iron are absorbed daily within the duodenum, which is equivalent to iron loss due to sloughing of enterocytes and skin cells in healthy populations [3]. The primary mechanism through which enhanced iron loss occurs is blood loss, often due to gastrointestinal bleeding, hemorrhage from either trauma or a medical procedure, or menorrhagia (in reproductive age women) [2,3]. In the face of high iron demands (or excessive loss), iron uptake is often slow to increase to compensate for diminishing iron stores, resulting in a propensity to experience iron deficiency (ID) [4].

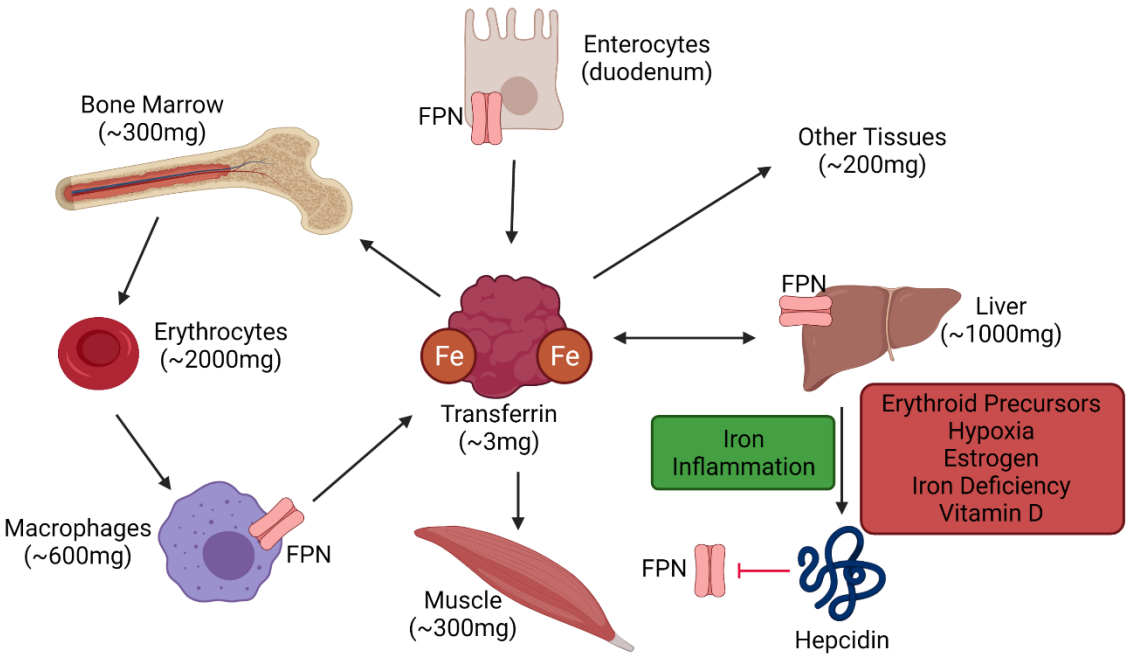

Figure 1.1: Overview of iron distribution and control. Estimated amounts of iron within each tissue are presented in parentheses. The central regulator of iron status, hepcidin, is primarily produced in the liver and is increased by high levels of iron or inflammation. The primary action of hepcidin is to inhibit and trigger internalization and degradation of ferroportin (FPN) which is primarily expressed in enterocytes, hepatocytes, and macrophages. As a result, iron absorption is reduced in the duodenum and remaining iron is sequestered within the liver and macrophages. Alternatively, hepcidin expression can be inhibited by stimuli such as iron deficiency, resulting in enhanced uptake and delivery of iron to target tissues. Created under licence with BioRender.com. Adapted from Sebastiani *et al.* 2016 [5].

Sufficient dietary iron intake is necessary to maintain life. Both recycling of iron from red blood cells and dietary intake of new iron contribute to the daily iron needs of individuals. In adults, approximately 5% of daily iron needs are met through dietary intake, albeit infants and children derive 30% of their daily needs through dietary intake

alone due to muscle growth and erythrocyte production [6]. The majority of absorbed dietary iron is contained within heme complexes, most commonly from hemoglobin and myoglobin proteins found in meat [7]. Additionally, non-heme iron salts can be found in vegetable and dairy food sources. The recommended daily allowance (RDA) for men and postmenopausal women is 8 mg of iron per day, whereas premenopausal women have an RDA of 18mg/day [7]. Reported median dietary intake of iron is 16-18mg/day in men, whereas the median in women in 12mg/day, despite premenopausal women having greater daily requirements [7]. Differences in dietary intake of iron, which may be tied to higher meat consumption in men versus women [8], may in part contribute to patterns of iron deficiency.

Mobilization and storage of iron within the body is controlled primarily via the actions of hepcidin [9]. Hepcidin is a peptide hormone, of which several isoforms exist with varying levels of activity [10]. Hepatocytes are responsible for the majority of hepcidin production within the body, which is then released into circulation to exert its biological effects [5]. Hepcidin regulates systemic iron status via its actions on ferroportin, which is the only known exporter of cellular iron [5]. Binding of hepcidin to ferroportin results in its internalization and degradation, thereby diminishing intestinal iron absorption by preventing its transfer through the basolateral membrane in the enterocyte. Moreover, hepcidin controls recycling and storage by modulating ferroportin expression in macrophages and hepatocytes [5,11]. When this occurs, availability of iron circulating to peripheral tissues is diminished [11]. Several known factors which induce and repress expression of hepcidin are summarized in **Figure 1.1** [12,13]. For instance, expression of hepcidin is suppressed by conditions associated with poor tissue oxygenation (i.e. erythropoiesis, hypoxia) to allow for increased iron mobilization in support of erythrocyte production [14]. Alternatively, hepcidin expression is induced by inflammation, infection, or by increased levels of circulating or intracellular iron [14].

Absorption of iron occurs primarily within the duodenum and proximal jejunum of the small intestine, albeit with markedly low efficiency compared to other nutrients [15]. Iron is most readily taken up by enterocytes in the form of heme (i.e. from meat, poultry,

or fish), where approximately 15-35% of ingested iron is absorbed. In contrast, less than 10% of non-heme iron, derived largely from plants or iron-fortified food sources [15,16], is absorbed. Lower uptake efficiency of non-heme iron is due to reliance on ferric reductase enzymes within the luminal brush border, required to convert insoluble Fe^{3+} to Fe^{2+}, which allows for uptake into enterocytes across the apical membrane via the divalent metal cation transporter 1 (DMT1) [1]. The efficiency of this process can be further reduced by ingestion of phytates, polyphenols, and the use of proton pump inhibitor medications, whereas ascorbic acid is known to increase iron absorption [15]. Currently, the mechanism and regulation of uptake of the heme form of iron remains poorly understood [9]. Once inside the enterocytes, iron is bound to ferritin, which is an iron storage protein with intrinsic catalytic activity allowing it to store iron in the Fe^{3+} form, and then convert it back to the Fe^{2+} form for transport through the basolateral membrane via ferroportin [1]. Ferritin is composed of 24 light and heavy chain monomers, and is capable of binding up to 4500 iron atoms, making it highly effective for storage [1].

When hepcidin levels are low, iron is exported via ferroportin into the circulation. Transferrin is the primary iron transport protein in the body and can bind to two Fe^{3+} molecules, requiring the serum enzyme ceruloplasmin to oxidize the iron to facilitate binding [13]. The vast majority of serum iron is bound to transferrin in an inert form, which is then taken up into target cells expressing transferrin receptors [1,13]. Notably, ferritin is also highly prevalent in the serum, although its function in circulation remains unclear. Serum ferritin is largely released into circulation by dying cells and arguably plays a negligible role in iron transport, with low levels of ferritin receptor expression on target cells being attributed to scavenger functions [17]. Consistent with this, serum ferritin is poorly saturated with iron [17]. Alternatively, some cells (i.e. hepatocytes, macrophages) actively secrete ferritin in the face of inflammation, potentially delineating a role of ferritin in mopping up any unbound iron in circulation to further limit oxidative stress [9,17]. Indeed, this is a principal mechanism through which ferritin acts as a positive acute phase reactant, meaning that serum levels rise in concert with inflammation and infection due to enhanced secretion from cells [18]. Notwithstanding, in the absence of systemic

inflammation, serum ferritin levels correlate with overall iron status within the body, and is one of the most utilized clinical tests to assess iron status [18,19]. As such, serum ferritin is regarded as a crucially important marker of iron status, despite its physiologic role remaining contentious [9,17].

Beyond central regulation of iron status via hepcidin, target tissues utilize post-transcriptional regulation of proteins involved in iron homeostasis to maintain local iron levels. This mechanism occurs primarily through the iron responsive elements (IRE) and iron regulatory proteins (IRP) [13]. IREs are DNA sequences within the untranslated regions (UTR) of numerous mRNA transcripts involved in iron status regulation, including the transferrin receptor and ferritin, which are bound by IRPs in response to cellular signals [1]. When tissue iron levels are low, IRPs bind to IREs (located in the 3` UTR of transferrin, or the 5` UTR of ferritin), thereby stabilizing transferrin receptor mRNA while simultaneously preventing translation of ferritin *via* steric hinderance [1]. In contrast, when tissue iron stores exceed cellular requirements, IRPs are unable to bind to IREs, which results in ferritin translation and degradation of transferrin receptor mRNA [1]. In the event of cellular damage due to iron overload, resident tissue macrophages play a role in recycling iron [20]. Thus, tissues can modulate their uptake and storage of iron to maintain cellular function, while also avoiding toxic accumulation of iron via these fine-tuning mechanisms, in concert with the central control mechanisms of hepcidin.

1.1.2 Clinical Characterization of Iron Deficiency (ID)

ID is defined by an inadequate level of iron stores to meet demand. ID is the most common nutritional deficiency worldwide, estimated to affect between 1-3 billion people [9,21]. Moreover, ID is the most common cause of anemia and anemia-related disability worldwide [22]. Common underlying mechanisms of ID include decreased iron absorption (i.e. celiac disease, bariatric surgery, drugs [i.e. proton pump inhibitors]), reduced iron intake (i.e. vegan/vegetarian diets, undernutrition), chronic blood loss (i.e. gastrointestinal bleeding, anticoagulant use, abnormal menstruation), multifactorial causes (i.e. chronic kidney disease, inflammatory bowel disease, peri-operative bleeding,

heart failure, etc.), or increased requirements (i.e. growth, pregnancy) [3]. As such, identification of ID in a patient requires a clinician to identify the underlying cause of deficiency, which is most often inadequate intake or blood loss (i.e. heavy menstruation, gastrointestinal bleeding) in adults, or increased demand in pregnant women and children [23].

The gold standard for diagnosis of ID is an absence of iron staining in bone marrow aspirates, though this procedure is too invasive for routine clinical practice [18]. Therefore, diagnosis of ID relies on surrogate markers of iron status, which can be assessed within the peripheral blood. In practice, serum ferritin levels are the first-line test to diagnose ID [24]. However, the degree to which serum ferritin correlates with depletion of iron within bone marrow is complicated by numerous factors, including but not limited to inflammation, infection, liver disease, and obesity [18]. For instance, a recent systematic review and meta-analysis showed that ferritin cut-offs for defining ID should be adjusted to account for the patient comorbidities outlined above, in order to accurately reflect depletion of bone marrow iron [25]. However, no current methodologies have been identified through which adequate correction of serum ferritin can be obtained on an individual patient basis, albeit research is ongoing to account for factors such as inflammation [26,27].

In addition to ferritin, many other peripheral blood markers for iron status are used clinically [19]. For example, serum iron is routinely used in clinical practice, and is almost exclusively bound to transferrin [9]. Direct quantification of total transferrin levels in the blood informs the total iron binding capacity (TIBC), with which transferrin saturation can be determined through the use of serum iron levels [11]. In contrast to ferritin, transferrin (and therefore serum iron) is a negative acute phase reactant, meaning that in the event of infection or inflammation the serum levels of iron and transferrin decrease [9]. Erythrocyte protoporphyrin is another peripheral blood marker of iron status. Erythrocyte protoporphyrin is a heme precursor which increases in abundance due to insufficient iron levels required for heme synthesis, which often complexes with other

divalent metal ion such as zinc in the setting of ID [19]. Finally, assays for additional markers such as soluble transferrin receptor and hepcidin are becoming more widely available, although their use is not currently widespread clinically [19,28]. While novel markers, such as the soluble transferrin receptor, appear to be quite promising in regards to their accurate reflection of iron status, no cut-off values have yet been validated for their use in identifying ID in patients [9,29].

If negative iron balance progresses sufficiently, alterations in functional iron (i.e. Hb levels) will be observed (**Figure 1.2**). Should ID progress to the extent that stored iron in the liver is diminished and no iron can be detected in the bone marrow, a condition described as microcytic anemia will result [9,30]. ID anemia manifests only with significant negative iron balance, as erythropoiesis is maintained at the expense of iron delivery to other tissues, despite the crucial role that iron plays in various processes within all cells [13,31]. Heme biosynthesis during the production of Hb requires the integration of adequate amounts of iron as a cofactor, without which increasing levels of non-functional precursors build up (i.e. erythrocyte protoporphyrin) [9]. As a result, fewer and smaller (microcytic) erythrocytes remain in circulation, as limited iron availability constrains production [9]. Anemia is defined as a circulating Hb level below a clinically determined threshold, which varies based on patient population [32]. Hematocrit, which reflects the ratio of erythrocyte volume to total blood volume, exhibits similar reductions in concert with Hb in the context of ID anemia [9]. Notably, although ID is the most common cause of anemia, several other conditions may result in reductions in circulating Hb [33]. As such, clinicians routinely investigate both Hb and serum ferritin levels to assess both iron and hematologic status simultaneously [34].

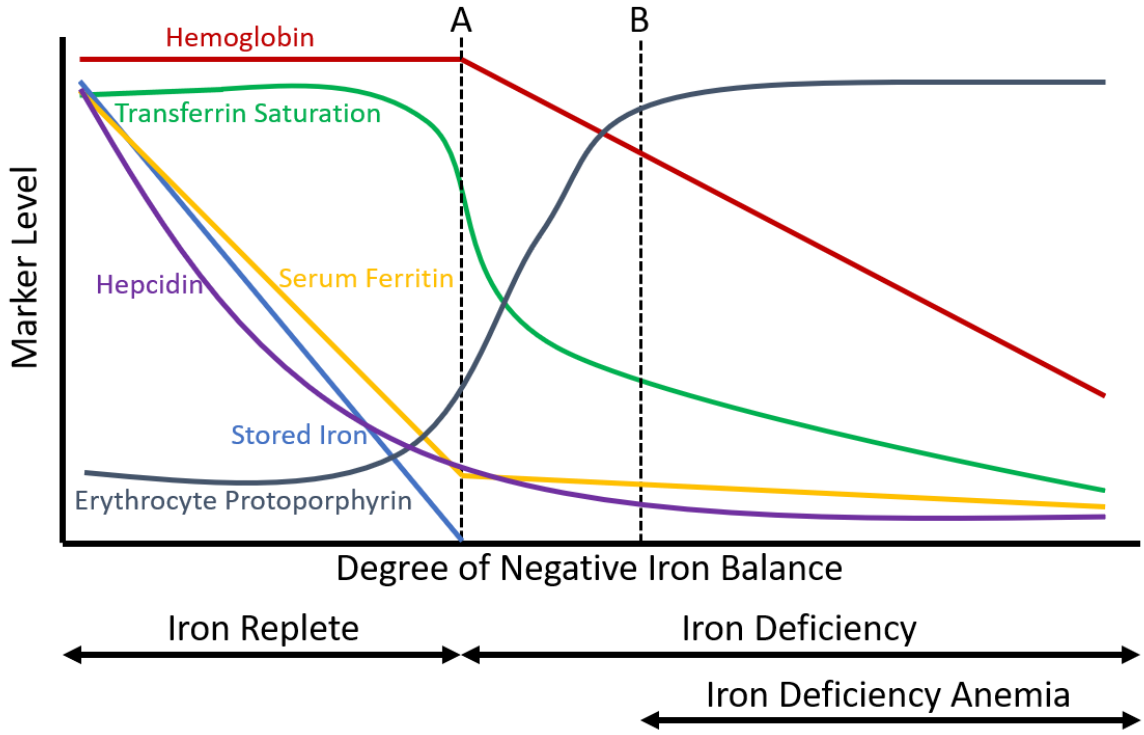

Figure 1.2: Iron status indicator levels over the spectrum of iron availability. Line A demarcates the point at which stored iron is no longer detectable, which is the definition of iron deficiency. Line B denotes the point at which hemoglobin levels reach a critical level, defined clinically as anemia. The general progression of iron deficiency is first depletion of stored iron (also reflected in serum ferritin levels), followed by reductions in iron transport (decreased serum iron; decreased transferrin saturation), and finally by reductions in functional iron (decreased hemoglobin). Figure adapted from Suominen *et al.* [35].

Clinically, it can often be challenging to identify either ID or ID anemia. Both ID and ID anemia cause similar non-specific symptoms, due to a lack of tissue-level functional iron, as well as reduced Hb. Weakness, fatigue, difficulty concentrating, and poor productivity at work can all be caused by either ID anemia or ID alone (insufficient functional iron; i.e. decreased enzymatic activity of iron-containing enzymes), or a combination of both factors [28]. As such, clinicians rely on biochemical assessments for iron status and hematologic indices to diagnose ID and anemia, respectively. While anemia may be a straightforward diagnosis based on hematologic indices with well-defined thresholds, assessment of iron status (and the ability to attribute anemia to ID) in

patients is often complicated by a variety of other factors. In healthy adults with no known co-morbidities which would alter iron status markers, a ferritin value of 15µg/L has been shown to correlate well with the depletion of iron in bone marrow [25]. Unfortunately, as previously mentioned above, several highly prevalent conditions impact the accuracy of serum ferritin as a measure of iron status (i.e. obesity, inflammation, infection, liver disease, etc.) [36]. For instance, ID may be masked by elevated ferritin levels due to chronic inflammation from a comorbid condition, which may or may not be identified by the clinician. Highlighting this issue, a recent Cochrane systematic review reported that use of 30µg/L ferritin as a cut-off for ID, elevated from 15 µg/L to account for artificial elevations of ferritin due to the reasons above, is prevalent despite the evidence supporting this practice being poor [36]. Current serum ferritin thresholds used for defining ID vary widely, emphasizing the need for establishing evidence-based cut-offs in a variety of patient sub-populations [18,19]. Furthermore, this point emphasizes the need for clinicians to order comprehensive iron status panels when assessing iron status in patients with comorbidities, not serum ferritin alone, as is currently common practice [24,25].

In pregnancy, considerable variation exists in the literature with respect to how ID and anemia are defined. For instance, a recent systematic review and meta-analysis highlighted that serum ferritin thresholds used in clinical studies varied from less than 6µg/L to less than 60µg/L; the most commonly used values were 12-15 µg/L, which are largely based on expert consensus guidelines rather than published evidence [29]. Similarly, anemia thresholds in pregnancy are lower than in non-pregnant women (12 g/dL) and vary based on trimester to account for physiological hemodilution and blood volume expansion. The World Health Organization (WHO) defines anemia as a Hb <11 g/dL (or hematocrit of <33%) at any time in pregnancy [34], whereas the Centers for Disease Control and Prevention (CDC) lowers this threshold to <10.5 g/dL (or hematocrit of <32%) in the second trimester [37]. Importantly, recent publications by our research group and others have shown that maternal iron and hematological status correlates poorly with fetal and neonatal iron status [19,38], suggesting more research is needed for evidence-based

ID thresholds in pregnancy which take into account both the mother and fetus. The importance of iron status optimization in pregnancy and early development will be highlighted within the following section.

1.1.3 ID & Pregnancy

The populations at the highest risk for developing ID are young children (under age 5) and pregnant women, largely due to increased iron demands [33]. ID is the chief cause of anemia in pregnant women, accounting for more than half of the 38% of women that become anemic over the course of their pregnancy worldwide [21]. However, the true rate of ID, which may not progress to overt anemia, is undoubtedly higher [39]. Indeed, up to 90% of women have sub-optimal iron stores prior to pregnancy (i.e. stores <500mg; serum ferritin <70μg/L) and 40% of women have low or absent iron stores [39], suggesting ID is likely to manifest in many pregnant women. Infant iron status is largely dependent on iron stores accumulated during gestation, their growth rate, and postnatal dietary iron intake [40]. Therefore, for the sake of brevity, this thesis will focus on the maternal factors associated with perinatal ID. Pregnant women are afflicted by ID at high rates in both developing and developed nations, albeit rates are far higher in developing nations [32]. Moreover, low socioeconomic status in developed nations has also been identified as a risk factor for developing ID in pregnant women [32,39]. Indeed, ID occurs in approximately 80% of infants in low income countries, and as many as 45% of infants in developed nations, reflecting in part that poor maternal iron status is widespread globally [41].

Insufficient iron status during pregnancy has numerous considerations beyond that of ID within non-pregnant individuals. First, one must consider the placenta both in terms of its own iron requirements and its capacity to transport iron to the fetus in the face of ID. The placenta regulates iron transport to the fetus, and responds robustly to ID, as reviewed by Roberts *et al.* [42]. ID alters placental structure, iron transporter expression, and iron metabolism within the placenta. However, the extent to which these mechanisms compensate to improve iron delivery to the fetus, versus acting as pathological changes triggered by hypoxia, oxidative stress, and inflammation remains unclear [42]. In mild ID,

studies suggest that delivery of iron to the fetus is maintained, supporting the notion that placental adaptations are beneficial to fetal iron delivery and development [41]. On the other hand, moderate to severe ID results in diminished iron status within the fetus, and several changes in placental structure may diminish placental functional capacity, such as the emergence of placental infarcts, syncytial knots, and fibrinoid necrosis [41,42]. As such, placental structure and functional changes in ID are thought to contribute, in part, to the pathogenesis of ID within the fetus.

There are several well-characterized acute impacts of ID on offspring health, such as reductions in offspring birth weight. Indeed, numerous studies have confirmed the association between maternal ID anemia and being born pre-term, small for gestational age, or having low birth weight [32,39,41,43–46]. Moreover, perinatal ID has been associated with increased risk of neonatal mortality [23,32,46]. Various factors are known to contribute to these effects, including altered placental function and structure, as described above. Furthermore, clear associations between the degree of growth restriction of the fetus and iron status exist, suggesting lack of functional iron itself may be a limiting factor for growth [43,47–49]. Physiologic adaptations to ID anemia made by the fetus may further predispose offspring to poorer growth, such as prioritization of blood flow to the brain, adrenals, and heart at the expense of other developing organs (i.e. liver, kidneys) in the face of presumed chronic hypoxemia [50–54]. As a result, this phenomenon known as asymmetric growth restriction may occur with increasing severity of ID anemia, likely contributing to long-term alterations in organ function [54]. Further discussion of perinatal outcomes and their relation to long-term health can be found in **Section 1.3**.

Iron demands over the course of gestation are estimated to be approximately 1200mg [39]. These increased demands are related to increased blood volume, placental and fetal development, and potential blood loss during delivery [39]. Approximately half of the iron required in pregnancy will be taken up by the fetus, which sequesters iron over the course of gestation to allow for continued growth and development postnatally [41]. Without sufficient iron stores prior to conception, most women are unable to meet their daily iron requirements through dietary intake, which increase from 0.8 mg/day in the

first trimester to 7.5 mg/day by the third trimester [15,39]. Enteral iron uptake of iron is slow to compensate for deficiency, such that enteral absorption of dietary iron is unlikely to achieve iron balance in this context, likely as a protective evolutionary mechanism to avoid iron overload [31]. Therefore, it is recognized that pre-conceptional iron status is critically important for the prevention of ID in pregnancy, albeit pre-pregnancy iron optimization is not always feasible. For instance, 45% of all pregnancies in the United States were unplanned in 2011[55]. Furthermore, even if pregnancies are planned, access to adequate pre-conception care, including screening for ID, may be difficult for many women worldwide [22,23,56]. As a result, In an effort to minimize poor birth outcomes due to perinatal ID, health agencies such as the WHO and Health Canada recommend daily oral iron supplementation in pregnancy to limit the risk of developing ID [33,57].

Iron supplementation in pregnancy has been shown to have substantial benefits, albeit drawbacks do exist. Iron supplementation improves maternal hematologic and iron indices [44,45]. However, without sufficient pre-conceptional iron stores, the prenatal vitamins routinely taken by pregnant women containing an average dose of 15-30 mg of iron may not be insufficient to meet iron demands due to poor absorption efficiency [15,24,28]. As such, higher dose oral supplementation may be warranted, albeit they stimulate hepcidin expression, thereby limiting iron of absorption for several days [23]. In addition, oral iron supplementation has several side effects. Iron supplements are associated with significant gastrointestinal discomfort, thereby limiting patient adherence [44]. Moreover, rare side effects associated with iron-overload have been reported, such as increased risk of glucose intolerance when supplementing in iron sufficient women [41]. As such, some controversy regarding adoption of universal iron supplementation in pregnancy exists, though it is viewed as beneficial to the vast majority of women [58].

Another potential issue with iron supplementation during pregnancy, in the context of perinatal ID, is limited efficacy in improving offspring outcomes. Recent Cochrane meta-analyses have shown that daily iron supplementation in pregnancy improves maternal hematologic indices and iron status, although no statistically significant reductions in premature birth or low birth weight were observed [44]. Similarly,

intermittent iron supplementation in pregnancy only improves maternal indices, albeit to a lesser extent than daily supplementation, with a notable benefit of reduced gastrointestinal discomfort versus daily supplementation [45]. In line with these findings, a recent study in Chinese mothers showed that anemia in the first trimester was associated with low birth weight, regardless of whether the anemia was subsequently corrected or not [59]. Together, these data demonstrate that oral iron supplementation during pregnancy after ID has developed may be sufficient to normalize maternal hematologic indices, but does not improve outcomes in offspring. Notably, treatment of ID in pregnancy with intravenous iron is highly effective in improving maternal indices and appears to have a favorable safety profile, albeit it remains unclear whether it improves offspring outcomes [60]. As such, prevention of ID in pregnancy remains paramount to minimize adverse offspring outcomes.

1.1.4 Cellular Pathophysiology of ID

Iron metabolism is regulated in part by oxidant status within cells. Cellular oxidant status describes the balance between reactive oxygen species (ROS), which are highly reactive molecules derived from oxygen produced through aerobic respiration or oxidation reactions within the cell that cause damage to cellular components [61], and antioxidant defenses. As a transition metal, Fe readily participates in reduction and oxidation reactions, implicating it in the formation of free radicals within the cell. When in excess, iron readily catalyzes the formation of hydroxyl and perhydroxyl radicals *via* Haber-Weiss and Fenton reactions [62]. However, intracellular iron pools must remain available to sustain biological functions, including synthesis of heme and Fe-S clusters, despite the potential for ROS generation. As such, it is unsurprising that IRPs are regulated in part by redox signaling itself, wherein Fe-S cluster oxidation and decomposition due to pro-oxidant conditions in IRP-1 promote its binding to IREs as an iron status independent "emergency brake" [61]. Nitric oxide (NO) levels, which depend on nitric oxide synthase (NOS) activity and reactivity of NO with ROS to form reactive nitrogen species such as peroxynitrite, are also known to modulate expression of ferritin

and transferrin receptors [61]. Together, these data suggest that changes in iron metabolism occur in concert with changes in cellular oxidant status. Furthermore, in conditions of overwhelming oxidant stress, intracellular iron stored in an 'inert' form bound to ferritin may become accessible to ROS and cause further damage [61]. Consistent with this, macrophages secrete ferritin when overwhelmed with oxidant stress, likely as a mechanism to limit the potential reactivity of stored intracellular iron [61]. In summary, iron metabolism is modulated by oxidant status, reflecting the role of iron in ROS generating processes within cells.

Iron status within a cell is critical for the regulation of several key functional processes necessary for life, such as energy production. Aerobic metabolism, the chief source of energy within most of our cells, is dependent on and regulated by iron status. Oxygen is delivered to tissues via hemoglobin. Inside the cell, oxygen is then utilized by mitochondria to produce ATP, where it acts as the final electron acceptor of the electron transport system. Interestingly, while glycolytic and anaerobic respiration are largely iron-independent, all components of the electron transport chain and many enzymes within the tricarboxylic acid (TCA) cycle (i.e. aconitase, succinate dehydrogenase) contain either Fe-S clusters or heme functional groups, or both [63]. Consequently, aerobic respiration is regulated in part by iron status through IRP/IRE mechanisms. For instance, succinate dehydrogenase and NADH dehydrogenase both have an IRE in their 5` UTR [64,65], meaning post-transcriptional regulation of their expression is linked directly to iron availability. Not surprisingly, energy demanding processes, such as tissue growth and repair, can be impaired by ID [66].

Both ID and excess iron are known to influence mitochondrial function. For instance, both insufficient and excess iron intake impair mitochondrial function in the livers of rats [67]. Similarly, ID in the absence of anemia impairs exercise performance via decreased electron transport chain complex I activity within skeletal muscle in mice [68]. Additionally, systemic perturbations in iron metabolism can alter local iron status, producing mitochondrial dysfunction. Exposure of cardiomyocytes to Ang-II or norepinephrine alters expression of IRPs, thereby decreasing intracellular iron stores,

resulting in impaired mitochondrial membrane potential and ATP production [69]. Similarly, infections and conditions which result in systemic inflammation may induce tissue-level ID due to activation of hepcidin, which may also predispose tissues to mitochondrial dysfunction [4,12,31]. Alternatively, diabetes mellitus, which has a complex association with iron dysmetabolism [70], has been shown to result in iron accumulation and subsequent mitochondrial dysfunction within the kidney; Interestingly, dietary iron restriction was shown to attenuate mitochondrial dysfunction within the kidney of streptozotocin induced diabetic rats [71]. As such, iron availability for mitochondrial respiration is critical for optimal function and energy production, regardless of the cause of local iron status changes.

The consequences of mitochondrial dysfunction secondary to ID can be profound. Beyond reductions in cellular energy production, mitochondrial dysfunction is of great concern due to potential for enhanced ROS generation. Even under optimal conditions, the reduction and oxidation reactions occurring within the mitochondria generate cellular ROS; in fact, it is estimated that~2% of total oxygen consumption by mitochondria contributes to ROS production [72,73]. Mitochondrial dysfunction is known to increase the proportion of ROS produced by mitochondria, thereby enhancing ROS generation [73]. Indeed, ID-induced mitochondrial dysfunction is associated with increased ROS generation and subsequent cellular damage to mtDNA, DNA, and lipids [67–69]. The extent to which this dysfunction is a direct reflection of a deficiency of iron-containing functional groups, versus the systemic and regulatory effects of iron status on mitochondrial function, remains unclear. However, each of the aforementioned mechanisms are likely to play a role. Importantly, ROS generation should not be viewed as strictly pathological, as ROS serve important cellular functions, including cell signaling [73]. Thus, while excess ROS can damage macromolecules and trigger cell death, too little ROS can result in reduced pro-survival signaling mechanisms, also resulting in cell death [73].

ID can also enhance ROS production through non-mitochondrial-dependent mechanisms. Iron is necessary for the function of certain antioxidant enzymes, and its

deficiency can impair cellular detoxification mechanisms. For instance, catalase requires iron as a cofactor for function [74]. Moreover, the iron-handling protein ferritin has intrinsic antioxidant properties, largely attributed to the ferroxidase activity of the heavy chain subunit [61]. Indeed, ferritin heavy chain has been shown to supress iron-mediated lipid peroxidation and is cytoprotective against oxidative stress [75,76]. Importantly, in addition to regulation of expression by IRPs, ferritin heavy chain expression is independently modulated by inflammatory cytokines (i.e. IFNγ, IL-1β, IL-6, TNF-α) and oxygen status, highlighting its role in modulating a variety of cellular stresses [77–82]. Ferritin secreted into circulation stimulated by increased inflammation has a higher than average proportion of heavy chains, consistent with its potential role as an antioxidant [17]. However, numerous studies have shown that the activities or levels of other antioxidant enzymes, such as superoxide dismutase (SOD) or glutathione peroxidase, are decreased by ID anemia [74,83–88]. Moreover, both glutathione depletion or overexpression trigger iron starvation-like responses, which highlights glutathione's important roles in regulating iron status and Fe-S cluster biogenesis [89,90].Decreased activities of key antioxidant enzymes in the face of ID may reflect cellular damage overwhelming antioxidant defenses, thereby worsening the oxidative damage.

Oxygen levels are also known to modulate iron metabolism, likely due in part to the role of iron in transporting oxygen throughout the body. Indeed, hypoxia is known to reduce hepcidin expression via the actions of hypoxia inducible factor (HIF)-1α and HIF-2α, thereby increasing enteric iron uptake to support erythropoiesis [61]. Additionally, HIF-2α stimulates several genes involved in iron metabolism directly, including DMT1 and duodenal cytochrome *b* (DcytB; which reduces luminal Fe^{3+} to Fe^{2+} for transport) in enterocytes, transferrin expression in the liver, and transferrin receptor expression in target tissues (i.e. bone marrow) [91]. Interestingly, HIF expression itself is iron regulated, as low levels of iron stimulate binding of IRPs to the IRE located in the 5` UTR of HIF-2α, a mechanism crucial for coordinating erythropoiesis with iron availability [91]. IRP-2 binding to IREs is stabilized by hypoxia, and acts as the predominant IRP responsible for iron regulation at low oxygen tensions, further supporting the critical role of oxygen

tension in the regulation of iron metabolism within cells [61]. Alternatively, high oxygen tension acts to limit iron availability. Cells exposed to supraphysiologic levels of oxygen exhibit enhanced binding of IRP-1 to IREs, thereby limiting the labile cellular iron pool which could react with oxygen to produce ROS [61]. Furthermore, iron-dependent prolyl hydroxylases act to target constitutively expressed HIF proteins for degradation in the presence of oxygen, suggesting a lack of functional iron may induce downstream HIF signaling [91,92]. The complex interplay between oxygen and iron status serves to provide tissue oxygenation, while simultaneously limiting potential ROS generation through reactions between iron and oxygen.

1.2 Cardiovascular Function & Disease

Cardiovascular disease is the leading cause of death worldwide [93]. Hypertension is a primary risk factor for ischemic heart disease and stroke, responsible for the majority of deaths from cardiovascular disease [93]. Moreover, hypertension is also an important risk factor for chronic kidney disease, which is the 12th leading cause of death worldwide as of 2017 [94,95]. Traditional risk factors for the development of cardiovascular disease are well-established, and include genetic (i.e. family history, ethnic background) and lifestyle factors (i.e. smoking, inactivity, obesity, high salt diets etc.) [94]. However, exposure to developmental stressors has been implicated in the dysregulation blood pressure control (see **Section 1.3**), thereby increasing offspring susceptibility for developing cardiovascular disease later in life.

A variety of factors contribute to blood pressure regulation, including alterations in genetics, epigenetics, endocrine function, and the structure and function of key organs (i.e. kidney, heart, vasculature) [96]. This introduction will focus primarily on the contributions of the vasculature and kidney, albeit the heart plays a critical role in the pathogenesis of cardiovascular disease, to which developmental programming likely also contributes [97–99]. The following sections will provide a brief overview of several systems that regulate blood pressure, which operate over a broad temporal spectrum ranging from acute (i.e. seconds) to chronic (i.e. days to years) effects.

1.2.1 Role of the Pressure Natriuresis in Blood Pressure Regulation

The most important determinant of long-term blood pressure is the kidney. The work of Guyton *et al*. has established that the kidney controls the long-term blood pressure set point through modulation of salt and water homeostasis [100]. Pressure natriuresis and diuresis describe the processes through which increased arterial pressure result in elevated renal output of salt and water in the urine, respectively. For instance, increased blood pressure will cause the kidneys to excrete more sodium and water, thereby reducing blood volume and lowering arterial pressure. Alternatively, low arterial pressure will cause the kidney to retain sodium and water, increasing blood volume and raising arterial pressure. Acutely, this process is constrained by the tubular capacity to reabsorb or excrete sodium; however, over a longer time-course the mechanism is considered to have infinite gain, such that sodium and water excretion will remain altered until arterial pressure has normalized [100,101]. Under this so-called 'Guytonian" view of hypertension, the capacity of a kidney to excrete sodium dictates long-term changes in blood pressure primarily through pressure natriuresis. As such, an abnormal pressure natriuresis relationship underlies chronic hypertension, wherein greater than normal elevations in arterial pressure are necessary to maintain sodium excretion and prevent extracellular fluid volume expansion [100,102]. Notably, several other physiologic factors alter the pressure natriuresis relationship. For example, NO promotes pressure natriuresis, through the mechanisms of blunting tubuloglomerular feedback, inhibiting tubular sodium reabsorption, and altering sympathetic input [103,104]. As such, pressure natriuresis must be viewed in light of the numerous integrated regulatory processes in the body, as highlighted by several recent publications [102,105,106].

Furthermore, the Guytonian view of hypertension has great utility for describing the pathogenesis of salt sensitivity of blood pressure. Salt sensitivity is characterized by an exaggerated change in blood pressure in response to alterations in dietary salt intake [107]. Salt sensitivity is estimated to occur in approximately one in four normotensive people, and half of those with hypertension [107]. Salt sensitivity is caused by abnormal pressure natriuresis, as well as alterations in the relationship between renal arterial

pressure and renal interstitial hydrostatic pressure (RIHP) [108,109]. RIHP is crucial for the urine concentrating abilities of the kidney, and is altered by changes in perfusion pressure [108,110]. This occurs via a small portion of renal medullary blood flow, which is poorly autoregulated, such that alterations in arterial pressure will alter medullary perfusion, and therefore RIHP [108,110]. Consequently, if medullary blood flow increases, enhanced RIHP will decrease tubular sodium reabsorption, facilitating enhanced sodium excretion [108]. As such, a blunted relationship between renal arterial pressure and RIHP will contribute to abnormal pressure natriuresis and salt sensitive hypertension, albeit vascular factors may also play a role [111].

1.2.2 Blood Pressure Regulation by the Sympathetic Nervous System

The sympathetic nervous system plays a prominent role in acute and long-term blood pressure regulation [112]. Sympathetic control of blood pressure occurs over the course of seconds, primarily acting through the arterial baroreceptors in the carotid sinus and aortic arch [112]. Increased blood pressure distends the vasculature and stretches the baroreceptors, causing a decrease in sympathetic neural outflow, thereby decreasing vasoconstrictor tone, myocardial contractility, and heart rate [112]. These reductions are achieved through the actions of decreased sympathetic input to vascular sympathetic nerves, the adrenal medulla (thereby decreasing epinephrine and norepinephrine release into circulation), and decreased stimulation of juxtaglomerular cells in the kidney which activate the renin angiotensin system (RAS) [112]. Indeed, the effects of the sympathetic nervous system also impact long-term blood pressure through reciprocal modulation of longer acting systems, such as the RAS [112]. Chronic changes in sympathetic activity may also be mediated in part by alterations in the set-point of the arterial baroreflex, albeit this process may be self-correcting over the course of days to weeks [112]. Moreover, chronic changes in sympathetic activity lead to structural remodelling of the heart and vasculature, such as hyperinnervation [113].As such, sympathetic nervous activity plays a role in both short and long-term blood pressure regulation.

1.2.3 Blood Pressure Regulation by the Renin Angiotensin System (RAS)

The systemic effects of the RAS play a central role in blood pressure and fluid regulation. The RAS regulates blood pressure through acting on the kidney, vasculature, and modulating the effects other regulatory mechanisms. In response to decreased blood pressure, renin is produced by the kidney and acts to convert circulating angiotensinogen, produced by the liver, into angiotensin-1 [114]. Consequently, angiotensin-1 is converted to angiotensin-II by angiotensin converting enzyme (primarily found in the lungs). The direct actions of angiotensin-II include mediating systemic vasoconstriction through AT1 receptors, and acting on the renal vasculature to mediate increased salt and water retention [114]. Additionally, angiotensin-II stimulates production of aldosterone in the adrenal gland, thereby further increasing salt and water retention [114]. Moreover, angiotensin-II has been shown to influence activity of the sympathetic nervous system [115]. The RAS is critically important to maintain normal arterial pressures despite variations in salt intake and hydration status, and has the potential to modulate long-term blood pressure through altering pressure natriuresis curve with chronic changes in activation [100,105,114].

1.2.4 Vascular Control of TPR and Blood Flow

The role of vasculature in the control of blood pressure is highlighted through its role in modulating total peripheral resistance (TPR). Resistance within a given vessel is related to the viscosity of blood, the length of the vessel, and the radius of the vessel lumen [116]. TPR describes the combined contributions to resistance of all vessels within the systemic vasculature. Mean arterial pressure can be calculated by multiplying cardiac output, or the product of stroke volume and heart rate, by TPR [116]. Elevations in TPR have been observed in idiopathic (also known as essential) hypertension, and in various preclinical models of hypertension, implicating the vasculature as a contributor to the pathogenesis of hypertension [102,116–118]. Moreover, local control of vascular resistance is critical to the regulation of organ perfusion, through a process known as autoregulation. Autoregulation describes the process through which alterations in vascular resistance

maintain tissue blood flow over a range of arterial pressures. Autoregulation occurs through several mechanisms, including sympathetic modulation, myogenic vascular responses, metabolic control, and vasoactive factors [119]. As such, changes in vascular resistance play a role in modulating blood flow and altering systemic blood pressure [102,105].

Acute blood flow regulation is achieved in part through myogenic vascular responses. Myogenic vascular responses are most pronounced in arterioles and other highly muscular blood vessels, which act to maintain tissue blood flow by altering vascular resistance [120]. Importantly, alterations in myogenic tone may contribute to the development of hypertension, due to their role in modulating total peripheral resistance [118]. Myogenic responses originate from the stretching and depolarization of vascular smooth muscle cells, thereby triggering constriction to counter high pressure within the lumen. Conversely, if blood pressure is low, vascular smooth muscle will relax, resulting in vasodilation and increased blood flow. Because myogenic responses are triggered through the stretch-mediated effects on vascular smooth muscle ion channels, this mechanism may act independently of, or in concert with, both neural and hormonal influences [120]. Should this mechanism be altered in vascular beds which contribute greatly to TPR, such as the mesenteric arteries, it may contribute to the pathogenesis of hypertension [121,122].

Numerous vasoactive substances acutely impact blood pressure and blood flow through modulation of vascular tone [123]. Many mediators cause vasoconstriction and raise TPR, including norepinephrine and epinephrine, angiotensin-II, vasopressin (anti-diuretic hormone), endothelin-1, and thromboxane [124]. Examples of physiologically important vasodilators, which contribute to decreased TPR, include bradykinin, histamine, prostacyclin (PGI_2), endothelial derived hyperpolarizing factor (EDHF), and NO [125]. Although alterations in these vasoactive mediators alone are often not sufficient to raise long-term blood pressure, they often precede the establishment of hypertension [126,127]. Importantly, many of these mediators act in concert with, or in opposition of one another. For instance, endothelin-1 production is stimulated by shear stress within vessels, and is

decreased by NO and PGI_2 [123]. In hypertension, an imbalance favoring the action of vasoconstrictors versus vasodilators is often observed, as reviewed elsewhere [123,128]. As such, the relative contributions of these mediators within the vasculature may be informative for vascular health. Since this thesis interrogates the role of NO signaling, the role of NO in this process is expanded upon below.

NO is viewed as being a critically important mediator of vascular function. Indeed, a deficiency of NO can be viewed as a biomarker of endothelial dysfunction, and for the subsequent development of hypertension [126]. Endothelial dysfunction is characterized by a pro-oxidant and pro-inflammatory state within the vasculature, corresponding to reductions in vasodilatory function [129]. In healthy vasculature, NO is produced primarily within the endothelium and causes relaxation of smooth muscle, thereby mediating vasodilation [104]. Increased vascular ROS are a primary cause of reduced NO bioavailability, either due to direct reaction of NO with ROS, or the uncoupling of endothelial NOS activity [129]. Moreover, loss of NO will reduce constraints on production of vasoconstrictors such as endothelin-1, which may further exacerbate production of ROS through stimulation of nicotinamide adenine dinucleotide phosphate (NADPH) oxidase [129]. Thus, NO bioavailability within the vasculature can have a profound impact on vascular tone and is implicated in the development of hypertension.

1.2.5 Vascular Remodelling

Long-term regulation of blood flow to maintain organ perfusion is largely dictated by organ-level structural and functional changes. For instance, a key mechanism through which long-term changes in organ perfusion occur is angiogenesis, the process of forming new blood vessels. Of particular importance in the context of development, formation of new blood vessels in neonates occurs within days, whereas angiogenesis in older animals where tissue structure is well-established is much slower [130]. Angiogenesis is stimulated through a variety of factors, the most important of which appear to be peak oxygen demands, wherein insufficient oxygen delivery to tissues stimulates the actions of vascular endothelial growth factor (VEGF) and platelet derived growth factor (PDGF)

[131,132]. The formation of new blood vessels helps to achieve chronic changes in organ perfusion, beyond the more acute processes involved in autoregulation.

Furthermore, vascular remodelling is an important mechanism contributing to long-term blood pressure alterations. Over time, transient-on-chronic increases in blood pressure will result in hypertrophy of vascular smooth muscle, wherein small resistance arteries and arterioles often exhibit inward eutrophic remodelling, whereas larger conduit vessels exhibit outward hypertrophic remodelling [133]. As a result, TPR will increase over time, contributing to the pathogenesis of hypertension[133]. In addition to changes in vascular smooth muscle, long-term alterations in vascular structure may also include altered sympathetic innervation, endothelial cell dysfunction, arterial calcification, and fibrosis[134]. As such, vascular remodelling is a mechanism through which acute alterations in vascular tone 'convert' to chronic changes over time.

1.3 The Developmental Origins of Health and Disease (DOHaD)

1.3.1 General Introduction to DOHaD

It has been long recognized in the scientific community that stressors encountered during early development can contribute to long-term susceptibility to chronic disease. The early works which helped to establish DOHaD as a field of study were epidemiologic studies utilizing birth records in the United Kingdom, published by Dr. David Barker and colleagues in the 1980s [135]. The early works of Barker and colleagues demonstrated that low birth weight and/or high rates of perinatal mortality were associated with increased risk of high blood pressure and mortality from ischemic heart disease later in life [136–138]. Initially, this phenomenon was referred to as fetal programming, and focused largely on the effects of the intrauterine environment on long-term outcomes. However, both epidemiologic and animal model studies have since shown that the early postnatal period is also critically important, resulting in a reframing from fetal programming to the DOHaD hypothesis [98,135]. The DOHaD hypothesis, perhaps known more colloquially as developmental programming, posits that both intrauterine and early postnatal exposure to stressors contribute to long-term disease susceptibility [98,135]. Following these landmark studies, numerous preclinical and clinical studies have provided further evidence in support of the DOHaD hypothesis, firmly establishing a link between early developmental stressors and long-term risk for cardiometabolic dysfunction, cognitive and behavioural deficits, reproductive dysfunction, and cancer in offspring [98,99,135,139–142].

To account for the long-term impacts of perinatal stressors on offspring health, numerous hypotheses have been proposed. Initially, the field of DOHaD reshaped the predominant notion that adult diseases were a result of genes and their interactions with an adverse environment in adulthood [140]. Instead, DOHaD emphasizes that a stressor encountered during development results in adaptations by the developing offspring to cope with their suboptimal environment, leading to permanent changes to offspring physiology and structure [135]. Indeed, this is the basis of developmental plasticity, which is the process through which one genotype can result in a large range of physiological states

in response to the differing stimuli and environmental conditions encountered [143]. It is recognized that developmental plasticity is highest *in utero*, and that while many adaptations provide a survival (and therefore evolutionary) advantage to the offspring in early life, it may come at the expense of disease susceptibility later in life [143]. Although developmental stressors may cause a clinically unambiguous phenotype in some cases (i.e. the more severe the stressor, the more obvious the adaptive response or phenotype), identification of many at risk offspring remains a great challenge.

Prematurity is an example of an unambiguous phenotype known to contribute to developmental programming. Prematurity, defined as being born prior to 37 weeks gestation, is a leading cause of perinatal morbidity and mortality, and also confers risk of long-term morbidity whose severity correlates with the degree of prematurity [144,145]. Rapid growth and development occur in the third trimester of pregnancy, and transitioning to the *ex utero* environment while this growth and development are actively occurring has long-term implications for function [145,146]. Moreover, with increasing degrees of prematurity, many offspring organs will not have the functional capacity to support life *ex utero*, leading to significant need for medical intervention [145,146]. As such, it is unsurprising that pre-term birth is a reliable marker for offspring likely to experience programming effects from a developmental stressor.

Similar to pre-term birth, significant attention has been paid to birth weight and intrauterine growth restriction (IUGR) and their usefulness in identifying at-risk offspring. Fetal growth restriction is a leading cause of perinatal morbidity and mortality and is estimated to occur in 5% of all pregnancies [147]. However, unlike pre-term birth, birth weight and IUGR share a more complicated relationship with long-term programming effects. Low birth weight can be categorized in absolute terms (i.e. any birth weight below 2500g) or as being small for gestational age (SGA), defined as weight $<10^{th}$ percentile of predicted when accounting for fetal sex and gestational age [148]. In contrast, IUGR is diagnosed via ultrasonography and is defined as being $<10^{th}$ percentile of predicted weight for gestational age, albeit significant variability in this definition may exist due to error associated with estimations of fetal size and the standard growth curve

utilized [147]. While growth restriction and low birth weight are indeed strongly associated with perinatal morbidity and mortality [147,149–151], and potentially to long-term programming effects, two important caveats must be considered. First, constitutional smallness, or small stature constrained by genetic factors rather than developmental stressors, must be considered. Second, long-term programming can occur in offspring where no overt growth restriction or reductions in birth weight are observed [99,139,152]. Together, this suggests that although growth restriction and birth weight are helpful for identifying offspring at risk of programming effects, they can result in false positives (i.e. constitutional smallness) and negatives (i.e. programming despite no change in birth weight). These factors, among others, contribute to the issues pertaining to identifying which offspring have been exposed to developmental stressors.

Furthermore, patterns of fetal growth restriction can be broken down into two broad categories, either asymmetric or symmetric. Asymmetric growth restriction refers to a condition in which some organs (i.e. heart, brain, adrenals) become proportionally larger, while other organs (i.e. kidneys, liver) are proportionally smaller [147]. This growth pattern is often caused by extrinsic developmental stressors (i.e. nutritional deficiencies, placental insufficiency), and reflects a diversion of resources to ensure function of "critical" organs at the expense of "dispensable" ones. This phenomenon has also been described as the fetal brain sparing effect in the context of chronic prenatal hypoxia exposure [54]. These processes are thought to enhance survival acutely, albeit contributing to long-term detrimental programming phenotypes [54,149,153,154]. In contrast, symmetric growth restriction, where fetal organs are all reduced in size in proportion to body size, is most commonly associated with intrinsic fetal issues (i.e. chromosomal abnormalities) or congenital infections in early pregnancy [147]. As such, the pattern of growth in offspring may help clinicians identify offspring exposed to extrinsic developmental stressors.

In addition to intrauterine growth, postnatal growth trajectories are also critically important for the long-term programming effects of developmental stressors. A phenomenon known as postnatal catch-up growth, which is characterized by abnormal growth and/or weight gain secondary to being born growth restricted, is a mechanism

through which developmental stressors contribute to long-term programming. For instance, several animal models of developmental programming have shown that IUGR offspring grow more rapidly than their control counterparts in the postnatal period when placed on a nutrient-replete diet. These accelerated postnatal growth trajectories are associated with enhanced adiposity and increased risk for development of cardiometabolic dysfunction [155–157]. The role of catch up growth, independent of a prenatal insult *per se*, has been demonstrated in studies wherein IUGR offspring maintained on nutrient restricted diets postnatally had improved long-term outcomes [158]. Therefore, it is recognized that all neonates, and especially those with IUGR, must be monitored closely in the postnatal environment to ensure optimal growth and development, and to avoid growth patterns that promote future cardiometabolic risk [158]. Moreover, body composition, and not just overall size, must be considered. In the context of perinatal ID, postnatal catch up growth may not be overt in perinatal ID, given that the low iron content in breast milk would continue to limit iron available for neonatal growth, until such a time that additional iron is provided in solid foods or supplemented formula [4,31]. As such, other metrics such as increased susceptibility for adiposity itself may be a useful indicator for postnatal catch-up growth [159,160].

To date, a variety of perinatal stressors have been linked with chronic disease. For instance, both clinical and mechanistic animal model studies have shown that a myriad of developmental stressors (i.e. micronutrient deficiencies, macronutrient restriction, maternal obesity, gestational diabetes, prenatal hypoxia, reduced uteroplacental perfusion, etc.) predispose offspring for increased risk of cardiovascular, metabolic, and cognitive dysfunction later in life [154,159,161–170]. Despite large differences in the nature of the various developmental stressors studied, many reviews highlight that offspring exhibit similar phenotypes in later life. Moreover, the mechanisms underlying the propensity for disease also show considerable overlap between models of developmental stress [139,153,171]. Therefore, treatment strategies which could be developed to prevent developmental programming of cardiovascular dysfunction may be applicable to a variety of stressors [171–173]. Notwithstanding, further mechanistic understanding of individual

developmental stressors, and how offspring respond to them, is necessary before perinatal therapeutics are a viable treatment option.

In cases where prevention of a developmental stressor may not be viable, it is temping to speculate that early interventions could be most effective [139,143]. Indeed, with higher developmental plasticity in early life, therapeutic interventions instituted during this time could be more effective by altering growth and developmental trajectories in such a way as to reduce the burden of chronic disease. Theoretically, this treatment paradigm could be more efficacious than treatments instituted once disease as manifest [143]. However, developing treatments for use during pregnancy or early postnatal life is fraught with challenges. In the same way that developmental plasticity confers greater potential efficacy for therapeutic interventions in this period, so too can the side effects of drugs be exacerbated. Moreover, the potential for long-term side effects in the various organ systems which are still developing would require substantial surveillance efforts. That said, the merits of early intervention cannot be understated, and early childhood or adolescence may be a more suitable time for therapeutics. Indeed, findings from the Pathobiological Determinants of Atherosclerosis in Youth (PDAY) study suggest that 90% of myocardial infarctions could be prevented through identifying and mitigating the progression of risk factors for atherosclerosis before age 15 [174]. Indeed, this viewpoint is in line with mitigating future cardiovascular disease through the lens of DOHaD, which stresses the importance of early detection and intervention. As medicine continues to progress, and we uncover new biomarkers which denote risk of future disease earlier, it is foreseeable that health optimization during early development will become a priority in treating a large variety of chronic health conditions.

1.3.2 Overview of Renal Development

The developing kidney is particularly susceptible to insults. To understand how stressors can influence long-term kidney structure and function, and brief description of kidney organogenesis is warranted. Nephrogenesis, the process through which nephrons are formed, begins early in gestation in humans and is complete by approximately gestational weeks 36-37 [175,176]. Notably, this is distinct from rats, wherein nephrogenesis ceases approximately 2 weeks postnatally [175]. The metanephric kidney, which gives rise to the permanent kidney, develops through the ureteric bud growing from the caudal region of the fetus into a loose grouping of nearby cells known as the metanephric mesenchyme. The ureteric bud, which will eventually form the collecting ducts, renal pelvis, and ureters, develops through elongation and branching processes [177]. Meanwhile, complex signaling interactions are occurring between the ureteric bud and the metanephric mesenchyme. The metanephric mesenchyme consists of many different cell types which ultimately form the vasculature, tubular structures, glomeruli, among other components of the kidney [177]. Numerous signaling pathways which are known to regulate the interactions between the ureteric bud and metanephric mesenchyme, thereby dictating congenital nephron number; these are summarized in **Figure 1.3**.

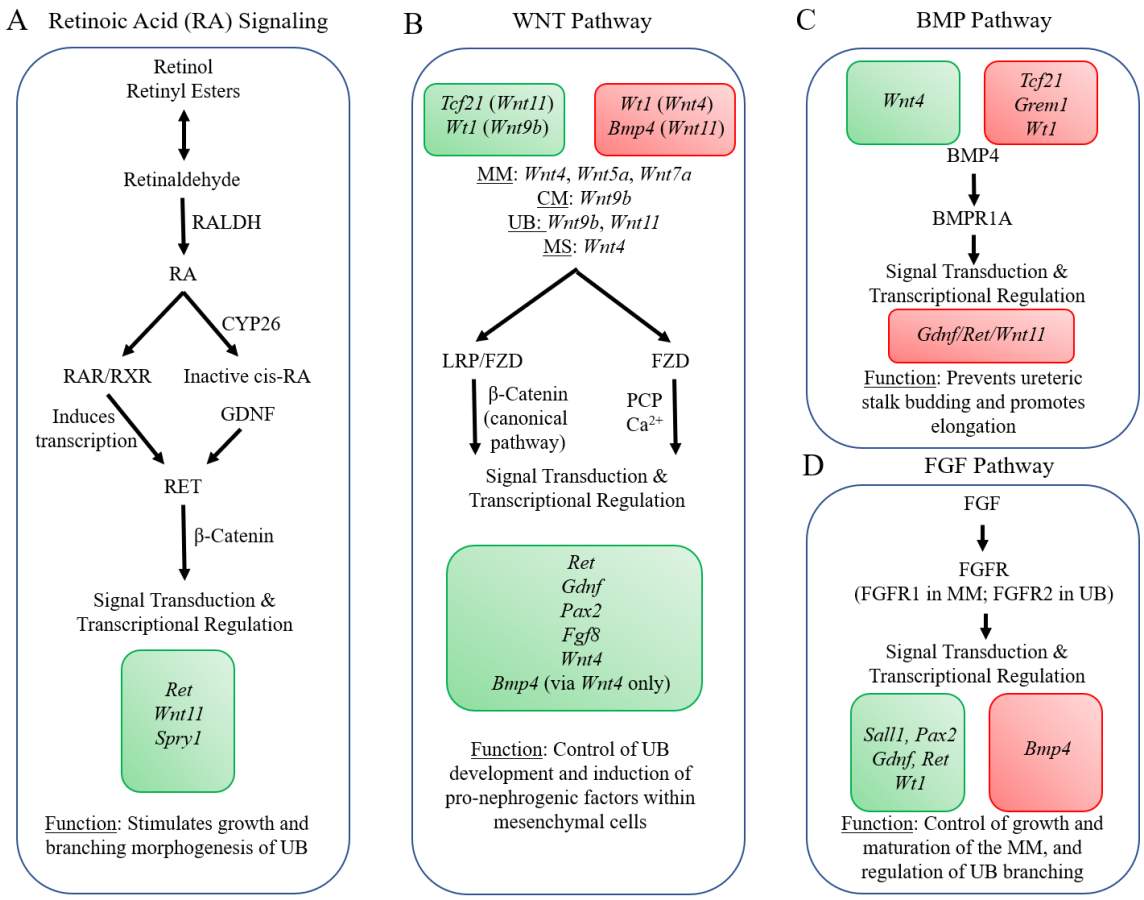

Figure 1.3: A simplified overview of nephrogenic signaling pathways. These pathways mediate the interactions between the ureteric bud and surrounding mesenchymal cells. (**A**) all-trans retinoic acid is generated through the action of retinaldehyde dehydrogenase (RALDH) activity, which can bind to nuclear retinoic acid receptor (RAR)/ retinoid X receptor (RXR) heterodimers leading to the transcription of receptor tyrosine kinase (RET). Glial derived neurotropic factor (GDNF) is the ligand for RET, leading to activation of downstream signaling mediated in part by β-catenin, thereby enhancing (green box) transcription of downstream mediators. (**B**) Wingless-related integration site (WNT) pathway signaling is enhanced (green box) and repressed (red box) by various factors. Several known WNT ligands and their regions of expression (metanephric mesenchyme, MM; cap mesenchyme, CM; ureteric bud, UB; medullary stroma, MS) may act through frizzled (FZD) receptors and downstream non-canonical WNT/Ca^{2+} or WNT/Planar Cell Polarity (PCP) pathways. Alternatively, low-density lipoprotein receptor (LRP)/FZD complexes and downstream β-catenin mediate canonical WNT signaling. (**C**) Bone morphogenic protein (BMP) pathway acts within the ureteric stalk via bmp-receptor 1a (BMPR1A; also known as ALK3) to antagonize pro-budding/branching signaling. (**D**) Fibroblast growth factor

(FGF) pathway functions via FGF-receptors (FGFR) in a similar fashion to the WNT pathway and the GDNF/RET axis, thereby stimulating coordinated growth, budding, and maturation of the ureteric bud through interactions with the MM. Each major pathway has been reviewed in-depth elsewhere in detail [178–184].

Regulation of cellular proliferation and death within the kidney is crucial, and has been shown to rely in part on the triggering of developmental senescence and apoptosis [185,186]. Indeed, developmental senescence and resultant senescence associated secretory phenotype (SASP) signaling, as well as apoptosis, are known to influence the signaling pathways described in **Figure 1.3** [177,187]. Best characterized in the mesonephros, genetic knockouts of developmental senescence induce abnormalities in kidney structure, which are partially abrogated by the enhanced induction of apoptosis [185,186]. In contrast to the stress-associated triggers of both apoptosis and cellular senescence in aging and disease (i.e. oncogenic DNA mutations, ROS-induced damage to the cell, etc.), the signaling pathways which underlie these developmental processes are distinct [185,186]; as such, it remains an open question how developmental stressors impact the balance of these reciprocally inhibited processes [188].

Over the course of development, large changes in oxygen availability and energy metabolism can impact levels of ROS within the kidney. Renal development *in utero* occurs in relative hypoxia, meaning that early growth is sustained largely through anaerobic respiration, in addition to low levels of aerobic respiration[189–191]. Over the course of gestation oxygen delivery to the fetus increases, leading to increases in aerobic respiration [192]. The most precipitous shift towards aerobic metabolism follows the transition to the extra-uterine environment, which is hyperoxic relative to the intrauterine environment [192]. As such, increased levels of lipid peroxidation, serum malondialdehyde, and lipoperoxide levels are observed in neonates [193–195], though these levels decrease to adult levels 10-20 days after birth [195,196]. While oxygen availability itself can increase formation of ROS through interactions with non-mitochondrial cellular components [197], mitochondria are implicated as a large source of the ROS in this transitional period, as

mitochondrial superoxide and H_2O_2 production is known to increase proportionally with pO_2 [198,199].

To compensate for the increased oxidative stress, numerous components of the antioxidant system are upregulated to prevent damage in neonates [200–203]. The rise in neonatal ROS also serves as a signal for growth and developmental processes, such that increases in antioxidant capacity must be tightly regulated in concert with changing levels of ROS [171]. Moreover, mitochondria increase in number substantially during development to meet the metabolic demands of the growing offspring. The heart and kidney have the highest energy demands and resting metabolic rates of all organs in adults[204]. Consequently, the heart has the highest oxygen consumption and mitochondrial content of any organ, followed closely by the kidney[205,206]. To limit oxidative damage in the kidney during the transition to the postnatal environment, commensurate rises in antioxidant defenses within these organs must occur [207]. Under this paradigm, stressors during development can disturb the finely tuned intracellular ROS levels, thereby altering development and causing damage to cells. Further, if the balance between mitochondrial content and antioxidant defense is perturbed, tissues may not be able to provide the energy to meet the metabolic demand of the growing tissues.

1.3.3 Developmental Programming of Cardiovascular & Renal Dysfunction

The impact of developmental stressors on the kidney has largely focused on congenital anomalies and alterations in nephron endowment. Additionally, abnormalities in tubular function and renal hemodynamics have also been reported due to developmental stressors such as gestational hypoxia and perinatal ID [170,208]; albeit these mechanisms are not within the focus of the work presented herein. Low birth weight and decreased kidney volume at birth, which are common effects of developmental stressors [209], have been identified as risk factors for developing hypertension and chronic kidney disease later in life [150]. Importantly, overall nephron endowment is associated with renal volume at birth [176,210,211]. Stemming from these observations, the Brenner hypothesis has

been proposed as a mechanistic explanation linking developmental stressors with long-term chronic kidney disease and hypertension.

The Brenner hypothesis posits that a congenital reduction in nephrons is a risk factor for hypertension and chronic kidney disease later in life [153]. Since being proposed in 1988 [212], numerous studies have substantiated the link between reductions in nephron endowment and hypertension and chronic kidney disease later in life [150,151,171,213]. Reductions in nephron complement reduce functional reserve, such that when secondary lifestyle stressors necessitate an increase in filtration (i.e. a high-salt diet), remaining nephrons must functionally adapt to a higher demand [153]. As a result, glomerular hypertrophy occurs to accommodate hyperfiltration, albeit over long periods of time this may result in glomerular sclerosis and accelerated loss of functional nephrons due to injury [153]. Therefore, developmental stressors which cause large reductions in congenital nephron numbers result in a feed-forward loop, wherein accelerated loss of nephrons due to lifestyle or other comorbidities result in the precipitation of hypertension and overt renal dysfunction in later life.

Perinatal ID has been shown to alter kidney development. Both gestational and postnatal iron restriction have been shown to decrease nephron endowment in rat offspring [214,215]. Additionally, recent studies have shown that perinatal ID results in delayed renal maturation, albeit ID-induced reductions in glomerular density were not observed in this study [216]. Similarly, gestational hypoxia, vitamin A deficiency, maternal protein restriction, and global maternal nutrient restriction have also been shown to reduce nephron endowment in offspring [217–223]. Although the mechanisms underlying altered nephrogenesis in perinatal ID remain unknown, models of similar etiology may offer some clues. For instance, gestational hypoxia causes dysregulation of both wingless-related integration site (WNT) and retinoic acid (RA) nephrogenic signaling pathways, suggesting they may contribute to in alterations in renal structure and associated long-term cardiovascular outcomes [208,218,224]. Moreover, ID is known to modify vitamin A metabolism [225–227], creating a strong impetus to assess vitamin A metabolism and nephrogenic signaling in long-term kidney dysfunction due to perinatal

ID. Furthermore, patterns of developmental senescence and apoptosis, and their interactions with cellular stress induced by perinatal ID, may alter nephrogenesis. Indeed, a variety of developmental stressors (i.e. ID, prenatal hypoxia, maternal protein restriction, etc.) have been shown to induce renal cellular stress [208,214,215,218,228,229], and as such it would be reasonable to postulate that they may patterns of developmental senescence and apoptosis.

Perinatal ID and developmental programming models of similar etiology provide evidence of long-term renal dysfunction in offspring. For instance, perinatal ID results in blunting of the relationship between renal arterial pressure and RIHP in adult male offspring, contributing to salt sensitivity of blood pressure [170]. Moreover, numerous studies report elevations in perinatal ID offspring blood pressures [159,160,170,215,230–232], further implicating the presence of kidney dysfunction due to its role in the regulation of long-term blood pressure set point [105]. Offspring exposed to prenatal hypoxia also exhibit hypertension and renal dysfunction, characterized by tubular dysfunction and abnormal collecting duct structure [208,218]. Given that antioxidant treatments improve cardiovascular outcomes in models of prenatal hypoxia, this may also suggest ROS underlie long-term renal dysfunction [233–235]. Indeed, mitochondrial dysfunction and enhanced ROS underlie renal dysfunction in a variety of experimental models, such as Dahl salt-sensitive rats and spontaneously hypertensive rats [236,237]. As such, it is possible that perinatal ID impacts long term renal function through impaired mitochondrial function bioenergetics and enhanced ROS generation.

In addition to long-term changes in renal function, developmental stressors such as prenatal hypoxia and perinatal ID also likely impact vascular function. Previous studies in adult offspring exposed to prenatal hypoxia show reduced vascular NO bioavailability, which be due in part to enhanced oxidative stress [233–235]. Prenatal hypoxia also results in long-term alterations in vascular myogenic tone [121,122], in addition to decreased responses to vasodilators and enhanced vasoconstrictor responses [121,162,233,238,239]. Moreover, sympathetic hyperinnervation and enhanced vascular smooth muscle sympathetic nerve activity have been observed in the vasculature of young adult

rat offspring exposed to prenatal hypoxia [127]. Given these data, an impetus exists to assess how perinatal ID impacts long-term vascular function.

Taken together, there are numerous mechanisms through which perinatal ID may alter vascular and renal function, thereby resulting in chronic elevations in offspring blood pressure. Importantly, hypertension is one of the most important risk factors for the development of cardiovascular disease, which is the number one cause of death globally [93]. Moreover, perinatal ID increases susceptibility for enhanced adiposity [159,160], an independent risk factor for the development of cardiovascular disease [174]. Finally, perinatal ID has been linked to altered renal development, which likely contributes to chronic elevations in offspring blood pressure [170,214–216]. Identification of mechanisms which contribute to cardiovascular dysfunction in perinatal ID offspring is critical for development of therapeutic strategies to ameliorate long-term detrimental outcomes.

1.3.4 Sex-Dependence of Developmental Programming

Interestingly, male and female offspring appear to exhibit markedly different outcomes when exposed to a variety of developmental stressors. As reviewed by Loria *et al*. [97], both short- and long-term cardiovascular outcomes in models of developmental programming differ between male and female offspring. Overall, the literature is suggestive that male offspring exhibit an increased propensity for development of cardiovascular dysfunction secondary to developmental stressors versus females [97,167]. Numerous mechanisms have been proposed to account for such differences, albeit no definitive answers have yet been found. Potential mechanisms include genetics (i.e. X- and Y-linked traits), epigenetics, and the actions of sex hormones. Each of the above factors may play a role in both modulating the degree of fetal exposure to a stressor, as well as the degree to which it causes dysfunction.

Despite similar maternal insults theoretically impacting male and female fetuses similarly, sexually dimorphic outcomes suggest this may not be the case. For instance, female fetuses invest more resources in placental development versus males [240]. As a result, female offspring likely have greater physiologic reserve when faced with maternal

stressors that impact the availability of nutrients or oxygen which must be efficiently transported to the fetus through the placenta. Additionally, male and female fetuses impact maternal physiology differently, which may place male fetuses at greater risk. For example, women pregnant with male fetuses are more likely to develop gestational diabetes mellitus, have poorer beta cell function, and have lower pregnancy-sustaining human chorionic gonadotropin (hCG) levels [241]. As such, poorer maternal health in pregnancies carrying male fetuses may place females at relatively lower risk.

Furthermore, genetic, epigenetic, and hormonal differences within the fetuses may explain why responses to similar exposures to developmental stressors may lead to divergent offspring phenotypes. For instance, the presence of higher levels of estrogen in females during development [242], or perhaps a less favorable ratio of testosterone to estrogen in males, may portend a protective effect during critical windows of development. Estrogen is known to transcriptionally control genes involved in mitochondrial function, antioxidant function, and cellular survival, the effects of which may reduce immediate cellular stresses thereby preventing long-term dysfunction [243–245]. Moreover, mitochondrial function may be a factor through which female offspring respond differentially to stressors, as mitochondria have evolved exclusively through maternal lineages, thereby optimizing their function in females [246–248].

Identification of mechanisms accounting for long-term dysfunction secondary to developmental stressors is critically important to development of treatment or preventative paradigms. For instance, preclinical studies utilizing antioxidant therapies in hopes of preventing cardiovascular dysfunction secondary to developmental stressors have showed that these may be detrimental to unaffected offspring [249,250]. As such, ascertaining the extent to which male and female offspring are exposed to developmental stressors, in addition to how they respond, is critical for the reduction of life-long cardiovascular disease risk. The mechanisms through which sex-dependent outcomes in DOHaD occur remains an open question, underscoring the necessity of studying both male and female offspring for all relevant outcomes.

1.4 Statement of Hypotheses and Aims

Iron deficiency is the most common nutritional deficiency worldwide, and pregnant women and infants are the most affected groups [4,21,41]. Gestational iron deficiency is associated a host of pregnancy complications, including increased risk of pre-term birth and intrauterine growth restriction [4,41]. Long-term, perinatal ID has been shown to cause hypertension, reduced nephron endowment, and altered renal function in adult offspring [170,215,216,230], albeit the mechanisms through which this occur remain unclear. Furthermore, whether these effects are present in both male and female offspring, and whether mechanisms through which dysfunction may occur in each sex, remains unclear. The overarching hypotheses to be tested are as follows:

1. Perinatal ID will result in organ-specific patterns of hypoxia, mitochondrial dysfunction, and oxidative stress during gestation (**Chapters 2 & 3**).
2. Perinatal ID will alter cellular health within the developing kidney, leading to altered nephrogenic signaling and ultimately a reduction in nephron endowment (**Chapters 4 & 5**).
3. Perinatal ID will result in increased risk for development of hypertension, vascular dysfunction, and renal injury; effects which can be exacerbated by consumption of a high-salt diet in adulthood (**Chapters 6 & 7**).

The specific aims of each study, which address specific portions of one or more of the above hypotheses, are listed below by chapter:

Chapter 2: Modest and severe maternal iron deficiency in pregnancy are associated with fetal anemia and organ-specific hypoxia in rats.

1. To determine which (if any) fetal or maternal organs are hypoxic due to differential severities of prenatal ID at the end of gestation.
2. Examine the extent of changes in uterine and umbilical artery blood flow due to differential severities of prenatal ID at the end of gestation.

3. Examine how different severities of prenatal ID impact patterns of growth restriction in fetuses at the end of gestation.

Chapter 3: Prenatal iron-deficiency causes sex-dependent mitochondrial dysfunction and oxidative stress in fetal rat kidneys and liver.

1. To determine how severe and moderate prenatal ID impact patterns of fetal growth restriction.
2. To determine if moderate and severe prenatal ID result in enhanced generation of superoxide concomitant with reductions in nitric oxide in the fetal liver and kidney.
3. To determine if moderate and severe prenatal ID cause mitochondrial dysfunction in the fetal liver and kidney.
4. To determine the impact of moderate and prenatal ID on mitochondrial biogenic factors in the liver and kidney.

Chapter 4: Perinatal iron deficiency causes sex-dependent changes in kidney oxidative stress, cellular senescence, and apoptosis during postnatal renal development.

1. To determine how perinatal ID impacts patterns of apoptosis and senescence over the course of postnatal renal development
2. To assess the impact of perinatal ID on antioxidant enzyme expression and levels of oxidative damage within the kidney throughout postnatal renal development

Chapter 5: Perinatal iron deficiency causes sex-dependent alterations in renal retinoic acid signaling and nephrogenesis.

1. To determine how perinatal ID impacts offspring renal vitamin A metabolism.
2. To determine if perinatal ID results in reduced nephron endowment in offspring following postnatal renal maturation.
3. To determine if alterations in nephrogenic signaling cascades following birth contribute to alterations in offspring nephron endowment.

Chapter 6: Perinatal iron deficiency and a high salt diet cause long-term kidney mitochondrial dysfunction and oxidative stress.

1. To determine how alterations in NO signaling contribute to hypertension in adult offspring born with perinatal ID.
2. To determine if perinatal ID results in chronic elevations in renal oxidative stress and mitochondrial dysfunction.
3. To determine if perinatal ID results in increased susceptibility to renal injury in adulthood.
4. To determine if the above effects of perinatal ID are exacerbated by introduction of a high-salt diet in adulthood.

Chapter 7: Perinatal iron deficiency combined with a high salt diet in adulthood causes sex-dependent vascular dysfunction.

1. To determine if perinatal ID results in resistance artery oxidative stress and a reduction in NO signaling.
2. To determine if perinatal ID results in impaired endothelial dependent and independent vasodilation.
3. To determine if perinatal ID results in hypersensitivity to vasoconstrictors, such as endothelin-1 and phenylephrine.
4. To determine if the above effects of perinatal ID are exacerbated by introduction of a high-salt diet in adulthood.

Chapter 2

Modest and Severe Maternal Iron Deficiency in Pregnancy are Associated with Fetal Anaemia and Organ-Specific Hypoxia in Rats

Andrew G. Woodman[1], Alison S. Care[2], Yael Mansour[3], Stephana J. Cherak[1], Sareh Panahi[3], Ferrante S. Gragasin[3], *Stephane L. Bourque[1, 3]

[1]Department of Pharmacology, University of Alberta

[2]Department of Obstetrics and Gynaecology, University of Alberta

[3]Department of Anesthesiology & Pain Medicine, University of Alberta.

PUBLISHED:

Woodman *et al Scientific Reports* 2017. 7:46573

2.1 Abstract

Prenatal iron-deficiency (ID) is known to alter fetal developmental trajectories, which predisposes the offspring to chronic disease in later life, although the underlying mechanisms remain unclear. Here, we sought to determine whether varying degrees of maternal anaemia could induce organ-specific patterns of hypoxia in the fetuses. Pregnant female Sprague Dawley rats were fed iron-restricted or iron-replete diets to induce a state of moderate (M-ID) or severe ID (S-ID) alongside respective controls. Ultrasound biomicroscopy was performed on gestational day (GD)20 to assess uterine and umbilical artery blood flow patterns. On GD21, tissues were collected and assessed for hypoxia using pimonidazole staining. Compared to controls, maternal haemoglobin (Hb) in M- and S-ID were reduced 17% ($P<0.01$) and 48% ($P<0.001$), corresponding to 39% ($P<0.001$) and 65% ($P<0.001$) decreases in fetal Hb. Prenatal ID caused asymmetric fetal growth restriction, which was most pronounced in S-ID. In both severities of ID, umbilical artery resistive index was increased ($P<0.01$), while pulsatility index only increased in S-ID ($P<0.05$). In both M-and S-ID, fetal kidneys and livers showed evidence of hypoxia ($P<0.01$ vs. controls), whereas fetal brains and placentae remained normoxic. These findings indicate prenatal ID causes organ-specific fetal hypoxia, even in the absence of severe maternal anaemia.

2.2 Introduction

Iron-deficiency (ID) is the most common nutritional deficiency worldwide[34]. ID anaemia, a condition in which circulating haemoglobin (Hb) levels are reduced, is estimated to affect 1.2 billion people globally[251]; the prevalence of latent ID, in which no overt signs of anaemia exist, is undoubtedly higher. One of the populations most at risk for ID and resultant anaemia is pregnant women, due blood volume expansion and demands from the fetal-placental unit[11,30]. Global rates of anaemia in pregnant women are estimated to be 38%[11], with 22% of pregnant women in developed nations affected[21], emphasizing the importance of iron status assessments in vulnerable groups regardless of geographical location.

ID during fetal and postnatal development is an important health concern that can have lasting effects on the offspring. ID during pregnancy and the postnatal developmental period causes altered growth trajectories, and is associated with long-term cognitive deficits[252,253], cardiovascular perturbations[170,230,231,254,255], and metabolic dysfunction[159,160,256]. Interestingly, iron supplementation and repletion of iron stores in children whose mothers had ID during pregnancy does not appear to alleviate the persistent health complications[257], suggesting adequate iron supply to the fetus throughout gestation is critical. Despite its well-described programming effects, the mechanisms by which ID during pregnancy alters fetal growth trajectories are unknown.

Hb is the molecular vehicle responsible for carrying atmospheric oxygen from the lungs to the tissues. Under normal circumstances (i.e. a non-pregnant state), the amount of oxygen delivered to tissues exceeds demands by a factor of approximately 4, with the notable exception of the heart, which extracts approximately 50% of its delivered oxygen[258]. This physiological reserve, coupled with cardiovascular compensatory mechanisms that alter blood flow and increase cardiac output, maintain adequate tissue oxygenation even in cases of severe anaemia[259]. During pregnancy, oxygen demands in the fetus are undoubtedly high, corresponding to a lower physiological reserve of oxygen delivery to tissues. In the case of anaemia during pregnancy, it is not presently clear whether adaptive increases in cardiac output and changes in blood flow[260] are capable of

mitigating hypoxia caused by decreased arterial oxygen delivery to the fetus[51,261]. Although hypoxia inducible factor-1α (HIF-1α) protein has been shown to accumulate in placentae and hearts of anemic fetuses[52,84,262], it is noteworthy that prolyl hydroxylase-activity is dependent on iron[263], and as such increased HIF-1α expression may be caused by ID *per se,* rather than hypoxia. Despite this, no other studies have explored organ-specific patterns of hypoxia in the fetuses of ID mothers.

Together, these studies provide a rationale for investigating the relationship of prenatal ID and oxygen status within the fetus during gestation. In this study, we utilized two groups of rats at different ages to induce different degrees of maternal anaemia, to assess the relationships between maternal and fetal iron status and oxygen tension; these groups are designated moderate (M-ID) and severe (S-ID) iron deficient groups on the basis of maternal iron status at the end of gestation. Using these models, we sought to determine: (1) whether maternal and fetal blood flow patterns are altered by prenatal ID using ultrasound biomicroscopy; and (2) the organ specific patterns of hypoxia in dams and fetuses.

2.3 Methods

2.3.1 Animals and Treatments

The experimental protocols described herein were approved by the University of Alberta Animal Care Committee in accordance with the guidelines established by the Canadian Council for Animal Care. Thirty-two female Sprague Dawley rats (16 at 12 weeks old, and 16 at 6 weeks old) were purchased from Charles River (Saint-Constant, Quebec, Canada) and housed in the University of Alberta Animal Care Facility. Dams had *ad libitum* access to food and water throughout the study. The animal care facility maintained a 12-hour light/dark cycle and an ambient temperature of 23°C.

Two weeks prior to mating, dams from both age groups were randomly assigned to receive either a control or an iron-restricted diet ; the two diets, based on the AIN-93G formula (Research Diets Inc.)[264], were identical in composition with the exception that control diets (D10012G) contained 35 mg/kg iron (in the form of ferric citrate), whereas

the ID diet (D15092501) had no added ferric citrate and contained only trace amounts of iron (3 mg/kg). This approach allowed us to feed dams an identical diet, but generate different degrees of ID anaemia in the dams, such that feeding the 6 week old female rats fed an iron-restricted diet generates a phenotype far more severe than that which occurs in 12 week old female rats fed the same iron-restricted diet. After two weeks on their respective diets, females were naturally bred (i.e. without synchronization of estrus) to age-matched males fed a standard iron-replete rodent chow (PicoLab 5L0D) by housing 1 male with 2 dams each night. Pregnancy was confirmed by the presence of sperm in a vaginal smear the following morning; this was considered gestational day(GD)0. Dams were housed individually starting on GD0, and food consumption, body weight, and Hb were assessed weekly. Maternal Hb levels was assessed using a HemoCue 201+ system from blood (~10 μL) collected via saphenous venipuncture.

2.3.2 Ultrasound Biomicroscopy

On GD20, ultrasound biomicroscopy was performed to assess uterine artery and fetal umbilical artery haemodynamic parameters, as previously described [265]. Rats were anaesthetized with isoflurane (5% induction, 2.5% maintenance in 100% O_2). The abdomen was shaved and pre-warmed gel was used as an ultrasound coupling medium. Rats were imaged transcutaneously using an ultrasound biomicroscope (model Vevo 2100, VisualSonics, Toronto, ON, Canada) with a 16-21 MHz MicroScan array transducer probe. A 0.2 to 0.5 mm pulsed Doppler gate was used, and the angle between the Doppler beam and the vessel was <45°. Doppler waveforms were obtained from uterine arteries near the lateral-inferior margin of the utero-cervical junction close to the iliac artery on each side, as well as from the umbilical artery from three fetuses per dam. Peak systolic velocity (PSV) and end diastolic velocity (EDV) averages were obtained from a minimum of three consecutive cardiac cycles. Both resistive index (RI=[PSV-EDV]/PSV) and pulsatility index (PI=[PSV-EDV]/time averaged velocity [TAV]) were calculated.

2.3.3 Tissue Collection and Analysis

After a minimum of 4 hours of recovery from anesthesia from ultrasound biomicroscopy assessments, rats were administered pimonidazole (60 mg/kg) by oral gavage. The next morning (GD21; term=GD22) dams were anesthetized (isoflurane, 5% induction, 3% maintenance in 100% O_2) and blood was collected from the inferior vena cava into EDTA coated tubes, and centrifuged at 1500 x g to isolate plasma. Rats were then euthanized by exsanguination and subsequent excision of the heart. Fetuses and their placentae were quickly removed, cleaned and weighed. Fetuses were decapitated and blood was collected for blood Hb assessments (HemoCue 201+ system). Fetal tissues were excised into ice-cold saline, cleaned, blotted dry and weighed; tissues were then fixed in 4% neutral-buffered formalin for 24 hours and subsequently embedded for histology as described [266]. Plasma transferrin and ferritin were assessed using kits (ab137993 and ab157732, Abcam), in duplicate for each dam, according to the manufacturer's instructions.

For hypoxyprobe analysis, embedded tissues from dams and male fetal offspring were sectioned at 6 μm. Maternal brain and kidneys were sampled from the cortical regions, whereas the entire cross-sections of fetal tissues were used (due to their small size). Following rehydration and antigen retrieval in sodium citrate buffer (10 mM sodium citrate, 0.05 % Tween-20, pH 6.0) for 20 min at 90°C, tissues were blocked using 1% bovine serum albumin in tris-buffered saline (50 mM Tris, 150 mM NaCl, 0.1% tween 20, pH 9.0). Sections were then probed with FITC-preconjugated hypoxyprobe mouse monoclonal antibodies (HP61000 Kit, Hypoxyprobe Inc.) in blocking buffer at a dilution of 1:50 (0.01 mg/mL) and incubated overnight at 4°C. After washing in tris-buffered saline, sections were mounted in DAPI-containing medium (Vectashield H-1200). Fluorescence intensities were measured using an Olympus IX81 fluorescent microscope. For each sample analyzed, mean fluorescence intensity was calculated from 6 separate fields of view. Thresholds of fluorescence images were normalized to average intensity of control group fluorescence (low threshold) and maximal fluorescence intensity of all samples (high threshold).

2.3.4 Statistical Analyses

In all cases, the n values reflect the number of litters (or dams) used, and not the number of fetuses. When multiple pups were sampled from the same litter, mean values were calculated and considered n=1; this corresponds to 1 pup per n in Hypoxyprobe data sets, and 2-6 pups for all other data sets presented. Parametric data (i.e. food intake, body weight gain, organ weights, and haemodynamic variables) were analyzed by unpaired Student's *t* test, or two-way analysis of variance with Bonferroni *post-hoc* tests; these data are presented as scatter plots with mean ±SEM. Non-parametric data (i.e. pimonidazole staining) were analyzed by Mann-Whitney *U*-test; these data are presented as bar and whisker plots showing as median, 25% and 75% quartiles, and range. Hypoxyprobe analyses were conducted in male fetal tissues, however trends were confirmed in select female tissues. All statistical analyses were conducted using Prism 5.0 (GraphPad Software, Inc.). $P<0.05$ was considered statistically significant.

2.4 Results

2.4.1 Maternal and Fetal Outcomes

Maternal iron restriction had no impact on total food consumption in M-ID and S-ID groups (M-ID: 709.4 ± 13.3g, controls: 698.1 ± 15.9 g, n=5, P=0.56; S-ID: 803.2 ±29.2 g, controls: 840.4 ± 13.1 g, n=8, P=0.19), nor did it affect maternal cumulative weight gain or litter sizes (**Figure 2.1**). Iron restriction in the M-ID group caused a 17% reduction in maternal Hb compared to controls by GD21 (**Figure 2.2A**), with no apparent changes in maternal plasma ferritin (**Figure 2.2B**) or transferrin (**Figure 2.2C**). In contrast, maternal Hb in the S-ID group was 48 % lower compared to controls (**Figure 2.2A**), plasma ferritin levels were 75 % lower than controls (**Figure 2.2B**), and transferrin levels were 25% higher than controls (**Figure 2.2C**). Fetuses in the M-ID group had Hb levels reduced by 39% compared to controls, whereas S-ID fetuses had Hb levels reduced by 65% (**Figure 2.2D**).

M-ID and S-ID resulted in 14% and 26% decreases in fetal bodyweight compared to controls, respectively (**Figure 2.3A**). M-ID caused modest changes in fetal growth trajectories with increased relative placental size (**Figure 2.3B**) and trends for increased brain (**Figure 2.3C**) and heart weight (**Figure 2.3D**), albeit no differences in liver or kidney weights were observed (**Figure 2.3E-F**). The S-ID group was characterized by more pronounced alterations in fetal organs weight at the end of gestation, including increased relative placental (**Figure 2.3B**), brain (**Figure 2.3C**), and heart weight (**Figure 2.3D**) which was accompanied by decreases in relative liver (**Figure 2.3E**) and kidney weight (**Figure 2.3F**).

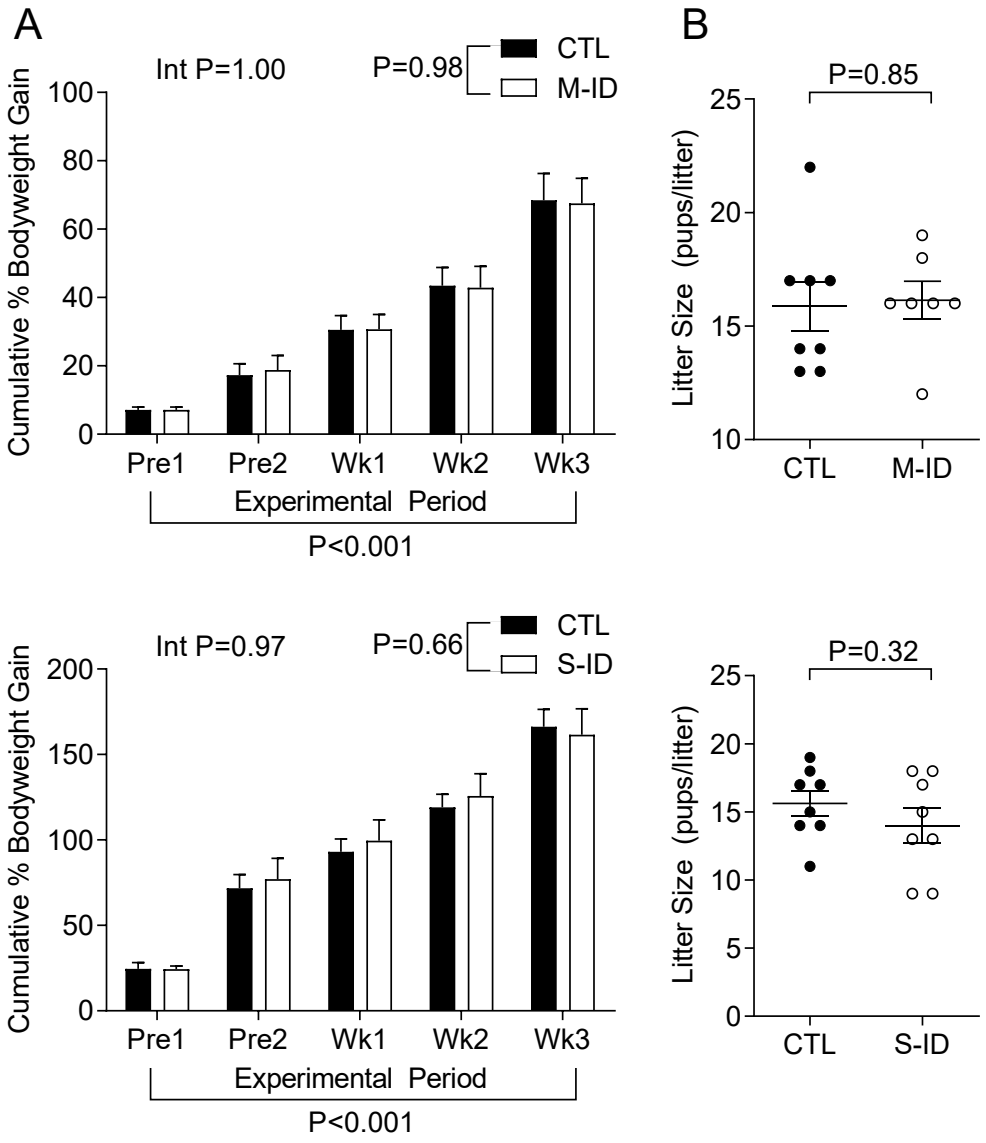

Figure 2.1: Maternal weight gain and litter outcomes. (**A**) Maternal cumulative weight gain over initial body weight and (**B**) litter sizes in moderate ID (M-ID) and severe ID (S-ID) groups. Top and bottom panels depict M-ID and S-ID data sets, respectively. Data is presented as mean ±SEM, and n=7-8. In panel A, P values reflect 2-way ANOVA outcomes; in panel B, P values reflect Student's t-test outcomes.

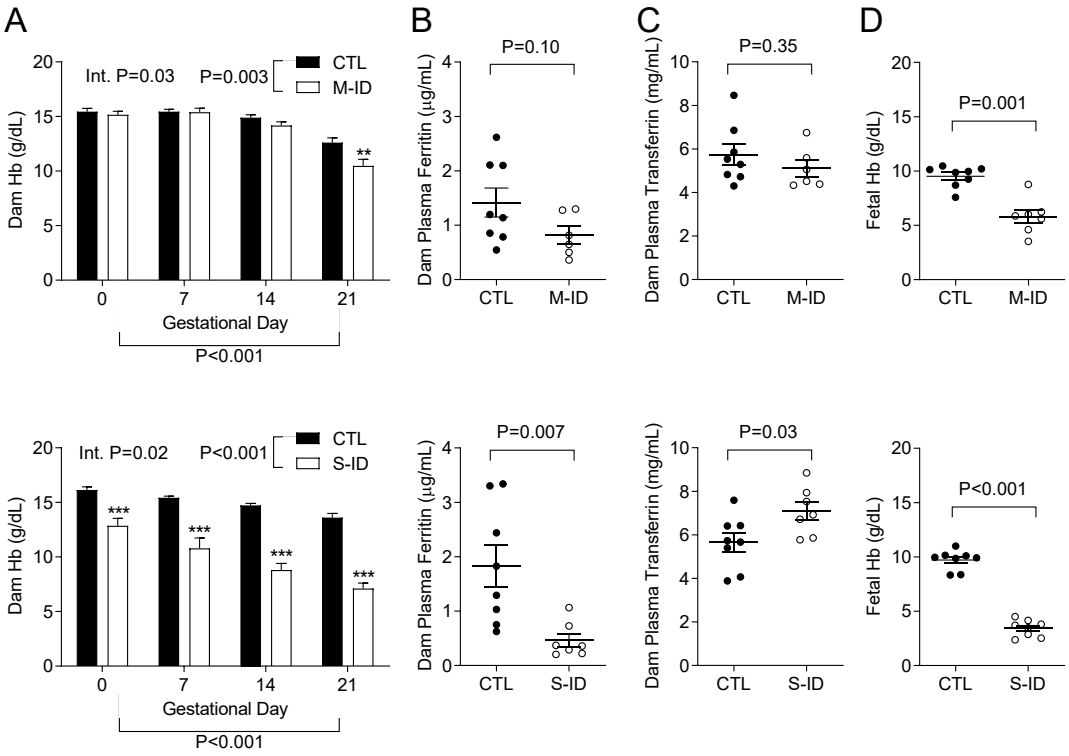

Figure 2.2: Maternal hematologic outcomes. (A) Dam Hb, (B) dam plasma ferritin on GD21, (C) dam plasma transferrin on GD21, and (D) fetal Hb on GD21 in M-ID and S-ID groups. Top and bottom panels depict M-ID and S-ID data sets, respectively. Data is presented as mean ±SEM, and n=6-8. In panel A, P values reflect 2-way ANOVA outcomes; in panels B-D, P values reflect Student's t-test outcomes.

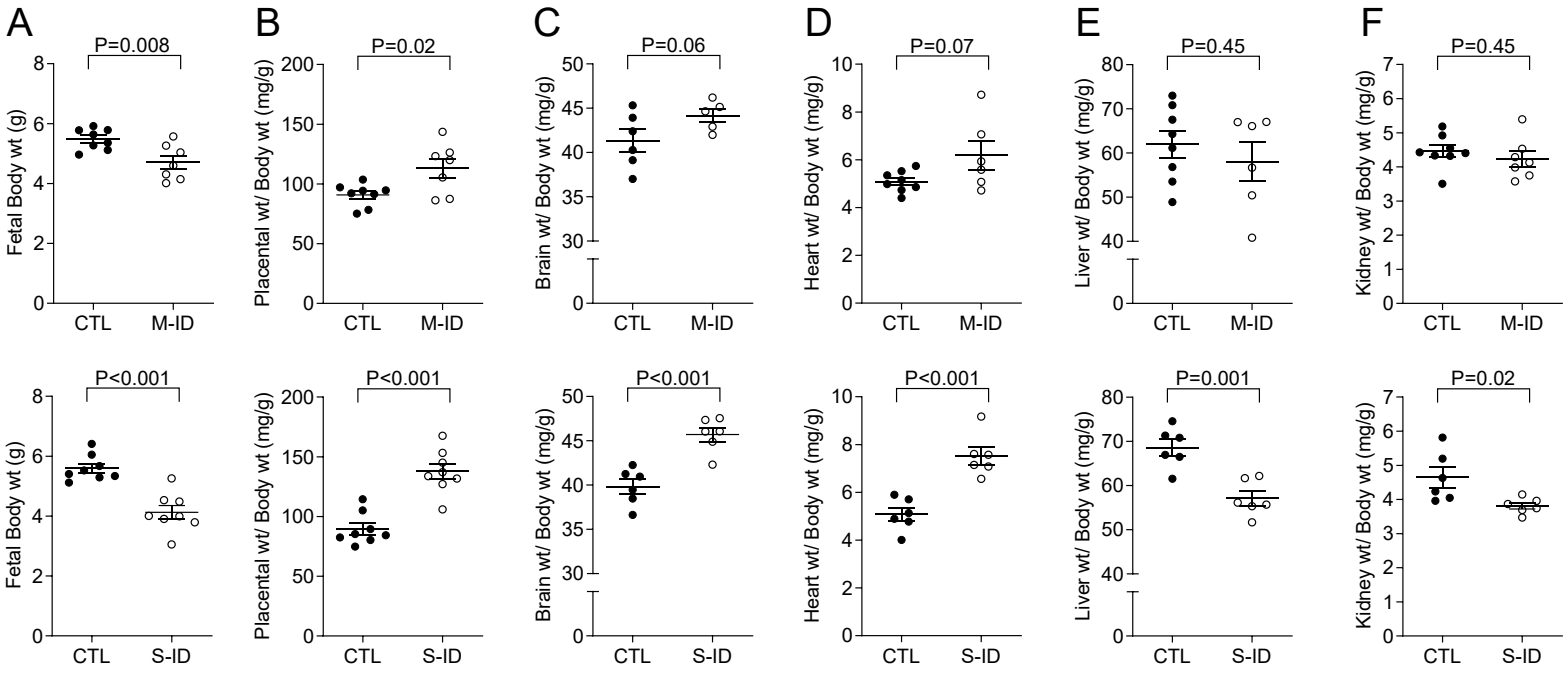

Figure 2.3: Fetal growth outcomes. (**A**) Fetal body weights, (**B**) relative placental weights, (**C**) relative brain weights, (**D**) relative heart weights, (**E**) relative liver weights, and (**F**) relative kidney weights in M-ID and S-ID groups. Top and bottom panels depict M-ID and S-ID data sets, respectively. Data is presented as mean ±SEM, and n=6-8. P values reflect Student's t-test outcomes.

2.4.2 Maternal and Fetal Haemodynamics

Neither M-ID nor S-ID dams exhibited alterations in uterine artery resistive index (0.60 ±0.04 M-ID vs. 0.62 ±0.03 controls, n=7-8, P=0.68; 0.62 ±0.04 S-ID vs. 0.63 ±0.02 controls, n=8, P=0.80) or pulsatility index (0.87 ±0.08 M-ID vs. 0.91 ±0.07 controls, n=7-8, P=0.69; 0.93 ±0.04 S-ID vs. 0.91 ±0.09 controls, n=8, P=0.88). However, fetal umbilical artery RI was increased in both groups (**Figure 2.4B**) compared to respective controls, with no change in fetal heart rates (**Figure 2.4D**). Umbilical artery PI was not changed in M-ID dams, whereas it increased in S-ID dams with respect to controls (**Figure 2.4C**). Underlying these changes, umbilical artery PSV was elevated by more than 35% in both the M- and S-ID groups with respect to controls (270.3 ±26.7 mm/s M-ID vs. 164.1 ±12.3 mm/s controls, n=7-8, P=0.002; 287.0 ±13.2 mm/s S-ID vs 216.4 ±15.3 mm/s controls, n=8, P=0.004). The S-ID group also has a trend for decreased EDV versus controls (9.9 ±1.4 mm/s S-ID vs. 13.1 ±1.0 mm/s controls, n=8, P=0.08), whereas the M-ID group did not (10.3 ±2.0 mm/s M-ID vs. 10.5 ±1.0 mm/s controls, n=7-8, P=0.96). Core body temperature, measured during ultrasound assessments, was not different between groups (35.1±0.3 ℃ M-ID vs. 35.3±0.3 ℃ controls, n=7-8, P=0.72; 35.0±0.3 ℃ S-ID vs 34.7±0.3 ℃ controls n=7-8, P=0.44).

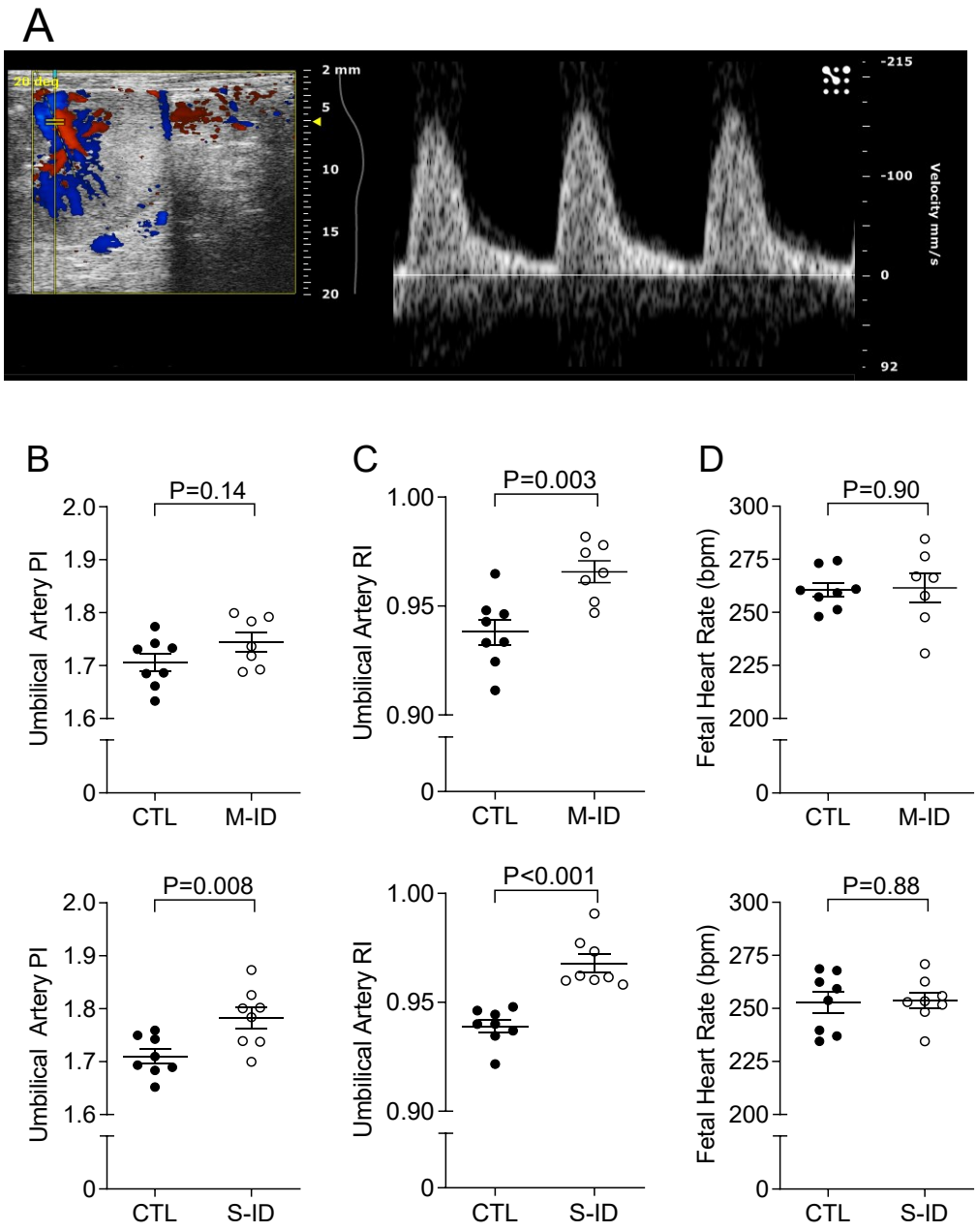

Figure 2.4: Umbilical Doppler outcomes. (**A**) Representative image of an umbilical artery Doppler from a moderate group control, (**B**) umbilical artery RI, (**C**) umbilical artery PI, and (**D**) fetal heart rate in M-ID and S-ID groups. Top and bottom panels in B-D depict M-ID and S-ID data sets, respectively. Data is presented as mean ±SEM, and n=7-8. P values reflect Student's t-test outcomes.

2.4.3 Hypoxyprobe Staining

Evidence of fetal hypoxia, as assessed by pimonidazole staining, was similar in both M-ID and S-ID groups. Pimonidazole staining was more pronounced in kidneys and livers of both M-ID and S-ID fetuses, relative to their respective controls (**Figure 2.5**). No pimonidazole staining was observed in fetal brain or in placentae of either group (**Figure 2.6**). Finally, increased levels of staining were observed in dam liver tissues in the S-ID group, which was not evident in the M-ID group (**Figure 2.7A & B**). No staining was observed in S-ID dam kidneys (**Figure 2.7C**) or brains (**Figure 2.7D**), and therefore these analyses were not performed in M-ID dams.

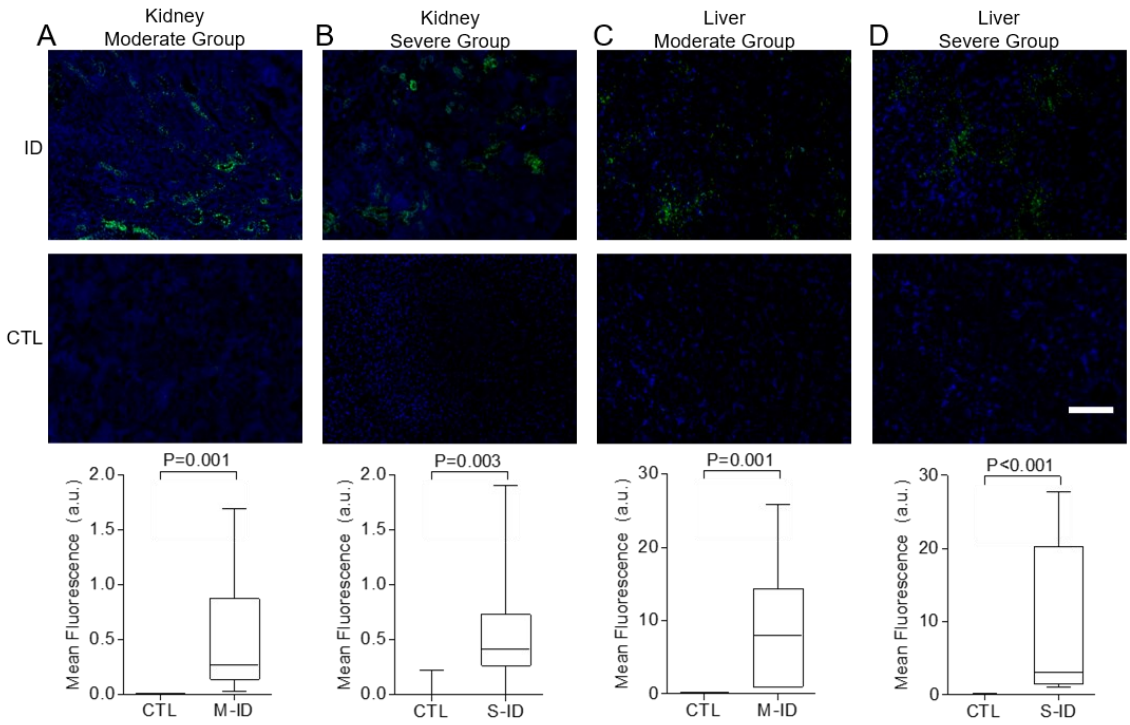

Figure 2.5: Fetal kidney and liver Hypoxyprobe staining. (**A**) moderate group kidney, (**B**) severe group kidney, (**C**) moderate group liver, and (**D**) severe group liver. Top and bottom panels depict representative staining and quantification, respectively. The white scale bar represents 75 μm of tissue. Data are presented as median, quartiles, and range. P values reflect Mann-Whitney U test outcomes, n=7-8.

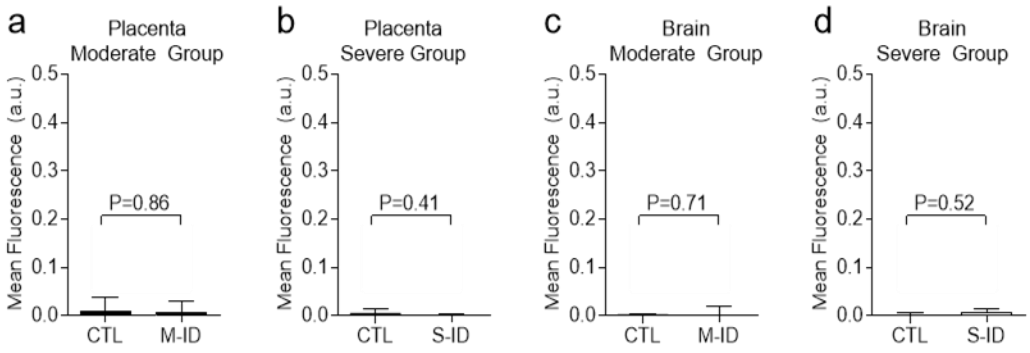

Figure 2.6: Placenta and brain Hypoxyprobe staining. (**A**) moderate group placentae, (**B**) severe group placentae, (**C**) moderate group brain, and (**D**) severe group brain. Data are presented as median, quartiles, and range. P values reflect Mann-Whitney U test outcomes, n=7-8.

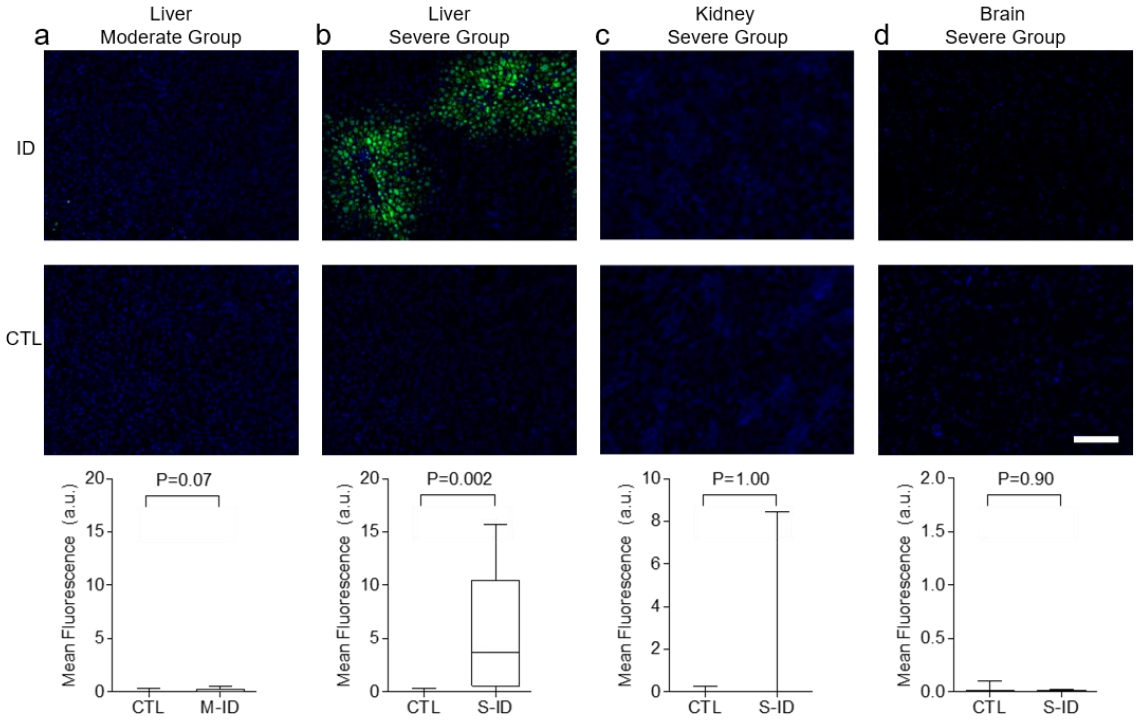

Figure 2.7: Maternal Hypoxyprobe staining. (**A**) M-ID liver, (**B**) S-ID liver, (**C**) S-ID kidney, and (**D**) S-ID brain. Top and bottom panels depict representative staining and quantification, respectively. The white scale bar represents 75 μm of tissue. Data are presented as median, quartiles, and range. P values reflect Mann-Whitney U test outcomes, n=7-8.

2.5 Discussion

In this study, we investigated the effects of maternal iron restriction during pregnancy to assess the impact on growth, iron status, and hypoxia in the developing fetus. To summarize, we report that prenatal ID caused: (1) asymmetric fetal growth restriction, which was dependent on the severity of fetal anaemia; (2) no changes in uterine artery blood flow patterns, but altered umbilical artery blood flow patterns; (3) hypoxia in fetal livers and kidneys, but not in the brain or placenta. Taken together these findings suggest that ID, which may or may not manifest as overt maternal anaemia by the end of gestation, causes fetal anaemia and tissue-specific patterns of hypoxia, which may have important implications in the programming of long-term health in the offspring.

The M-ID rat model used in this study is one in which ID develops in the dam over the course of gestation, and only begins to show signs of anaemia at the end of pregnancy. In contrast, reductions in maternal Hb are observed throughout gestation in the S-ID group, which caused more pronounced fetal growth asymmetry. The M-ID group is intended to mimic a common clinical scenario in which the increased demands of pregnancy coupled with insufficient iron intake or poor gastrointestinal absorption[267,268] causes the gradual depletion of iron stores, which can proceed without clinical manifestations until the end of gestation. As blood volume expansion continues and iron demands from the fetal-placental unit increase throughout gestation, reduced maternal Hb levels become apparent. The M-ID group models this clinical scenario well, as maternal Hb levels reside within the range considered normal in non-pregnant women (12-16 g/dL[39]), and only reach a modest degree of anaemia in the last week of gestation (<11 g/dL[33]). In the M-ID dams, we observed no changes in plasma ferritin or transferrin levels, which is in contrast to the S-ID model, further demonstrating that this treatment regimen produces a modest insult more likely to be overlooked in the clinical setting. Whereas the S-ID fetuses exhibited severe growth restriction and marked changes in organ grown patterns, the M-ID fetuses group exhibited lesser growth restriction, and no marked alterations in certain organ weights. However, we did observe subtle alterations

in brain and heart weights (relative to body weight; Figure 3), which likely reflects cardiovascular adaptations contributing to a brain-sparing effect (see below), suggesting this moderate anaemia does in fact cause iron depletion in the developing fetus by the end of pregnancy. Moreover, Mihaila *et al.* reported differences in embryo iron content as early as embryonic day 15 using a rat model of iron deficiency of similar severity as the M-ID group used herein[269], suggesting that the fetus is exposed to a prolonged period of stress in the absence of maternal anaemia.

As noted above, ID *per se* can upregulate endogenous markers generally associated with hypoxia, such as HIF-1α[92,263] and can therefore confound hypoxia assessments. The present study therefore relies on the suitability of exogenous pimonidazole as a more accurate marker of hypoxia. In non-ID contexts, pimonidazole staining correlates well with HIF-1α and other endogenous markers of hypoxia[270,271], suggesting it is well-suited to detect physiologically relevant degrees of hypoxia (~10 mmHg)[271,272].

The majority of oxygen transported in the blood is bound to Hb, and consequently anaemia has a direct and profound impact on oxygen carrying capacity[51,273]. S-ID dams, unlike M-ID dams, exhibited signs of liver hypoxia at the end of pregnancy, indicating compromised oxygen transport and an inability to fully compensate via increases in blood flow. In the case of S-ID fetuses, concomitant reductions in both maternal and fetal Hb predictably resulted in hypoxia in certain tissues (e.g. kidneys, liver) but not in others (i.e. brain). Although blood gas parameters were not assessed in the present study owing to technical limitations, Darby *et al.* previously showed in an ovine model that a similar degree of fetal anaemia as seen in the present study causes reduced fetal blood O_2 content, with changes in fetal blood pH and pCO_2[261]. These hypoxia patterns are consistent with altered organ growth patterns, which may be indicative of fetal cardiovascular compensatory mechanisms. Indeed, coronary and cerebral blood flow in ovine fetuses tend to increase disproportionally in chronic anaemia[274] suggesting a redistribution of blood flow towards the brain and heart at the expense of other organs (e.g. liver and kidney). Bastian *et al.* also reported increased blood vessel branching and

elevated expression of angiogenic and vasculogenic genes in various brain regions[275], suggesting other compensatory mechanisms are involved in the mitigating the hypoxia induced by anaemia.

Interestingly, in contrast with previous reports in ovine models of fetal anaemia[260,273], no compensatory increases in fetal heart rate were observed in either the M or S-ID group. Although this could be attributed to the use of isoflurane anesthesia (the studies by Mostello *et al.* and Davis *et al.* were done in non-anesthetized sheep), it is noteworthy that anaemia-induced increases in cardiac output are thought to stem largely from decreases in blood viscosity (resulting primarily in reduced afterload) and increased contractility[260] rather than autonomic nervous system-driven changes in cardiac function[276]. In this regard, it is not surprising that fetal heart rates were not affected. However, whether fetal cardiac responses to anaemia differ from adults, and whether there are developmental differences between rats and sheep in heart rate regulation[273,277] may provide some insights into the mechanisms of fetal cardiovascular compensation to anaemia.

The marked increase in placental size in both the M-ID and S-ID groups suggest that the placenta is sensitive to oxygen (or iron) deficiencies, despite no increases in blood flow with anaemia[260,274]. Although the consequences of this excessive placental growth are not clear, this may reflect a compensatory mechanism to increase oxygen and nutrient exchange and therefore offset the reduced oxygen delivery caused by lower maternal and fetal Hb levels and mitigate a hypoxic insult to the fetus. However, Lewis *et al.* reported that prenatal ID is associated with reduced vascularity and capillary volume in the placenta[278], and the authors speculate that the alterations in placental morphology (and possibly abnormal vascular structure/function) may be a cause of altered fetal growth trajectories in this model. As such, increased umbilical artery resistive index in both M-ID and S-ID groups may reflect an abnormal placental vascular development, and may be a cause of altered fetal growth trajectories, rather than a beneficial adaptive mechanism. Moreover, our results showing that S-ID, but not M-ID, contributes to an elevated PI may indicate of a greater level of pathology with increasing severity of ID.

Our study implicates fetal hypoxia as a possible mechanism that contributes to the programming of chronic diseases in later life. We have previously shown that perinatal ID can induce long-term health complications, ranging from cardiovascular perturbations[170], to increased propensity for obesity and metabolic dysfunction[159,160], to cognitive deficits[253]. These effects are said to be 'programmed' because the phenotypic and functional consequences persist long after the stressor is removed. The observation that fetal kidneys become hypoxic may be a contributing factor to the cardiovascular dysfunction seen in adult PID offspring, which is characterized by reduced nephron endowment[215], hypertension[230,231,254], and alterations in the intrarenal haemodynamics associated with salt sensitivity[170]. Consistent with this hypothesis, prenatal hypoxia has also been shown to cause reduced nephron endowment in rats[163], and result in hypertension in adult offspring[239] .

Although prenatal hypoxia has been shown to induce similar programming effects on cardiovascular and metabolic function as prenatal ID, the precise role of hypoxia *per se* in our M-ID and S-ID models requires further investigation. Persistent neurological deficits, including long-term changes in neurotransmitter function, cognition and behaviour[279,280] are well described in models of perinatal ID anaemia, yet no evidence of brain hypoxia was observed in the present study. Thus alternative mechanisms (e.g. changes in functional iron levels, alterations in inflammatory and oxidant status, perturbations in energy metabolism[67,84,281,282]) may also be implicated in the pathophysiology of prenatal ID. Given the intimate relationships between iron, oxygen transport, energy, and inflammation, it is likely that the multiple mechanisms are involved. Moreover, we cannot discount the possibility that the compensatory mechanisms that mitigate the development of hypoxia are implicated in the programming of altered nervous system function. For example, hypoxia-induced increases in cerebral blood flow can result in blood brain barrier leakiness that accompanies accelerated vasculogenesis/angiogenesis[283]. In prenatal ID fetal rats, vasculogenic and angiogenic mediators implicated in this process are shown to be upregulated[275], potentially

implicated compromised integrity of the fetal blood brain barrier— a condition associated with a numerous of brain pathophysiologies[284].

In summary, we have demonstrated that ID results in an organ-specific pattern of fetal hypoxia, and this can even occur in the absence of marked changes in maternal iron status. While it is well-established that prenatal ID is linked to long-term health outcomes, our results suggest the mechanisms underlying the programming of cardiovascular, metabolic, and neurological function in the offspring may be different based on the heterogeneous patterns of hypoxia within the fetus. Indeed, longstanding assumptions regarding the patterns of organ injury/dysfunction in the context of prenatal ID may be incorrect in the case of the fetal brain, in which no evidence of hypoxia observed, but may be warranted in the case of other organs (e.g. liver and kidney). Although we recognize that there are inherent limitations to the applicability of these results to human pregnancies, our findings nevertheless emphasize the potential pitfalls of relying exclusively on maternal iron status as a predictor of fetal pathology, given that maternal anaemia can occur at the end of gestation, or may not appear at all. Consequently, alternative diagnostic markers of fetal ID and anaemia are needed so interventions can be instituted before these fetal complications alter developmental trajectories and cause long-term health consequences in the offspring.

Acknowledgements

The authors are indebted to the Cardiovascular Research Centre at the University of Alberta for the use of the confocal microscope.

Author Contributions

SLB conceived and designed the experiments. AGW, ASC, YM, SJC, and SP collected data, and all authors analyzed data. AGW and SLB wrote the manuscript. FSG and SLB provided financial support. All authors approve of the final manuscript.

Competing Interests

No conflicts, financial or otherwise, to declare.

Funding

This work is funded by a Women and Children's Health Research Institute (WCHRI) Innovation Grant and an operating grant from the Canadian Institutes of Health Research (CIHR; MOP14239). AGW is supported by studentships from Alberta Innovates Health Solutions (AIHS) and CIHR. ASC is supported by fellowships from National Health and Medical Research Council of Australia, AIHS, and the Heart and Stroke Foundation of Canada. SJC is supported by a WCHRI studentship. SLB is supported by a CIHR New Investigator Salary Award.

Chapter 3

Prenatal Iron-Deficiency Causes Sex-Dependent Mitochondrial Dysfunction and Oxidative Stress in Fetal Rat Kidneys and Liver

[1]Andrew G. Woodman, [2]Richard Mah, [2]Danae Keddie, [2]Ronan MN Noble, [2]Sareh Panahi, [2]Ferrante S. Gragasin, [3]Hélène Lemieux, [1,2]Stephane L Bourque

[1]Department of Pharmacology, University of Alberta

[2]Department of Anesthesiology & Pain Medicine, University of Alberta

[3]Faculty Saint-Jean, University of Alberta

PUBLISHED:

Woodman *et al. FASEB Journal* 2018. 32(6):3254-3263

3.1 Abstract

Prenatal iron-deficiency alters fetal developmental trajectories, resulting in persistent changes in organ function. Here we studied the effects of prenatal iron-deficiency on fetal kidney and liver mitochondrial function. Pregnant Sprague Dawley rats were fed partially or fully iron-restricted diets to induce a state of moderate or severe iron-deficiency alongside iron-replete controls. We assessed mitochondrial function *via* high-resolution respirometry and reactive oxygen species generation *via* fluorescence microscopy on gestational day 21. Hemoglobin levels were reduced in dams in the moderate moderate (-31%) and severe groups (-54%) compared with controls, which was accompanied by 55% reductions in fetal hemoglobin in both moderate and severe groups versus controls. Male iron-deficient kidneys exhibited globally reduced mitochondrial content and respiration, as well as increased cytosolic superoxide and decreased nitric oxide. Female iron-deficient kidneys exhibit complex II downregulation and increased mitochondrial oxidative stress. Male iron-deficient livers exhibit reduced complex IV respiration and increased cytosolic superoxide, whereas female liver tissues exhibit no alterations in oxidant levels or mitochondrial function. These findings indicate prenatal iron deficiency causes changes in mitochondrial content and function as well as oxidant status in a sex and organ-dependent manner, which may be an important mechanism underlying the programming of cardiovascular disease.

3.2 Introduction

Iron deficiency (ID) occurs when iron demands chronically exceed intake and stores. A negative iron balance can progress to anemia, its most severe form, when circulating hemoglobin (Hb) levels fall below clinical thresholds[39]. ID is the most common nutritional deficiency worldwide[33], and pregnant women are most at risk due to increased iron demands stemming from maternal blood volume expansion and growth of the fetal placental unit that exceed reduced losses [39]. Despite widespread iron supplementation efforts, ID remains a global health burden, with 38% of women worldwide developing ID anemia at some point in pregnancy[21]. Even in higher-income countries, ID anemia during pregnancy affects 1 in 5 women[21].

ID during pregnancy has important health implications for the growing fetus. In addition to increasing the risk of perinatal mortality, ID has been shown to affect fetal developmental trajectories, resulting in neurocognitive[253,280], metabolic[159,160] and cardiovascular[170,215,254] consequences which persist long after iron repletion[11]. The long-term cardiovascular perturbations include hypertension[170,215,254], and alterations in kidney structure and function[170,215]. Although the long-term effects of prenatal ID are known, the mechanisms underlying these changes remain poorly understood. Interestingly, sex differences have been reported with respect to the programming of renal function and co-morbid illness, such that males are at a higher risk of developing kidney dysfunction than females[285,286]. As such, prenatal ID may affect male and female kidney development differently[215].

Prenatal ID has been shown to impair oxygen delivery to the fetus, resulting in tissue-specific patterns of hypoxia[164]. As iron is critical for oxygen transport and is a component of numerous hemoproteins and metalloproteins containing iron-sulfur clusters, including those within the electron transport chain, ID can impact mitochondrial function[287]. Studies in adult rats indicate tissues types respond differently to ID; for instance, skeletal muscle mitochondrial function is markedly disrupted by ID, whereas liver mitochondrial function is relatively spared[288]. In this regard, the relative

susceptibility to mitochondrial dysfunction may provide insights as to why certain developing organs are more prone to long-term dysfunction than others.

On the basis of these studies, we sought to investigate whether prenatal ID results in organ- and sex-specific patterns of mitochondrial dysfunction and oxidative stress. Using high-resolution respirometry, we assessed mitochondrial function in fetal kidneys and livers—organs prone to hypoxia secondary to fetal ID—in models of moderate and severe maternal iron restriction.

3.3 Methods

All reagents described herein were purchased from Sigma-Aldrich (St. Louis, MO, USA) unless otherwise stated.

3.3.1 Animals and Treatments

The protocols described here were approved by the University of Alberta Animal Care Committee in accordance with the guidelines established by the Canadian Council for Animal Care. Twenty-five female Sprague Dawley rats (6wk of age) were purchased from Charles River (Saint-Constant, QC, Canada) and housed at the University of Alberta. The animal care facility maintained a 12h light/dark cycle and an ambient temperature of 23ºC. Dams had *ad libitum* access to food and water throughout the study.

All purified diets used in this study are based on the AIN-93G formula (Research Diets Inc., New Brunswick, NJ, USA), which contained varying amounts of iron in the form of ferric citrate. Two weeks prior to mating, 8 dams were randomly assigned to a control diet group (37mg/kg iron diet, D10012G), and 17 dams to the iron-restricted diet group (3mg/kg iron diet, D03072501). After two weeks on their respective diets, females were bred to age-matched males fed a standard rodent chow (5L0D; PicoLab, St. Louis, MO, USA). Pregnancy was confirmed by the presence of sperm in a vaginal smear the following morning (GD0), and dams were singly housed thereafter. Dams in the control group were maintained on the same control diet throughout pregnancy (n=8); dams fed the iron-restricted diet prior to pregnancy were further divided into the M-ID group, fed a diet containing 10mg/kg iron (D15092501; n=8), or the S-ID group, continuing on the

3mg/kg iron diet (n=9). Throughout pregnancy, food consumption, body weight, and Hb were assessed weekly. Maternal Hb levels were assessed using a HemoCue 201+ system (HemoCue, Angelholm, Sweden) from blood (~10uL) collected via saphenous venipuncture.

On GD21 (term=GD22), dams were anesthetized with isoflurane (5% induction, 3% maintenance in pure O_2), and then euthanized by exsanguination and subsequent excision of the heart. Fetuses and their placentae were removed, weighed, and euthanized by decapitation. Sex of fetuses was determined by anogenital distance, which was confirmed by at least two researchers. A core blood sample was used to assess fetal Hb levels, and organs were collected and weighed; tissues used for mitochondrial function experiments were processed immediately without freezing. Tissues collected for Western blotting were frozen in liquid nitrogen, whereas those used for fluorescence microscopy were embedded in Tissue-Tek optimal cutting media (Sakura, Torrance CA) and then frozen in liquid nitrogen; all frozen tissues were stored at -80°C until processing.

3.3.2 High-Resolution Respirometry

Respirometry measurements were performed using the Oroboros system (Oxygraph-2k, Innsbruck, Austria). Tissues from one male and female pup from each litter (~20mg of kidney or ~40mg of liver) were gently homogenized in 2mL of MiR05 buffer (110mM sucrose, 60mM K-lactobionate, 0.5mM EGTA, 1g/L bovine serum albumin (fatty acid free), 3 mM $MgCl_2$, 20mM taurine, 10mM KH_2PO_4, and 20mM K-N-2-hydroxyethylpiperazine-N_2-ethanesulphonate, pH 7.1) and 150µL of homogenate was added to each chamber. The remaining homogenate was frozen at -80ºC for measurement of citrate synthase (CS) activity (see mitochondrial content). The mitochondrial titration protocol used allowed for evaluation of mitochondrial function at three different respiratory states[289]: 1) LEAK is the respiration in the presence of substrate but in the absence of ADP; 2) Oxidative phosphorylation (OXPHOS) is coupled oxidative phosphorylation with saturating ADP; and 3) Electron transport system (ETS) capacity is

the noncoupled state of maximum oxygen flux after titration up to an optimal uncoupler concentration.

OXPHOS (coupled, with saturating ADP) and ETS capacities were measured in the presence of substrates feeding electron in different pathways or steps: NADH-linked substrates (N-pathway; pyruvate and malate, feeding electrons into complex I), NADH & succinate-linked substrates (NS-pathway; pyruvate, malate, and succinate, feeding electrons into complexes I and II simultaneously), succinate and rotenone (S-pathway, feeding electrons into complex II), and complex IV substrates (ascorbate and tetramethyl-p-phenylenediamine [TMPD]). The single titration protocol included sequential addition of the following substrates, uncoupler, and inhibitors (final concentration): pyruvate (5mM) and malate (5mM), ADP (2.5mM), cytochrome *c* (10µM), dinitrophenol (10µM steps, up to 30µM), rotenone (0.5µM), antimycin A (2.5µM), ascorbate (0.5mM) and TMPD (2mM), and sodium azide (15mM). Mitochondrial respiration was corrected for oxygen flux due to instrumental background noise and residual oxygen consumption after inhibition of complexes I and III with rotenone and antimycin A, respectively. For complex IV respiration (ascorbate and TMPD), the chemical background measured in the presence of sodium azide was substracted. Flux control ratio (FCR) was normalized for maximal ETS capacity with substrates feeding electrons into NADH and succinate pathways (complexes I and II) simultaneously.

3.3.3 Mitochondrial Content

CS activity was measured at 37˚C using a UV/Vis spectrophotometer (Ultrospec 2100 pro; Biochrom, Cambridge, USA) equipped with a heated cell holder and a circulating water bath[290]. After thawing the tissue homogenates, an additional cycle of homogenization with a conical glass homogenizer was performed on ice for 10 sec. to ensure complete homogeneity of the sample. The absorbance was measured for 5 min at 412 nm following the reduction of 0.1mM 5,5’ dithiobis-2-nitrobenzoic acid (DTNB, ε: 13.6 mL/cm.µmol) in the presence of 0.25% triton X-100, 0.5mM oxaloacetatic acid,

0.31mM acetyl-coenzyme A, 100mM Tris-HCl and triethanolamine-HCl buffer, pH 8.0[290].

3.3.4 Fluorescence microscopy

Tissues from one male and female pup from each litter were sectioned (8µm thickness) by cryostat at -20ºC onto SuperFrost Plus microscope slides and then stored at -80ºC. Dihydroethidium (DHE; ThermoFisher Scientific, Waltham, MA, USA) was used to assess cytosolic superoxide anion levels; DAF-FM Diacetate (4-Amino-5-Methylamino-2`,7`-Difluorofluorescein Diacetate; ThermoFisher Scientific) was used to assess nitric oxide (NO) levels; and MitoSOX Red (ThermoFisher Scientific) was used to assess mitochondrial superoxide levels. Sections were thawed, washed three times with Hank's balanced salt solution (HBSS), and warmed to 37ºC in a humidified chamber for 10 minutes. Slides were then washed and incubated with either DHE (20µM, 30min), DAF-FM (20µM, 30min), or MitoSOX (5µM, 10min). Following incubation, slides were washed 3 times with HBSS and mounted in either HBSS (for DHE) or Vectashield Antifade Mounting Medium with DAPI (Vector Laboratories) to provide a nuclear counterstain (for DAF-FM and MitoSOX). Fluorescence was visualized on an Olympus IX81 fluorescent microscope.

3.3.5 Western Blotting

Livers and kidneys from one male and female pup from each litter were homogenized in lysis buffer at 0.1mg tissue per mL (20mM Tris pH 7.4, 5mM EDTA, 10mM $Na_4P_2O_7$, 100mM NaF, 1% NP-40) containing sodium orthovanadate (2mM), phosphatase inhibitor (20µg/mL, Calbio catalogue #524628) and protease inhibitor (10µL/mL, Sigma Aldrich catalogue #P8340). Total protein concentration of the lysate was determined by BCA assay (Pierce, Rockford IL, USA). Total protein (100µg/well) was separated on 12% SDS-polyacrylamide gels (with a 3.5% stacking gel) and transferred onto a nitrocellulose membrane. Membranes were incubated with 100% blocking reagent (Odyssey PBS blocking buffer, Li-Cor Biosciences) for 1 hour at room temperature. After washing with PBS solution, membranes were incubated overnight at

4ºC in 5% blocking buffer and 0.05% tween PBS with primary antibodies for AMPK (1µg/mL, Abcam ab3759), p-AMPK (56ng/mL, ThermoFisher PA5-35573), PGC1α (0.75µg/mL, Abcam ab54481), SIRT1 (0.2µg/mL, Santa Cruz sc-15404), SIRT3 (1.31µg/mL, Abcam ab189860), β-actin (0.5µg IgG/mL, Abcam ab6276), and COX IV (0.5µg/mL, Abcam ab16056). Donkey anbti-rabbit IgG H&L (Alexa Fluor 680; Abcam ab175772) and donkey anti-mouse IgG H&L (Alexa Fluor 790; Abcam ab175782) secondary antibodies (both 0.2µg/mL) were incubated with 25% blocking buffer in 0.05% tween PBS for one hour at room temperature, and blots were visualized with an Odyssey near-infrared fluorescence Imager and quantified by densitometry with Odyssey V3.0 software (Li-Cor Biosciences).

3.3.6 Statistical Analyses

All statistical analyses were performed on GraphPad (La Jolla, CA, USA) Prism 7.0 software. An alpha value of 0.05 was used for the threshold for significance.

3.4 Results

3.4.1 Pregnancy Outcomes

Two-week pre-treatment with a fully iron-depleted diet resulted in a reduction in maternal hemoglobin (Hb) at gestational day (GD)0 (**Figure 3.1A**). Continued treatment with the moderate and severe iron-restricted diets resulted in a differential degree of anemia, which was evident by GD14, and culminated in 31% and 54% reductions in maternal Hb by GD21 in moderate-ID (M-ID) and severe-ID (S-ID), respectively. While both M-ID and S-ID fetuses exhibited an approximate 55% decrease in Hb compared to controls (CTL) (**Figure 3.1B**), these treatments resulted in 22% and 33% reductions in fetal bodyweight, respectively (**Table 3.1**). M-ID and S-ID fetuses displayed asymmetric growth restriction, characterized by increased relative placental, brain, and heart weights, with reduced kidney and liver weights (**Table 1**). In accordance with these results, S-ID dams had more resorptions than controls and exhibited reduced litter sizes with respect to

the CTL and M-ID groups **(Table 3.2**). As expected, on the basis of these results, S-ID dams had reduced food intake compared to their M-ID and CTL counterparts (**Table 3.2**).

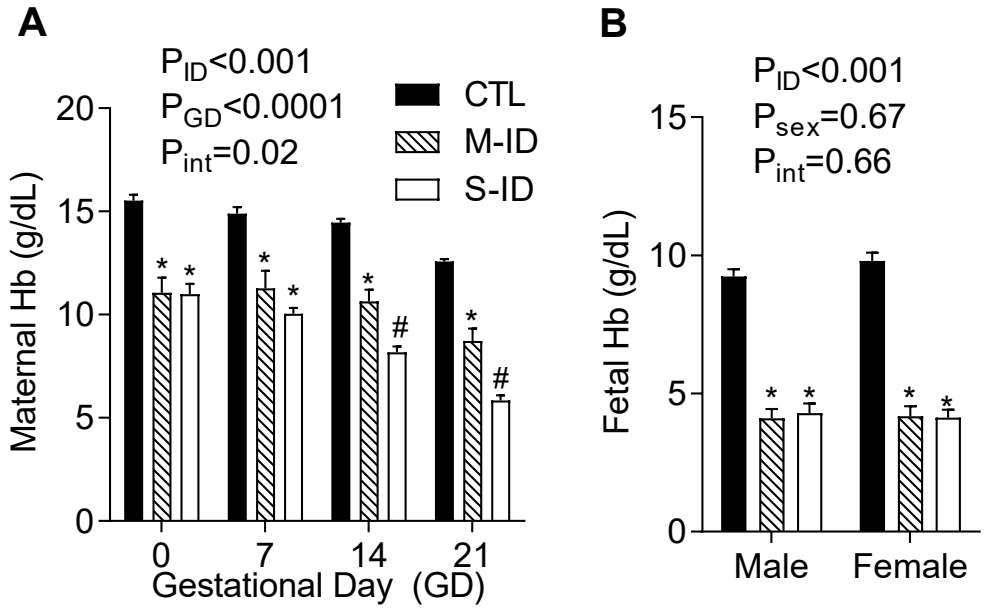

Figure 3.1: Maternal and fetal hemoglobin. (**A**) Maternal and (**B**) fetal hemoglobin (Hb) in control (CTL), moderate iron-deficient (M-ID), and severe iron-deficient (S-ID) groups. Data were analyzed by two-way ANOVA and Tukey's *post hoc* tests, where * denotes P<0.05 vs. CTL and # denotes P<0.05 vs. M-ID. Error bars indicate SEM. N=7-8 litters per group.

Table 3.1. Fetal growth parameters.

Parameter	Sex	CTL (n=7)	M-ID (n=8)	S-ID (n=8)	P Value		
					Sex	ID	Int.
Body Weight (g)	M	5.76 ± 0.22^{a}	4.73 ± 0.18^{b}	3.85 ± 0.19^{c}	0.11	<0.001	0.91
	F	5.60 ± 0.20^{a}	4.44 ± 0.20^{b}	3.55 ± 0.15^{c}			
Relative Placental Weight. (mg/g)	M	84.0 ± 3.5^{a}	126.7 ± 4.4^{b}	131.3 ± 7.8^{b}	0.22	<0.001	0.81
	F	88.3 ± 6.2^{a}	131.4 ± 8.3^{b}	143.4 ± 7.9^{b}			
Relative Brain Weight (mg/g)	M	36.2 ± 1.0^{a}	38.1 ± 1.1^{a}	40.9 ± 1.7^{a}	0.18	0.002	0.73
	F	36.8 ± 0.8^{a}	39.5 ± 2.0^{a}	43.9 ± 1.5^{b}			
Relative Liver Weight (mg/g)	M	60.8 ± 4.0^{a}	53.2 ± 2.4^{a}	47.4 ± 4.3^{a}	0.16	0.02	0.86
	F	63.3 ± 5.7^{a}	60.2 ± 4.0^{a}	52.2 ± 4.0^{a}			
Relative Heart Weight (mg/g)	M	5.4 ± 0.1^{a}	6.3 ± 0.3^{a}	7.1 ± 0.5^{b}	0.03	<0.001	0.68
	F	5.8 ± 0.2^{a}	7.3 ± 0.5^{b}	7.7 ± 0.4^{b}			
Relative Kidney Weight (mg/g)	M	8.4 ± 0.3^{a}	8.0 ± 0.3^{a}	7.3 ± 0.5^{a}	0.89	0.04	0.77
	F	8.8 ± 0.5^{a}	7.7 ± 0.3^{a}	7.5 ± 0.6^{a}			

Data are presented as mean ± SEM. P values denote two-way ANOVA outcomes and different superscript letters denote $P<0.05$ by Tukey *post-hoc* test. Control, CTL; moderate iron-deficient, M-ID; severe iron-deficient, S-ID; male, M; female, F; interaction, int.

Table 3.2. Pregnancy outcomes.

Parameter		CTL (n=7)	M-ID (n=8)	S-ID (n=8)	P Value
Maternal Body Weight (g)	GD0	313.3 ± 7.9[a]	274.2 ± 15.3[a]	296.7 ± 12.2[a]	<0.001
	GD7	363.2 ± 10.4[a]	319.4 ± 15.6[a]	342.6 ± 11.4[a]	
	GD14	423.8 ± 10.5[a]	380.7 ± 13.5[a]	391.7 ± 11.1[a]	
	GD21	532.7 ± 12.1[a]	468.2 ± 16.2[b]	448.3 ± 12.6[b]	
Total Food Intake (g)		564.3 ± 21.2[a]	519.1 ± 13.0[a]	493.5 ± 15.9[b]	0.02
Litter Size (No.)		16.0 ± 0.9[a]	14.0 ± 1.0[a]	8.7 ± 1.3[b]	0.01
Resorptions (No.)		0.0 ± 0.0[a]	0.6 ± 0.3[a]	6.8 ± 1.2[b]	0.007

Data are presented as mean ± SEM, where P value represents the outcome of the overall treatment effect as indicated by ANOVA. Superscript letters indicate whether column means are significantly different by Tukey *post-hoc* test. Control, CTL; moderate iron-deficient, M-ID; severe iron-deficient, S-ID; gestational day, GD.

3.4.2 Mitochondrial Content and Function

Citrate synthase (CS) activity was used as a marker of mitochondrial content. In kidney homogenates, CS activity was associated with fetal Hb in males (P=0.009), but not females (P=0.26; **Figure 3.2A**). In contrast, in liver homogenates, there was no change in CS activity associated with prenatal ID in either male or female fetuses (**Figure 3.2B**).

Mitochondrial function data are expressed as flux per unit tissue mass or as FCR (see methods). The FCR is indicative of qualitative changes in mitochondrial respiratory control, independent of mitochondrial density[289,291]. LEAK respiration is the oxygen flux compensating mainly for proton leak, and not available for performing biochemical work[289,292] -- it is used as an indicator of coupling in the oxidative phosphorylation (OXPHOS) process. LEAK respiration was measured in the presence of NADH-linked substrates-- pyruvate and malate-- and did not vary as a function of fetal Hb in either the kidney or liver tissues (**Figures 3.3 and 3.4**).

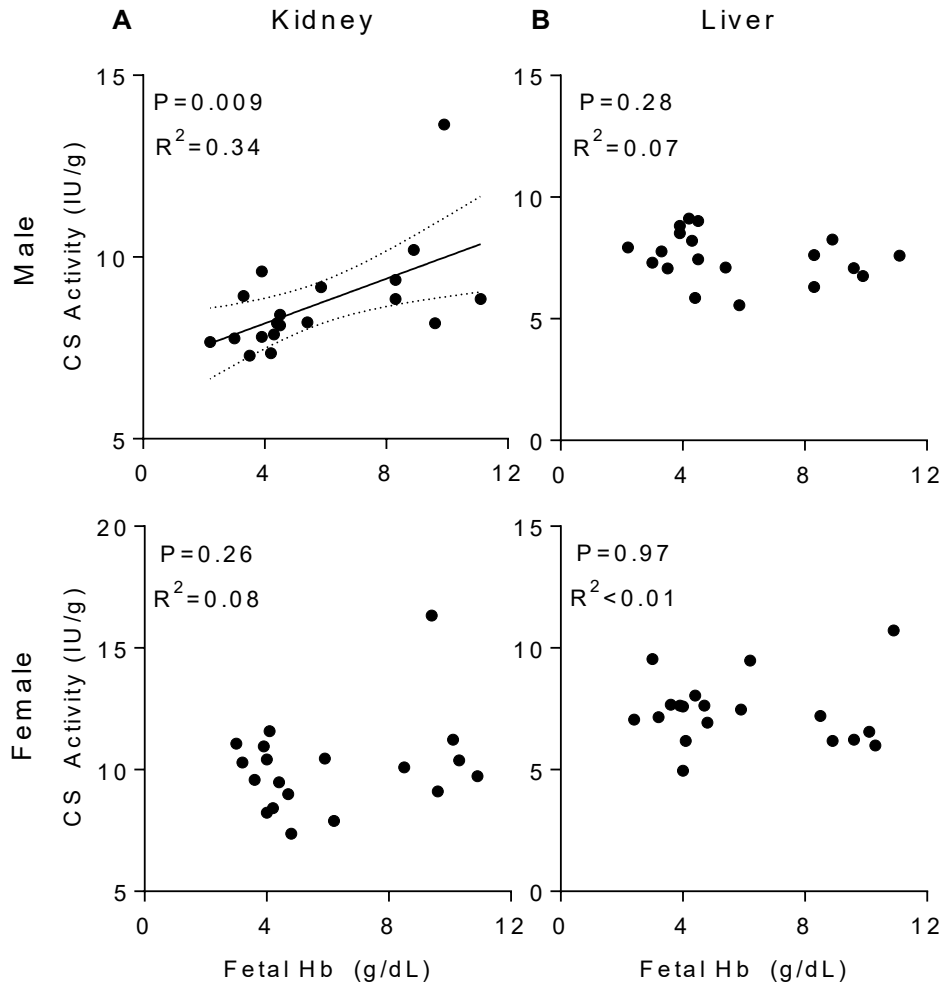

Figure 3.2: Citrate synthase (CS) activities. (**A**) fetal kidney and (**B**) fetal liver homogenates versus hemoglobin (Hb) levels from the same fetus. Linear regression with 95% confidence intervals are shown where significant. Each point represents a separate litter.

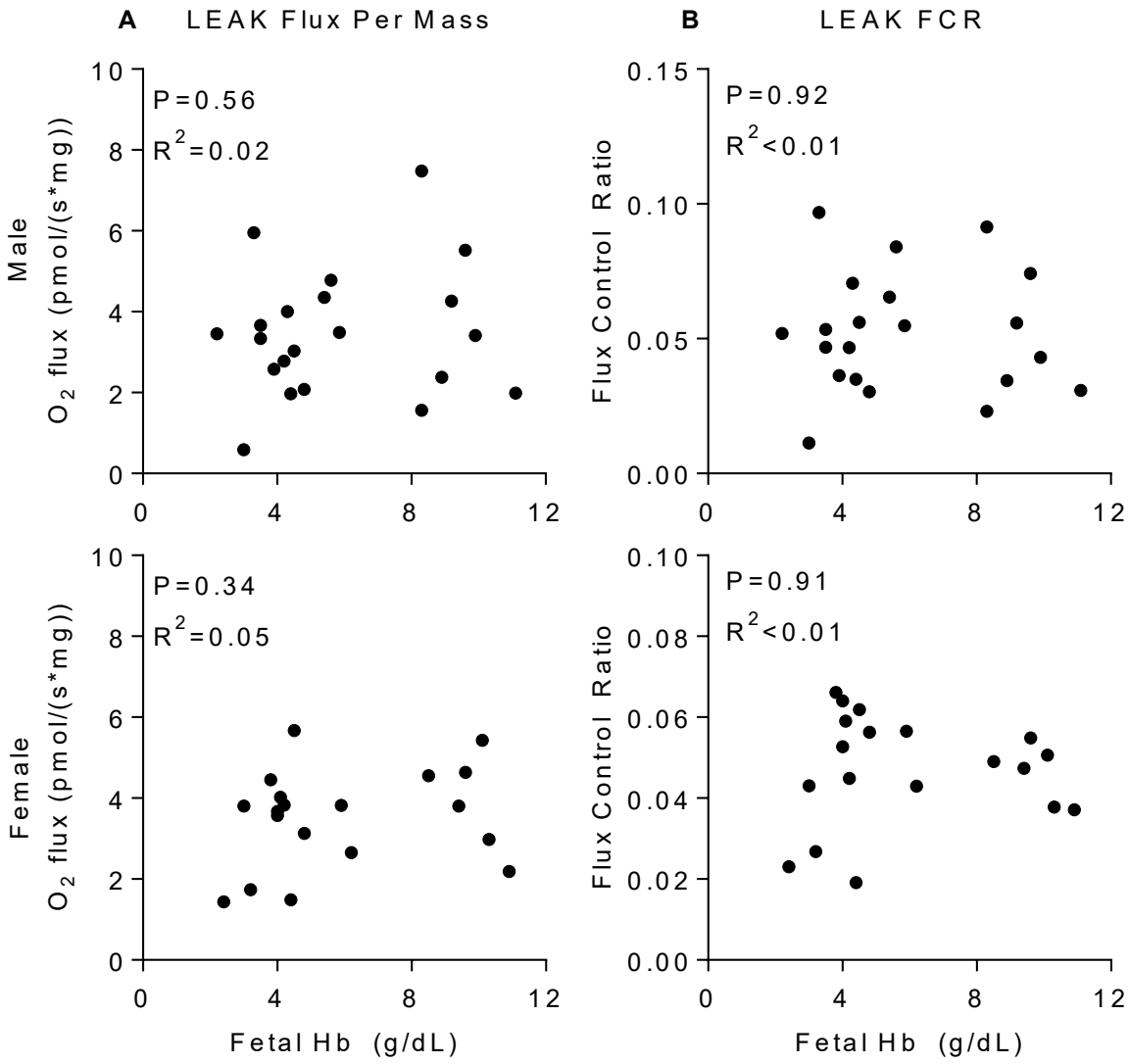

Figure 3.3: Kidney LEAK respiration. (**A**) oxygen flux per unit of tissue mass and (**B**) Flux Control Ratio (FCR) versus fetal Hemoglobin (Hb). Linear regression with 95% confidence intervals are shown where significant. Each point represents a separate litter.

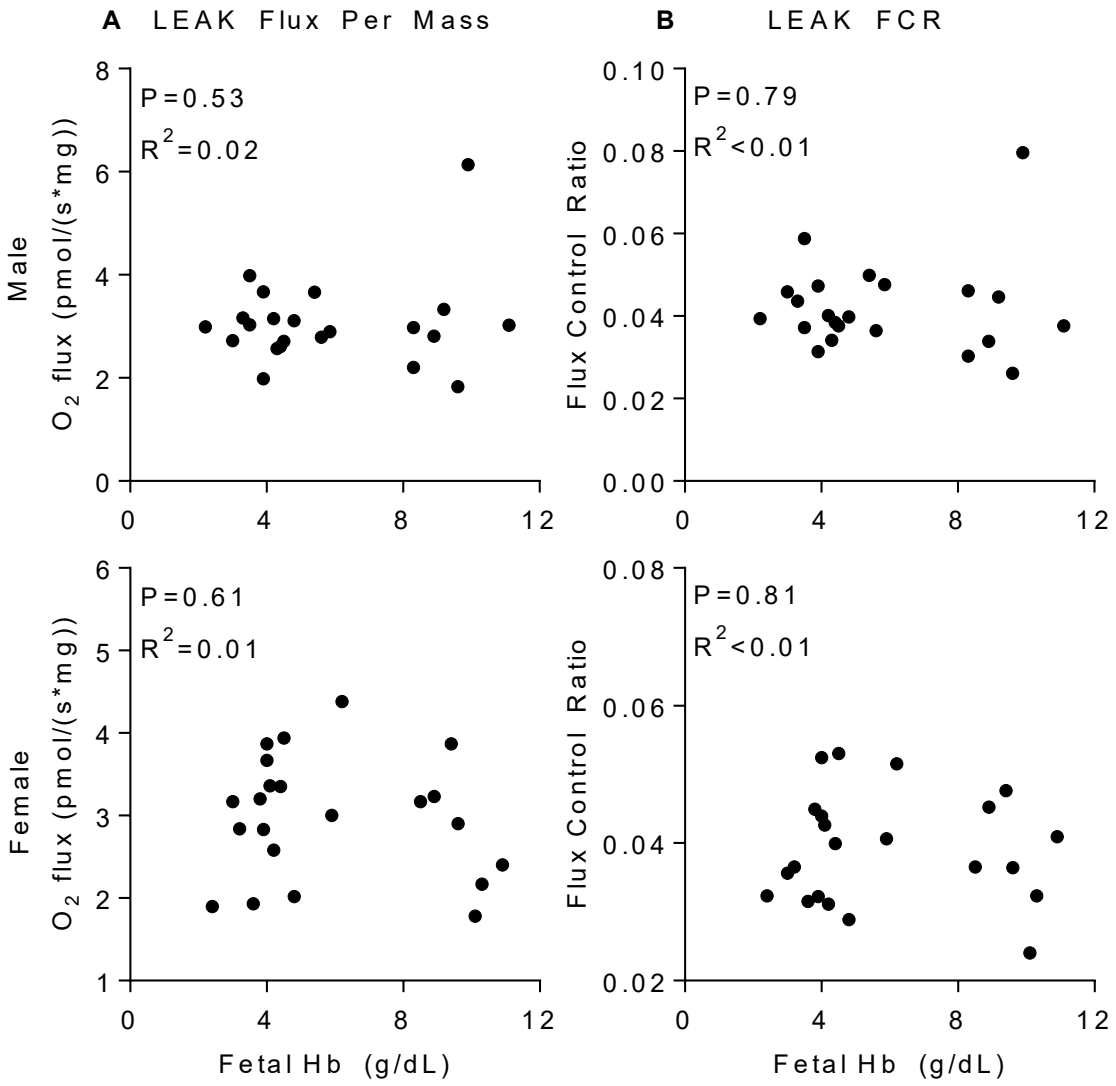

Figure 3.4: Liver LEAK respiration. (**A**) oxygen flux per unit of tissue mass and (**B**) Flux Control Ratio (FCR) versus fetal Hemoglobin (Hb). Linear regression with 95% confidence intervals are shown where significant. Each point represents a separate litter.

In male fetal kidneys, N-pathway OXPHOS capacity, NS- and S-pathway ETS capacities, as well as complex IV activity were positively correlated with fetal Hb (all $P<0.05$, **Figure 3.5**), albeit no changes in FCR were apparent for any of the above parameters (**Figure 3.6**). In the female fetal kidney, no changes in oxygen flux per tissue mass were observed (**Figure 3.5**), albeit a trend for a positive correlation between S-pathway ETS capacity and Hb level was noted ($p=0.07$). Female fetal kidney NS-pathway FCR was found to be negatively associated with fetal Hb (**Figure 3.6B**), however a positive association was observed for S-pathway FCR (**Figure 3.6C**). In the liver, none of the pathway capacities, expressed in flux per tissue mass (**Figure 3.7A-D**) or in FCR (**Figure 3.8A-C**), were found to correlate with fetal Hb in male or female fetuses. Complex IV activity in the male liver, however, exhibited a positive correlation with fetal Hb both when expressed in flux per tissue mass and as a FCR (both $P<0.05$, **Figures 3.7E** & **8D)**. By virtue of the fact that fetal Hb levels were not different between the M-ID and S-ID groups, we also performed correlation analysis between mitochondrial respiration parameters with fetal body weights, which reflected the severity of maternal iron restriction (**Table 3.1**). Results from this analysis were consistent with correlations between fetal Hb levels and mitochondrial respiration parameters (**Tables 3.3** & **3.4**).

Addition of cytochrome *c* after pyruvate, malate, and ADP was used as an indicator of mitochondrial outer membrane damage. A zero percent increase in respiration following addition of cytochrome *c* indicates full integrity of the outer mitochondrial membrane[289]. A slight and equivalent increase in respiration was indicative of good mitochondrial membrane integrity in all male kidney groups (CTL: 6.9±1.2%, M-ID: 5.0±2.2%, and S-ID: 7.1±1.3%, one-way ANOVA $P=0.60$). In the female kidneys, however, there was a slight increase in membrane fragility in the control group (CTL: 12.5±1.2%, M-ID: 8.3±1.7%, and S-ID: 5.9±1.3%, one-way ANOVA $P=0.006$). In the liver, there were no changes in membrane fragility with ID in both males (CTL: 12.5±2.1%, M-ID: 13.1±2.3%, S-ID: 14.1±2.6%, one-way ANOVA $P=0.89$) and females (CTL: 15.0±1.9%, M-ID: 18.0±2.2%, S-ID: 16.7±3.6%, one-way ANOVA $P=0.75$). All

OXPHOS and ETS capacities were presented with exogenous cytochrome *c* added, avoiding any possible bias between groups induced by limitation of cytochrome *c* availability resulting from damage to mitochondrial outer membrane.

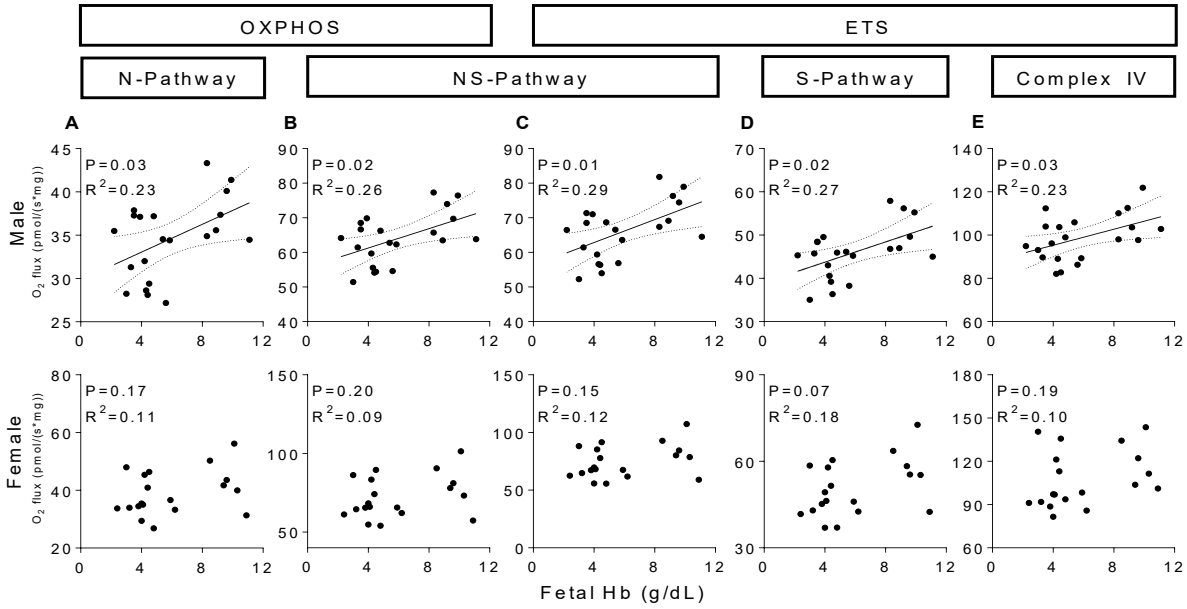

Figure 3.5: Kidney mitochondrial respiration (expressed as oxygen flux per unit of tissue mass) versus hemoglobin (Hb) from the same fetus. Two states were measured, oxidative phosphorylation (OXPHOS) with saturating ADP (**A** & **B**) and electron transport system (ETS) after addition of an optimal concentration of uncoupler (**C**-**E**). (**A**) OXPHOS capacity was measured for the NADH pathway (N-pathway, NADH-linked substrates pyruvate and malate entering through complex I); (**B**) NADH and succinate pathways simultaneously (NS-pathway; pyruvate, malate, and succinate feeding electrons into complex I and II simultaneously); (**C**) ETS capacity was measured with NS-pathway (after uncoupling); (**D**) succinate pathway (S-pathway, after addition of rotenone; and (**E**) complex IV activity (ascorbate and TMPD). Linear regression and dotted 95% confidence intervals are shown where significant. Each point represents a separate litter.

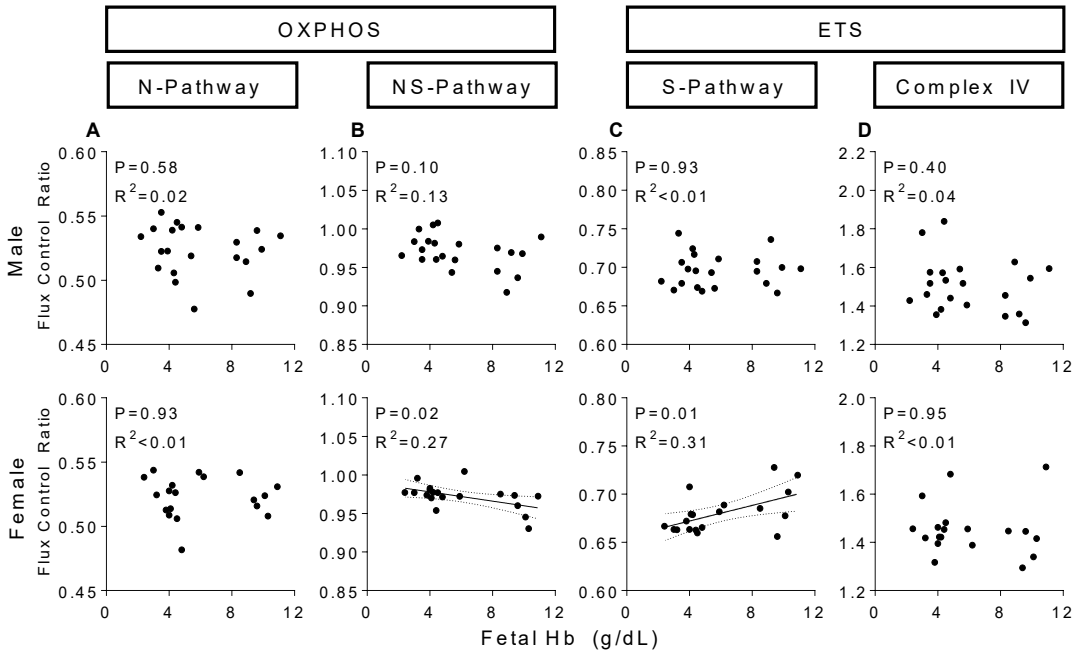

Figure 3.6: Kidney mitochondrial respiration (expressed as flux control ratio [FCR]) versus hemoglobin (Hb) from the same fetus. Two states were measured, oxidative phosphorylation (OXPHOS) with saturating ADP (**A** & **B**) and electron transport system (ETS) after addition of an optimal concentration of uncoupler (**C** & **D**). OXPHOS capacity was measured with (**A**) NADH-linked substrates (N-pathway; pyruvate and malate), and (**B**) NADH and succinate pathways simultaneously (NS-pathway; pyruvate, malate, and succinate); ETS capacity was measured in the NS-pathway (not shown, 1.00 by definition), (**C**) succinate pathway (S-pathway; after addition of rotenone), and for (**D**) complex IV (ascorbate and TMPD). Linear regression and dotted 95% confidence intervals are shown where significant. Each point represents a separate litter.

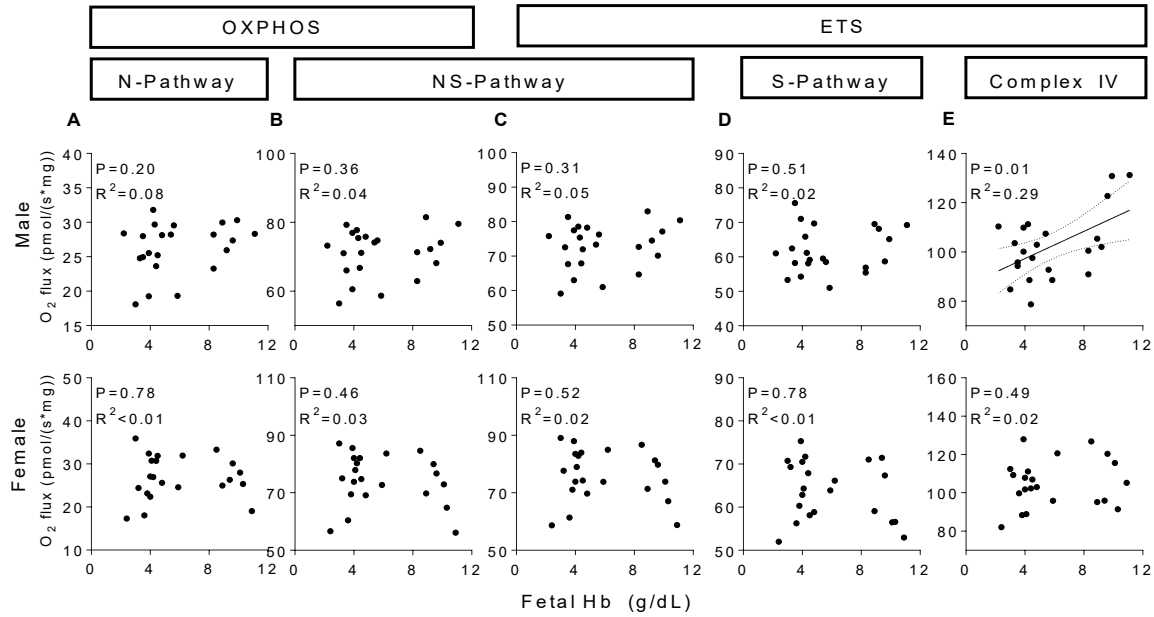

Figure 3.7: Liver mitochondrial respiration (expressed as oxygen flux per unit of tissue mass) versus fetal hemoglobin (Hb) in the same fetus. Two states were measured, oxidative phosphorylation (OXPHOS) with saturating ADP (**A** & **B**) and electron transport system (ETS) after addition of an optimal concentration of uncoupler (**C**-**E**). (**A**) OXPHOS capacity was measured for the NADH pathway (N-pathway, NADH-linked substrates pyruvate and malate entering through complex I); (**B**) NADH and succinate pathways simultaneously (NS-pathway; pyruvate, malate, and succinate feeding electrons into complex I and II simultaneously); (**C**) ETS capacity was measured with NS-pathway (after uncoupling); (**D**) succinate pathway (S-pathway, after addition of rotenone; and (**E**) complex IV activity (ascorbate and TMPD). Linear regression and dotted 95% confidence intervals are shown where significant. Each point represents a separate litter.

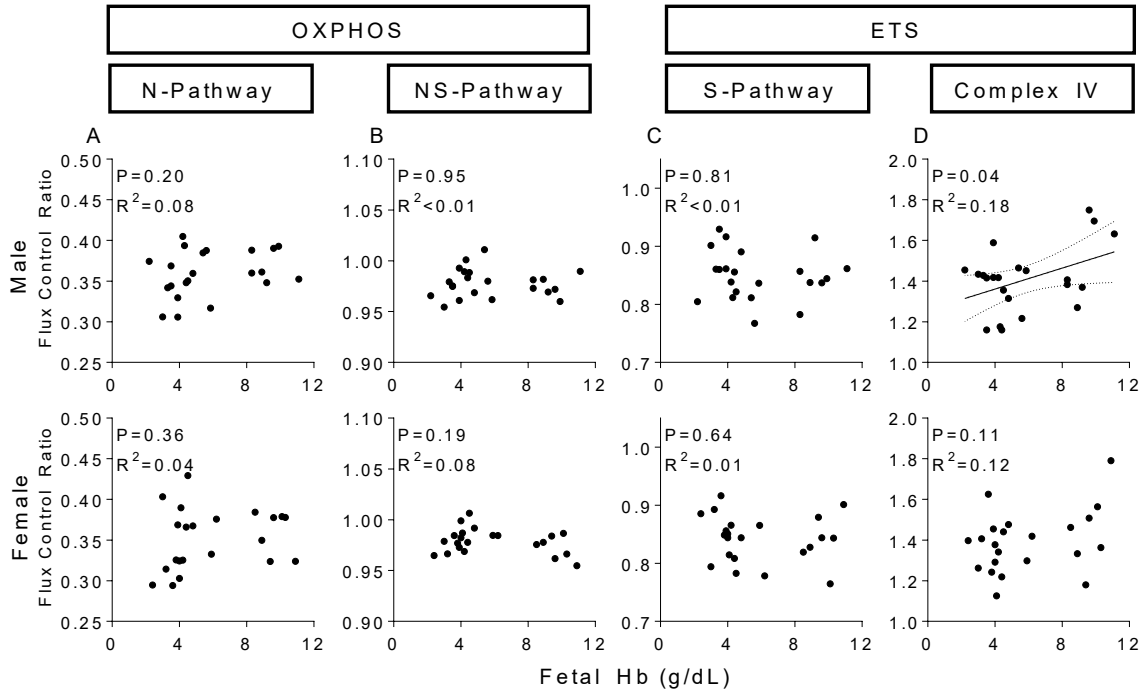

Figure 3.8: Liver mitochondrial respiration (expressed as flux control ratio [FCR]) versus hemoglobin (Hb) from the same fetus. Two states were measured, oxidative phosphorylation (OXPHOS) with saturating ADP (**A** & **B**) and electron transport system (ETS) after addition of an optimal concentration of uncoupler (& **D**). OXPHOS capacity was measured with (**A**) NADH-linked substrates (N-pathway; pyruvate and malate), and (**B**) NADH and succinate pathways simultaneously (NS-pathway; pyruvate, malate, and succinate); ETS capacity was measured in the NS-pathway (not shown, 1.00 by definition), (**C**) succinate pathway (S-pathway; after addition of rotenone), and for (**D**) complex IV (ascorbate and TMPD). Linear regression and dotted 95% confidence intervals are shown where significant. Each point represents a separate litter.

Table 3.3. Kidney mitochondrial flux per mass and flux control ratio correlated with fetal bodyweight in male and female offspring.

		Sex	Flux Per Mass			FCR		
			Slope	P	R^2	Slope	P	R^2
OXPHOS	Leak	M	-	0.65	0.01	-	0.65	0.01
		F	-	0.92	<0.01	-	0.92	<0.01
	N-Pathway	M	2.8 ±0.8	0.003	0.39	-	0.81	<0.01
		F	-	0.13	0.13	-	0.48	0.03
	NS-Pathway	M	4.6 ±1.3	0.002	0.41	-	0.15	0.11
		F	-	0.19	0.10	-7.5±3.3	0.04	0.23
ETS	NS-Pathway	M	5.3±1.3	0.001	0.43	-	-	-
		F	-	0.15	0.12	-	-	-
	S-Pathway	M	3.8 ±1.1	0.002	0.41	-	0.74	<0.01
		F	-	0.07	0.18	9.9 ±4.2	0.03	0.25
	Complex IV	M	5.8 ±2.0	0.009	0.31	-	0.35	0.05
		F	-	0.19	0.10	-	0.88	>0.01

Linear regressions were performed, where slope is the flux per mass (units: pmol O_2/s*mg_{tissue}*$g_{bodyweight}$) and FCR (units: FCR/ $mg_{bodyweight}$) as a function of fetal bodyweight. The FCR for NS-pathway ETS is 1.00 by definition (see methods). Non-significant slope values were omitted. ETS, electron transport system; F, female; FCR, flux control ratio; M, male; N- pathway, NADH dependent pathway; OXPHOS, oxidative phosphorylation; S-pathway, succinate dependent pathway.

Table 3.4. Liver mitochondrial flux per mass and flux control ratio correlated with fetal bodyweight in male and female offspring.

		Sex	Flux Per Mass			FCR		
			Slope	P	R^2	Slope	P	R^2
OXPHOS	Leak	M	-	0.78	<0.01	-	0.78	<0.01
		F	-	0.06	0.17	-3.4 ±1.6	0.047	0.18
	N-Pathway	M	-	0.72	<0.01	-	0.67	<0.01
		F	-	0.45	0.03	-	0.48	0.03
	NS-Pathway	M	-	0.77	<0.01	-	0.24	0.07
		F	-	0.41	0.03	-7.0 ±2.3	0.006	0.32
ETS	NS-Pathway	M	-	0.89	<0.01	-	-	-
		F	-	0.56	0.02	-	-	-
	S-Pathway	M	-	0.70	0.01	-	0.30	0.05
		F	-	0.99	<0.01	-	0.14	0.11
	Complex IV	M	7.0 ±2.7	0.02	0.26	97.1±29.0	0.003	0.36
		F	-	0.65	0.01	-	0.20	0.08

Linear regressions were performed, where slope is the flux per mass (units: pmol O_2/s*mg_{tissue}*$g_{bodyweight}$) and FCR (units: FCR/ $mg_{bodyweight}$) as a function of fetal bodyweight. The FCR for NS-pathway ETS is 1.00 by definition (see methods). Non-significant slope values were omitted. ETS, electron transport system; F, female; FCR, flux control ratio; M, male; N- pathway, NADH dependent pathway; OXPHOS, oxidative phosphorylation; S-pathway, succinate dependent pathway.

3.4.3 Reactive Species Quantification

Quantities of mitochondrial and cytosolic superoxide, in addition to nitric oxide were measured in the fetal tissues. Mitochondrial superoxide was quantified by MitoSOX fluorescence. In the kidney, MitoSOX staining was negatively associated with fetal Hb in female (P=0.01), but not male fetuses (P=0.39; **Figure 3.9A**). Dihydroethidium (DHE) fluorescent intensity, a marker of cytosolic superoxide, was inversely correlated with fetal Hb in male (P=0.02), but not female, offspring (P=0.56; **Figure 3.9B**). 4-Amino-5-Metyhylamino-2`,7`-Difluorofluorescein Diacetate (DAF-FM) mean fluorescence intensity, a marker of nitric oxide (NO), was associated with fetal Hb in male (P=0.006), but not female, fetuses (P=0.97; **Figure 3.9C**). In the fetal liver, mitoSOX staining indicated that changes in neither male nor female mitochondrial superoxide was associated with decreases in fetal Hb (**Figure 3.10A**). DHE fluorescence in the liver was negatively associated with fetal Hb in male (P=0.01), but not female offspring (P=0.60; **Figure 3.10B**). DAF-FM fluorescence in the liver showed no change in cytosolic NO association with decreased fetal Hb in males or females (**Figure 3.10C**). Representative images of fluorescence for the kidney and liver are contained in **Figures 3.11** & **3.12.**

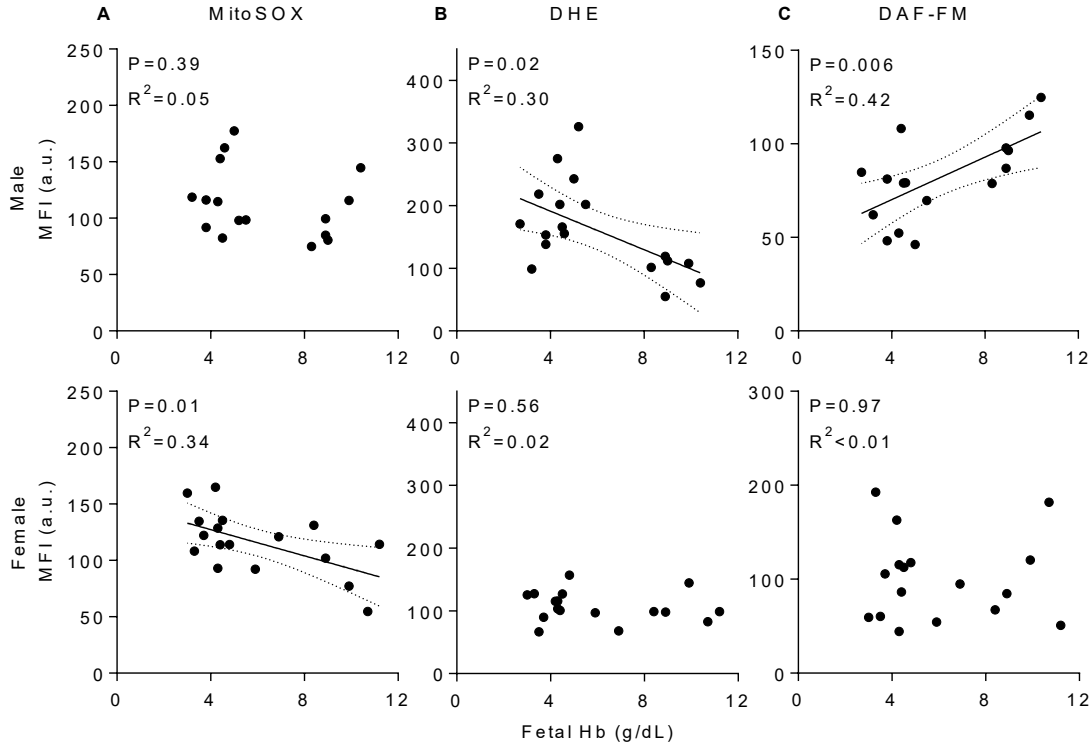

Figure 3.9: Kidney reactive species. Mean fluorescence intensity (MFI) of (**A**) mitochondrial superoxide with mitoSOX (**B**) cytosolic superoxide with DHE, and (**C**) cytosolic nitric oxide with DAF-FM, versus fetal hemoglobin (Hb) in the same fetus. Linear regression and dotted 95% confidence intervals are shown where significant. Each point represents a separate litter. Representative images of fluorescence are shown in **Figure 11**. a.u., arbitrary units.

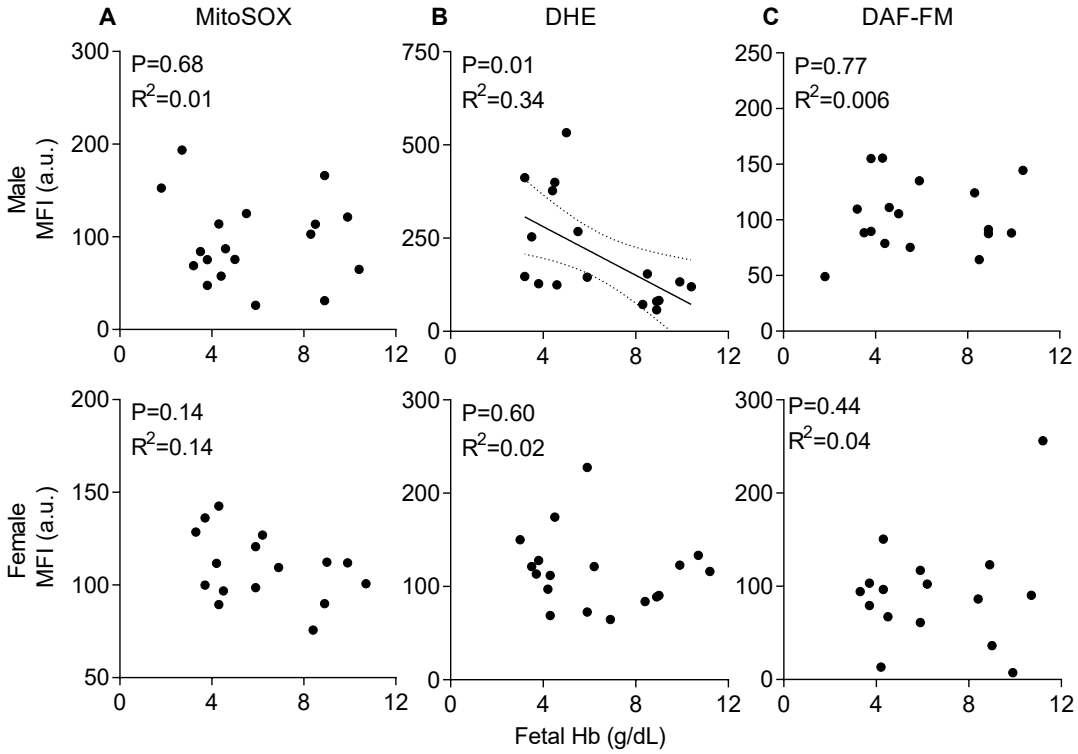

Figure 3.10: Liver reactive species. Mean fluorescence intensity (MFI) of (**A**) mitochondrial superoxide with mitoSOX (**B**) cytosolic superoxide with DHE, and (**C**) cytosolic nitric oxide with DAF-FM, versus fetal hemoglobin (Hb) in the same fetus. Linear regression and dotted 95% confidence intervals are shown where significant. Each point represents a separate litter. Representative images of fluorescence are shown in **Figure 12**. a.u., arbitrary units.

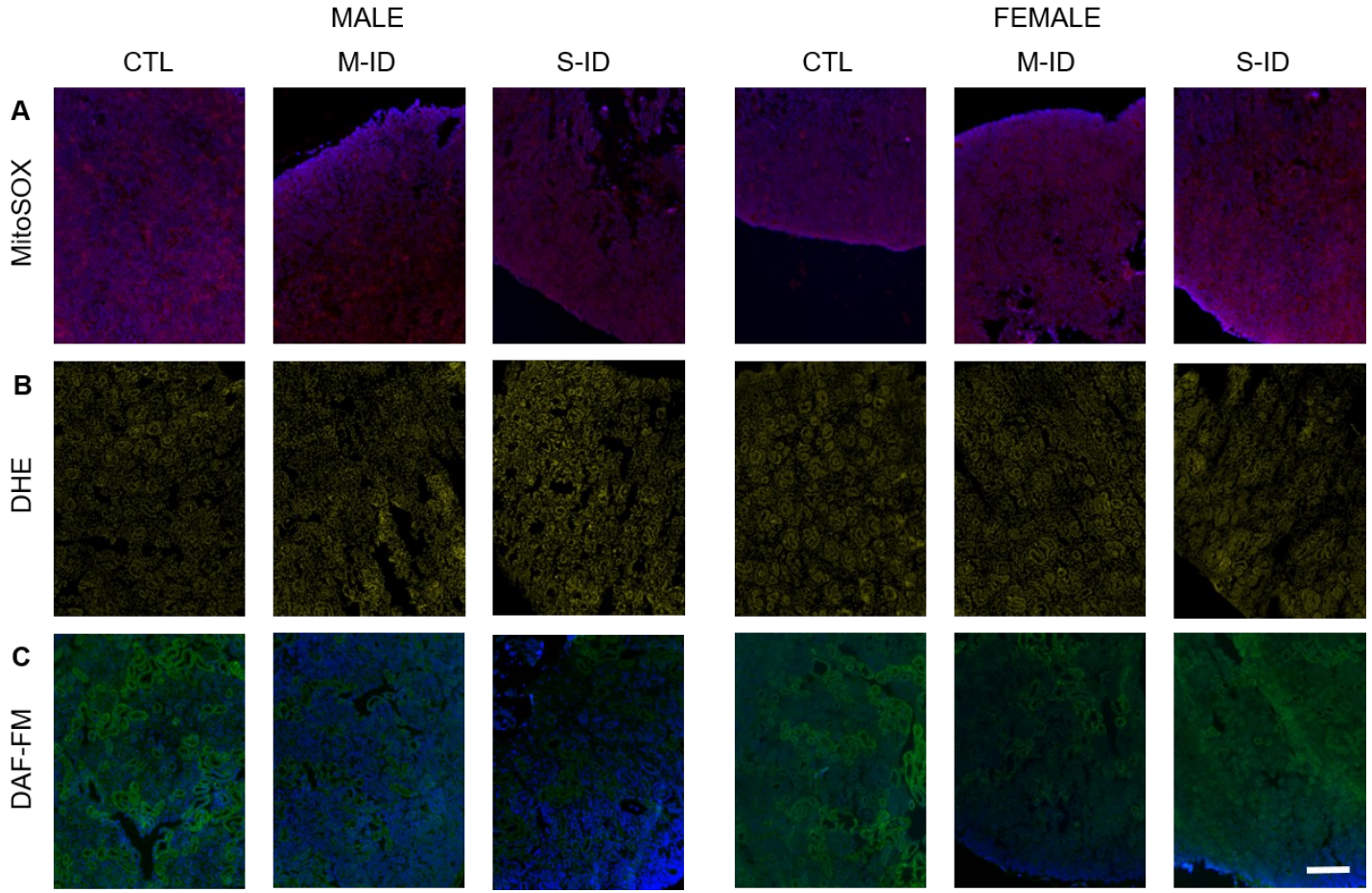

Figure 3.11: Representative images of kidney reactive species. (**A**) red MitoSOX, (**B**) yellow DHE, and (**C**) green DAF-FM fluorescence intensity. DAPI counterstain was used where applicable, visualized as blue fluorescence. White scale bar indicates 150μm. Quantification of intensity can be seen in **Figure 3.9**.

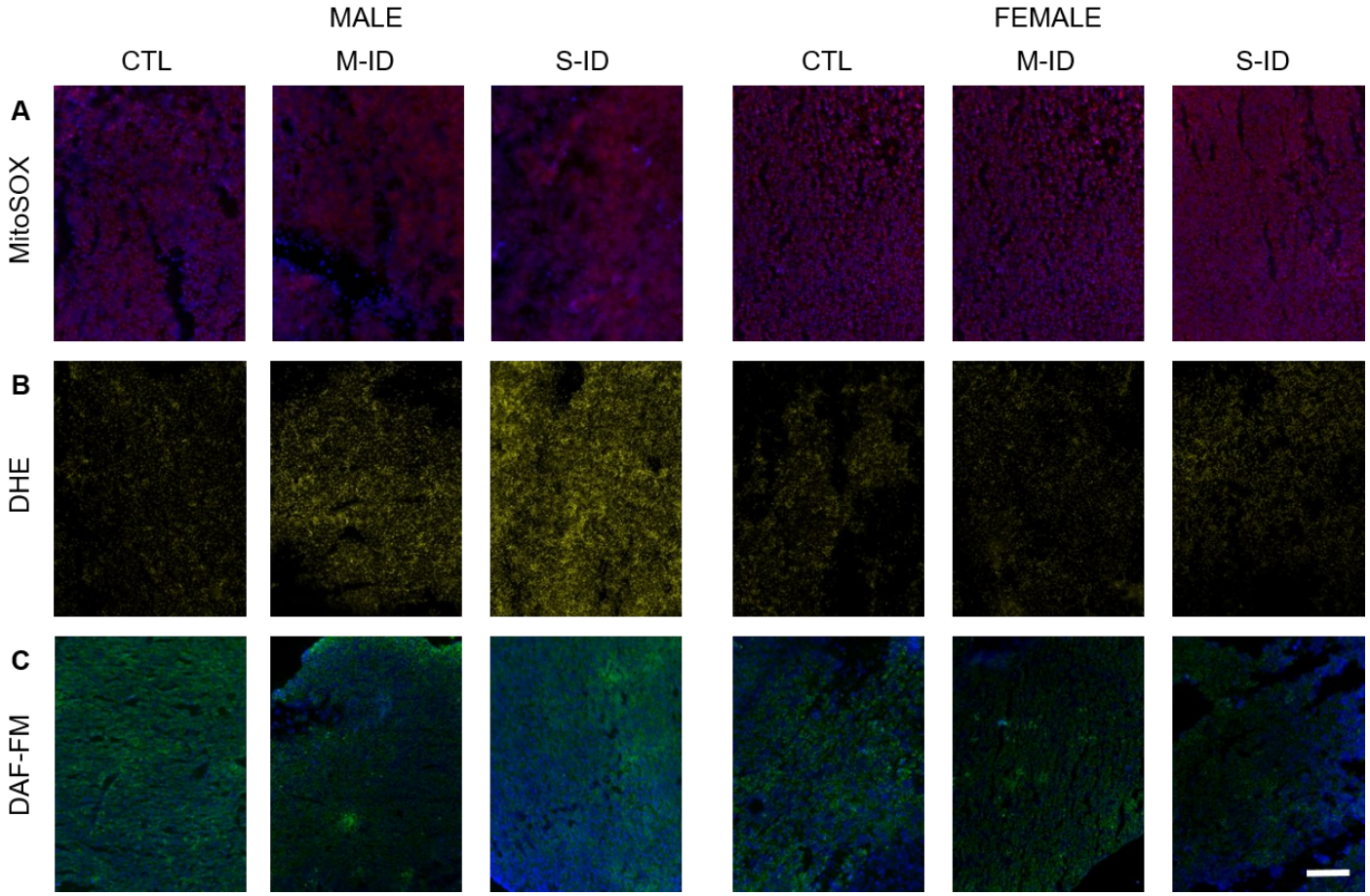

Figure 3.12: Representative images of liver reactive species. (**A**) red MitoSOX, (**B**) yellow DHE, and (**C**) green DAF-FM fluorescence intensity. DAPI counterstain was used where applicable, visualized as blue fluorescence. White scale bar indicates 150μm. Quantification of intensity can be seen in **Figure 3.10**.

3.4.4 Markers of Mitochondrial Biogenesis & Cellular Energy Status

In both the male and female fetal kidney, overall levels of AMP-activated protein kinase (AMPK) remained unchanged, with no increases in phosphorylation in M-ID and S-ID (**Figure 3.13**). Peroxisome proliferator-activated receptor gamma coactivator 1α (PGC1α), sirtuin 1 (SIRT1), or sirtuin 3 (SIRT3) levels were not affected by ID in male or female kidneys (**Figure 3.13**). In the male and female liver, no expression levels of any proteins studied were altered (**Figure 3.14**). These data demonstrate a lack of alteration in mitochondrial biogenic signalling in both the kidneys and liver of male and female ID offspring.

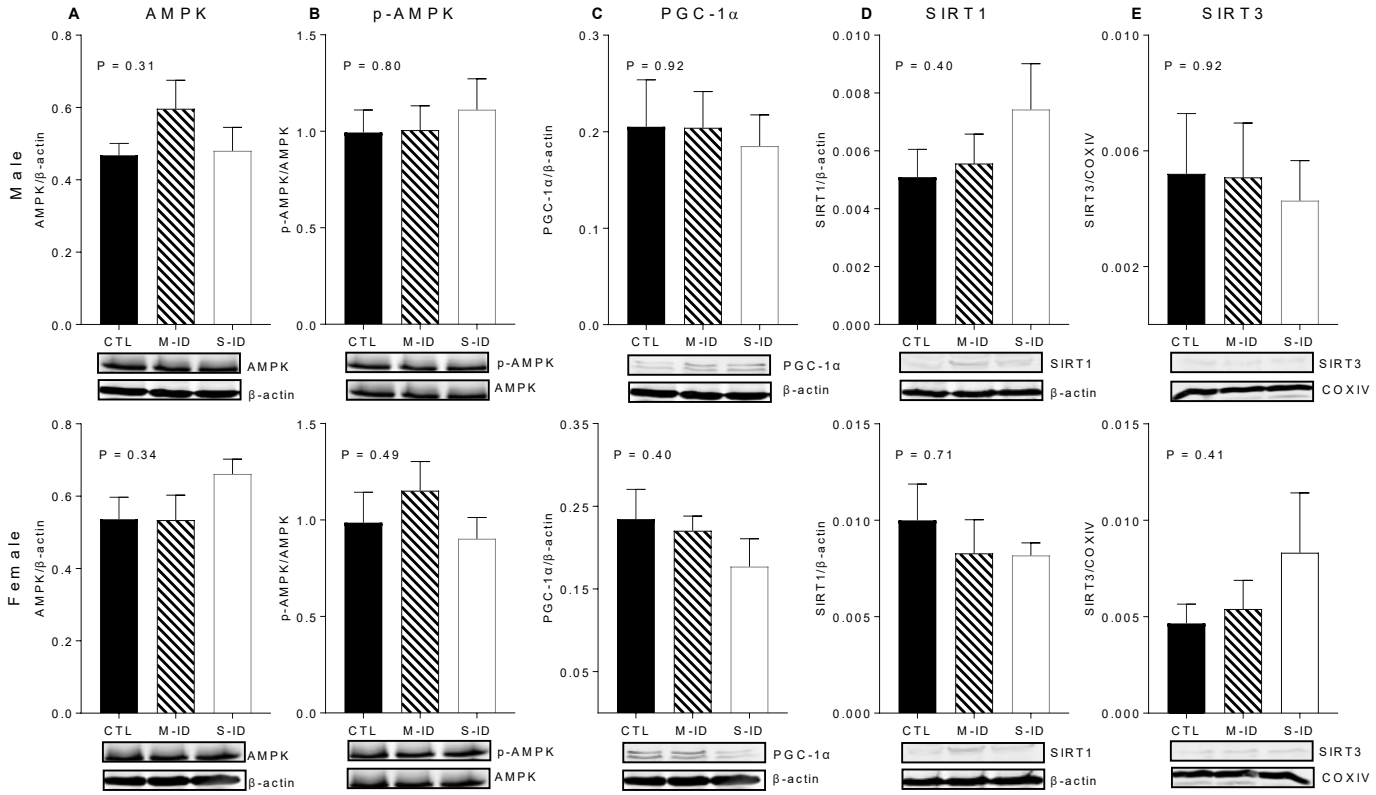

Figure 3.13: Markers of kidney mitochondrial biogenesis and cellular energy status. Western blot results from whole fetal kidney homogenates from control (CTL), moderate iron-deficient (M-ID), and severe-ID (S-ID) groups. Quantification of (**A**) AMPK, (**B**) phosphorylated-AMPK, (**C**) PGC-1α, (**D**) SIRT1, (**E**) SIRT3 expression in male (top row) and female (bottom row) offspring. Data were analyzed by one-way ANOVA. N=5-7 litters per group.

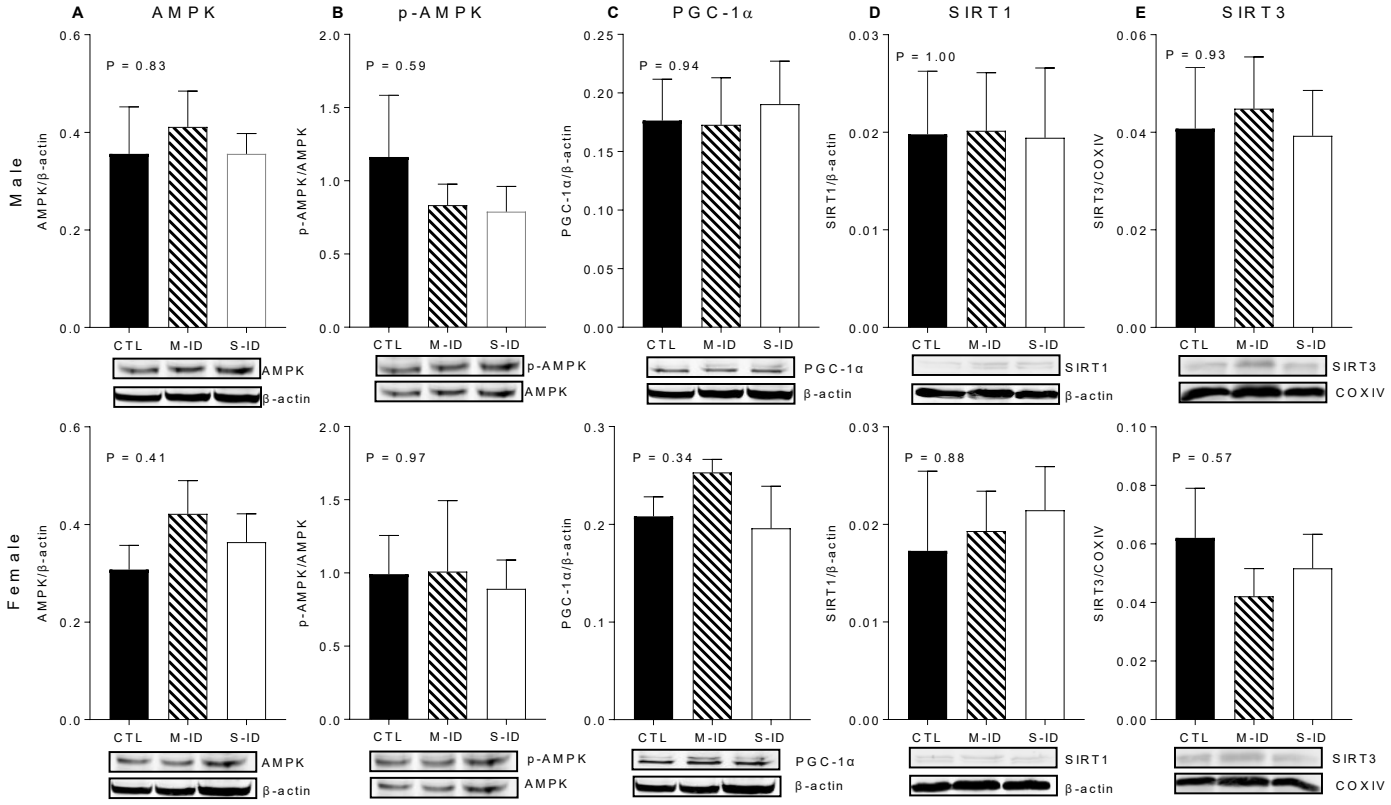

Figure 3.14: Markers of liver mitochondrial biogenesis and cellular energy status. Western blot results from whole fetal liver homogenates from control (CTL), moderate iron-deficient (M-ID), and severe-ID (S-ID) groups. Quantification of (**A**) AMPK, (**B**) phosphorylated-AMPK, (**C**) PGC-1α, (**D**) SIRT1, (**E**) SIRT3 expression in male (top row) and female (bottom row) offspring. Data were analyzed by one-way ANOVA. N=5-7 litters per group.

3.5 Discussion

In this study, we investigated the effects of maternal iron restriction on fetal kidney and liver mitochondrial function, oxidative stress, and markers of mitochondrial biogenesis. To summarize, we report that prenatal ID caused: (1) reduced mitochondrial content in only male kidneys (and not in female kidneys or in livers from either sex); (2) reduced complex II respiration in the female kidney, and reduced complex IV activity in the male liver; (3) increased cytosolic superoxide in male kidneys and livers, but not in females; (4) increased mitochondrial superoxide in female ID kidneys only; and (5) no alterations in biogenic factors studied. Taken together, these findings suggest that male ID fetuses are more prone to mitochondrial dysfunction and oxidative stress than females, and that the fetal kidney is more vulnerable to such perturbations than the liver. Our findings may have uncovered a mechanism through which cardiovascular disease is programmed by in prenatal ID offspring in a sex-dependent manner.

The models of maternal ID employed in this study rely on treating both the M-ID and S-ID groups with a fully iron-restricted diet during the pre-treatment period to partially deplete iron stores before pregnancy. During pregnancy, dams in the M-ID group were fed a diet with a modestly higher iron content, which caused a less marked drop in maternal Hb by GD14 and GD21. Whereas Hb levels were different between CTL, M-ID and S-ID dams at GD21, offspring from M-ID and S-ID groups had similar Hb levels, confirming our previous reports that maternal Hb can be a poor surrogate for fetal Hb[164]. Interestingly, despite the similar degree of anemia in the offspring, fetal body weights were reduced in the S-ID group (of both sexes) compared to both CTL and M-ID groups, suggesting the ID was more pronounced during the last week of pregnancy, when weight gain is greatest in the fetus. In agreement with previous findings[164], we found that prenatal ID causes reduced relative growth of the kidney and liver but not the heart or brain. The severity of anemia in the S-ID group was such that reduced litter sizes were seen, likely due to an increase in resorption rate. This observation may explain the modest reduction in maternal weight gain and food intake in the S-ID group due to reduced demands from their litter. However, we cannot discount the possibility that

maternal undernutrition is contributing to some extent, however small, to the effects on fetal growth restriction and development.

We previously reported that prenatal ID causes organ-specific patterns of hypoxia, where the brain is spared at the expense of other organs such as the liver and kidneys[164]. Our results are the first to describe organ- and sex-specific patterns of fetal mitochondrial dysfunction in the context of prenatal ID, despite evidence of hypoxia in both these tissues. In male fetal kidneys, the positive correlations between Hb and global oxygen flux, with no effect on FCR for any complex, suggests a reduced quantity of mitochondria. This is consistent with positive correlation between Hb levels and citrate synthase activity—a marker of mitochondrial content. In contrast, the prenatal ID female fetal kidneys had normal citrate synthase activity, with reductions only in complex II FCR. Remarkably, the liver is spared compared to the kidney, with female mitochondrial function being unaffected while males experienced reduced complex IV activity.

We observed sex-dependent alterations in oxidative stress within the kidneys. In females, we observed a reduction in FCR for the succinate pathway through complex II. Complex II has been reported to be highly sensitive to hypoxia[293], and therefore its downregulation may be due to reduced oxygen delivery, as previously shown in our model[164]. Moreover, impaired respiration at complex II is associated with increased intramitochondrial reactive oxygen species generation[294,295], which is in agreement with the observed increase in mitochondrial superoxide only in the female kidneys. The absence of elevated mitochondrial superoxide in ID male kidneys, as assessed by MitoSOX staining, may be due to a global reduction in mitochondrial content, thereby reducing overall signal even though proportional increases may have occurred. Male fetal kidneys had reduced cytosolic NO bioavailability concomitant with an increase in cytosolic superoxide, whereas female cytosolic superoxide and NO were unaffected. This may be because complex II derived superoxide is largely intramitochondrial[294], and therefore less likely to affect cytosolic oxidant levels in females. However, differences in antioxidant pathways and reactive oxygen species derived from other sources (i.e. uncoupled nitric oxide synthase[296]) may also be implicated.

In the liver of male, but not female fetuses, decreases in complex IV activity and increases in cytosolic superoxide production were observed. Liver cytosolic superoxide may be a consequence of downregulation of complex IV[297], whose normal function limits the production of superoxide by maintaining efficient function of the ETS[298]. Indeed, female livers without perturbations in complex IV function do not have elevated cytosolic superoxide like their male counterparts. While prenatal ID has been shown to reduce antioxidant capacity in pooled male and female fetal tissues[84], more recent studies have shown that perinatal ID reduces male antioxidant capacities more than in females[85]. Potential differences in compartmentalized antioxidant capacities in both the liver and kidney warrant further investigation, and may help explain the observed patterns of oxidative stress in our model.

The mechanisms underlying the heightened susceptibility for mitochondrial dysfunction in males remain unclear. It has been proposed the maternal inheritance of mitochondria results in their evolution favoring functional optimization in females due to more time under selection[299]. Sex hormones, notably testosterone, may also be implicated[247]. At end of gestation, testosterone levels are higher in male fetuses than females, whereas estradiol and progesterone levels are equivalent[242,300]. Therefore, future studies investigating testosterone signaling in the context of prenatal ID and mitochondrial function are warranted.

The organ-specific patterns of pathology in our model emphasize the importance of physiological reserve *in utero*. In chronically anemic fetuses, blood flow to the kidney can increase two-fold, whereas blood flow to the liver can increase four-fold[260]. The limited increase in renal blood flow (and hence oxygen delivery) could result in a pathological level of sustained hypoxia, particularly since the kidney develops in an environment of relative hypoxia under normal circumstances[91]. Sustained hypoxia may cause changes in metabolic function and mitochondrial biogenesis. Interestingly, prenatal ID had no effect on fetal biogenic and metabolic modulators studied, which included AMPK, SIRT1 and 3, and PGC1α. Although these mediators are exquisitely sensitive to metabolic perturbations, their ability to act as homeostatic regulators depends on the

ability to signal in a wide range of conditions. It is therefore possible that a sustained state of ID and hypoxia in the fetus results in new signaling set points, and changes in these metabolic mediators may only be evident earlier in pregnancy. Indeed, in cultured cells, ID only transiently affects mitochondrial biogenesis[301,302]. Evidence also suggests that iron-mediated changes in mitochondrial biogenesis can occur independently of the mediators studied herein[302].

The results presented herein suggest perturbations in energy production secondary to ID may be involved in abnormal kidney development and function, as seen in animal models and humans[170,214,215,303]. Importantly, the impact of prenatal ID on mitochondrial function in male kidneys, which is greater than on female kidneys, may contribute to sexually-dimorphic outcomes seen in the programming of long-term cardiovascular and renal function, and may contribute to the imbalanced burden of cardiovascular disease in men compared to women. Although ID is highly prevalent, particularly in pregnant women, our findings may have important implications for programming models that may share hypoxia and oxidative stress as etiological mechanisms (e.g. prenatal hypoxia, reduced placental perfusion, maternal smoking). Indeed, in a model of maternal smoking, offspring exhibit persistent alterations in mitochondrial dysfunction in adulthood[304]. Offspring that are exposed to maternal nutrient restriction during pregnancy also exhibit sex-dependent changes in mitochondrial gene expression[305], suggesting altered mitochondrial function may be programming mechanism common to many models of developmental stress. In the context of prenatal ID, whether the observed the fetal mitochondrial dysfunction persists in adulthood, or whether it occurs transiently during development, leading to abnormalities in kidney structure and function requires further investigation.

In summary, we have demonstrated that prenatal ID results in organ- and sex-specific patterns of mitochondrial dysfunction. Our results implicate mitochondrial function and compartmental oxidative stress as mechanisms underlying the sex-specific programming of cardiovascular and metabolic function in of offspring. These results may suggest that intervention strategies directed towards improving energy metabolism and

antioxidant capacity in the fetus may improve long-term cardiovascular outcomes secondary to prenatal ID.

Author Contributions

A.G. Woodman, H. Lemieux, F.S. Gragasin, and S.L. Bourque designed research; A.G. Woodman, R. Mah, D. Keddie, R. Noble, and S. Panahi performed research; A.G. Woodman, R. Mah, D. Keddie, and H. Lemieux analyzed data; and A.G. Woodman and S.L. Bourque wrote the manuscript.

Funding Sources

This work is supported by grants from the Canadian Institutes of Health Research (CIHR, MOP142396) and the Women and Children's Health Research Institute to SLB, and a discovery grant from the National Sciences and Engineering Research Council to HL (RGPIN 402636). AGW holds studentships from CIHR and Alberta Innovates-Health Solutions. SLB holds a CIHR New Investigator Salary Award.

Disclosures

None.

Chapter 4

Perinatal Iron Deficiency Causes Sex-Dependent Changes in Kidney Oxidative Stress, Cellular Senescence and Apoptosis During Postnatal Renal Development

Andrew G. Woodman[1,2,3*], Richard L. Mah[1,3*], Claudia D. Holody[1,2,4], Ronan M.N. Noble[1,2,4], Robin D. Clugston, Stephane L. Bourque[1,2,3,4,5]

Women and Children's Health Research Institute, University of Alberta[1]

Cardiovascular Research Centre, University of Alberta[2]

Department of Pharmacology, University of Alberta[3]

Department of Pediatrics, University of Alberta[4]

Department of Anesthesiology and Pain Medicine, University of Alberta[5]

*Denotes equal contribution

UNDER PREPARATION FOR PUBLICATION

4.1 Abstract

Kidney structure and function has been shown to be permanently altered by perinatal stressors, such as iron deficiency (ID). Here, we sought to assess how perinatal ID alters cellular oxidative stress, senescence, and apoptosis within the developing kidney. Pregnant Sprague Dawley rats were fed either an iron-restricted or iron-replete diet, and offspring were studied on postnatal day (PD)1 and 28. Maternal iron-restriction caused offspring anemia and growth restriction that was evident on PD1. Kidneys from male perinatal ID offspring on PD1 exhibited decreased total glutathione levels (P=0.01), enhanced caspase 3 activity (P=0.009), and altered autophagosome-associated levels of LC3 protein (P=0.03), concomitant with increased expression of antioxidant enzymes *Sod1*, *Sod2*, and *Gsr* (all P<0.05). Senescence-associated β-galactosidase (SA-βGal) activity was decreased by perinatal ID in both sexes on PD1 concomitant with increased *p21* (P=0.04) and decreased *P16* (P=0.04). By PD28, perinatal ID offspring were no longer anemic, and kidney weights relative to bodyweight were increased relative to controls (P=0.0001), despite decreased gross kidney weight (P=0.0002) and offspring body weights (P<0.0001) remaining lower. On PD28, male perinatal ID offspring kidneys exhibit enhanced lipid peroxidation (P=0.03) and decreased *Sod1* (P=0.03) expression. Perinatal ID offspring of both sexes exhibit enhanced SA-βGal activity (P=0.002) and expression of *Tgfβ1* (P=0.04) and *Tgfβ2* (P=0.04) on PD28. Female offspring irrespective of perinatal group exhibited higher SA-βGal activity (P=0.01), and enhanced expression of *Smad3* and *Tgfβ2* (P=0.02) on PD28. Together, these results indicate that perinatal ID is associated with inhibition and subsequent upregulation in cellular senescence. In males, these effects are also associated with oxidative stress, altered autophagy, and enhanced apoptosis. The absence of long-term renal dysfunction in female offspring suggest that the combination of disrupted senescence and enhanced apoptosis and oxidative stress may underlie dysfunction, rather than disrupted senescence alone.

4.2 Introduction

The overall mortality rate from chronic kidney disease has increased more than 40% since 1990 and is currently the 12th leading cause of death globally [95]. An increasingly recognized risk factor for the development of chronic kidney disease is a sub-optimal environment during development, as indicated by pre-term birth, low birth weight, or being small for gestational age [306,307]. Studies in animals show that a variety of perinatal stressors cause renal impairments that persist in adulthood, emphasizing the vulnerability of the developing kidney to insults [171]. Preclinical models remain invaluable for studying the mechanisms through which perinatal stressors impact renal function later in life due to the logistical challenges associated with studying these phenomena in humans over decades.

Iron deficiency (ID) is the most common nutritional deficiency worldwide [21], and affects pregnant women at staggering rates. Perinatal ID anemia results in long-term cardiovascular sequelae in the offspring, including hypertension, vascular dysfunction, and renal injury [170,308,309]. Notably, these persistent cardiovascular consequences occur predominantly in male offspring, whereas female offspring are largely spared. The early mechanisms contributing to these effects are unclear, but we and others have shown that pre- and perinatal ID causes patterns of hypoxia [164], mitochondrial dysfunction and increased superoxide levels in the fetal kidney [165], reduced nephron endowment [214,215], and delayed postnatal renal maturation [216]. Yet how these factors translate to cellular stress responses and altered renal development is not clear.

Apoptosis and senescence are generally regarded as cellular responses to stress (i.e. oxidative stress), though recent studies have highlighted an important role for these processes in normal development. Organ development requires tight control of cell proliferation to achieve and maintain patterning for the formation of complex structures, and both senescence and apoptosis have evolved as mechanisms for this process. Developmental senescence, which is stimulated by the transforming growth factor (TGF) pathway rather than replicative stress, is highly active in renal development [185,186]. Interestingly, apoptosis has been shown to compensate for deficiencies in developmental

senescence resulting from genetic manipulation [310], suggesting a degree of functional redundancy between these processes.

Here, we sought to determine how iron deficiency affects patterns of cellular senescence and apoptosis during and after kidney development.

4.3 Methods

4.3.1 Animals and Treatments

The studies described herein were approved by the University of Alberta Animal Care Committee (reference number AUP974) in accordance with the guidelines established by the Canadian Council of Animal Care. Twenty experimentally naïve and nulliparous female Sprague Dawley rats (initially 6 weeks of age) were purchased from Charles River (Saint-Constant, QC, Canada) and housed at the University of Alberta animal care facility under a 12h light/dark cycle and ambient temperature of 23°C. Rats were housed in wire top cages fitted with mesh filter tops, enriched with wooden blocks and shredded paper pucks. Rats were provided *ad libitum* access to food and water throughout the study.

Throughout the exposure period, female rats were fed one of three AIN-93G purified diets (Research Diets Inc., New Brunswick, NJ, USA), which were identical in composition with the exception of the amount of added ferric citrate. Two weeks prior to pregnancy, rats were randomly allocated to either the iron-restricted group and fed a diet low in iron (3mg/kg iron; D03072501), or the control group fed an iron-replete diet (37mg/kg iron; D10012G). After a minimum of two weeks, females were co-housed with age-matched males overnight for breeding, and pregnancy was confirmed by the presence of sperm in a vaginal smear the following morning. Thereafter, all pregnant dams were single-housed, and those in the iron-restricted group were fed a diet moderately low in iron (10mg/kg iron; D15092501) for the duration of pregnancy; dams in the control group were maintained on the same iron-replete diet throughout pregnancy. Maternal Hb levels, body weight gain and food consumption were monitored throughout gestation. Within 24h of giving birth, all dams were fed a standard rodent chow (5L0D; PicoLab, St. Louis,

MO, USA), and litters sizes were standardized to 8-10 offspring to prevent under- or overfeeding in the postnatal period. Offspring were weaned from their mothers on postnatal day (PD)21 and maintained on rodent chow thereafter.

Pups culled within 24h of birth (referred to as PD1 offspring) were euthanized by decapitation, and mixed blood samples were collected to assess Hb levels using a HemoCue201+ system. Organs were then collected, cleaned and weighed, and then snap frozen in liquid nitrogen or embedded in optimal cutting temperature (OCT) medium (TissueTek, Inc.) and then frozen. Offspring were euthanized on PD28 under isoflurane anesthesia (3% isoflurane in medical grade oxygen, flow rate 1L/min) by exsanguination and subsequent excision of the heart. Blood samples were taken from the vena cava for Hb assessment, and tissues were collected and stored as described above.

4.3.2 RT-qPCR Experiments

Kidneys (~50mg) from one male and one female pup from each litter were homogenized in TRIzol reagent (Life Technologies, Carlsbad, CA) in two intervals of 30s with a Precellys Minilys homogenizer (Bertin Instruments) using 2mL tubes containing ceramic beads (Precellys CK14; Bertin Instruments). RNA extraction was performed with Qiagen RNeasy kit (Venlo, Netherlands). Briefly, homogenates in TRIzol were separated with chloroform and spun down at 12,000x *g* for 10min at 4°C. The aqueous RNA phase was purified in multiple spin columns at 17,000x *g* for 15s sequentially with 70% ethanol, and proprietary buffers contained in the kit. RNA concentration and purity was assessed by A_{260}/A_{280} absorbance with a NanoDrop1000 spectrophotometer (Thermo Fisher Inc.). RNA was reverse transcribed using the High Capacity cDNA Reverse Transcription Kit (Applied Biosystems, Cheshire, UK) according to manufacturer's instructions. All reactions contained 2000ng of RNA.

Gene sequences of interest were obtained from NCBI's Gene database (https://www.ncbi.nlm.nih.gov/gene). Primer sequences designed with the LightCycler Probe Design Software 2.0 (Roche) are shown in **Table 4.1**. Each qPCR reaction was carried out in duplicate in either a 96-well optical reaction plate on a QuantStudio3 Real-

Time PCR System (Applied Biosystems) or LightCycler 480 (Roche) 384-well plate with PowerUP SYBR Green Master Mix (Applied Biosystems). The thermocycling conditions consisted of an initial step of 50°C for 120s, 40 cycles of denaturation at 95°C for 15s and annealing and extension steps at 60°C for 60s. Where more than one transcript variant or isoform was found for a given gene, a primer suitable for quantifying expression of all variants was used. The relative gene expression was calculated by comparing cycle thresholds using the following equation: relative gene expression$=2^{(\Delta Ctsample—\Delta Ctcontrol)}$ as previously described [311]. Expression of genes of interest was normalized to ribosomal *18s* expression in the study, which was confirmed to be uniformly expressed across all samples.

Table 4.1: Primers for RT-q-PCR experiments.

Gene (Gene ID)	Primer Sequence	
18s (100861533)	Fwd	CGG ACA GGA TTG ACA GAT TGA TAG C
	Rev	CGT TCG TTA TCG GAA TTA ACC AGA C
Bad (64639)	Fwd	ACT GCA ACA CAG ATG CGA CAA
	Rev	TCC GGG AAT GTG GAG CAG ATC A
Bax (24887)	Fwd	GCG AGT GTC TCA GGC GAA T
	Rev	CTG CCA CAC GGA AGA AGA CC
Bcl2 (24224)	Fwd	GAG GAT TGT GGC CTT CTT TGA GTT
	Rev	GCA GAT GCC GGT TCA GGT
Casp3 (25402)	Fwd	TGG ACA TGA CGA CAG GGT GCT A
	Rev	TTT GAG GCT GCT GCA TAA TCG C
Cat (24248)	Fwd	CGG ATT CCT GAG AGA GTG GTA CA
	Rev	TGT GGA GAA TCG GAC GGC AAT AG
Gclc (25283)	Fwd	GCT GAC CAG GGT GAT CCT CTC ATA
	Rev	CCT GTA AGA CGG CAT CTC GC
Gclm (29739)	Fwd	ACT GCA TTT GCT AAA CAG TTT GAC A
	Rev	GGA TGC TTT CTT GAA GAG CTT CCT
Gpx1 (24404)	Fwd	GGC TCA CCC GCT CTT TAC C
	Rev	AAT GTC GTT GCG GCA CAC
Gsr (116686)	Fwd	GGG ATT GGC TGC GAT GAG AT
	Rev	TTC TGA AGA GGT AGG ATG AAT GGC G
Gss (25458)	Fwd	CTG TCG CTG AGG CCC TT
	Rev	CTC CAG AGC GTG TAC CAT TTC C
P16 (25163)	Fwd	CCC GAA CAC TTT CGG TCG T

	Rev	GGT CCT CGC AGT TCG AAT CT
P21 (114851)	Fwd	CCT GGT TCC TTG CCA CTT CTT AC
	Rev	TCA TCC TAG CGG GCC TTA GAG
P53 (24842)	Fwd	ACC ATG AGC GTT GCT CTG AT
	Rev	CAC CAC GCT GTG CCG AA
P62 (113894)	Fwd	TGG GTT TCT CGG ATG AAG GCG
	Rev	GGT GGA GGG TGC TTT GAA TAC T
P66shc (85385)	Fwd	GCC GAT CAC TCT CAC TGT GT
	Rev	CCC ACC AGA CGC GAA TGA GAT A
Smad2 (29357)	Fwd	GTT TGC CGA GTG CCT AAG TGA T
	Rev	GGT TAC AGC CTG GTG GGA TTT
Smad3 (25631)	Fwd	GTG CAA ACA GGC TGC CCT AGA
	Rev	AAA GAT GGC TCC AAT TTC CTT GTG A
Sod1 (24786)	Fwd	GCA GAA GGC AAG CGG TGA
	Rev	GGT ACA GCC TTG TGT ATT GTC CC
Sod2 (24787)	Fwd	GTC TGT GGG AGT CCA AGG TT
	Rev	GTT CCT TGC AGT GGG TCC TGA TTA
Tfeb (316214)	Fwd	ACT TAA TTG AGA GAA GAC GCA GGT T
	Rev	CTT GAG GAT GGT GCC CTT GT
Tgfβ1 (59086)	Fwd	CCG GGT GCT TCC GCA TCA
	Rev	TGT TGG ACA ACT GCT CCA CCT
Tgfβ2 (81809)	Fwd	TGG AAC CAC TGA CCA TCC TCT ACT
	Rev	TTT CCC GAG GAC TTT AGC TGC ATT T
Zkscan3 (306977)	Fwd	TGG GTG AAG ACA CTG TCC AGA TT
	Rev	CCC ACA TTC ACG GCA GTA GA

4.3.3 β-Galactosidase Activity Assay

Histochemical detection of senescence associated β-Galactosidase (SA-βGal) activity was performed using a kit (ab65351; Abcam Inc.) according to the manufacturer's instructions. Briefly, kidneys embedded in OCT medium were cryosectioned at 8μm and stored at -80°C. Slides were then thawed, and tissue sections incubated in fixative solution (provided in kit) at room temperature for 10-15min. Slides were washed twice with phosphate buffered saline (PBS; pH 7.4), and then incubated with staining solution overnight in a sealed humidified container at 37°C. Sections were imaged with an EVOS XL Core microscope at 4X magnification; intensity of blue staining, reflecting SA-βGal activity, was quantified using ImageJ software.

4.3.4 Caspase Activity Assays

Activities of caspases 3 and 9 were measured using commercially available kits (ab39383 and ab65607; Abcam Inc.) per manufacturer instructions. Briefly, kidney tissue (100mg) was homogenized in cell lysis buffer (provided in kit), centrifuged at 12,000x*g*, and pellets were discarded. Supernatant protein concentration was determined through the bicinchoninic acid (BCA) assay. 50µg of protein (1µg/µL) was loaded in duplicate into 96 well plates and incubated with 50µL of 2X Reaction Buffer containing 10mM dithiothreitol (DTT). Finally, 5µL of probe (50µM final concentration) was added and plates were incubated at 37˚C for 1hr and subsequently analyzed using a fluorescent plate reader (excitation 400nm; emission 505nm). Levels of caspase activity in perinatal ID offspring samples were compared directly as fold-changes versus the average value of controls of the same sex at each timepoint.

4.3.5 Western Blotting

Western blots were performed as previously described [165]. Antibodies utilized for Western blotting experiments, and their dilutions/concentrations, are as follows: LC3 protein rabbit polyclonal primary antibody (Abcam ab48394; dilution of 1:1000 for final concentration of 1µg/mL), β-actin mouse monoclonal primary antibody (Abcam ab6276; dilution of 1:5000 for final concentration of 0.4µg/mL), Alexa Fluor 680 donkey anti-rabbit secondary antibody (Abcam ab175772; dilution of 1:10000 for final concentration of 0.2µg/mL), and Alexa Fluor 790 donkey anti-mouse secondary antibody (Abcam ab175782; dilution of 1:10000 for final concentration of 0.2µg/mL). Intensities of LC3-I and LC3-II bands were compared, with β-actin serving as a loading control for each sample. Western blots were imaged with a an Odyssey imaging system (LI-COR Biosciences).

4.3.6 Oxidative Stress Markers

Lipid peroxidation in whole kidney homogenates (~10mg sample) was assessed using a commercially available malondialdehyde (MDA) assay kit (ab118970; Abcam Inc.). Kidney tissue was homogenized in lysis buffer (provided in kit) using a Minilys

Homogenizer (Precellys Inc.) for 30s at high speed. Samples were centrifuged at 13,000x *g* for 10min, and the supernatant was collected. 200µL of supernatant (containing standards or sample) was incubated with 600µL of thiobarbituric acid solution and incubated at 95˚C for 1hr then cooled on ice for 10min. Turbidity in samples was eliminated via passage through 0.2µm filters and loaded into a 96 well plate for quantification in a fluorescent reader (excitation 532nm; emission 553nm).

Levels of glutathione (reduced and oxidized forms) were assessed in homogenized tissues (~50mg) using commercial kits (ab138881; Abcam Inc.). Renal tissue was homogenized with a Minilys Homogenizer (Precellys Inc.) for 30s on high speed in phosphate buffered saline (PBS; pH 6.0) containing 0.5% (v/v) NP40. Samples were centrifuged (10min; 13,000x *g*) and supernatants were deproteinated by acidification with trichloroacetic acid using a commercially available kit as directed (ab204708; Abcam Inc.). Samples (1:20 dilution) were incubated with probes for GSH and GSSG as directed at room temperature for 1hr, and fluorescence intensity was quantified by spectrophotometry (excitation 490nm; emission 520nm).

Assessments on DNA for 8-hydroxy-2`-deoxyguanosine (8-OHdG) were conducted using commercially available kits (ab201734; Abcam Inc.). DNA was isolated from snap frozen tissue (~25mg) using the DNEasy blood & tissue kit per manufacturer directions (Qiagen Inc.). DNA concentration and purity were confirmed by A_{260}/A_{280} absorbance with a NanoDrop1000 spectrophotometer (Thermo Fisher Inc.). DNA samples were boiled for 5min, cooled on ice, and digested with 100U nuclease P1 (M0660S; New England BioLabs Canada) for every 100µg DNA at 37˚C for 15min. Following digestion, DNA was further digested with 1U alkaline phosphatase (M0371S; New England BioLabs Canada) per 100µg DNA at 37˚C for 15min. DNA samples were then boiled for 10min and placed on ice until use. Digested nucleosides (1-1.5µg/well) were assessed by ELISA in triplicate per manufacturer instructions and quantified by spectrophotometry (OD_{450}).

4.3.7 Statistical Analyses

For all data sets, *n* values reflect the number of offspring of each sex from separate litters (i.e. treated dams are the experimental unit, and any values derived from one litter are averaged and treated as a single unit). With the exception of caspase activity data, all data were analyzed by mixed-model or two-way ANOVA for the main effects of perinatal ID and offspring sex, and Sidak's *post hoc* tests were completed to assess differences between CTL and ID groups of each sex. For caspase activity assays, data are analyzed by unpaired *t*-test to minimize inter-assay variability (due to lack of internal standards accompanying the kits); thus, only intra-assay comparisons between CTL and ID offspring of the same sex were made. Data are presented as mean±SEM unless otherwise indicated. $P<0.05$ was considered significant. Grubb's test was used to identify statistical outliers, which were excluded from analyses as appropriate. All statistical analyses were conducted using GraphPad Prism 9.0 software.

4.4 Results

4.4.1 Growth Outcomes

The impacts of iron restriction prior to and throughout gestation on maternal outcomes in this model have been described in detail previously [159,165,253,308,309], and include anemia and impaired weight gain throughout pregnancy. The consequences of maternal iron restriction on offspring growth and hematological offspring parameters are summarized in **Table 4.2**. Perinatal ID offspring exhibit ~50% reductions in Hb levels on PD1 ($P<0.0001$), with no differences between the sexes. Perinatal ID male and female offspring were growth restricted at PD1 ($P<0.0001$), and male offspring are larger than their female littermates irrespective of perinatal treatment group ($P<0.0001$). Kidney weights from perinatal ID offspring were smaller than those from controls in both sexes ($P=0.001$) but were no longer different when normalized to bodyweight.

By PD28, Hb levels were no longer different between perinatal treatment groups, albeit female offspring tended to have slightly elevated levels regardless of perinatal group ($P=0.053$; **Table 4.2**). Offspring body weights on PD28 remained lower in perinatal ID offspring ($P<0.0001$), and male offspring remained larger than their female counterparts irrespective of treatment group ($P=0.0004$). At PD28 absolute kidney weights of perinatal ID offspring were smaller than control kidneys in both males and females ($P=0.0002$) but were larger when normalized to bodyweight ($P=0.0001$).

Table 4.2: Offspring Growth Outcomes & Characteristics.

Age	Parameter	Males		Females		P Values		
		CTL	ID	CTL	ID	ID	Sex	Int.
PD1	Hb (g/dL)	11.3 ±1.9	5.2 ± 0.9#	11.2 ± 2.0	5.4 ± 1.2#	<0.0001	0.81	0.59
	Body wt. (g)	6.91 ±0.38	5.41 ± 0.39#	6.30 ± 0.39	5.18 ± 0.31#	<0.0001	<0.0001	0.006
	Kidney wts. (mg)	76.2 ± 13.5	56.5 ± 8.3#	71.0 ± 11.6	54.1 ± 6.5*	0.001	0.04	0.63
	Kidney wt/ body wt. (mg/g)	10.8 ± 1.2	10.0 ± 1.3	11.2 ± 1.2	10.5 ± 0.9	0.14	0.13	0.92
PD28	Hb (g/dL)	10.0 ± 0.5	10.0 ± 0.8	10.4 ± 0.5	10.2 ± 0.9	0.70	0.05	0.52
	Body wt. (g)	113.0 ± 7.9	86.0 ± 11.2#	100.1 ± 5.5	78.7 ± 6.6#	<0.0001	0.0004	0.30
	Kidney wts. (g)	1.35 ± 0.08	1.14 ± 0.15#	1.20 ± 0.08	1.01 ± 0.08*	0.0002	0.0002	0.80
	Kidney wt/ body wt. (mg/g)	11.9 ± 0.4	13.3 ± 0.8#	12.0 ± 0.5	13.0 ± 0.7*	0.0001	0.80	0.34

Data are presented as mean±SD. n=8-9 for all measurements. Data was analyzed by mixed model ANOVA, where male and female offspring from the same litter were paired for analysis. * P<0.01 # P<0.001 vs CTL of the same sex. Control, CTL; iron deficiency, ID; interaction, int.; postnatal day, PD; weight, wt.

4.4.2 Cellular Senescence

SA-βGal activity was decreased by perinatal ID on PD1 (P<0.001; **Figure 4.1A**). Expression of *Tgfβ1* and *Tgfβ2*, which encode ligands that bind to transforming growth factor β receptors and induce developmental senescence via SMAD2/SMAD3 signaling, were not altered by perinatal ID or offspring sex (**Figure 4.2A** & **4.2B**). Expression of *Smad2* exhibited a significant interaction effect (P=0.03; **Figure 4.1B**), and expression was elevated in females versus males irrespective of perinatal group (P=0.008). No alterations were observed in *Smad3* expression (**Figure 4.1C**). Expression of *P21* on PD1 was induced by perinatal ID in offspring of both sexes (P=0.04; **Figure 4.1D**). Expression of *P16* was unchanged by perinatal ID in male offspring, whereas females exhibited reductions due to perinatal ID relative to high baseline expression in CTL offspring (P=0.006; **Figure 4.1E**).

In contrast to PD1, perinatal ID resulted in elevated cellular senescence, which was most prominent in female offspring on PD28. SA-βG activity was increased by both perinatal ID (P=0.002) female sex (P=0.01), the former effect being most prominent in the female perinatal ID group (**Figure 4.1F**). Expression of *Tgfβ1* and *Tgfβ2* was increased by perinatal ID (both P=0.04), with an overall increase in *Tgfβ2* due to female sex (P=0.02; **Figure 4.2C** & **4.2D**). Neither *Smad2* or *P21* expression were altered by perinatal ID or offspring sex on PD28, whereas *Smad3* expression was increased in females (P=0.03; **Figure 4.1H**). Expression of *P16* was not detectable in any group on PD28 (**Figure 4.1J**).

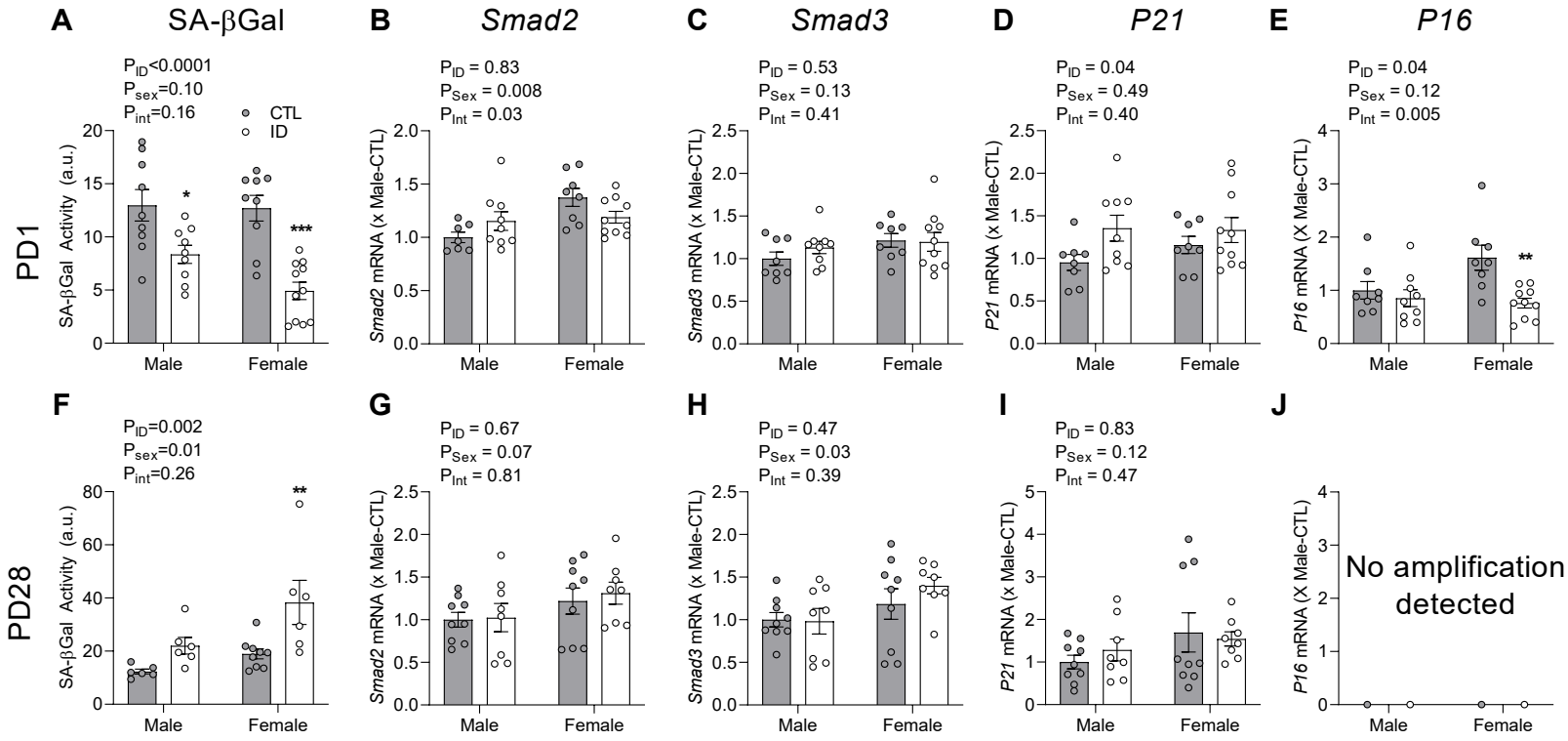

Figure 4.1: Renal cellular senescence. Markers of cellular senescence in kidneys from perinatal iron deficient (ID) and control (CTL) offspring on postnatal day (PD)1 and 28. **(A&F)** senescence-associated β-Galactosidase (SA-βGal) activity, **(B&G)** *Smad2* expression, (**C**&**H**) *Smad3* expression, **(D&I)** *P21* expression, **(E&J)** *P16* expression. Data are summarized by bar graphs showing mean±SEM. Data are analyzed by two-way or mixed model ANOVA and Sidak's *post hoc* test, where data from male and female littermates was paired when possible. * P<0.05, ** P<0.01, *** P<0.001 versus CTL of the same sex.

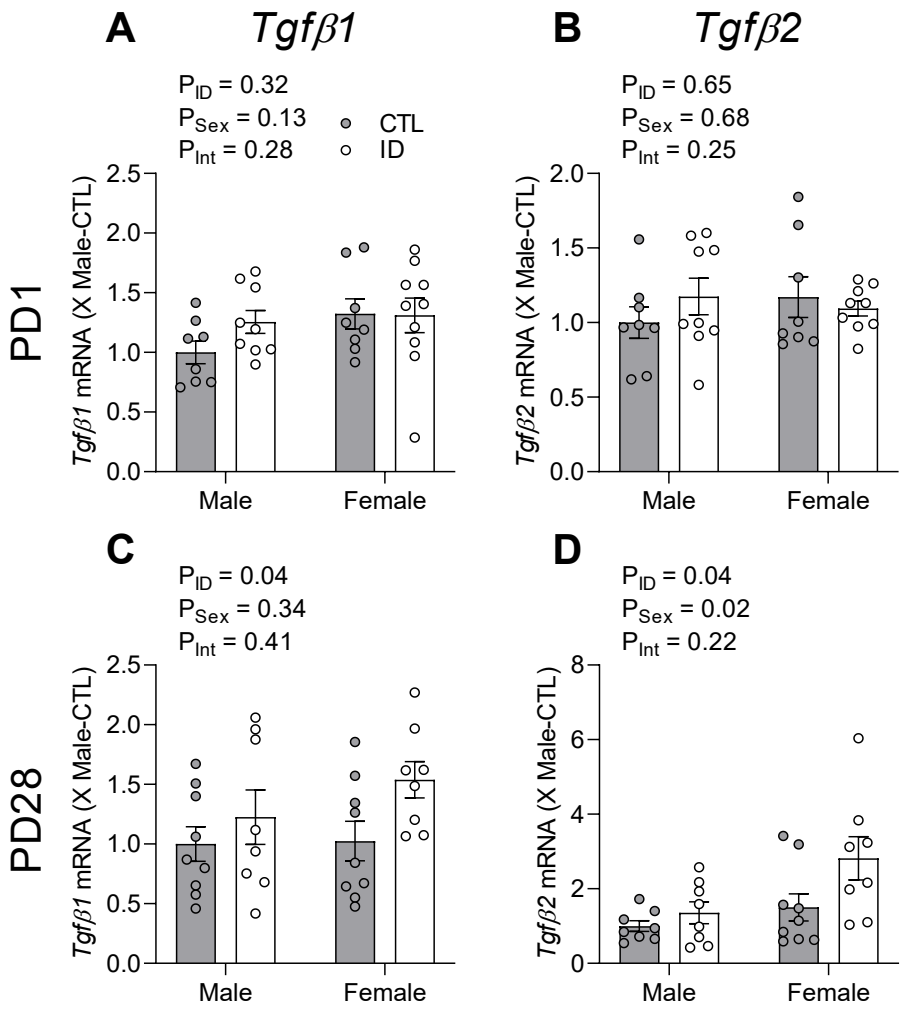

Figure 4.2: Transforming growth factor expression. Expression of (**A**&C) *Tgfβ1* and (**B**&**D**) *Tgfβ2* in kidneys from perinatal iron deficient (ID) and control (CTL) offspring on postnatal day (PD)1 and 28. Data are summarized by bar graphs showing mean±SEM. Data are analyzed by two-way or mixed model ANOVA and Sidak's *post hoc* test, where data from male and female littermates was paired when possible.

4.4.3 Apoptosis

On PD1, male but not female perinatal ID offspring exhibited enhanced caspase 3 activity (P=0.009; **Figure 4.3A**), despite no differences in caspase 9 activity between groups (**Figure 4.3B**). Perinatal ID did not alter expression of *P53* on PD1, although expression was increased in females versus males irrespective of perinatal treatment group (P=0.003; **Figure 4.3C**). Expression of apoptosis mediators, such as *Bcl2, Bax, Bad*, and *Cas3* were not altered by perinatal ID or offspring sex (**Figure 4.4A-D**).

On PD28, no alterations in either caspase 3 or caspase 9 activities were observed due to perinatal ID (**Figure 4.3D & E**). Similarly, no alterations in expression of *P53* (**Figure 4.3F**), nor *Bcl2*, *Bax*, *Bad,* or *Cas3* were observed due to either perinatal ID or offspring sex (**Figure 4.4E-H**).

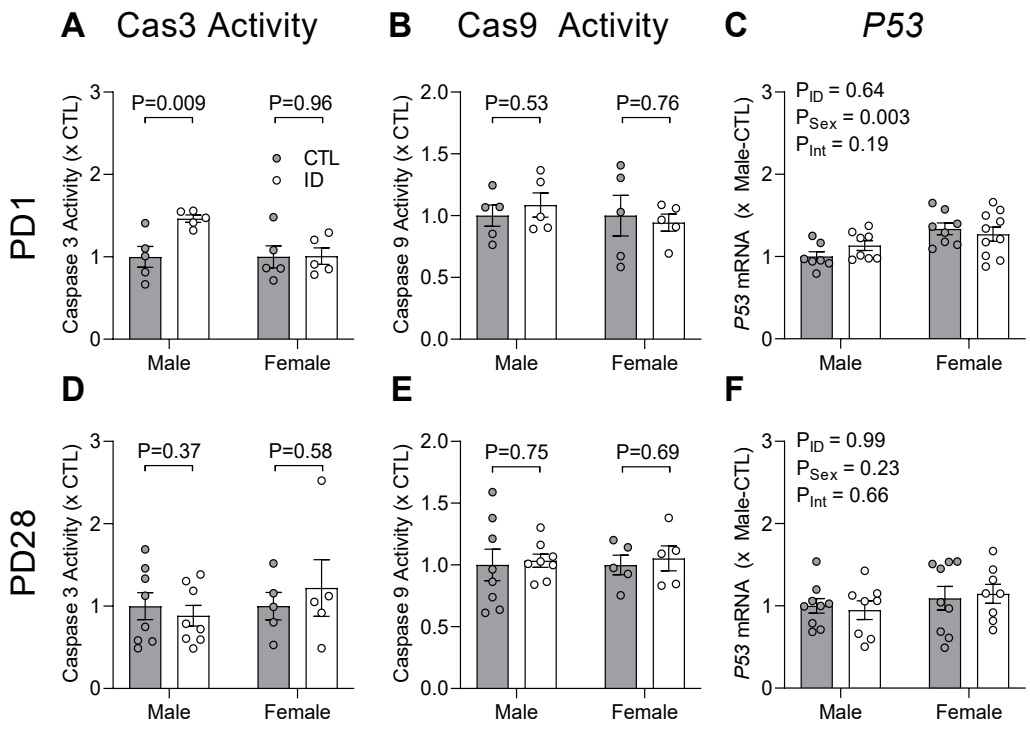

Figure 4.3: Renal apoptosis mediators. Markers of apoptosis in kidneys from perinatal iron deficient (ID) and control (CTL) offspring on postnatal day (PD)1 and 28. (**A**&**D**) Caspase 3 activity, (**B**&**E**) Caspase 9 activity, (**C**&**F**) *P53* expression. Data are summarized by bar graphs showing mean±SEM. Data are analyzed by two-way or mixed model ANOVA and Sidak's *post hoc* test (where data from male and female littermates was paired when possible), or by unpaired *t*-test (see statistical analyses section of methods).

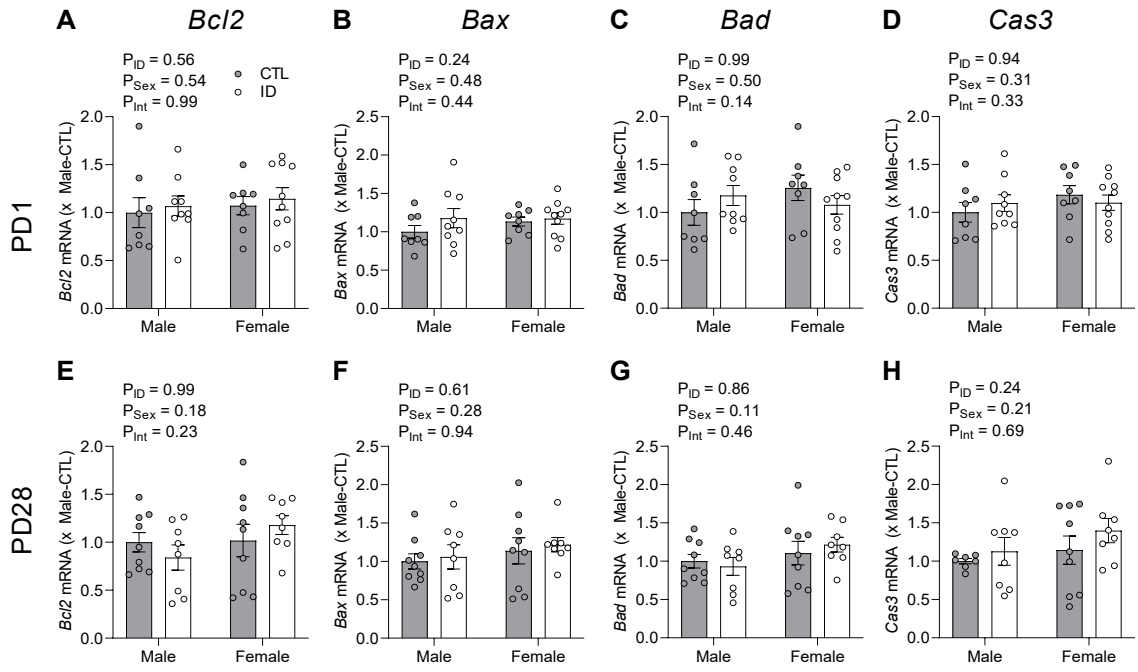

Figure 4.4: Renal apoptosis regulation. Mediators/markers of apoptosis in kidneys from perinatal iron deficient (ID) and control (CTL) offspring on postnatal day (PD)1 and 28. (**A**&**E**) *Bcl2* expression, (**B**&**F**) *Bax* expression, (**C**&**G**) *Bad* expression, (**D**&**H**) *Cas3* expression. Data are summarized by bar graphs showing mean±SEM. Data are analyzed by two-way or mixed model ANOVA and Sidak's *post hoc* test, where data from male and female littermates was paired when possible.

4.4.4 Autophagy

On PD1, reductions in the ratio of LC3-I:LC3-II protein were observed due to both perinatal ID (P=0.03) and female sex (P=0.009; **Figure 4.5A**). However, no alterations in other autophagy mediators, such as *P62*, *Tfeb*, or *Zkscan3* were observed due to either perinatal ID or offspring sex (**Figure 4.5B-D**). On PD28, no alterations in LC3 protein ratios or autophagic mediators were observed due to either perinatal ID or offspring sex (**Figure 4.5E-H**).

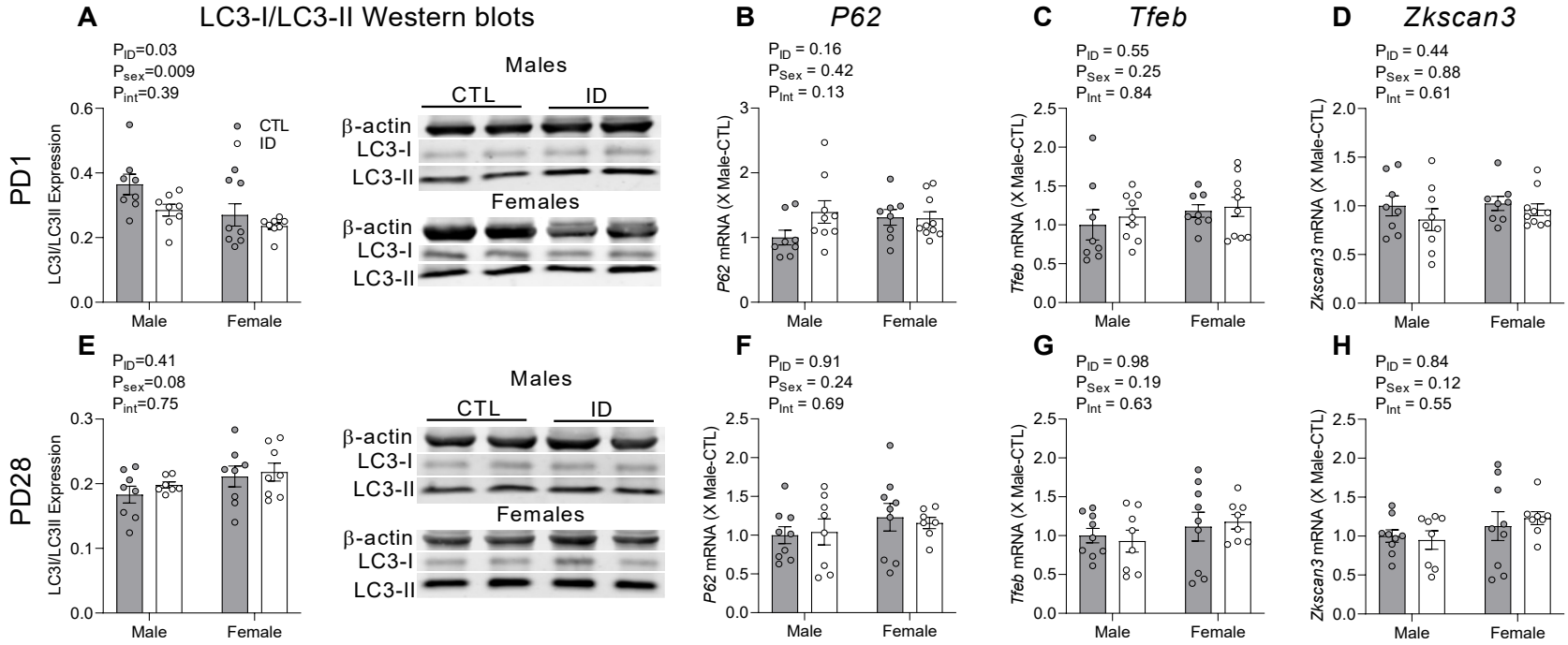

Figure 4.5: Renal autophagy. Markers of autophagy in kidneys from perinatal iron deficient (ID) and control (CTL) offspring on postnatal day (PD)1 and 28. (**A**&**E**) Ratio of LC3-I:LC3-II protein levels with representative images, (**B**&**F**) *P62* expression, (**C**&**G**) *Tfeb* expression, (**D**&**H**) *Zkscan3* expression. Data are summarized by bar graphs showing mean±SEM. Data are analyzed by two-way or mixed model ANOVA and Sidak's *post hoc* test, where data from male and female littermates was paired when possible.

4.4.5 Oxidative Stress

Perinatal ID resulted in changes in oxidant status on PD1, and many of these differences resolved by PD28. MDA levels were reduced due to perinatal ID in male and female offspring on PD1 (P=0.02; **Figure 4.6A**). Total cellular glutathione levels were reduced by perinatal ID in male, but not female, offspring on PD1 (P=0.01; **Figure 4.6B**). Interestingly, the ratios of reduced to oxidized glutathione (GSH:GSSG) were not altered by perinatal ID, albeit lower ratios were observed in female offspring regardless of perinatal group (P=0.04; **Figure 4.6C**). 8-OHdG, a marker of DNA oxidation, was not altered by perinatal ID on PD1, albeit females tended to show higher oxidant damage to their DNA irrespective of perinatal treatment group (P=0.046; **Figure 4.6D**). Expression of *P66shc*, a trigger of apoptosis and indicator of oxidative stress, did not vary due to perinatal ID or offspring sex on PD1 (**Figure 4.6E**).

On PD28, MDA levels were increased by perinatal ID in male, but not female, offspring (P=0.03; **Figure 4.6F**). An interaction effect was observed for total glutathione levels in PD28 offspring (P=0.05), wherein perinatal ID increased levels in males but decreased them in females (**Figure 4.6G**). Despite differences in total glutathione levels, GSH:GSSG ratios were not altered by either perinatal ID or offspring sex on PD28 (**Figure 4.6H**). Neither 8-OHdG levels or expression of *P66shc* were altered in PD28 offspring (**Figure 4.6I** & **J**).

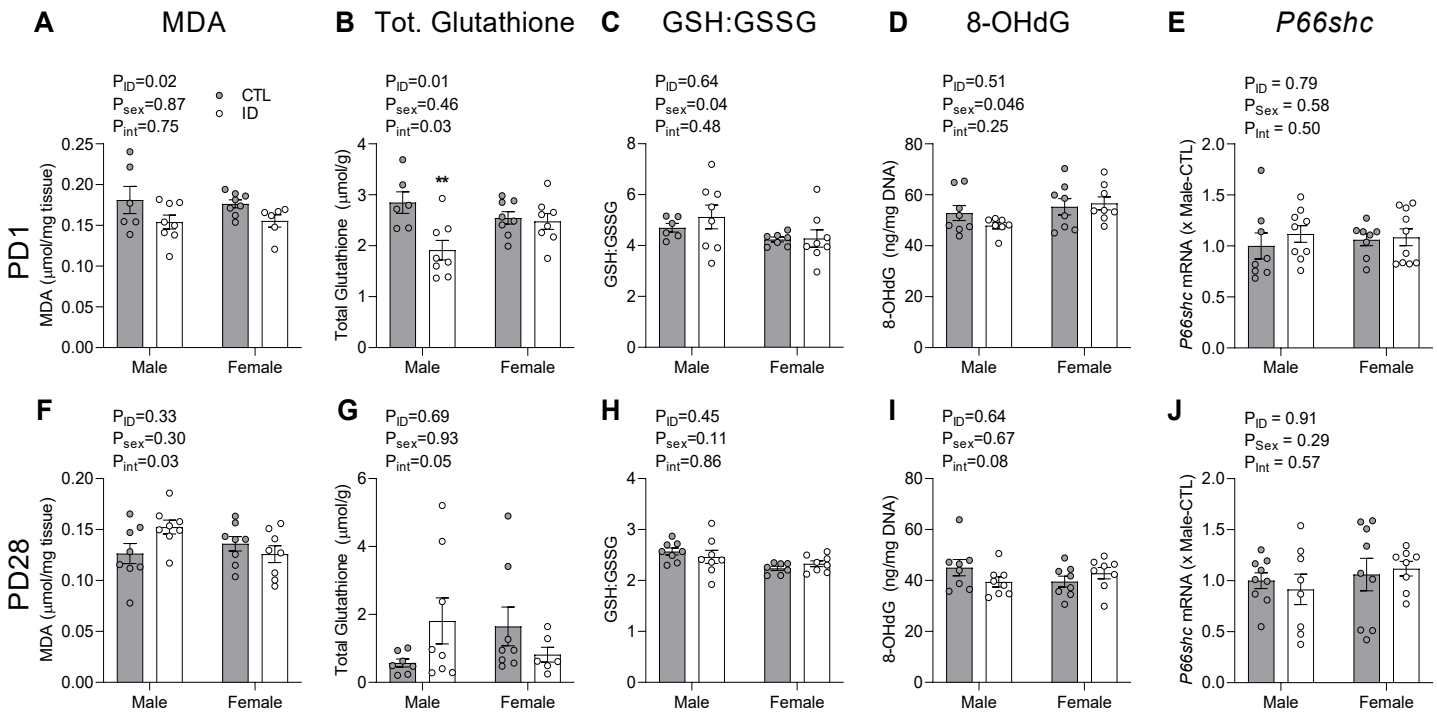

Figure 4.6: Renal oxidative stress. Oxidative stress measurements in kidneys from perinatal iron deficient (ID) and control (CTL) offspring on postnatal day (PD)1 and 28. **(A&F)** levels of lipid peroxidation product malondialdehyde (MDA), **(B&G)** Total glutathione (GSH+GSSG) concentration, (**C&H**) Ratio of GSH:GSSG, **(D&I)** Levels of DNA damage marker 8-OHdG, **(E&J)** Expression of *P66shc*. Data are summarized by bar graphs showing mean±SEM. Data are analyzed by two-way or mixed model ANOVA and Sidak's *post hoc* test, where data from male and female littermates was paired when possible. ** denotes P<0.01 versus CTL of the same sex. Reduced glutathione, GSH; oxidized glutathione, GSSG.

4.4.6 Antioxidant Defenses

On PD1, expression of both superoxide dismutase *(Sod)1* and *Sod2* exhibited an interaction effect in which perinatal ID increased expression versus controls in males, whereas the opposite effect was observed in females (both P<0.01; **Figure 4.7A** & **B**). Glutathione reductase (*Gsr*) exhibited an interaction effect (P<0.001), where perinatal ID resulted in an increase in expression in males and a decrease in females (**Figure 4.7C**). No alterations were observed in the expression of glutathione peroxidase 1 (*Gpx-1*) or catalase (*Cat*) on PD1 (**Figure 4.7D** & **E**). Neither offspring sex nor perinatal group altered expression of glutathione synthetic enzymes, including glutathione synthetase (*Gss*), glutamate-cysteine ligase catalytic subunit (*Gclc*), or glutamate-cysteine ligase regulatory subunit (*Gclm*; **Figure 4.8A-C**).

On PD28 an interaction effect was observed for expression of *Sod1*, wherein expression was decreased by perinatal ID in males but increased in females (P=0.03; **Figure 4.7F**). Neither *Sod2*, *Gsr, Gpx-1,* or *Cat* expression were altered by perinatal ID or offspring sex (**Figure 4.7G-J**). Similarly, neither perinatal group or offspring sex altered expression of glutathione synthetic enzymes *Gss, Gclc, or Gclm* (**Figure 4.8D-F**).

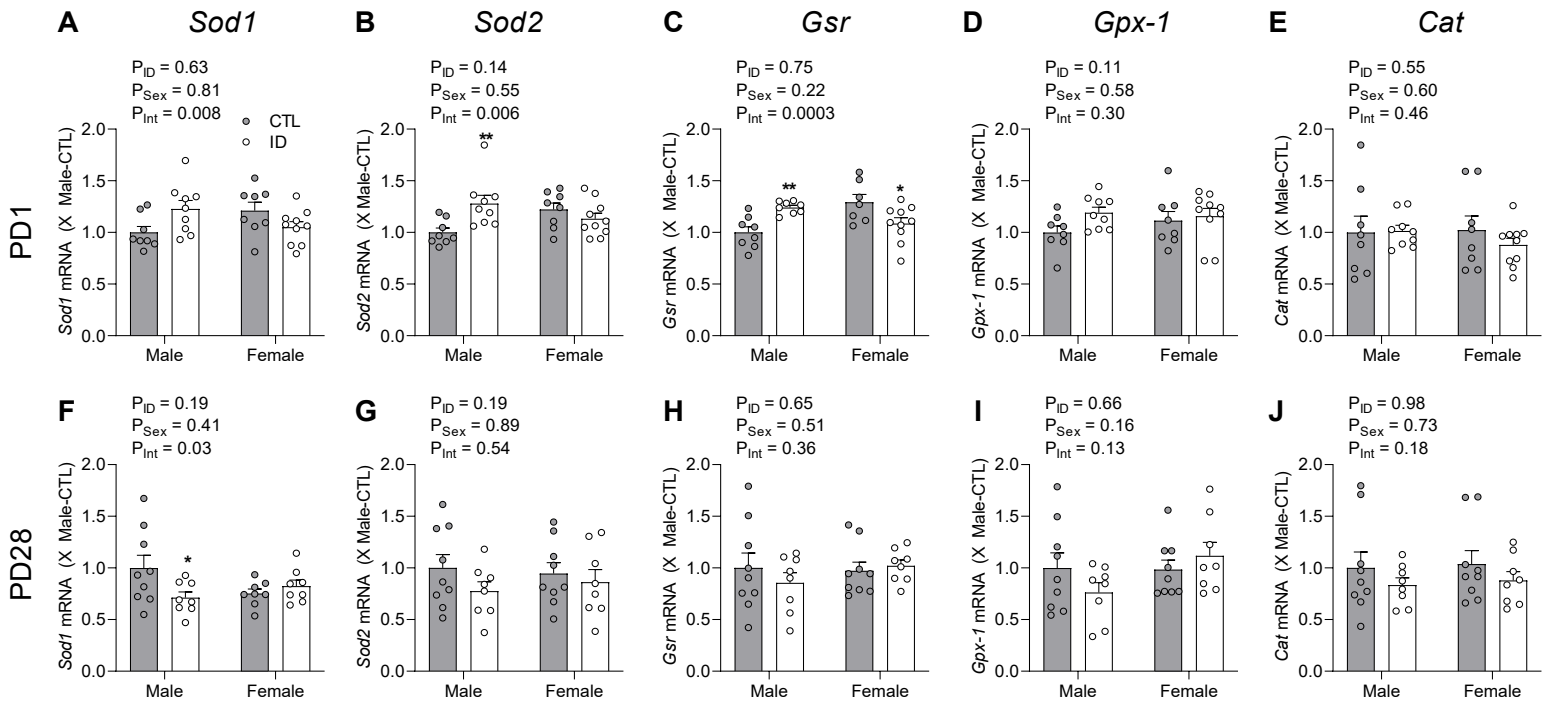

Figure 4.7: Renal antioxidant enzyme expression. RT-qPCR in kidneys from perinatal iron deficient (ID) and control (CTL) offspring on postnatal day (PD)1 and 28. **(A&F)** Superoxide dismutase (*Sod*)1 expression, **(B&G)** *Sod2* expression, (**C**&**H**) Glutathione reductase (*Gsr*) expression, **(D&I)** Glutathione peroxidase (*Gpx-1*) expression, **(E&J)** catalase (*Cat*) expression. Data are summarized by bar graphs showing mean±SEM. Data are analyzed by two-way or mixed model ANOVA and Sidak's *post hoc* test, where data from male and female littermates was paired when possible. * P<0.05, ** P<0.01 versus CTL of the same sex.

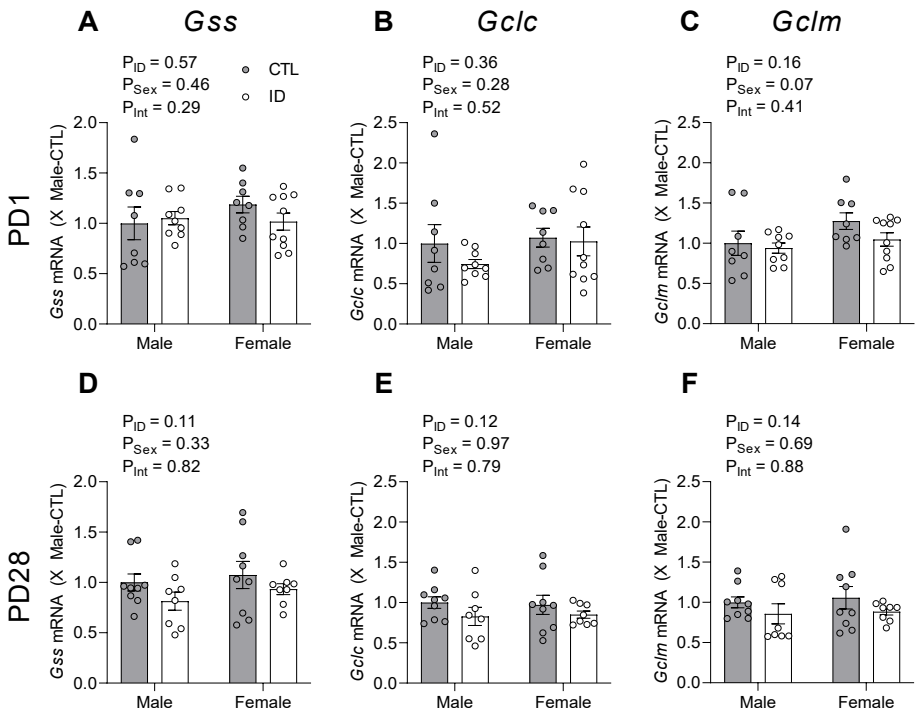

Figure 4.8: Expression of glutathione synthetic enzymes. RT-qPCR in kidneys from perinatal iron deficient (ID) and control (CTL) offspring on postnatal day (PD)1 and 28. (**A**&**D**) *Gss* expression, (**B**&**E**) *Gclc* expression, (**C**&**F**) *Gclm* expression. Data are summarized by bar graphs showing mean±SEM. Data are analyzed by two-way or mixed model ANOVA and Sidak's *post hoc* test, where data from male and female littermates was paired when possible.

4.5 Discussion

In this study we investigated the impact of perinatal ID on patterns of oxidative stress, cellular senescence, and apoptosis in PD1 and PD28 offspring kidneys. While the PD1 timepoint serves as an immediate exposure to perinatal ID, PD28 was chosen because systemic iron status has largely normalized in offspring (as indicated by Hb levels) and renal maturation is largely complete. To summarize, we report that perinatal ID caused: (1) enhanced oxidative stress concomitant with reduced antioxidant capacity and an induction of antioxidant enzyme expression in male but not female offspring; (2) decreases in cellular senescence on PD1, despite upregulation of developmental senescence pathway constituents, followed by an increase in cellular senescence on PD28; (3) increased apoptosis and alterations in autophagic flux, particularly in male offspring, on PD1; and (4) increased relative kidney size in perinatal ID offspring by PD28. Together, these results suggest that altered cellular oxidant status differentially triggers compensatory mechanisms (i.e. induction of antioxidant defenses, apoptosis) in offspring of both sexes, which may extend into the postnatal period despite iron repletion. These mechanisms likely contribute to altered cellular patterning and development during a phase of rapid renal growth and maturation, leading to longstanding changes in kidney health and function over the lifespan.

Oxidative stress is likely a critical trigger for altering patterns of senescence and apoptosis during development. Iron is a critical co-factor for antioxidant enzyme function, as well as function of reduction-oxidation reactions processes for cellular energy production, which generate large amounts of reactive oxygen species [74]. Paradoxically, reductions in MDA formation were observed in perinatal ID offspring of both sexes on PD1 despite previous evidence of renal oxidative stress in male ID offspring at the end of gestation [165]. However, measures of lipid peroxidation in the context of ID are often contentious, with studies reporting reductions [312–314], increases [315,316], or no changes [317,318]. Iron is involved in generating hydroxyl and perhydroxyl radicals via the Haber-Weiss and Fenton reactions [62], which are responsible for lipid and DNA oxidative damage [319]. Therefore, ID is hypothesized to reduce lipid peroxidation

through decreasing formation of hydroxyl and perhydroxyl radicals, which therefore may not correlate with increases in other markers of oxidative stress, such as superoxide levels. Conversely, ID is thought to increase lipid peroxidation in some circumstances through increased accumulation of other transition metals (i.e. Cu) which can also catalyze such reactions, or by increased mitochondrial membrane fragility [67,315,320]. Similarly, the lack of DNA oxidation in perinatal ID offspring on PD1 may indicate a lack of iron for the formation of excess hydroxyl and perhydroxyl radicals, albeit antioxidant defenses may be capable of mitigating damage despite depletions of the glutathione observed in male perinatal ID offspring. Interestingly, our results indicate higher basal levels of DNA oxidation, reduced GSH:GSSG, and increased expression of *P53* and *P16* mediators in females versus males, suggesting the relative susceptibility of females to oxidative damage may be greater than previously thought. Following iron replenishment, enhanced lipid peroxidation in perinatal ID males on PD28 is further suggestive of oxidative damage occurring in these offspring throughout the developmental period. Consistent with previous studies in kidneys of both fetuses and adult offspring exposed to perinatal ID [165,309], female perinatal ID offspring do not exhibit altered levels of oxidative stress versus controls.

The striking differences in oxidative stress patterns between male and female offspring may underlie other sex specific differences observed in this model. Oxidative stress in the male offspring may trigger enhanced apoptosis [321], induction of antioxidant enzyme expression [207], and perturbations in autophagy [322]. One possible reason could be differential production of oxidant species between male and female offspring derived from mitochondrial function. Mitochondrial dysfunction has been observed in the kidneys of male but not female offspring exposed to perinatal ID [165,309], suggestive that oxidant production may be higher in males [323]. Alternatively, studies have shown that females tend to have higher antioxidant capacities than their male counterparts [324,325]. While our study suggests that female offspring may have higher levels of expression of key antioxidant enzymes such as *Sod1, Sod2,* and *Gsr* in CTL offspring, perinatal ID did not result in further increases. Although the oxidative stress in female perinatal ID

offspring may have been insufficient to trigger a transcriptional upregulation, other mechanisms are likely contributing to the apparent decreases in expression. For instance, perinatal ID may disrupt sex hormone signaling, resulting in a decrease in estrogen-stimulated expression of antioxidant defenses such as *Sod* [326]. Notwithstanding, the reduced ratio of GSH:GSSG and enhanced DNA oxidation in female offspring irrespective of perinatal treatment group suggests that higher antioxidant defenses in female offspring are not contributing to the sex differences observed herein and may actually be mitigating them.

To our knowledge, this study is the first to identify a decrease in renal cellular senescence due to a perinatal stressor. Pathologic hypoxia is known to inhibit cellular senescence [327,328], which occurs in the kidneys of perinatal ID offspring secondary to anemia *in utero* [164]. Although reductions due to cellular senescence were observed in both male and female offspring due to perinatal ID, the reduction in males may also be partially explained by inhibition of senescence via the induction of apoptosis [188]. Alternatively, knockout models examining the developmental senescence pathway exhibit compensatory increases in apoptosis [185,186], which may imply increased apoptosis is a consequence of reduced senescence rather than a cause. In contrast with our results, murine models of cigarette smoke exposure *in utero* exhibit enhanced oxidative stress and upregulated cellular senescence in the fetus [329], suggesting the etiology of perinatal ID extends beyond the effects of hypoxia and oxidative stress. The upregulation of *P21* expression observed due to perinatal ID on PD1 is consistent with enhanced signaling for senescence, albeit senescence remains lower overall. Cellular senescence may also be supressed by a lack of iron itself; senescent cells are known to accumulate vast amounts of iron [330], which would be highly detrimental to an organism with inadequate stores. While sufficient iron supply is not necessary for cellular senescence to occur (i.e. iron chelation does not prevent induction of cellular senescence in culture conditions) [330], it is possible this factor contributes to reducing senescence through an unknown evolutionary mechanism. More studies are needed to characterize the mechanisms underlying these changes.

In contrast to PD1, cellular senescence is enhanced in the kidneys of perinatal ID offspring on PD28. Our data may suggest the increase in senescence in perinatal ID offspring on PD28 is caused by an upregulation of the developmental pathway (i.e. increased *TGFβ1/TGFβ2*), as part of a 'catch-up' for a delayed developmental process. Indeed, recent studies have shown nephrogenesis and nephron maturation is delayed by iron deficiency on PD15, whereas morphologic features were similar by PD30 [216]. Therefore, enhanced senescence at PD28 may indicate delayed maturation following normalization of iron status. Indeed, in a model of maternal protein restriction during gestation, offspring kidneys at the time of weaning exhibited increased expression of cellular senescence mediators [228]. The increase in relative size of the kidneys in perinatal ID offspring by PD28 also reflects catch-up growth within the kidney, albeit the extent to which it may induce or contribute to increased senescence in otherwise healthy developing kidney tissues requires further investigation. Further supporting the potential role of transiently upregulated developmental senescence in catch-up growth, markers of renal senescence are not altered in offspring at 4 months of age in a model of prenatal hypoxia [331]. The enhanced senescence on PD28 may represent a response to cellular stress, though low levels of oxidative stress (especially in perinatal ID females), undetectable *P16* expression, and a lack of perturbation in LC3-II: LC3-I suggest this this is unlikely [330]. More work is needed to understand how developmental senescence may underlie these changes. In particular, the reason why females see the largest upregulation in senescence on PD28 while exhibiting no alterations in apoptosis on PD1 must be investigated further.

Consistent with elevated DNA oxidation, we observed transcription of *P53* was elevated in female versus male offspring on PD1. Transcription of *P53* occurs primarily in the S-phase of the cell cycle as a protective mechanism against DNA damage during the replication process [332]. As such, higher expression of *P53* may explain why female perinatal ID offspring did not exhibit elevated levels of apoptosis on PD1 like their male littermates. Elevation of *P21* expression due to perinatal ID in both male and female PD1 offspring does suggest activation of *P53* activity as a transcription factor in both sexes,

albeit apoptosis does not appear negatively regulated by *P21* in males to the same extent [188]. Both ID and iron excess are known to cause genomic instability [333], and are associated with increased cancer risk [334]. Elevated levels of *P53* in female offspring coinciding with subtly higher basal levels of DNA oxidation may decrease susceptibility to further DNA damage associated cellular dysfunction and death. The cellular regulation regarding how apoptosis and senescence are triggered in both male and female offspring must be studied further in the context of ID.

In summary, we have shown that altered cellular senescence appears central to renal pathology observed adult perinatal ID offspring. Importantly, we have shown that male and female offspring exhibit differential levels of baseline antioxidant capacities and oxidant levels (as indicated by GSH:GSSG and DNA oxidation), and that their responses to further induction of oxidative stress appear divergent. In male offspring, the combination of decreased cellular senescence concomitant with enhanced apoptosis likely underlies future deficiencies in renal function. Although female offspring exhibit largely normal renal health and function in later life [309], more work is needed to understand how perinatal ID impacts renal development in both sexes.

Funding

A.G.W. held a Canadian Institutes of Health Research (CIHR) Vanier Scholarship and an Alberta Innovates Graduate Studentship. S.L.B. is a Canada Research Chair in Developmental and Integrative Pharmacology (Tier 2). Project funding was provided by a CIHR Operating Grant (MOP142396) and a Heart and Stroke Foundation of Canada Bridge Grant (G-20-0029380) held by S.L.B.

Acknowledgements

The authors are indebted to the University of Alberta Cardiovascular Research Centre for the use of their Roche Lightcycler 480.

Author Contributions

A.G.W., R.D.C., and S.L.B. designed the research; A.G.W., R.L.M., C.D.H., and R.M.N.N. performed the experiments; A.G.W. and R.L.M. analyzed the data; A.G.W. and S.L.B. wrote the manuscript. A.G.W., R.D.C., and S.L.B. critically reviewed the manuscript.

Chapter 5

Perinatal Iron Deficiency Causes Sex-Dependent Alterations in Renal Retinoic Acid Signaling and Nephrogenesis

Andrew G. Woodman[1,2,3*], Richard L. Mah[1,3*], Samantha Kinney[1,4], Claudia D. Holody[1,2,5], Ronan M.N. Noble[1,2,5], Robin D. Clugston[1,4], Stephane L. Bourque[1,2,3,5,6]

Women and Children's Health Research Institute, University of Alberta[1]

Cardiovascular Research Centre, University of Alberta[2]

Department of Pharmacology, University of Alberta[3]

Department of Physiology, University of Alberta[4]

Department of Pediatrics, University of Alberta[5]

Department of Anesthesiology and Pain Medicine, University of Alberta[6]

*Denotes equal contribution

UNDER PREPARATION FOR PUBLICATION

5.1 Abstract

Long-term alterations in kidney structure and function have been observed in offspring exposed to perinatal stressors such as iron deficiency (ID). ID is known to influence vitamin A metabolism, a critical mediator of nephrogenic signaling pathways. Here, we sought to assess how perinatal ID alters renal vitamin A metabolism and nephrogenic signaling in the developing kidney. Pregnant Sprague Dawley rats were fed either an iron-restricted or -replete diet throughout gestation, and offspring were studied on postnatal day (PD)1 and 28. Maternal iron restriction results in neonatal anemia, low birth weight, and reduced renal retinoid levels on PD1. Nephron endowment was reduced 21% in male perinatal ID offspring on PD28, whereas female nephron endowment was unaffected. Male perinatal ID offspring exhibit sex-specific enhancements of retinoic acid pathway signaling on PD1, coinciding with elevations in mediators of the fibroblast growth factor, and wingless-related integration site pathways, despite concomitant elevations in the antagonistic bone morphogenetic protein pathway. In contrast, female perinatal ID offspring exhibit reductions in the expression of retinoic acid receptors, bone morphogenetic protein receptors, and fibroblast growth factor receptors on PD1. Finally, expression of angiogenic factors such as vascular endothelial growth factor A and renin were elevated by perinatal ID on PD1. By PD28, renal retinoid levels were elevated in perinatal ID offspring, coinciding with enhanced signaling through the retinoic acid pathway in both sexes, albeit this effect was most pronounced in females. Furthermore, female perinatal ID offspring exhibited reduced plasma retinol concentrations, as well as sex-specific elevations in renal expression of renin. Perinatal ID was shown to elevate expression of platelet derived growth factor β and decrease expression of angiotensinogen on PD28 in offspring of both sexes, albeit no differences in vascular density were observed on PD28 In summary, perinatal ID was shown to reduce nephron endowment in male offspring, primarily through sex-specific perturbations in the pathways studied herein.

5.2 Introduction

The rapidly growing fetus and neonate are uniquely susceptible to injury from sub-optimal environments, such that stressors during early development can influence life-long functional capacity of many organ systems [143]. The kidney is one such organ. The total number of nephrons, the functional units of the kidney, is set at birth in humans and shortly thereafter in rodents [175]. Nephron endowment at birth is thought to contribute to functional capacity of the kidney, and indeed an inverse relationship between nephron number and the risk of hypertension and chronic kidney disease in later life has been described. Commonly referred to as the Brenner hypothesis, the theory posits that a reduced nephron complement in early life can result in glomerular hyperfiltration, resulting in renal damage and blood pressure dysregulation, thus perpetuating a cycle of progressive cardio-renal injury [335]. The number of nephrons a person is born with is determined both by genetic and environmental factors, and thus may be affected by adversity during these periods of development [150]. In addition to gestational hypoxia [218], micro- and macronutrient deficiencies during early development have been associated with reductions in nephron endowment [215,219,221,305].

Iron deficiency (ID) is the most common nutritional deficiency worldwide, which has a high incidence in pregnancy due to blood volume expansion and increased iron demands of the growing fetus and placenta [4,21]. While ID during pregnancy has long been recognized as a risk factor for pre-term birth, low birth weight, and neonatal mortality [44], the consequences of perinatal ID on cardiovascular function persist throughout life. Perinatal ID has been associated with hypertension, salt sensitivity of blood pressure, and renal dysfunction in later life [159,230,309]. Similar to many models of perinatal stress, perinatal ID also affects nephron endowment in offspring [214–216], and the long-term cardiovascular consequences are consistent with those predicted by the Brenner hypothesis [170,212,308,309].

Despite these links, it remains unclear how perinatal ID alters nephrons growth and maturation during development. Renal development, and the determination of nephron number, largely depends on the complex processes governed by interactions

between the branching ureteric bud and the metanephric mesenchyme [177]. The branching ureteric bud forms the collecting ducts, upon which glomeruli, tubular structures, and the vascular system of the kidney develop. Numerous signaling processes are important in dictating nephron endowment, including the wingless-related integration site (WNT), fibroblast growth factor (FGF), bone morphogenetic protein (BMP), and the retinoic acid and receptor tyrosine kinase (RA-RET) pathways [177]. Moreover, concurrent vascular development is modulated by these and other pathways, including the renin angiotensin system (RAS) and vascular endothelial growth factor (VEGF) [282,336].

In this study, we assessed numerous signalling pathways through which nephron endowment is established in male and female ID offspring. We hypothesized that perinatal ID disrupts offspring nephrogenic signaling, thereby contributing to a reduction in nephron endowment.

5.3 Methods

5.3.1 Animals and Treatments

The studies described herein were approved by the University of Alberta Animal Care Committee (reference number AUP974) in accordance with the guidelines established by the Canadian Council of Animal Care. Thirty-seven experimentally naïve and nulliparous female Sprague Dawley rats (initially 6 weeks of age) were purchased from Charles River (Saint-Constant, QC, Canada) and housed at the University of Alberta animal care facility under a 12h light/dark cycle and ambient temperature of 23˚C. Rats were housed in wire top cages fitted with mesh filter tops, enriched with wooden blocks and shredded paper pucks. *Ad libitum* access to food and water was provided for all rats throughout the study.

Prior to and throughout gestation, female rats were fed AIN-93G purified diets (Research Diets Inc., New Brunswick, NJ, USA), which were identical in composition except for the amount of added ferric citrate; all purified diets used herein contained 4000 IU/kg vitamin A acetate. Rats allocated to the iron-restricted group were fed a diet low in iron (3 mg/kg iron; D03072501), whereas those in the control group were fed an iron-

replete diet control group (37 mg/kg iron; D10012G). Females were co-housed with age-matched males for breeding, and pregnancy was confirmed by the presence of sperm in a vaginal smear the following morning. Pregnant dams were single-housed during pregnancy, and those in the control group were maintained on the same diet throughout pregnancy, whereas the iron-restricted dams were fed a diet moderately low in iron (10 mg/kg iron; D15092501) for the duration of pregnancy. Maternal parameters such as Hb levels, body weight gain and food consumption were recorded weekly.

A subset of non-fasted pregnant dams (6 iron-restricted and 6 controls) were euthanized on gestational day (GD)21, one day prior to full term. Dams were anesthetized in isoflurane (3-5% in medical grade oxygen at 1L/min) and euthanized by exsanguination and subsequent excision of the heart. Maternal plasma and liver samples were collected for analysis. The remaining twenty-five dams (14 iron-restricted, 11 controls) and their offspring were studied postnatally. After giving birth, all dams were fed a standard rodent chow (5L0D; PicoLab, St. Louis, MO, USA), and all pups were weighed, and litters were standardized to 8 offspring (four males and four females). In cases where litters contained fewer than 4 males or 4 females, tissue collection was prioritized for a single time point only, thereby avoiding confounding effects of variable litter sizes.

For PD1 experiments, offspring were euthanized by decapitation within 12h of birth. Hemoglobin (Hb) levels were measured using a HemoCue 201+ system, and pup organs were quickly harvested, weighed, and snap frozen in liquid nitrogen. The remaining pups remained with their mothers until PD21, at which time they were weaned onto the standard rodent chow. At PD28, offspring were anesthetized in isoflurane (3-5% in medical grade oxygen at 1L/min) and euthanized by exsanguination and subsequent excision of the heart; tissues were quickly harvested, and snap-frozen in liquid nitrogen, or processed for nephron endowment assay (described below).

5.3.2 RT-qPCR Experiments

Offspring kidneys (~50mg) were homogenized in TRIzol reagent (Life Technologies, Carlsbad, CA) in two intervals of 30 seconds using a homogenizer (Percellys Minilys Tissue Homogenizer; Bertin Instruments, France) using 2 mL tubes containing ceramic beads. RNA extraction was performed with Qiagen RNeasy kit (Venlo, Netherlands). Briefly, homogenates in TRIzol were separated with chloroform and centrifuged at 12,000 g for 10 min at 4℃. The aqueous phase was sequentially purified in multiple spin columns at 17,000 g for 15 seconds with 70% ethanol, and proprietary buffers provided in the kit. RNA concentration and purity was assessed by absorbance at $A260_{nm}$ and $A280_{nm}$ with a NanoDrop1000 spectrophotometer (Thermo Fisher). Purified RNA was then reverse transcribed using the High Capacity cDNA Reverse Transcription Kit (Applied Biosystems, Cheshire, UK) according to manufacturer's instructions. All reactions contained ~2000 ng of RNA.

Gene sequences of interest were obtained from NCBI's Gene database (https://www.ncbi.nlm.nih.gov/gene). Primer sequences were designed with the LightCycler Probe Design Software 2.0 (Roche) and are shown in **Table 5.1**. Each qPCR reaction was carried out in duplicate in a 96- or 384-well optical reaction plate on a QuantStudio3 Real-Time PCR System (Applied Biosystems) or LightCycler 480 (Roche) with PowerUP SYBR Green Master Mix (Applied Biosystems), respectively. The thermal cycling conditions consisted of an initial step of 50°C for 120 s, 40 cycles of denaturation at 95°C for 15 s and annealing and extension steps at 60°C for 60 s. Where more than one transcript variant or isoform was found for a given gene, a primer suitable for all variants was used. The relative gene expression was calculated by comparing cycle thresholds using the following equation: relative gene expression$=2^{(\Delta Ctsample—\Delta Ctcontrol)}$ as previously described [311]. Expression of ribosomal 18s was used as the reference gene in the study and was validated to be uniformly expressed across all samples (data not shown).

Table 5.1: Primer sequences used for RT-qPCR

Gene (other names) [Gene ID]	Primer Sequence	
18s [100861533]	Fwd	CGG ACA GGA TTG ACA GAT TGA TAG C
	Rev	CGT TCG TTA TCG GAA TTA ACC AGA C
Agt [24179]	Fwd	CTG AGC AGT CCG TTC CTG TT
	Rev	AGG AGG CAT CAC ACC ACA TT
Aldh1a1 (Raldh1) [24188]	Fwd	GAG AGA GGA CGC TTG CTG AAC
	Rev	GCC TCC TAA ATC CGA CAA GTA CG
Aldh1a2 (Raldh2) [116676]	Fwd	ACA TGA GCC CAT CGG AGT
	Rev	GCA GGC TTG ATG ACC ACA GTG TTA
Aldh1a3 (Raldh3) [266603]	Fwd	CCA CAG TGG GAG CAG CAA
	Rev	CTC CTG GAG GCA GCT TCT TTA AC
Bmp4 [25296]	Fwd	CCC GGA TTA CAT GAG GGA TCT
	Rev	GGC TCT GCT GGC AGG AC
Bmpr1a (Alk3) [81507]	Fwd	TTA CAA CAT GGT GCC TAG TGA CCC
	Rev	ATT CAT CAC TGT TCC AGC GGT TAG A
Crabp1 [25061]	Fwd	CGA CCG CTC CTC AGC AGA
	Rev	TAC CGG CGA AGT TGG GC
Crabp2 [29563]	Fwd	GGA GCC GAG AAC TGA CCA AT
	Rev	GTT CTT GGG ACA TAG GCA CTC AC
Ctnnb1 (β-catenin) [25453]	Fwd	AGA ATG CCG TTC GCC TTC ATT A
	Rev	CGG GCA AGG TTT CGG ATC AA
Cyp26a1 [154985]	Fwd	ACC CAT GAC GTG GCA GAC
	Rev	GAA TGA AAC TGA ACC TGG AGG TGT
Cyp26b1 [312495]	Fwd	GAC GCC CTG GAC ATT CTC ATT G
	Rev	TGC TGG CAC TGG CCG TA
Cyp26c1 [308190]	Fwd	TCA GGC AGC TCG GAA GAC T
	Rev	CTC CAG GCG ACA AGA AGG TT
Fgf7 [29348]	Fwd	AGT CCA GAG CAG ACG GC
	Rev	ACA GTC TCC TCA CCC TTA TAT CCC
Fgf10 [25443]	Fwd	TTG GTG TCT TCC GTC CCT GT
	Rev	CTG GAG GTG ATT GTA GCT TCG C
Fgfr1 [79114]	Fwd	GCA CAT CGA GGT GAA TGG GAG TAA
	Rev	ATC CTC AAA GGA GAC ATT CCG TAG A
Fgfr2 [25022]	Fwd	CCA CCT TGA TGT TGT TGA GCG A
	Rev	CCT TGC AGA CAA ATT CTA CGT CCC
Fzd4 [64558]	Fwd	GCA GAT TCT GCC CTT ACT CAC G
	Rev	TAC AGC CTG GCT AGT CAG CTA C
Gdnf [25453]	Fwd	CGC CGG ACG GGA CTC TA
	Rev	GCG CTT CGA GAA GCC TCT TAC

Lrp6 [312781]	Fwd	TAT CCA CAG CCT TCG GAA CGT C
	Rev	ACC ATC TTC TTG TGC CTT TCG TAT
Pax2 [293992]	Fwd	CCT GGG CAG GTA CTA CGA G
	Rev	GTC GGG TTC TGT CGC TTG TAT
Pdgfb (Pdgfβ) [24628]	Fwd	GCC TGC AAG TGT GAG ACA GTA G
	Rev	CGA ACG GTC ACC CGA GTT T
Rara (Rarα) [24705]	Fwd	CCT GGA CAT CCT GAT TCT GCG
	Rev	AAG CCA GCG TTG TGC AT
Rarb (Rarβ) [24706]	Fwd	ACT TTC TCT GAT GGC CTT ACC CTA
	Rev	AGA AGA CCT GTT TCT GTG TCA TCC
Rarg (Rarγ) [685072]	Fwd	GGC ATG TCC AAG GAA GCT GTA AG
	Rev	CCT CTA ACT GTG GAC TCA GTT CGT A
Ren [24715]	Fwd	CTT TGA CAC GGG TTC AGC C
	Rev	AGC TAG AGG ATT CCG AGG AGT CAT A
Ret [24716]	Fwd	TGG AGC ACA CAC CCA ACG
	Rev	AGG ACT CGG CTC TCT GAG AT
Rxra (Rxrα) [25271]	Fwd	GAG CCC AAG ACT GAG ACA TAC G
	Rev	GCC CAC TCC ACA AGA GTG AAG
Sall1 [307740]	Fwd	GCA AGC GAA GCC TCA ACA TTT
	Rev	CGT GGG CAT CTT TGC TCT TAG T
Spry1 [294981]	Fwd	GCC TTC CCT TCG CAC CC
	Rev	CCA GGA GCC AAA GGC ACC TTA
Tcf21 [252856]	Fwd	CGA GGA GAT TCG TTT CCA AAC CG
	Rev	CAG CCA GGC TCA CAG TCA T
Vegfa (Vegfα) [83785]	Fwd	CCT TCT TAG AGA GGC CGA AGT C
	Rev	AGG GAT GGG TTT GTC GTG T
Wnt4 [84426]	Fwd	TGC AGC AGT GGA GAT CTG GAG AA
	Rev	GCT ACG CCA TAG GCG ATG T
Wnt5a [64566]	Fwd	GTC GGC AGA GGA CAG GAA CTA A
	Rev	CCA CTG CCT GTG TAT AAA TGC TTC A
Wnt7a [114850]	Fwd	GCC GCC TTC ACC TAT GCA ATT A
	Rev	CCC ACT TCC AGC CCT CG
Wnt9b [303586]	Fwd	AGG AAC CAC AGT GAC CCG A
	Rev	CTT CAG TGG GAA GCA GTT CTC AAT C
Wnt11 [140584]	Fwd	GTC AGG GCA GGG ATG GGT A
	Rev	CCA AGT TAG TGG TTC CAT GTG GTG
Wt1 [24883]	Fwd	CGG TGT CTT CCG AGG CAT T
	Rev	GCA CAC ATG AAA GGA CGC TTC T

5.3.3 Determination of Glomerular Number

Estimation of nephron endowment was determined by the technique of acid maceration, as described [337]. Briefly, the left kidney from each PD28 offspring was excised, decapsulated, and placed in phosphate-buffered saline (PBS). Each kidney was weighed, cut into ~2mm pieces, then digested in 5mL of 6M HCl at 37˚C for 2h. Following digestion, tissue solutions were poured into syringes and homogenized by passage through 18G and then 21G needles. Homogenates were then washed several times with PBS, and final volume was adjusted to 50mL, and incubated at 4˚C overnight. In a 6-well plate, 500µL of homogenate was mixed with 500µL of PBS in 3 wells, and the number of intact spherical glomeruli in each well was counted with an EVOS XL microscope under 20x magnification. Nephron endowment was estimated by multiplying the average number of glomeruli per well by 100.

5.3.4 Retinoid Levels

Liver, kidney, and plasma retinoid levels were analyzed by HPLC, according to previously described protocols [338]. Briefly, liver (~50mg) and kidney samples (~75mg) were homogenized in PBS and then extracted in hexane, whereas plasma samples (50-100µL) were directly extracted into hexane. Following extraction, hexane was evaporated, and the samples were redissolved in mobile phase (70% acetonitrile, 15% v/v methanol, and 15% v/v methylene chloride). Samples were analyzed with an Agilent 1200 HPLC system (Santa Clara, CA, USA) with a Zorbax Exclipse Plus C18 separating column (4.6 x 250mm, 5µm particle size). Peak absorbance at 325nm was measured with an Agilent diode array detector, and the area under the curve was used to calculate retinol and retinyl ester concentration, which factored in the recovery of the retinyl acetate internal standard. Liver retinol and retinyl ester values are expressed as a percentage of average male control values due to running samples over multiple separate runs, thereby minimizing inter-assay variability. Total tissue retinoid levels are calculated by addition of free retinol and the amount of retinol present as retinyl ester.

5.3.5 Determination of Vascular Density by Immunofluorescence

Kidneys were fixed and embedded as previously described [164]. Embedded tissues were prepared as 6μm sections. Slides were rehydrated and antigen retrieval was performed in sodium citrate buffer (10 mM sodium citrate, 0.05% Tween-20, pH 6.0) via microwaving on high until boiling (~80s), followed by a 30min cooling period. Slides were then washed in PBS and blocked in Tris-buffered saline with tween (TBST; 50mM Tris, 150mM NaCl, 0.05% Tween-20, pH 9.0) with bovine serum albumin (BSA; 1% w/v) and 10% v/v goat serum (ab7481, Abcam) for 1h at room temperature. Slides were incubated with CD34 antibody (ab81289, Abcam) diluted 1:200 (final concentration 2.75 μg/mL) in PBS containing 1% w/v BSA at 4˚C overnight in a humidified chamber. Slides were washed with PBS and incubated at room temperature with Goat Anti-Rabbit IgG FITC secondary antibody (ab6717, Abcam) diluted 1:200 (final concentration 100 μg/mL) in PBS for 1h. Slides were then washed, and subsequently mounted in Vectashield Antifade Mounting Medium containing DAPI. Slides were imaged on an Olympus XI81 Fluorescent Microscope at 20 X magnification using Olympus cellSens software. Quantification of the areas positive for staining was completed on ImageJ using the MaxEntropy algorithm [339]. The average area positive for CD34 staining, as a percentage of total area, was reported from 4 representative cortical images containing similar numbers of glomeruli from each animal.

5.3.6 Statistical Analyses

Data obtained from the same litter were averaged and treated as a single value; thus *n* values (individual data points within each graph) reflect the number of litters (i.e. treated dams). Data were analysed by mixed-model or two-way ANOVA for the effects of perinatal ID and offspring sex with Sidak's *post hoc* test; data sets were paired for analysis when possible (i.e. male and female offspring data from the same dam). Data are presented as mean ± SEM unless otherwise stated. All statistical analyses were conducted using GraphPad Prism 9.1 (GraphPad Software Inc, San Diego USA). Investigators were not blinded for analyses.

5.4 Results

5.4.1 Characteristics of Perinatal ID Model

We utilized our previously characterized model of perinatal ID [165,308,309], outcomes of which have been described in detail previously. Briefly, offspring Hb levels on PD1 were reduced by 49% by perinatal ID (P<0.001; **Table 5.2**), and body weights were reduced by ~19% (P<0.001; **Table 5.2**). Female offspring were smaller than males, irrespective of perinatal treatment group. Kidney weights on PD1 were also reduced by perinatal ID, albeit this effect was most pronounced in male offspring (P=0.004; **Table 5.2**). When normalized to body weight, kidney weights on PD1 were not altered by perinatal ID (**Table 5.2**).

By PD28, hemoglobin values of perinatal ID offspring largely normalized, albeit they remained lower than CTL offspring, particularly in males (P=0.002; **Table 5.2**). Male and female perinatal ID offspring remained growth restricted at PD28 (P<0.001; **Table 5.2**). Kidney weights of perinatal ID offspring remained lower than those of the larger-bodied CTL offspring on PD28 (P<0.001; **Table 5.2**). When normalized to body weights, relative kidney weights were not different between groups on PD28 (**Table 5.2**).

Table 5.2. Offspring outcomes on PD1 and PD28.

Timepoint	Parameter	CTL		ID		ANOVA P-Values		
		Male	Female	Male	Female	ID	Sex	Int.
PD1	Hb (g/dL)	11.1 ± 2.0	10.7 ± 2.4	5.5 ± 0.9 ***	5.7 ± 0.9 ***	<0.001	0.81	0.52
	Body weight (g)	7.10 ± 0.88	6.53 ± 0.60	5.64 ± 0.42 ***	5.37 ± 0.55 ***	<0.001	0.02	0.37
	Kidney weight (mg)	67.1 ± 6.1	62.9 ± 8.4	56.4 ± 8.6 *	56.3 ± 9.0	0.004	0.43	0.46
	Kidney/body weight (mg/g)	9.63 ± 0.69	9.82 ± 1.32	9.92 ± 1.32	10.54 ± 1.54	0.26	0.36	0.63
PD28	Hb (g/dL)	10.1 ± 0.3	10.4 ± 0.5	9.2 ± 1.1 *	9.8 ± 0.7	0.002	0.06	0.46
	Body weight (g)	111.4 ± 7.3	99.2 ± 6.1	76.1 ± 13.5 ***	71.5 ± 10.4 ***	<0.001	0.02	0.26
	Kidney weight (g)	1.31 ± 0.08	1.18 ± 0.10	0.95 ± 0.19 ***	0.87 ± 0.11 ***	<0.001	0.02	0.61
	Kidney/body weight (mg/g)	11.8 ± 0.4	11.9 ± 0.7	12.5 ± 1.0	12.0 ± 1.1	0.15	0.52	0.28

Data are analyzed by two-way ANOVA with *Sidak's* post-hoc test. * P<0.05 and *** P<0.001 vs. CTL of the same sex. *n*=7-13 for PD1 data, *n*=8-10 for PD28 data. Control, CTL; hemoglobin, Hb; interaction, int; iron deficient, ID; postnatal day, PD.

5.4.2 Renal Nephron Endowment & Vascular Density

Nephron endowment was assessed in PD28 offspring, a time at which total nephron number is established in rats, using an acid maceration technique [337]. Perinatal ID resulted in a 21% reduction in nephron endowment in male offspring ($P<0.001$), with no significant reduction observed in females (**Figure 5.1A**). Vascular density was assessed by staining for CD34, an endothelial cell marker, and was not altered by perinatal ID or offspring sex on PD28 (**Figure 5.1B & C**).

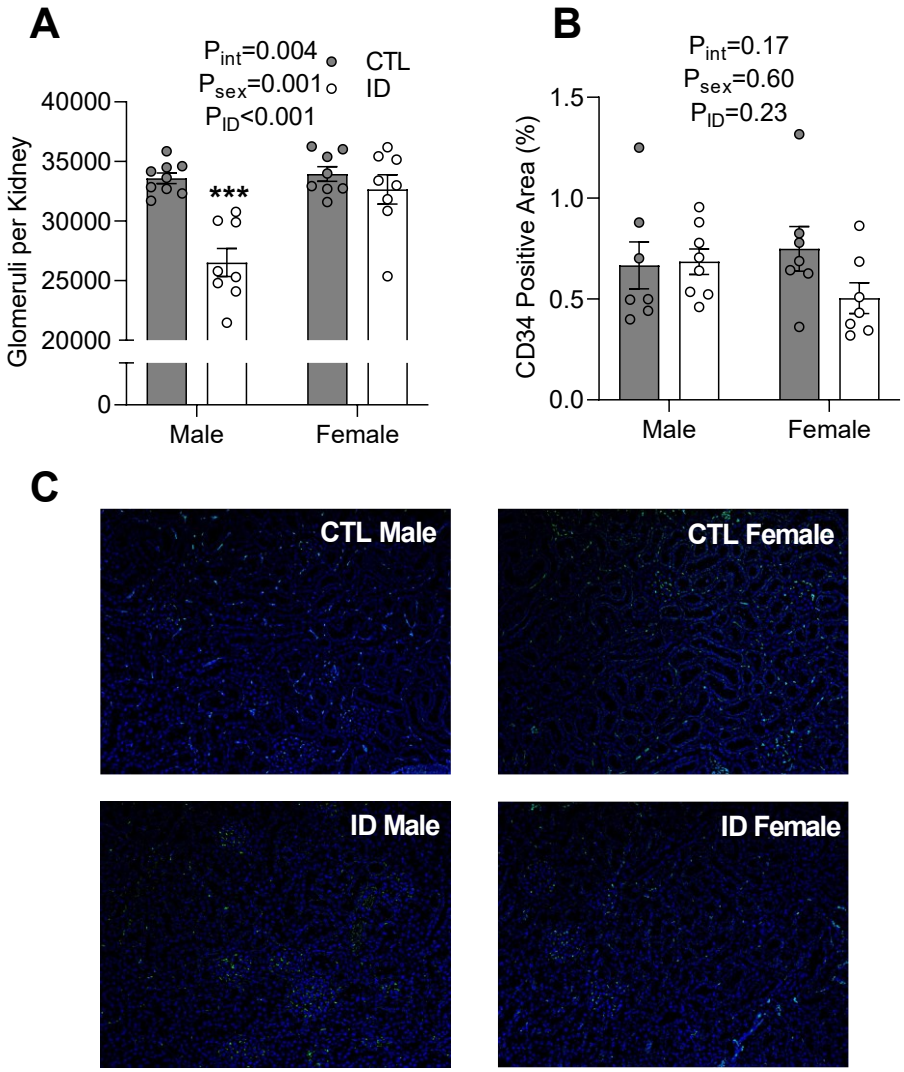

Figure 5.1: Offspring nephron endowment & Vascular Density. Postnatal day (PD)28 control (CTL) and perinatal iron deficient (ID) offspring (**A**) nephron endowment, (**B**) quantified vascular density, and (**C**) representative 20x images of CD34 staining (green) with DAPI nuclear counterstain (blue). Data are analyzed by two-way ANOVA with *Sidak's* post-hoc test. *** P<0.001 vs. CTL of the same sex.

5.4.3 Retinoid Status

One day prior to full term on GD21, a subset of dams were euthanized and their vitamin A status was assessed. Perinatal ID caused a 35% reduction in plasma retinol levels (P=0.02), although hepatic retinol levels were unchanged (P=0.59; **Figure 5.2A** & **B**). Levels of retinyl esters in maternal livers at term tended to increase due to perinatal ID, albeit this was not significant (P=0.08; **Figure 5.2C**).

In PD1 offspring, there were no differences in plasma retinol due to either sex or perinatal ID (**Figure 5.2D**). Liver retinol in PD1 offspring was not altered by perinatal ID, nor did they vary due to offspring sex (**Figure 5.2E**). Interestingly, retinyl esters in PD1 offspring livers were decreased by perinatal ID offspring of both sexes (P=0.03; **Figure 5.2F**). In the kidneys of PD1 offspring, retinol levels were reduced by perinatal ID (P=0.001), which was most pronounced in males (P=0.01; **Figure 5.3A**). Retinyl ester levels in kidneys of PD1 offspring were elevated by female sex (P=0.02; **Figure 5.3B**), with a significant reduction due to perinatal ID in females alone (P=0.047). Together, total retinoid levels (retinol and retinyl esters) in PD1 offspring kidneys were higher in females (P=0.02) and reduced by perinatal ID (P=0.005), albeit the latter effect was predominantly seen in females (P=0.02; **Figure 5.3C**).

At PD28, plasma retinol levels were reduced in female perinatal ID offspring, and was unchanged in males (P_{int}=0.049; **Figure 5.2G**). Hepatic retinol levels did not differ between perinatal treatment group nor offspring sex, nor did retinyl ester levels (**Figure 5.2H** & **I**). In the kidney, whereas retinol was decreased by perinatal ID at PD1, retinol was increased by perinatal ID in both male and female offspring on PD28 (P=0.0005; **Figure 5.3D**). Although renal retinyl ester levels were not different between groups on PD28, total renal retinoids were elevated by perinatal ID on PD28 (P=0.02; **Figure 5.3E**). Together, total retinoid levels in PD28 offspring kidneys were increased by perinatal ID (P=0.02), with no sex differences observed (**Figure 5.3F**).

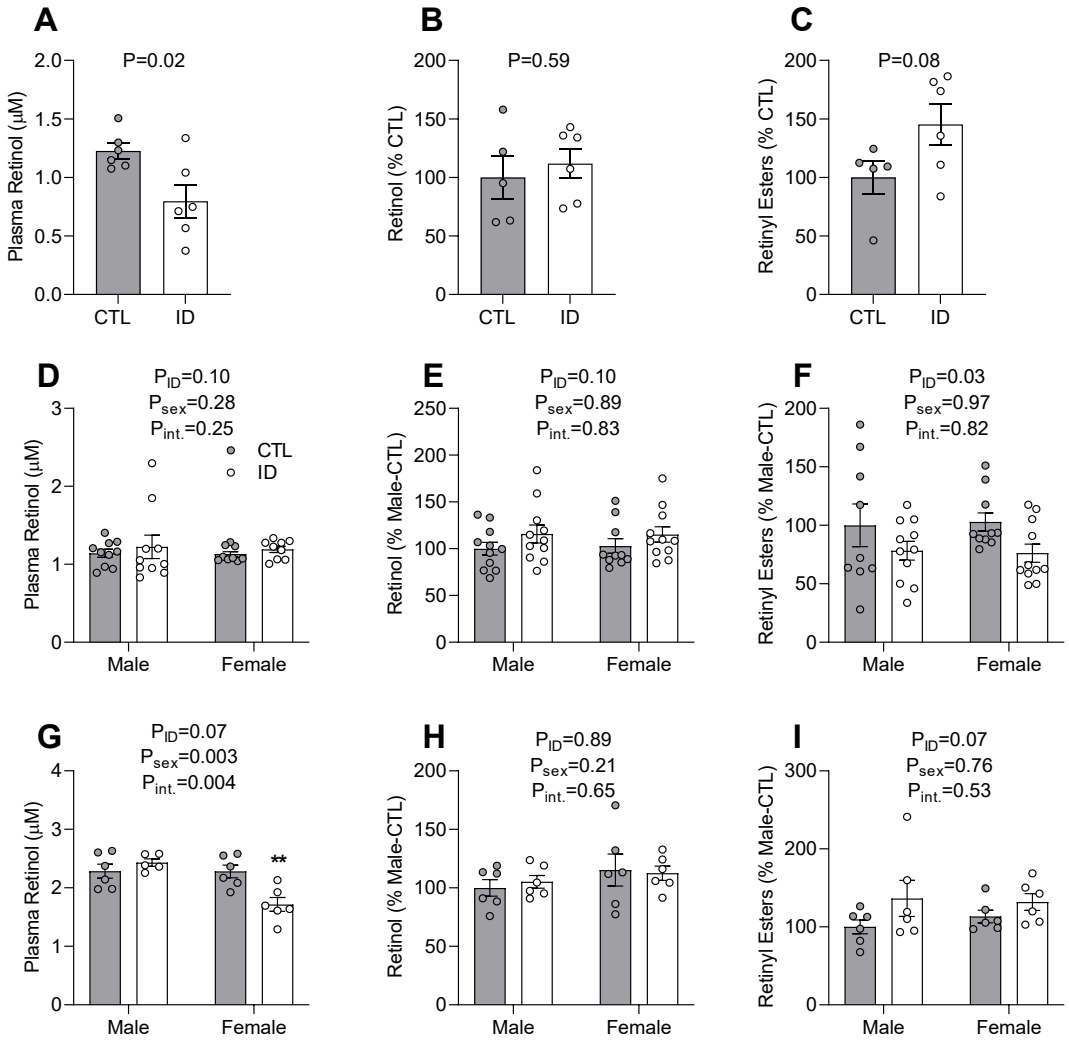

Figure 5.2: Systemic retinoid status in perinatal iron-deficient (ID) and control (CTL) group (**A-C**) dams on gestational day 21, (**D-F**) postnatal day (PD)1 offspring, and (**G-I**) PD28 offspring. (**A, D, G**) Plasma retinol concentration, (**B, E, H**) normalized liver retinol concentration (nmol retinol/g liver), (**C, F, I**) normalized liver retinyl ester concentration (nmol retinyl-ester/g liver). Data are analyzed by unpaired *t*-test or two-way ANOVA with *Sidak's* post-hoc test, as applicable. ** P<0.01 vs. CTL of the same sex.

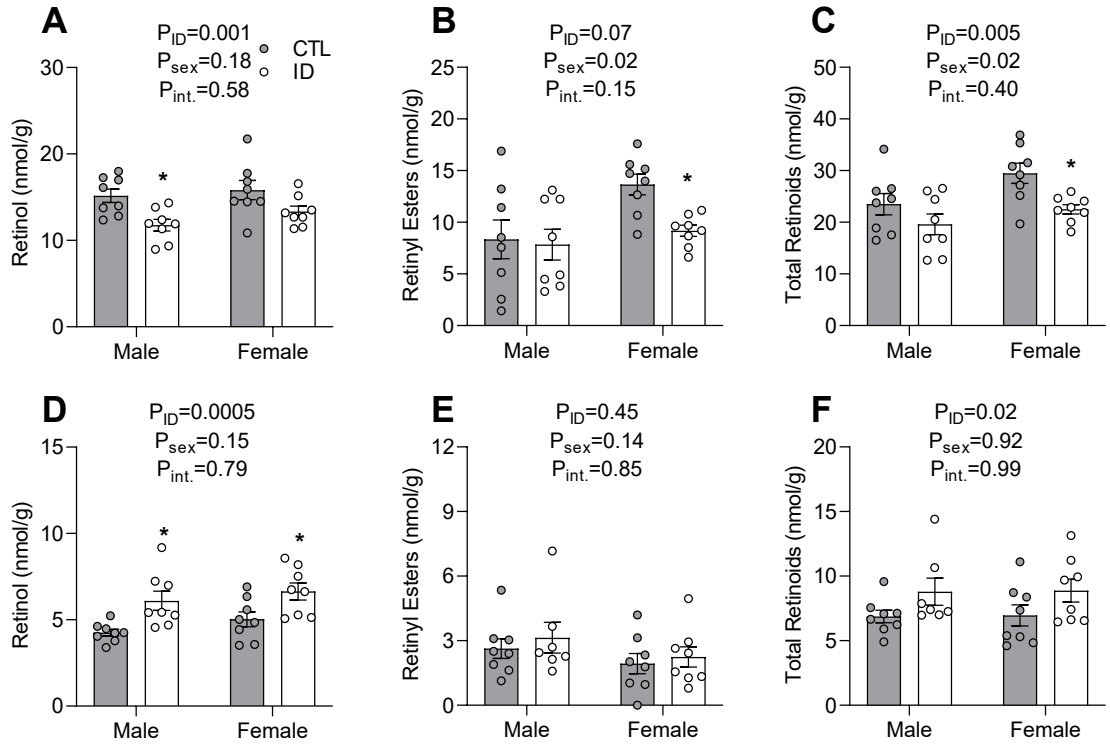

Figure 5.3: Kidney retinoid status in perinatal iron-deficient (ID) and control (CTL) group (**A-C**) postnatal day (PD)1 offspring and (**D-F**) PD28 offspring. (**A, D)** Renal retinol concentration (nmol/g kidney), (**B, E**) renal retinyl ester concentration (nmol/g kidney), and (**C, F**) combined retinol and retinyl ester concentration (nmol/g kidney). Data are analyzed by two-way ANOVA with *Sidak's* post-hoc test. * P<0.05 vs. CTL of the same sex.

5.4.4 Kidney Retinoic Acid Signaling

Gene expression profiles for components of the RA signaling pathway were assessed in kidney tissue on both PD1 and PD28, albeit the physiologic function of which changes over the course of renal development. RA Receptors (RARs) primarily function as heterodimers associated with Retinoid X Receptor (RXR) subunits, with several isoforms of each subunit expressed within the kidney [340]. On PD1, the dominant RAR isoform, *Rar-α*, was upregulated in perinatal ID males but not females (P_{int}=0.002; **Figure 5.4A**). Notably, *Rar-β*, *Rar-γ*, and *Rxr-α* showed interaction effects, wherein receptor expressions of each were decreased in perinatal ID females, but increased in perinatal ID male offspring compared to respective controls (all P<0.01; **Figure 5.4B-D**). Moreover, expression of *Rar-γ* was higher in females vs. males regardless of perinatal group (P=0.03; **Figure 5.4C**).

Several isoforms of the rate-limiting enzyme for the RA synthetic pathway retinaldehyde dehydrogenase 1 (*Raldh*), also known as aldehyde dehydrogenase 1 (*Aldh1a*), were studied. Expression profiles for each isoform vary during fetal and postnatal renal development, as previously described [341]. Briefly, During early postnatal renal development expression of *Raldh1* (*Aldh1a1*) is predominant in the renal cortex in collecting and proximal tubules, *Raldh2* (*Aldh1a2*) expression is present in the peripheral stroma and developing glomerular anlagen, and *Raldh3* (*Aldh1a3*) is expressed in the ureteric bud epithelium and medullary portions of the collecting duct system [341]. In the current study, *Raldh2* was found to be upregulated by perinatal ID in males but not female offspring on PD1 (P=0.02; **Figure 5.4E**). Interestingly, no alterations due to perinatal ID or sex were observed in expression of either *Raldh1* or *Raldh3* on PD1 (**Figure 5.5A & B**).

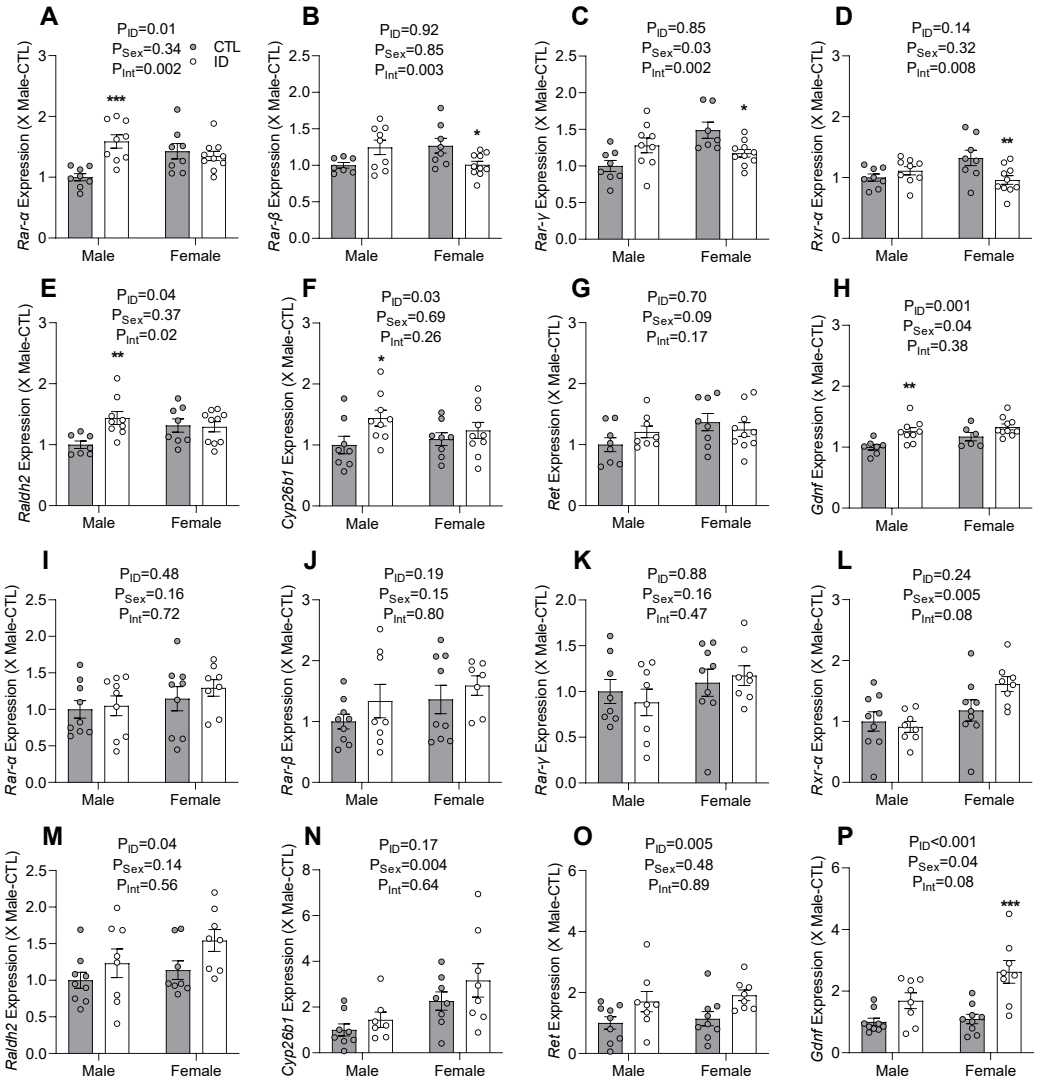

Figure 5.4: RT-qPCR expression of retinoic acid (RA) signaling pathway components in control (CTL) and perinatal iron-deficient (ID) groups from (**A-H**) postnatal day (PD)1 offspring kidneys and (**I-P)** PD28 offspring kidneys. (**A, I**) Retinoic acid receptor α (*Rar-α*), (**B, J**) Retinoic acid receptor β (*Rar-β*), (**C, K**) Retinoic acid receptor γ (*Rar-γ*), (**D, L**) Retinoid X receptor α (*Rxr-α*), (**E, M**) Retinaldehyde dehydrogenase 2 (*Raldh2*), (**F, N**) Cytophrome P450 family 26 subfamily B member 1 (*Cyp26b1*), (**G, O**) Ret Receptor tyrosine kinase (*Ret*), (**H, P**) Glial derived neurotrophic factor (*Gdnf*). Data are analyzed by two-way ANOVA with *Sidak's* post-hoc test. * P<0.05, ** P<0.01, and *** P<0.001 vs. CTL of the same sex.

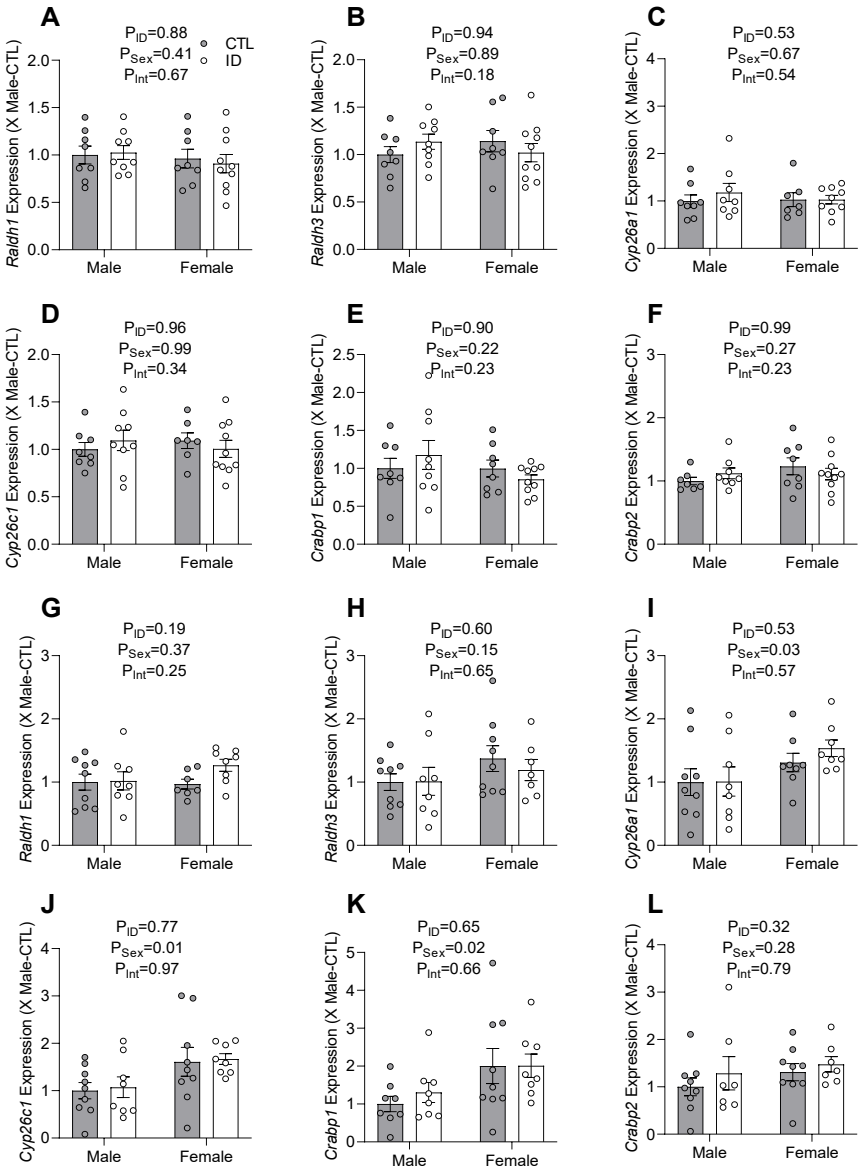

Figure 5.5: RT-qPCR expression of retinoic acid (RA) signaling pathway components in control (CTL) and perinatal iron-deficient (ID) groups from kidneys of (**A-F**) postnatal day (PD)1 and (**G-L)** PD28 offspring. (**A, G**) Retinaldehyde dehydrogenase 1 (*Raldh1*), (**B, H**) *Raldh3*, (**C, I**) Cytochrome P450 family 26 subfamily A member 1 (*Cyp26a1*), (**D, J**) Cyp26 subfamily C member 1 (*Cyp26c1*), (**E, K**) cellular retinoic acid binding protein 1 (*Crabp1*), (**F, L**) *Crabp2*. Data are analyzed by two-way ANOVA with *Sidak's* post-hoc test.

Expression of RA-degrading cytochrome P450 enzyme *Cyp26* is known to constitute primarily of the *Cyp26b1* isoform postnatally throughout S-shaped bodies and in the glomerular visceral layer, with lower levels of expression of both *Cyp26a1* and *Cyp26c1* [341]. On PD1, expression of *Cyp26b1* was increased by perinatal ID predominantly in male offspring (P=0.03; **Figure 5.4F**), whereas isoforms *Cyp26a1* and *Cyp26c1* were not altered by perinatal ID or sex (**Figure 5.5C** & **D**). Expression of cellular retinoic acid binding proteins (*Crabp*)1 and *Crabp2* were not altered by perinatal ID or sex on PD1 (**Figure 5.5E** & **F**). Expression of receptor tyrosine kinase (*Ret*) was not altered by perinatal ID or sex on PD1 (**Figure 5.4G**). Finally, expression of glial derived neurotropic factor (*Gdnf*), which encodes for the ligand of RET, was increased by perinatal ID, particularly in male offspring on PD1 (P=0.001; **Figure 5.4H**). Moreover, an overall sex effect was observed for *Gdnf* expression wherein females produced higher levels regardless of perinatal treatment group (P=0.04; **Figure 5.4H**).

Gene expression of numerous RA signaling pathway constituents within the kidney remained altered on PD28. *Rxr-α* levels were higher in female offspring regardless of perinatal treatment group (P=0.005), with no alterations observed in either *Rar-α, Rar-β,* or *Rar-γ* (**Figure 5.4I-L**). Although expression of *Raldh1* and *Raldh3* were not altered on PD28 (**Figure 5.5G** & **H**), *Raldh2* expression was increased in the perinatal ID group (P=0.04; **Figure 5.4M**). All three isoforms of *Cyp26* studied (*a1, b1, c1*) exhibited higher expression in female offspring, with no effect of perinatal ID (all P<0.05; **Figure 5.4N**; **Figure 5.5I** & **J**). Expression of *Crabp2* was not altered by perinatal ID or offspring sex, whereas *Crabp1* exhibited higher expression in female offspring (P=0.02; **Figure 5.5K & L**). *Ret* expression was increased by perinatal ID (P=0.005), with no evident effect of offspring sex (**Figure 5.4O**). Finally, expression of *Gdnf* was enhanced in the perinatal ID group (P<0.001), where overall expression was also higher in females (P=0.04; **Figure 5.4P**).

5.4.5 Renal Nephrogenic Gene Expression

Several key pathways involved in nephrogenesis were studied herein. In the canonical WNT pathway, WNT ligands bind receptor complexes composed of both the low-density lipoprotein receptor (LRP) and Frizzled (FZD) receptor, downstream signaling from which is mediated by β-catenin [179]. Alternatively, WNT signaling may occur through FZD receptors with downstream signaling mediated through either Ca^{2+}-dependent or planar cell polarity (PCP) mechanisms [179]. Expression of *Wnt4, Wnt5a, Wnt7a,* and *Wnt11* ligands were unchanged by perinatal ID or sex on PD1 (**Figure 5.6A-E**). Expression of *Wnt9b* was decreased by perinatal ID, particularly in female offspring (P=0.04; **Figure 5.6D**). Although *Fzd4* expression was not altered by perinatal ID or offspring sex (**Figure 5.6G**), *Lrp6* exhibited an interaction effect wherein perinatal ID increased expression in males alone (P=0.002; **Figure 5.6F**). Finally, β-catenin expression was enhanced by perinatal ID, particularly in male offspring (P=0.04; **Figure 5.6H**).

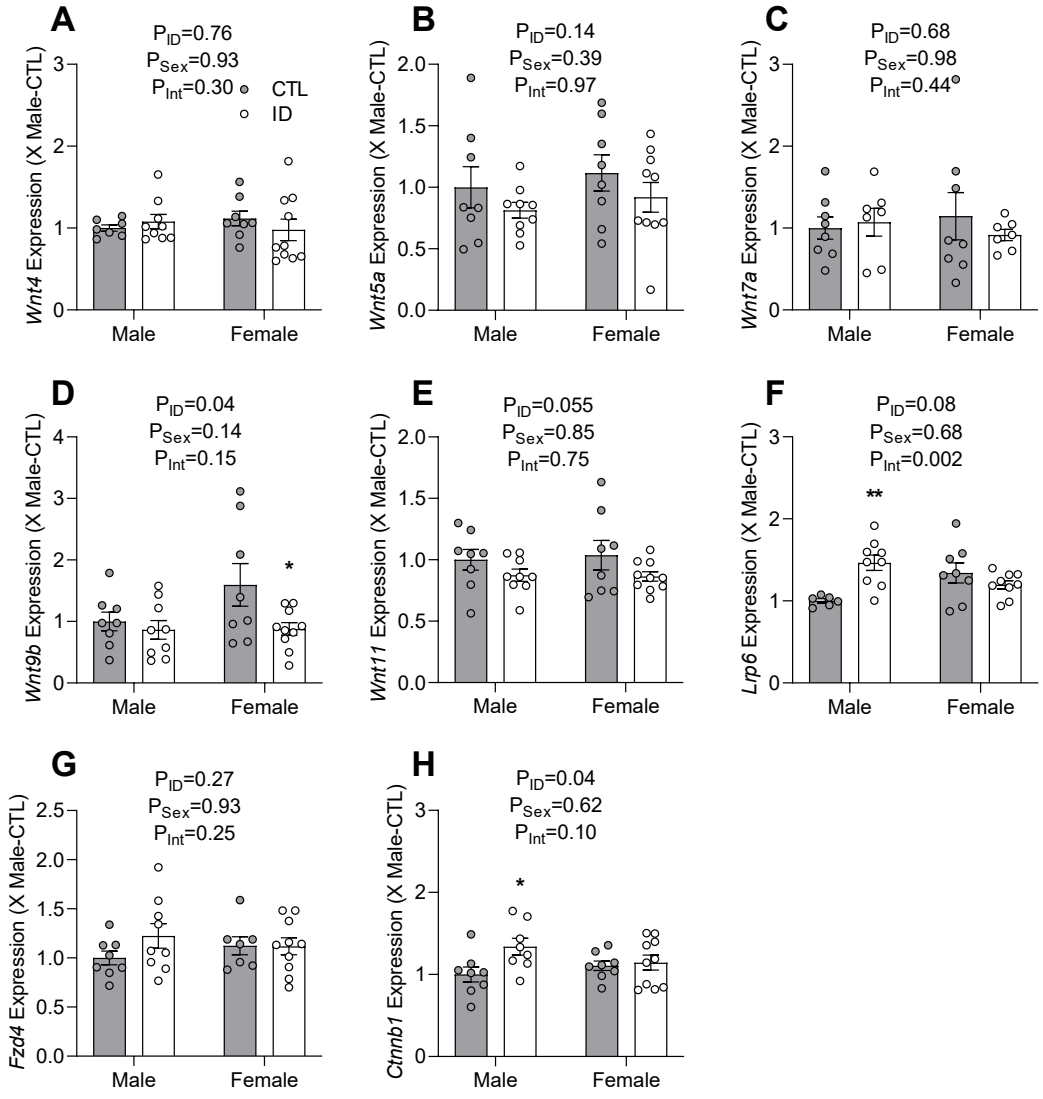

Figure 5.6: RT-qPCR expression of wingless-related integration site (*Wnt*) pathway components in postnatal day 1 kidneys from control (CTL) and perinatal iron deficient (ID) offspring. (**A**) *Wnt4*, (**B**) *Wnt5a*, (**C**) *Wnt7a*, (**D**) *Wnt9b*, (**E**) *Wnt11*, (**F**) Low density lipoprotein receptor related protein 6 (*Lrp6*), (**G**) Frizzled class receptor 4 (*Fzd4*), (**H**) β-catenin (*Ctnnb1*). Data are analyzed by two-way ANOVA with *Sidak's* post-hoc test. * P<0.05 and ** P<0.01 vs. CTL of the same sex.

Key elements of both the FGF and BMP pathways were also assessed herein. In PD1 offspring kidneys, expression of *Fgf7* was not altered by either perinatal ID or offspring sex (**Figure 5.7A**). In contrast, *Fgf10* exhibited an interaction effect (P=0.048), wherein expression was increased by perinatal ID only in male offspring (P=0.04; **Figure 5.7B**). Expression of *Fgfr1* was not altered by perinatal ID or offspring sex, albeit a trend towards an interaction effect was observed (P=0.07; **Figure 5.7C**). In contrast, expression of *Fgfr2* showed a robust interaction effect (P=0.007), wherein perinatal ID increased expression in males but decreased it in females (**Figure 5.7D**). Expression of *Bmp4*, a key mediator preventing branching of the ureteric stalk, was found to be upregulated by perinatal ID in male but not female offspring (P=0.008; **Figure 5.7E**). Perinatal ID also caused an interaction effect for the expression of the *Bmp4* receptor *Bmpr1a* (also known as *Alk3*), wherein it resulted in an increase in male but not female offspring (P=0.04; **Figure 5.7F**).

Finally, additional key mediators for interactions between the metanephric mesenchyme and the ureteric bud were assessed in PD1 offspring kidneys. Expression of Wilms tumor suppressor protein 1 (*Wt1*) exhibited robust upregulation due to perinatal ID, particularly in male offspring (P=0.006; **Figure 5.7G**). While no effect of perinatal ID was observed on expression of paired box gene 2 (*Pax2*), higher expression was observed in females irrespective of perinatal group (P=0.03; **Figure 5.7H**). Neither perinatal ID or offspring sex were observed to impact expression of sprouty receptor tyrosine kinase signaling antagonist 1 (*Spry1*) or transcription factor 21 (*Tcf21*) (**Figure 5.7I & J**). Lastly, expression of spalt like transcription factor 1 (*Sall1*) was increased by perinatal ID in male and female offspring (P=0.04; **Figure 5.7K**).

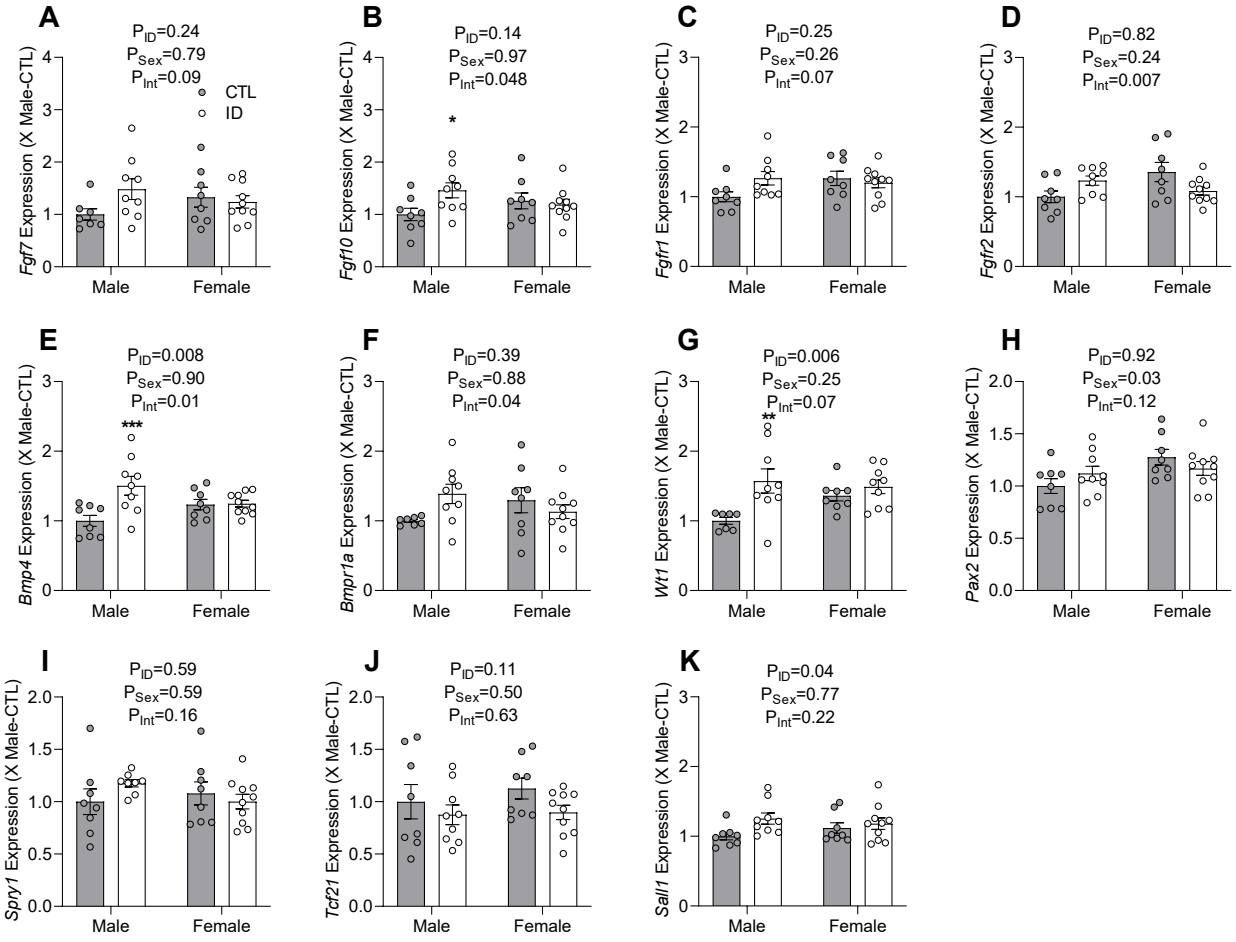

Figure 5.7: RT-qPCR expression of fibroblast growth factor (*Fgf*) pathway, bone morphogenetic protein (*Bmp*) pathway, and nephron progenitor cell regulatory factor expression in postnatal day 1 kidneys from control (CTL) and perinatal iron deficient (ID) offspring. (**A**) *Fgf7*, (**B**) *Fgf10*, (**C**) Fgf receptor 1 (*Fgfr1*), (**D**) Fgf receptor 2 (*Fgfr2*), (**E**) *Bmp4*, (**F**), Bmp receptor type 1A (*bmpr1a*), (**G**) Wilms' tumor suppressor gene 1 (*Wt1*), (**H**) Paired box gene 2 (*Pax2*), (**I**) Sprouty receptor tyrosine kinase signaling antagonist 1 (*Spry1*), (**J**) Transcription factor 21 (*Tcf21*), (**K**) Spalt like transcription factor 1 (*Sall1*). Data are analyzed by two-way ANOVA with *Sidak's* post-hoc test. * P<0.05, ** P<0.01, *** P<0.001 vs. CTL of the same sex.

5.4.6 Renal Vasculogenic Gene Expression

Marked changes in expression of mediators related to angiogenesis and vasculogenesis were observed in offspring kidneys on PD1. Vascular endothelial growth factor A (*Vegfa*), which induces angiogenesis, vasculogenesis, and endothelial cell growth, exhibited enhanced expression due to perinatal ID in male and female offspring (P=0.003; **Figure 5.8A**). Expression of renin (*Ren*), which regulates several renal growth factors during development in addition to its physiologic role in blood pressure control, exhibited an interaction effect wherein expression was increased in male but not female perinatal ID offspring (interaction P=0.047; **Figure 5.8C**). Interestingly, neither angiotensinogen (*Agt*) nor platelet derived growth factor β (*Pdgfβ*) expression patterns were altered by perinatal ID on PD1 (**Figure 5.8B &D**).

Strikingly, the patterns of alterations in angiogenic/vasculogenic mediators on PD28 share few similarities with the results observed on PD1. Expression of *Vegfa* exhibited a trend for increase due to perinatal ID (P=0.07), particularly in female offspring, likely contributing to an overall higher level of transcription in females regardless of perinatal group (P=0.048; **Figure 5.8E**). *Pdgfβ* expression was enhanced by perinatal ID in both male and female offspring (P=0.007; **Figure 5.8F**). Perinatal ID increased expression of *Ren* (P=0.03), albeit this effect was largely only seen in females, reflected by higher overall expression in females irrespective of perinatal group (P=0.01; **Figure 5.8G**). Finally, perinatal ID resulted in decreased expression of *Agt* in both male and female offspring (P<0.001; **Figure 5.8H**).

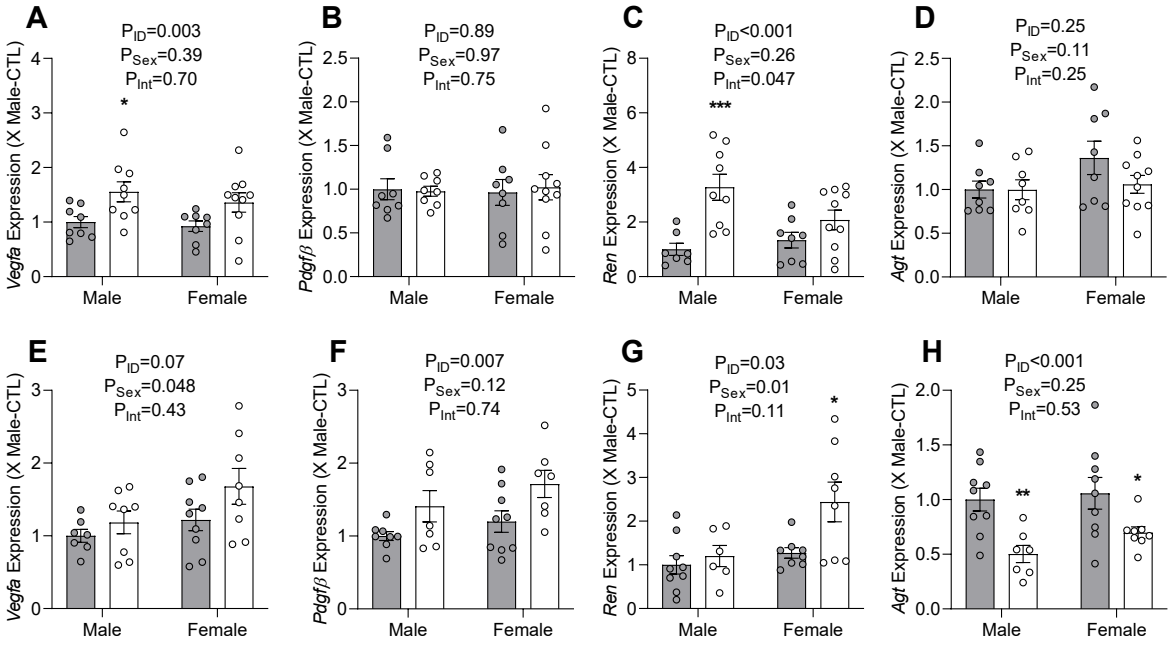

Figure 5.8: RT-qPCR expression of mediators involved in angiogenesis and vasculogenesis in the kidney. (**A-D**) Postnatal day (PD)1 and (**E-H**) PD28 control (CTL) and perinatal iron deficient (ID) offspring. (**A, E**) Vascular endothelial growth factor A (*Vegfa*), (**B, F**) Platelet derived growth factor β (*Pdgfβ*), (**C, G**) Renin (*Ren*), (**D, H**) Angiotensinogen (*Agt*). Data are analyzed by two-way ANOVA with *Sidak's* post-hoc test. * P<0.05, ** P<0.01, *** P<0.001 vs. CTL of the same sex.

5.5 Discussion

Alterations in the complex signaling interactions governing nephrogenesis have lasting impacts on kidney structure and function. We have shown that perinatal ID is associated with sex-specific changes in expression of factors from all nephrogenic signaling pathways studied herein, which are associated with reduced nephron endowment in male but not female offspring on PD28. Outcomes on PD1 serve to inform how perinatal ID impacts nephrogenic processes acutely, whereas PD28 is a time at which iron repletion has largely occurred and nephrogenesis is complete [159,216]. Male perinatal ID offspring exhibit upregulation of factors in RA/RAR, WNT, FGF, and BMP signaling pathways, whereas females exhibited no change or even decreased expression due to perinatal ID. Since blood vessel formation and growth formation coincides with nephrogenesis, it was perhaps not surprising that large alterations in pro-angiogenic factors were observed due to perinatal ID, despite no differences in vascular density being observed. As a whole, our data show that while both male and female offspring exhibit similar restrictions in iron status and growth restriction, strongly dimorphic responses in signaling based on offspring sex are observed on both PD1 and PD28, potentially contributing to previously observed cardiovascular outcomes in male but not female offspring exposed to perinatal ID [308,309].

The key finding of this study is that perinatal ID caused a sex-dependent reduction in nephron endowment. Numerous preclinical and clinical studies have previously reported that ID during development can affect kidney development and function. For instance, clinical studies have shown that higher doses of maternal iron supplementation during pregnancy are associated with improvements in estimated GFR in children aged 4-5 years [342]. Additionally, maternal ID has been reported to result in decreased renal parenchymal volume with enhanced proliferation of the stroma, coinciding with a significant increase in immature renal structures in humans [343]. Preclinical studies have been far more focused on nephron endowment. First, Lisle *et al*. reported that perinatal ID results in a reduction in nephron number in male and female rat offspring at an age of 18 months [215]. Another study conducted by Drake *et al*. reported

that strictly postnatal iron restriction in rat offspring reduces nephron endowment, albeit offspring sex was not factored into the experimental design [214]. Finally, Sun *et al*. reported that although perinatal ID in rats delayed renal maturation over the postnatal period, offspring nephron endowment was not different between controls and ID offspring post-weaning [216]. In contrast to the results of Lisle *et al.*, we observed reductions in nephron endowment in male but not female perinatal ID offspring, a finding which has also been observed in models of prenatal hypoxia and maternal global nutrient restriction [149,218,220]. The results reported herein are also consistent with previous findings in our model, where male but not female offspring exhibited hypertension and evidence of glomerular hyperfiltration and renal injury in adulthood [309]. The observed sex-differences may in part be explained by sex-specific alterations in signaling cascades studied, in addition to numerous mechanisms reviewed elsewhere [344], such as the potential roles of estrogen and innate differences in renal biology and development.

The role of vitamin A in renal development has also been studied. A recent systematic review identified several clinical studies reporting lower kidney size at birth being associated with lower maternal vitamin A levels [166]. These studies are consistent with previous reports that overall renal mass is directly tied to vitamin A status [345]. Preclinical studies have also demonstrated that maternal vitamin A levels have a linear correlation with offspring nephron number [219]. Furthermore, genetic knockout models for mediators of vitamin A signaling demonstrate that RA signaling is necessary for renal development [223].

ID is associated with large changes in vitamin A metabolism, which may have implications for vitamin A status of fetuses in pregnancies complicated by ID. For instance, ID has been shown to increase stored hepatic vitamin A at the expense of reductions in plasma retinol levels in non-pregnant rats [226,346]. During pregnancy, it is critical that maternal hepatic vitamin A storage is decreased, thereby providing retinoids to the developing fetus and placenta [225]. However, rodent studies suggest that ID during pregnancy interferes with this process through stimulating enhanced hepatic storage of retinoids [225], as previously mentioned. Moreover, rodent studies have shown that ID

interferes with retinoid delivery to the fetus, resulting fetal hepatic adaptations to maintain adequate supply of retinoids for growth and development [225]. Consistent with this notion, vitamin A dysmetabolism is implicated in the pathogenesis of congenital heart disease caused by perinatal ID [227]. In the study herein, we found minimal changes in systemic offspring vitamin A status on PD1, despite reduced maternal circulating retinol and a tendency for increased maternal storage. Conversely, in the kidneys of male offspring, there was a robust reduction in renal retinol levels due to perinatal ID, whereas female offspring primarily exhibited a reduction in retinyl ester levels. The extent to which these reductions represent reduced uptake of retinoids or altered RA conversion is unclear, but altogether suggest that levels of RA metabolites required for nephrogenesis are reduced at a critical time in both males and females.

Interestingly, we observed concomitant increased expression of mediators of RA/RAR signaling in perinatal ID males at PD1, and this could be the cause of the reduced retinol levels in the tissue. Indeed, WT1 upregulates *Raldh/Raldh2* expression, which may contribute to upregulated RA generation, resulting in reduced retinol levels in perinatal ID males [347]. Alternatively, the increased RA/RAR signaling could constitute a compensatory response to maintain adequate signaling RA in the wake of reduced retinol levels. Walton *et al.* have reported that prenatal hypoxia causes reduced RA/RAR signaling in developing kidneys of male offspring [208], and since perinatal ID causes similar patterns of kidney hypoxia [164], it is tempting to speculate that upregulations in the RA/RAR pathway in perinatal ID males is a compensatory response. Indeed, *Ret* expression, a transcriptional target of RA-RAR/RXR signaling and primary mechanism through which RA impacts renal development [348], was not increased in perinatal ID males at the same time. Finally, it is noteworthy that other models of congenital nephron impairment (e.g. induced by maternal protein restriction) can be rescued by retinoic acid supplementation, suggesting RA deficiency is an critical factor in these models of perinatal stress [221].

Notably, several other pathways also modulate *Ret* expression and signaling, and could suggest RA signaling is upregulated in male perinatal ID offspring on PD1.

Although expression of *Ret* is unchanged on PD1, increased *Gdnf* may result in enhanced signaling downstream through regulation via other pathways. Indeed, *Gdnf* and *Ret* are upregulated by signaling through *Wnt* and *Fgf*, but downregulated by *Bmp* signaling [180,349,350]. Genetic studies have shown that overexpression of *Gdnf* prolongs postnatal kidney maturation, consistent with previous observations in perinatal ID kidneys and an overall increase in *Gdnf* signaling via *Ret* [216,351]. Moreover, RA signaling is known to be a potent stimulator of *Ren* expression, which is robustly increased in PD1 kidneys of male perinatal ID offspring [336]. A recent study has shown that severe gestational iron deficiency in mice causes an upregulation of RA signaling in the developing heart, which contributes to congenital heart defects [227]. Importantly, rates of congenital heart defects caused by gestational ID were reduced by concomitant dietary reductions in vitamin A [227]. Under this paradigm, the interaction effects observed for expression of all *Rar/Rxr* studied on PD1 would support a protective decrease in expression due to perinatal ID in females, thus preserving nephron endowment by decreasing aberrant RA signaling. Alternatively, transient robust upregulation of RA signaling *in utero* may cause a secondary deficiency in RA signaling within the kidney thereafter, the effects of which could be rescued by subsequent low dose RA supplementation [352]. Indeed, either teratogenic doses of RA or RA deficiency in the developing kidney result in similar phenotypes [352], suggesting that temporal alterations in RA dynamics may contribute to the reduction in nephron endowment in male offspring. More work is necessary to elucidate the nature of the physiologic changes within the RA signaling pathway in perinatal ID offspring kidneys.

In addition to the RA/RAR pathway, several renal morphogenic pathways are altered by perinatal ID and likely contribute to sex-specific reductions in nephron endowment. *Wt1* plays numerous roles within the kidney over the lifespan, including regulation of kidney development and maintenance of renal function [353–355]. Mice with null mutations in *Wt1* lack a ureteric bud and exhibit renal agenesis [184]. However, the effect of increased expression of *Wt1,* as seen in perinatal ID males, is largely unknown. WT1 is anti-apoptotic in nephron progenitor cells during development, and this effect is

dependent on nitric oxide signaling [353]. NO levels are reduced in male, but not female, perinatal ID offspring kidneys during gestation, concomitant with increased reactive oxygen species levels [165,308,309]. Therefore reduced nephrogenesis, attributed at least in part to increased apoptosis (unpublished observations; see **Chapter 4**) may occur despite increased *Wt1* due to impaired NO signaling within the kidney. Consistent with this, *Pax2*, which is repressed by *Wt1* [356], was not altered by perinatal ID, suggesting that *Wt1* function is impaired despite its overexpression. WT1 is also known to modulate FGF and BMP signaling, wherein *Wt1* increases FGF signaling but decreases BMP signaling [357]. Therefore, while increased *Bmp4* and *Bmpr1a* expression in male perinatal ID offspring are consistent with reduced WT1 signaling, increased *Fgf10* and *Fgfr2* expression are difficult to reconcile. Enhanced BMP signaling in perinatal ID males may also be attributed, in part, to increased *Sall1*, which regulates nephron progenitor expansion [358]. Taken together, perinatal ID dysregulates numerous nephrogenic pathways which dictate interactions between the ureteric bud and nephron progenitors, albeit the extent to which each individual change contributes to reduced nephron endowment in perinatal ID males remains unclear.

The WNT pathway is intimately involved in several processes during renal development, reviewed in-depth elsewhere [179]. Of the WNT ligands studied, perinatal ID primarily impacted*Wnt9b*, which regulates progenitor cells within the metanephric mesenchyme and the extension of tubular epithelium [359,360]. However, since perinatal ID female offspring exhibit no evidence of altered hemodynamic function, even when challenged with a high-sodium diet in adulthood [309], the consequences of observation are likely modest. Perinatal ID also tended to reduce *Wnt11*, an important autocrine mediator promoting ureteric bud branching and determination of total renal size [360], and whose expression is enhanced via RA/RAR signaling through GDNF/RET [350]. Notably, upregulation of both *Lrp6* and *Ctnnb1* were observed in male perinatal ID offspring, potentially indicating enhanced signaling through the canonical WNT pathway despite no substantial upregulation of any WNT ligands studied herein. Consistent with this, upregulation of the expression of GDNF is observed in male perinatal ID offspring on

PD1, which is stimulated through WNT signaling [350]. Alternatively, enhanced BMP pathway signaling may inhibit the GDNF/RET/WNT11 signaling axis, acting to antagonize the pro-WNT actions of the RA/RAR pathway.

Furthermore, findings which are highly supportive of reductions in nephron endowment in perinatal ID male offspring include upregulation of the BMP pathway and high levels of *Vegfa* expression. BMP4 signaling via BMPR1A is a principal mechanism which antagonizes ureteric bud branching stimuli (i.e. FGF, RA/RAR, and WNT pathways) [183]. In addition, further inhibition of nephrogenesis in male perinatal ID offspring is likely occurring through enhanced *Vegfa* on PD1 [361]. Therefore, it is possible these mechanisms supersede the previously discussed enhancements in RA/RAR, WNT, and FGF pathway signaling, which are broadly considered pro-branching.

The renin angiotensin system (RAS) is known to play a critical role in kidney development. Constituents of the RAS system are expressed at higher levels in development than adulthood, and perturbations in systemic and intrarenal RAS during development have been implicated in the pathogenesis of kidney disease, as reviewed by [173]. Previous studies have shown that perinatal ID offspring exhibit hypertension as well as renal vascular function abnormalities in adulthood [170], providing an impetus for studying RAS components and angiogenesis during development. Importantly, no alterations in vascular density were observed due to perinatal ID on PD28. However, enhanced expression of *Vegfa* on PD1 due to perinatal ID denotes increased pro-angiogenic signaling within the endothelium, likely due to chronically limited oxygen delivery secondary to anemia [362], albeit upregulation of *Pdgfa* to stimulate vascular smooth muscle proliferation was not observed until PD28. Furthermore, *Ren* expression was enhanced by perinatal ID on PD1, indicative of increased systemic RAS signaling [114]. This result is in contrast to findings of decreased *Ren* expression in models of placental insufficiency at birth, and gestational hypoxia on PD7 [208,229]. Elevations in *Ren* expression have also been observed in male but not female offspring exposed to prenatal hypoxia on PD21, albeit this elevation is observed in both sexes in adulthood [218]. Increased *Ren* expression in perinatal ID female offspring on PD28 may be partially

explained by *Vegfa* expression, which could indicate poor renal perfusion triggering RAS activation [114]. While the liver is the predominant source of circulating AGT, intra-renal expression of *Agt* largely occurring in the proximal tubules is known to contribute to regulation of blood pressure independently of systemic RAS function [363]. Perinatal ID offspring have been shown to exhibit reduced blood pressure versus controls on PD20 [231], with another study observing elevated blood pressure in perinatal ID males at 6 weeks whereas a reduction was seen in females [230]. Taken together, reduced renal *Agt* expression in PD28 perinatal ID offspring of both sexes would be consistent with reduced blood pressure, whereas enhanced *Ren* expression on PD28 in only female perinatal ID offspring may be partially explained by NO deficiencies previously observed in male perinatal ID offspring [165,308,309].

Interestingly, female perinatal ID offspring exhibited reduced plasma retinol levels on PD28. Given that a U-shaped association between all-cause mortality and plasma retinol levels exists, this may indicate a potential pathological dysregulation of retinoid metabolism in female perinatal ID offspring [364], warranting further investigation. Interestingly, by PD28 renal retinol levels fall approximately 4-fold when compared to PD1 levels, indicating the physiologic importance of vitamin A in early renal development. Perinatal ID results in increased retinol levels in the kidneys of PD28 perinatal ID offspring, combined with enhanced expression of *Ret* and *Gdnf*. Taken together, these data likely suggest an upregulation of both retinoid uptake and signaling due to perinatal ID occurring over the course of postnatal kidney development, consistent with delayed renal maturation as described above [216,351]. Furthermore, sex specific enhancements in *Gdnf, Rxr-α*, and *Cyp26b1* in female offspring on PD28 may explain in part the depletion of circulating plasma retinol levels in perinatal ID female offspring. Importantly, RA signaling through RET plays a plethora of roles following development which must also be considered. Perinatal ID induces significant oxidative stress and mitochondrial dysfunction in the developing kidney, particularly in male offspring [165]. As such, RA signaling through RAR/RXR may be acting to modulate cellular differentiation, cell cycle arrest, anti-inflammatory responses, or modulate cellular survival via pro- and

anti-apoptotic pathways [365]. The extent to which RA signaling is detrimental to kidney health following development depends largely on receptor and downstream mediator expression, with signaling through RAR-β and RAR-γ sub-units being linked to podocyte toxicity [365]. As such, long-term dysregulation of vitamin A metabolism may be a potential mechanism through which renal injury may be exacerbated in perinatal ID offspring.

Our study has several limitations. First, we rely on the implicit assumption that gene expression profiles reflect their functional relevance, and this may not be the case due to translational and post-translational regulation. The interpretation of our data relies heavily on data obtained from gene knockout models, which poses challenges in deciphering how modest changes in signaling pathways affect immediate and long-term outcomes. Therefore, future studies would benefit from utilization of mouse models, or another platform where inducible gene knockouts are feasible in the presence of perinatal ID. Furthermore, use of a LacZ gene reporter for RA/RAR signaling in conjunction with a model of perinatal ID would alleviate many of the interpretation issues described herein. Finally, quantitative RA assessments could not be performed due to its instability, but would provide insights into the cumulative effects of altered RA production (i.e. *Raldh*) and metabolism (i.e. *Cyp26*), and how these contribute to RA signaling during development.

In conclusion, perinatal ID causes robust changes in renal vitamin A metabolism and nephrogenic signaling, which appear to contribute, at least in part, to the sex-specific reductions in nephron endowment in male offspring. This study is the first to assess the impact of dysregulated vitamin A metabolism on renal development in the context of perinatal ID. Together with our previous findings within the fetal kidney [164,165], it suggests that the impacts of perinatal ID on kidney development span the perinatal period. Thus, our results emphasize the importance of identifying and treating ID in women of reproductive age, as well the importance of considering perinatal health as a risk factor for subsequent cardiovascular disease.

Funding

A.G.W. held a Canadian Institutes of Health Research (CIHR) Vanier Scholarship and an Alberta Innovates Graduate Studentship. S.L.B. is a Canada Research Chair in Developmental and Integrative Pharmacology (Tier 2). Project funding was provided by a CIHR Operating Grant (MOP142396) and a Heart and Stroke Foundation of Canada Bridge Grant (G-20-0029380) held by S.L.B., and a University of Alberta Faculty of Agricultural, Life and Environmental Sciences Vitamin Research Fund Grant held by A.G.W.

Author Contributions

A.G.W., R.D.C. and S.L.B. designed the research; A.G.W., R.L.M., S.K., C.D.H., R.M.N.N., and R.D.C. performed the experiments; A.G.W., R.L.M., S.K., and R.D.C. analyzed the data; A.G.W. and R.L.M. wrote the manuscript; R.D.C. and S.L.B. provided critical feedback and editorial comments for the manuscript.

Chapter 6

Perinatal Iron Deficiency and a High Salt Diet Cause Long-Term Kidney Mitochondrial Dysfunction and Oxidative Stress

Andrew G. Woodman[1,5], Richard Mah[1,5], Danae L. Keddie[1,5], Ronan M.N. Noble[2,5], Claudia D. Holody[2,5], Sareh Panahi[3,5], Ferrante S. Gragasin[3,5], Helene Lemieux[4,5,6], Stephane L. Bourque[1,2,3,5].

Department of Pharmacology, University of Alberta[1]
Department of Pediatrics, University of Alberta[2]
Department of Anesthesiology & Pain Medicine, University of Alberta[3]
Department of Medicine, University of Alberta[4]
Women and Children's Health Research Institute, University of Alberta[5]
Faculty Saint-Jean, University of Alberta[6]

PUBLISHED:
Woodman *et al. Cardiovascular Research* 2020. 116(1):183-192
(First appeared as E-Pub January 2019)

6.1 Abstract

Aims: Perinatal iron deficiency alters developmental trajectories of offspring, predisposing them to cardiovascular dysfunction in later life. The mechanisms underlying this long-term programming of renal function have not been defined. We hypothesized perinatal iron deficiency causes hypertension and alters kidney metabolic function and morphology in a sex-dependent manner in adult offspring. Furthermore, we hypothesized these effects are exacerbated by chronic consumption of a high salt diet.

Methods and Results: Pregnant Sprague Dawley rats were fed either an iron-restricted or replete diet prior to and throughout pregnancy. Adult offspring were fed normal or high salt diets for six weeks prior to experimentation at six months of age. Blood pressure was assessed via indwelling catheters in anesthetized offspring; kidney mitochondrial function was assessed via high-resolution respirometry; reactive oxygen species and nitric oxide were quantified via fluorescence microscopy. Adult males, but not females, exhibited increased systolic blood pressure due to iron deficiency ($P=0.01$) and high salt intake ($P=0.02$). In males, but not in females, medullary mitochondrial content was increased by high salt ($P=0.003$), while succinate-dependent respiration was reduced by iron deficiency ($P<0.05$). The combination of perinatal iron deficiency and high salt reduced complex IV activity in the cortex of males ($P=0.01$). Perinatal iron deficiency increased cytosolic superoxide generation ($P<0.001$) concomitant with reduced nitric oxide bioavailability ($P<0.001$) in male offspring, while high salt increased mitochondrial superoxide in the medulla ($P=0.04$) and cytosolic superoxide within the cortex ($P=0.01$). Male offspring exhibited glomerular basement membrane thickening ($P<0.05$), increased collagen deposition ($P<0.05$), and glomerular hypertrophy (interaction, $P=0.02$) due to both perinatal iron deficiency and high salt. Female offspring exhibited no alterations in mitochondrial function or morphology due to either high salt or iron deficiency.

Conclusions: Perinatal iron deficiency causes long-term sex-dependent alterations in renal metabolic function and morphology, potentially contributing to hypertension and increased cardiovascular disease risk.

6.2 Introduction

Cardiovascular disease (CVD) is a leading cause of mortality, responsible for approximately a third of all deaths worldwide.[93] The etiology of CVD is complex, and the developmental origins of health and disease (DOHaD) hypothesis has identified new risk factors, which are dictated by the quality of the fetal and early postnatal environment. The DOHaD theory, first articulated by the late Sir David Barker, posits that stressors, such as nutrient deficiencies and hypoxemia, can alter the growth trajectories of the developing organism and in turn predispose the offspring to chronic disease in later life.[139]

Iron-deficiency (ID) is the most common nutritional deficiency worldwide. It occurs when iron demands chronically exceed intake, resulting in depletion of tissue iron stores and eventually leading to reduced circulating haemoglobin (Hb). During gestation and early childhood, increased iron demands due to growth and blood volume expansion contribute to the increased risk of ID and anaemia.[4] Globally, an estimated 38% of pregnant women are anemic,[21] and the prevalence of latent ID in pregnancy, in which overt anaemia is not yet manifest, is undoubtedly higher. Even in many developed countries where prenatal iron supplementation is common, approximately one in four pregnant women still develop anaemia,[21] emphasizing the need to better understand long-term implications of ID on offspring health outcomes.

In addition to increasing the risk of fetal death, preterm birth and intrauterine growth restriction,[366,367] ID during pregnancy is associated with long-term neurocognitive,[252] metabolic[159] and cardiovascular complications.[170,230] However, the mechanisms underlying these adverse long-term outcomes remain unclear. We recently showed that prenatal ID anaemia causes hypoxia, mitochondrial dysfunction and increased generation of reactive oxygen species (ROS) in the term rat fetus.[164,165] These adverse outcomes were organ- and sex-specific, such that kidneys of male fetuses exposed to prenatal ID were most affected,[164,165] suggesting that renal development is particularly sensitive to programming effects. Indeed, adult offspring born to pregnancies complicated by perinatal ID exhibit hypertension and enhanced blood pressure

responsiveness to high salt intake,[159,160,170] implicating intrinsic changes in renal function.[100] However, the long-term effects of perinatal ID on kidney function have not been studied. The objective of this study was to determine whether perinatal ID causes long-term kidney mitochondrial dysfunction and oxidative stress within the kidney, which has been described in other models of hypertension and salt sensitivity.[236,237] Moreover, we sought to determine whether these outcomes would be exacerbated by chronic consumption of a high salt diet.

6.3 Methods

6.3.1 Animals and Treatments

The protocols described herein were approved by the University of Alberta Animal Care Committee (AUP974) in accordance with guidelines established by the Canadian Council of Animal Care, consistent with NIH guidelines. Experimentally naïve and nulliparous six-week old Female Sprague-Dawley rats were purchased from Charles River (Saint-Constant, QC, Canada) and housed at the University of Alberta animal care facility, which maintained a 12h light/dark cycle and ambient temperature of 23ºC. Rats were housed in conventional wire-top cages fitted with filter tops and had *ad libitum* access to food and water throughout the study. Enrichment for the rats in the study included wooden blocks and shredded paper pucks.

All purified diets used in this study were purchased from Research Diets Inc. (New Brunswick, NJ, USA), and are identical in composition except for the amount of added ferric citrate. Two-weeks prior to pregnancy, female rats were randomly assigned to the iron-restricted group, in which they were fed a purified diet low in iron (containing 3mg/kg elemental iron; D03072501); the remaining females were assigned to the control group, in which they were fed a purified control diet (containing 37mg/kg elemental iron diet; D10012G). After 2wk on their respective diets, female rats were bred by co-housing overnight with age-matched males fed a standard rodent chow (5L0D; PicoLab, St. Louis, MO, USA). Pregnancy was confirmed by the presence of sperm in a vaginal smear the following morning [gestational day (GD)0]. Upon confirmation of pregnancy, dams

in the iron-restricted group were fed a moderately iron-restricted diet (containing 10mg/kg elemental iron; D15092501), and those in the control group were maintained on the control diet. Throughout pregnancy, food consumption, body weight, and haemoglobin (Hb) levels were monitored weekly. Hb levels were assessed using a HemoCue 201+ system (HemoCue, Angelholm, Sweden) from blood (~10µL) collected *via* saphenous venipuncture from dams, or blood collected after decapitation in neonates. Within 12h of giving birth, all dams were fed the standard rodent chow, and pup weights were recorded, and litters were standardized to 8 offspring (four males, four females). Postnatal body weights were recorded weekly, and offspring were weaned from their dams at PD21 and fed standard rodent chow.

At four and a half months of age (6wks prior experimentation), male and female offspring from each litter were fed either a high salt diet (HS, 5.0% NaCl *w/w*; D17053103DW) or a normal salt diet (NS, 0.27% NaCl *w/w*; D06041501DW) for six weeks. Body weights, food intake and water consumption were monitored weekly during this six-week treatment period.

6.3.2 Haemodynamic Assessments

Direct haemodynamic assessments were performed in spontaneously breathing adult offspring under isoflurane anaesthesia (in medical grade oxygen at a flow rate of 1mL/min; 3-5% for induction, 1.5% for maintenance) on a 37^{o}C warming bed (heated by a circulating water bath). Catheters (PE50, 0.58 mm i.d., 0.97 mm o.d., Becton Dickson, Sparks, MD, USA) connected to a pressure transducer (ADInstruments, Colorado Springs, CO, USA) were implanted into the left femoral artery for direct blood pressure measurements, and a catheter (Silastic ®, 0.51 mm i.d., 0.94 mm o.d. Cole-Parmer, Montreal, QC, Canada) was implanted into the left femoral vein for drug delivery. Following completion of surgery, rats were given a minimum of 15min to achieve steady haemodynamics, and baseline parameters were recorded for the next 5-10min. After baseline recordings, haemodynamic responses to the pan-nitric oxide (NO) synthase inhibitor L-Nitro-G-Arginine Methyl ester (L-NAME; 60mg/kg IV) were assessed over

15min. Isoflurane anaesthesia was then increased to 5% and rats were euthanized by exsanguination and subsequent excision of the heart. Organs were collected and weighed; hearts were dissected to isolate the right ventricle (RV) from the left ventricle and septum (LVS) before weighing. Blood pressure measurements in offspring of the same litter were performed on the same day, and male offspring were always assessed first; female offspring were thus housed in an adjacent room in the laboratory 2-3 hours prior to undergoing blood pressure assessments. After hemodynamic assessments, organs were weighed, but tissues were not used for further data collection to the potential confounding effects of prolonged isoflurane exposure and intravenous drug administration.

6.3.3 High-Resolution Respirometry

Respirometry was performed using the Oroboros Oxygraph-O2k system (Innsbruck, Austria). Kidneys were separated into cortical and medullary components under a microscope, and approximately 20 mg of each tissue region were subsequently homogenized in 2mL of MiR05 buffer (110mmol/L sucrose, 60mmol/L K-lactobionate, 0.5mmol/L EGTA, 1g/L fatty acid free bovine serum albumin, 3mmol/L $MgCl_2$, 20mmol/L taurine, 10mmol/L KH_2PO_4, and 20mmol/L K-N-2-hydroxyelthylpiperazine-N_2-ethanesulphorate, pH 7.1), and 100µL of tissue homogenate was added to each chamber. The remainder of homogenate was flash frozen and stored at -80ºC for citrate synthase (CS) activity assay (see mitochondrial content section). The titration protocol used herein allows evaluation of the mitochondrial function at three different respiratory states [LEAK (respiration in the presence of substrate, but in the absence of ADP; includes a variety of processes and is not limited to electron leak, thus it is expressed in capitalized to note the distinction), oxidative phosphorylation (OXPHOS), and electron transfer (ET)] as previously described.[165,289]

OXPHOS (coupled respiration with saturated ADP) and ET capacities (uncoupled) were measured in the presence of substrates feeding electrons into the NADH-linked pathway (N-pathway; pyruvate and malate, feeding electrons into complex I), NADH and succinate-linked pathway (NS-pathway; pyruvate, malate and succinate

feeding electrons into complexes I and II simultaneously), succinate-linked pathway (S-pathway; succinate and rotenone, the latter to inhibit complex I), and complex IV [ascorbate and tetramethyl-p-phenylenediamine (TMPD)]. The single titration protocol utilizes sequential addition of the following substrates, inhibitors and uncouplers (final concentration): 5mmol/L pyruvate and 5mmol/L malate; 2.5mmol/L ADP; 10µmol/L cytochrome *c*; dinitrophenol at 10µmol/L steps, up to 30µmol/L; 0.5µmol/L rotenone; 2.5µmol/L antimycin A; 0.5mmol/L ascorbate and 2mmol/L TMPD; and 15mmol/L sodium azide. Corrections for oxygen flux due to instrumental background noise and residual oxygen consumption by complexes I and III were made by subtraction of values following administration of both rotenone and antimycin A. Complex IV respiration was corrected through subtraction of chemical background following administration of sodium azide. Flux control ratio (FCR) was normalized for maximal ET capacity with substrates feeding into the NS-pathway.

6.3.4 Mitochondrial Content

Citrate synthase (CS) activity was measured using a UV/Vis spectrophotometer (Ultrospec 2100 Pro; Biochrom, Cambridge, MA, USA) heated to 37ºC by a cell holder and circulating water bath, as previously described[165,368]. Medullary and cortical tissue homogenates were thawed and underwent an additional cycle of homogenization with a conical glass homogenizer for 10s. Absorbance was measured for 5min at 412nm after the reduction of 0.1mmol/L 5,5/ dithiobis-2-nitrobenzoic acid (ε: 13.6 mL cm^{-1} μM^{-1}) in the presence of 0.25% Triton X-100, 0.5mmol/L oxaloacetic acid, 0.31mmol/L acetyl co-enzyme A, 100mmol/L Tris-HCl, and triethanolamine-HCl buffer pH 8.0, as previously described.

6.3.5 Fluorescence Microscopy

As previously described[165], reagents were purchased from Thermo Fisher Scientific (Waltham, MA, USA) for experimentation: dihydroethidium (DHE; for assessment of cytosolic superoxide), 4-amino-5-methylamino-2`,71-difluorofluorescein diacetate (DAF-FM; for assessment of cytosolic nitric oxide), and MitoSox Red (for

assessment of mitochondrial superoxide). Kidneys were embedded in optimal cutting temperature compound (OCT, Tissue Tek, Sakura Inc.), were sectioned (8 µm thickness) at -20ºC by cryostat onto SuperFrost Plus microscope slides (Fisher Scientific), and then stored at -80ºC. Sections were thawed and washed 3 times with Hanks Buffered Salt Solution (HBSS), and warmed to 37ºC in a humidified chamber for 10min. Slides are then washed again with HBSS and then incubated with either DHE (20µmol/L for 30min), DAF-FM (20µmol/L for 30min) or MitoSox (5µmol/L for 10min). Afterward, slides were washed for two minutes with HBSS three times and were subsequently mounted in HBSS (DHE and MitoSox) or Vectashield Antifade Mounting Medium with DAPI (Vector Laboratories, Burlingame, CA, USA). Nuclear counterstain was only used for DAF-FM fluorescence because DHE and MitoSox rely on DNA intercalation. Fluorescence was visualized for both cortical and medullary regions of the kidney sections using an Olympus IX81 fluorescent microscope (Tokyo, Japan).

6.3.6 Renal Morphology Assessments

Kidneys were fixed in 4% neutral-buffered formaldehyde for 24 hours and subsequently embedded for histology and sectioned at 6µm as previously described[164]. Jones silver staining was performed per manufacturer instructions (HT100A-1KT, Sigma-Aldrich) with alcoholic Eosin Y and Harris hematoxylin counterstain. Twenty separate glomerular basement membranes per animal (with 10 points of measurement per glomerular membrane) were measured. Masson's trichrome staining was performed per manufacturer instructions (HT15-1KT, Sigma-Aldrich) for the assessment of interstitial and glomerular collagen deposition. Intensity of blue staining for collagen in a minimum of 6 fields of view in 4 separate tissue sections per animal were quantified with ImageJ as previously described.[369] In trichrome-stained sections, glomerular cross-sectional area was calculated using Adobe Photoshop. Glomerular cross-sectional areas were calculated in 4 separate tissue sections, and an average was calculated from the maximum value for each section. Maximum values were used to reduce a potential underestimation caused by sectioning glomeruli outside a central axis.[370]

6.3.7 Statistical Analyses

In all data sets, n values reflect the number of litters (i.e. treated dams are the experimental unit); instances where more than one offspring per litter were used to obtain a value (e.g. neonatal weights and haemoglobin levels), the litter average was treated as a single data point. Data were analyzed by unpaired Student's *t*-test, or two-way ANOVA for the main effects of perinatal ID and salt treatment, with a Sidak's *post hoc* test. All male and female offspring data were analyzed separately. Data are presented as mean±SEM. $P<0.05$ was considered significant. Grubb's test was used to identify statistical outliers, which were excluded from analysis. All statistical analyses were conducted using GraphPad Prism 8.0 software.

In total, data was collected from 136 adult offspring from 30 litters; 76 animals were allocated to hemodynamics experiments and 60 to mitochondrial function and oxidative stress measurements. Technical issues with oxygraph chamber calibration and improper separation of the medulla and cortex in initial experiments resulted in the exclusion of the following data points from respirometry and citrate synthase results: 2 male ID NS; 1 male CTL NS; 1 female CTL NS; 1 female ID NS; and 1 female ID HS sample; the need for fresh tissues for these analyses precludes the ability to repeat these experiments when complications arise. Finally, one cryopreserved kidney block from the male ID NS group was shattered during sectioning, resulting in the loss of one data point.

6.4 Results

6.4.1 Pregnancy Outcomes and Offspring Growth

Iron restriction prior to and throughout pregnancy resulted in a 34% decrease in maternal Hb levels by gestational day (GD)21, one day prior to full term (**Table 6.1**). ID dams gained 14% less weight during pregnancy and had a 19% reduction in litter size (**Table 6.1**) compared to control (CTL) dams, despite no differences in food intake during pregnancy (CTL 580.4±23.7g vs. ID 541.6±16.3g, P=0.21). On PD1, male and female pups born to ID dams had ~40% decreases in circulating Hb and ~11% lower body weights (**Table 6.1**). In these offspring, the growth restriction persisted in the pre-weaning phase, such that they were ~27% smaller than their CTL counterparts on PD21 (male CTL 49.8±1.5g vs. ID 36.4±3.2g, P=0.006; female CTL 49.2±1.7g vs. ID 35.4±2.9g, P=0.003). Prior to beginning the 6-wk HS treatment, adult male perinatal ID offspring remained ~10% smaller than their CTL counterparts, with no initial differences in size when comparing the groups allocated to NS and HS treatments (ID effect P=0.003, HS effect P=0.61, interaction P=0.20; data not shown). In contrast, female offspring exhibited no differences in bodyweight between groups (ID effect P=0.42, HS effect P=0.53, interaction P=0.56; data not shown). Notably, the smaller male perinatal ID offspring ate and drank less than their control counterparts during the 6-wk treatment period (**Table 6.2**). The HS diet increased water intake by greater than two-fold in both male and female offspring, despite HS not altering food intake (**Table 6.2**).

At the end of the 6wk salt treatment period, male perinatal ID offspring remained ~10% smaller than their CTL counterparts, with shorter crown-rump lengths and reduced abdominal girth (**Table 6.3**). Male offspring had increased relative (i.e. normalized to bodyweight) right ventricular (RV) weight due to both perinatal ID and HS, whereas only HS causes an increase in relative left ventricle and septum (LVS) weight (**Table 6.3**). No differences in relative kidney weights in male offspring were observed (**Table 6.3**). In contrast, female offspring exhibited no alterations in size or weight, or differences in

organ weights due to perinatal ID or HS, with the exception of a trend for increased RV weight due to perinatal ID (P=0.06; **Table 6.3**).

Table 6.1. Pregnancy and neonatal outcomes.

Parameter		Treatment		P Value
		CTL	ID	
Maternal Weight Gain GD0-GD21 (g)		227.2 ± 7.5	195.5 ± 9.0	**0.01**
Litter Size (No. pups)		18.1 ± 0.9	14.6 ±0.6	**0.003**
Maternal Hb (g/dL)	GD0	15.3 ± 0.2	11.8 ± 0.6	**<0.001**
	GD7	14.7 ± 0.2	11.7 ± 0.5	**<0.001**
	GD14	14.0 ± 0.2	10.7 ± 0.5	**<0.001**
	GD21	12.5 ± 0.3	8.3 ± 0.4	**<0.001**
PD1 Hb (g/dL)	Males	11.2 ± 0.4	6.8 ± 0.5	**<0.001**
	Females	11.0 ± 0.3	6.3 ± 0.5	**<0.001**
PD1 Body Weight (g)	Males	6.49 ± 0.14	5.76 ± 0.15	**0.004**
	Females	6.13 ± 0.20	5.54 ± 0.14	**0.02**

All groups n=8-11 offspring from separate litters Data are expressed as mean ± SEM and analyzed by unpaired *t*-test. CTL, control; GD, gestational day; Hb, haemoglobin; ID, perinatal iron deficient group; PD, postnatal day.

Table 6.2. Food and water intake during the 6-week high salt diet feeding.

Sex	Parameter	Treatment				P-Values		
		CTL		ID		ID	HS	Int.
		NS	HS	NS	HS			
M	Food (g/day)	30.1±1.5	28.9±1.1	26.0±1.1	25.9±0.8	**0.007**	0.62	0.69
	Water (mL/day)	31.3±2.0	72.7±2.2#	26.3±1.1	66.1±3.1#	**0.02**	**<0.001**	0.73
F	Food (g/day)	19.5±2.1	19.6±0.9	19.9±0.7	18.5±0.7	0.76	0.58	0.54
	Water (mL/day)	22.3±1.4	47.6±2.9#	21.7±1.7	48.3±4.2#	0.98	**<0.001**	0.83

All groups n=8-11 offspring from different litters. Data are expressed as mean ± SEM and analyzed by two-way ANOVA with Sidak's *post hoc* test, where # denotes P<0.001 vs. NS of the same group. CTL, control; F, female; HS, high salt diet; ID, perinatal iron deficiency group; int, interaction; M, male; NS, normal salt diet.

Table 6.3. Body measurements and organ weights of 6-month old offspring.

	Parameter	Treatment				P-Value		
		CTL		ID		ID	HS	INT.
		NS	HS	NS	HS			
M	Body Wt. (g)	757.7±24.7	699.4±23.5	640.5±19.3	638.5±10.8	**<0.001**	0.17	0.19
	CR Length (cm)	21.5±0.3	21.1±0.2	20.3±0.3	20.5±0.1	**<0.001**	0.74	0.26
	Ab. Girth (cm)	26.0±0.5	24.6±0.4	23.9±0.4	23.9±0.4	**0.003**	0.14	0.14
	LVS (mg/g)	1.62±0.03	1.79±0.06*	1.75±0.05	1.83±0.07	0.11	**0.02**	0.36
	RV (mg/g)	0.41±0.01	0.44±0.02	0.46±0.02	0.51±0.03	**0.002**	**0.03**	0.80
	Kidneys (mg/g)	5.93±0.23	6.34±0.12	6.45±0.36	6.21±0.20	0.42	0.72	0.16
F	Body Wt. (g)	434.5±21.8	422.6±12.7	391.8±17.3	410.9±12.8	0.13	0.84	0.38
	CR Length (cm)	17.6±0.3	17.4±0.2	17.3±0.2	17.4±0.2	0.51	0.88	0.64
	Ab. Girth (cm)	21.0±0.6	20.3±0.3	19.8±0.4	20.4±0.4	0.27	0.92	0.16
	LVS (mg/g)	1.90±0.06	1.94±0.06	1.90±0.06	1.94±0.07	0.96	0.56	0.99
	RV (mg/g)	0.46±0.02	0.48±0.02	0.51±0.03	0.52±0.03	0.06	0.54	0.87
	Kidneys (mg/g)	5.80±0.26	6.48±0.17	6.11±0.38	6.21±0.27	0.94	0.19	0.33

All groups n=8-11 offspring from different litters. Data are expressed as mean ± SEM, and are analyzed by two-way ANOVA with *Sidak's post hoc test* where * denotes P<0.05 vs. NS group. Ab, abdominal; CR, crown-rump; CTL, control; F, female; HS, high salt diet; ID, perinatal iron deficiency group; int, interaction; LVS, left ventricle-septum; M, male; NS, normal salt diet; RV, right ventricle.

6.4.2 Haemodynamics

At 6-months of age, there was an overall effect of perinatal ID and HS on systolic BP (SBP) in male offspring (**Figure 6.1A**). Furthermore, HS increased diastolic BP (DBP) and mean arterial pressure (MAP) in male offspring, whereas perinatal ID increased MAP but not DBP (P=0.09; **Table 6.4**). In contrast, there was no effect of perinatal ID or HS on haemodynamic parameters in female offspring (**Table 6.4**), albeit the interaction between perinatal ID and HS in SBP approached significance (P=0.06, **Figure 6.1A**).

In male offspring, intravenous administration of pan-NOS inhibitor L-NAME caused a gradual rise in SBP, culminating in a 20-42% increase over baseline which was least pronounced in the perinatal ID offspring fed the HS diet (**Figure 6.1B**). The magnitude of SBP rise was reduced by perinatal ID and HS (**Figure 6.1B**), resulting in similar SBP between groups after L-NAME treatment (**Figure 6.1C**). In female offspring, the L-NAME-mediated rise in SBP ranged from 6-17% and was mitigated by the effects of HS — an effect that was most pronounced in the perinatal ID offspring (**Figure 6.1B**).

Table 6.4. Offspring blood pressures at 6 months of age.

Parameter		Treatment				P-Values		
		CTL		ID		ID	HS	Int.
		NS	HS	NS	HS			
M	SBP (mmHg)	112.5±2.7	124.0±6.5	124.9±2.6	137.3±7.9	**0.01**	**0.02**	0.93
	MAP (mmHg)	86.4±2.0	95.0±5.4	94.5±2.6	102.6±4.5	**0.03**	**0.03**	0.94
	DBP (mmHg)	72.1±1.5	80.5±5.3	79.3±2.7	85.2±4.2	0.09	**0.045**	0.71
F	SBP (mmHg)	137.2±5.5	131.3±9.2	127.2±4.9	147.4±7.9	0.66	0.30	0.06
	MAP (mmHg)	101.3±3.9	100.3±6.1	96.8±3.7	109.9±5.2	0.59	0.20	0.14
	DBP (mmHg)	83.4±3.4	84.8±5.2	81.6±3.4	91.2±4.3	0.57	0.18	0.32

All groups n=8-11. Data are expressed as mean ± SEM and analyzed by two-way ANOVA with Sidak's *post hoc* test. CTL, control; DBP, diastolic blood pressure; F, female; HS, high salt diet; ID, perinatal iron deficient group; int, interaction; M, male; MAP, mean arterial pressure; NS, normal salt diet group; SBP, systolic blood pressure.

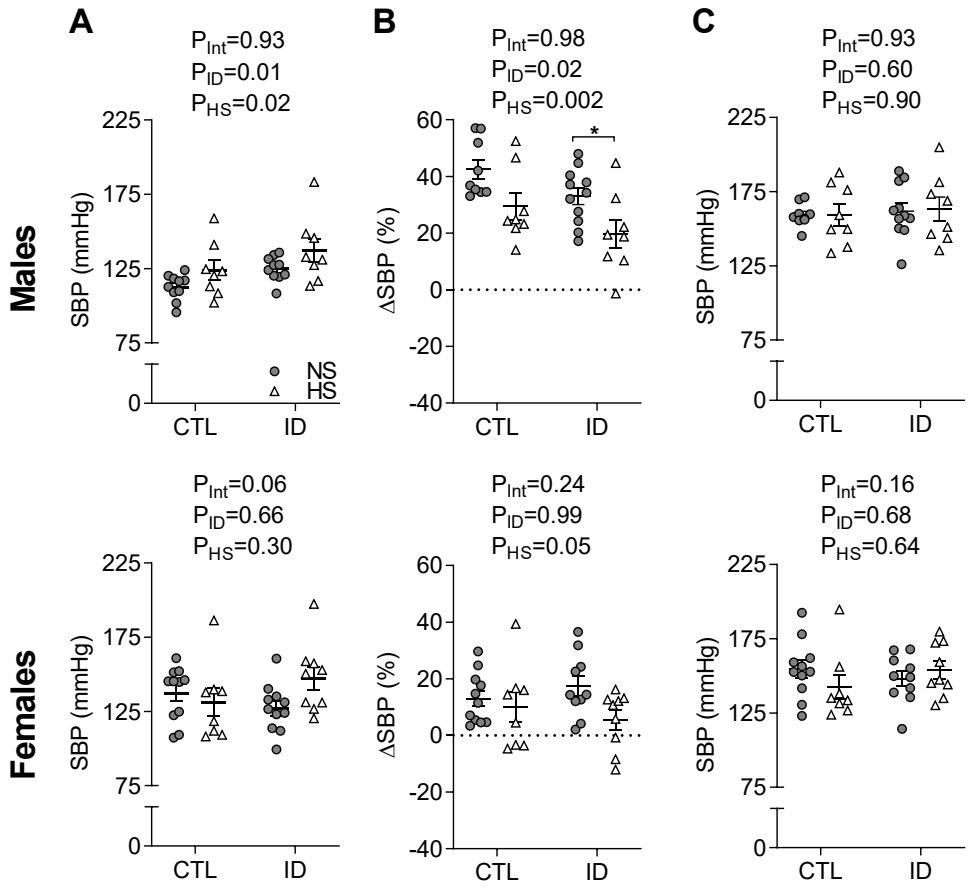

Figure 6.1: Haemodynamics & Nitric Oxide (NO) Signalling. Systolic blood pressure (SBP) and systemic nitric oxide NO signalling interrogated by NO synthase inhibitor L-LAME in six-month-old offspring fed a normal salt (NS) or high salt (HS) diet, born from control (CTL) or iron deficient (ID) dams. (**A**) Baseline SBP, (**B**) percentage increase in SBP with the addition of L-NAME, and (**C**) SBP in the presence of L-NAME. All groups n=8-11. Data analyzed by two-way ANOVA with *Sidak's post hoc test* where * denotes P<0.05 vs. NS.

6.4.3 Mitochondrial Content and Function

Mitochondrial respiration in renal tissues is expressed both as flux per unit homogenate mass, as well as flux control ratio (FCR; see online supplement), where FCR is indicative of qualitative changes in mitochondrial respiratory control and independent of mitochondrial density.[289] Within the medulla and cortex, LEAK respiration (oxygen flux in the absence of ADP unavailable for performing biochemical work)[289] was not affected by either ID or HS in male or female offspring (**Figure 6.2**). The magnitude of LEAK respiration was low and indicative of well coupled mitochondria in all groups (**Figures 6.3** & **6.4**). Moreover, addition of cytochrome *c* resulted in similar fractional increases in N-pathway respiration between groups (**Table 6.5**), indicating integrity of the outer mitochondrial membrane was similar in tissues among treatment groups.[289] Notwithstanding, all coupled oxidative phosphorylation (OXHPOS; in the presence of saturating ADP) and electron transfer (ET; non-coupled respiration after the addition of uncoupler) capacities presented herein reflect measurements taken after the addition of exogenous cytochrome *c*, avoiding possible bias resulting from damage to the outer mitochondrial membrane during tissue preparation.

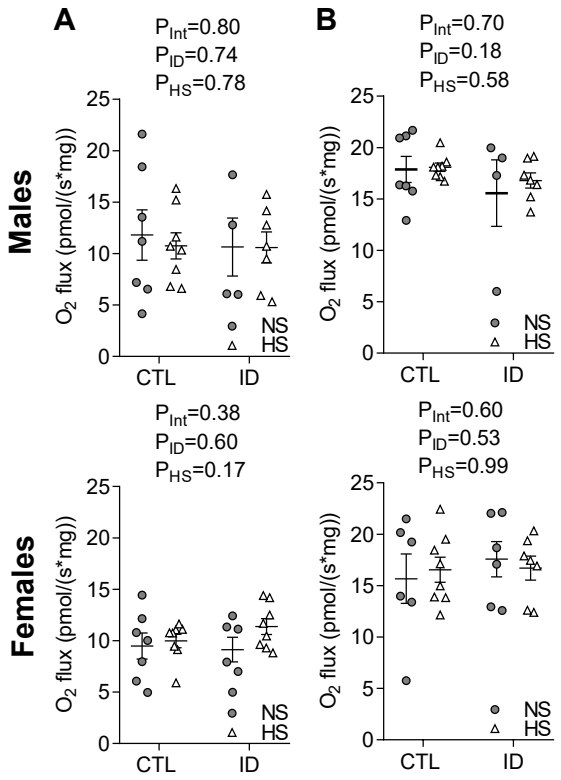

Figure 6.2: Kidney LEAK respiration. (**A**) medulla and (**B**) cortex LEAK respiration (in the absence of ADP) expressed as flux per unit mass tissue from 6-month-old offspring born to iron deficient (ID) or control (CTL) dams challenged with a normal salt (NS) or high salt (HS) diet for 6 weeks prior to experimentation. In the male ID-NS group n=4, and n=6-8 in all others. Data are analyzed by two-way ANOVA and Sidak's *post hoc* test.

Table 6.5. Fractional increases over N-pathway oxygen flux with the addition of cytochrome c in respirometry experiments.

Tissue		Treatment				P-Value		
		CTL		ID		ID	HS	Int.
		NS	HS	NS	HS			
Kidney	M	0.16±0.01	0.17 ±0.01	0.16±0.03	0.18±0.02	0.73	0.42	0.80
Medulla	F	0.16±0.02	0.14 ±0.01	0.18±0.02	0.16±0.02	0.44	0.20	0.94
Kidney	M	0.25±0.02	0.25 ± 0.02	0.31±0.03	0.23±0.03	0.63	0.16	0.14
Cortex	F	0.29±0.04	0.26 ± 0.03	0.32±0.03	0.25±0.02	0.71	0.10	0.51

In male ID-NS group n=4, and n=6-8 in all others. Data are expressed as mean ± SEM and analyzed by two-way ANOVA and Sidak's *post hoc* test. CTL, control; F, female; HS, high salt diet; ID, perinatal iron deficient group; int, interaction; M, male; NS, normal salt diet group.

In adult male offspring, medullary oxygen flux per unit mass through the NADH- and Succinate- (N- and S-) pathways as well as complex IV activity were increased by HS (**Figure 6.5A-E**), while perinatal ID reduced flux through the S-pathway (**Figure 6.5B-D**). FCR in the medulla of male offspring are unaffected by ID and HS (**Figure 6.3**). Within the cortex, ID and HS did not alter oxygen flux per unit mass for any parameter (**Figure 6.6A-E**), nor did it alter FCR for N- and S-pathways (**Figure 6.4A-D**). An interaction between perinatal ID and HS was observed in the cortex of male offspring, where complex IV FCR was reduced by HS only in ID offspring (**Figure 6.4E**); a similar trend was observed in flux per mass (interaction P=0.07, **Figure 6.6E**). There were no effects of perinatal ID or HS in oxygen flux per unit mass in either the renal medulla (**Figure 6.5**) or cortex (**Figure 6.6**) in adult female offspring, nor when data were expressed as FCR (**Figures 6.3** & **6.4).** Mitochondrial content of the renal medulla, as assessed by CS activity assay, was increased by HS in male, but not female offspring (**Figure 6.7A**). Within the cortex, no alterations in mitochondrial content were observed in either male or female offspring due to perinatal ID or HS (**Figure 6.7B**).

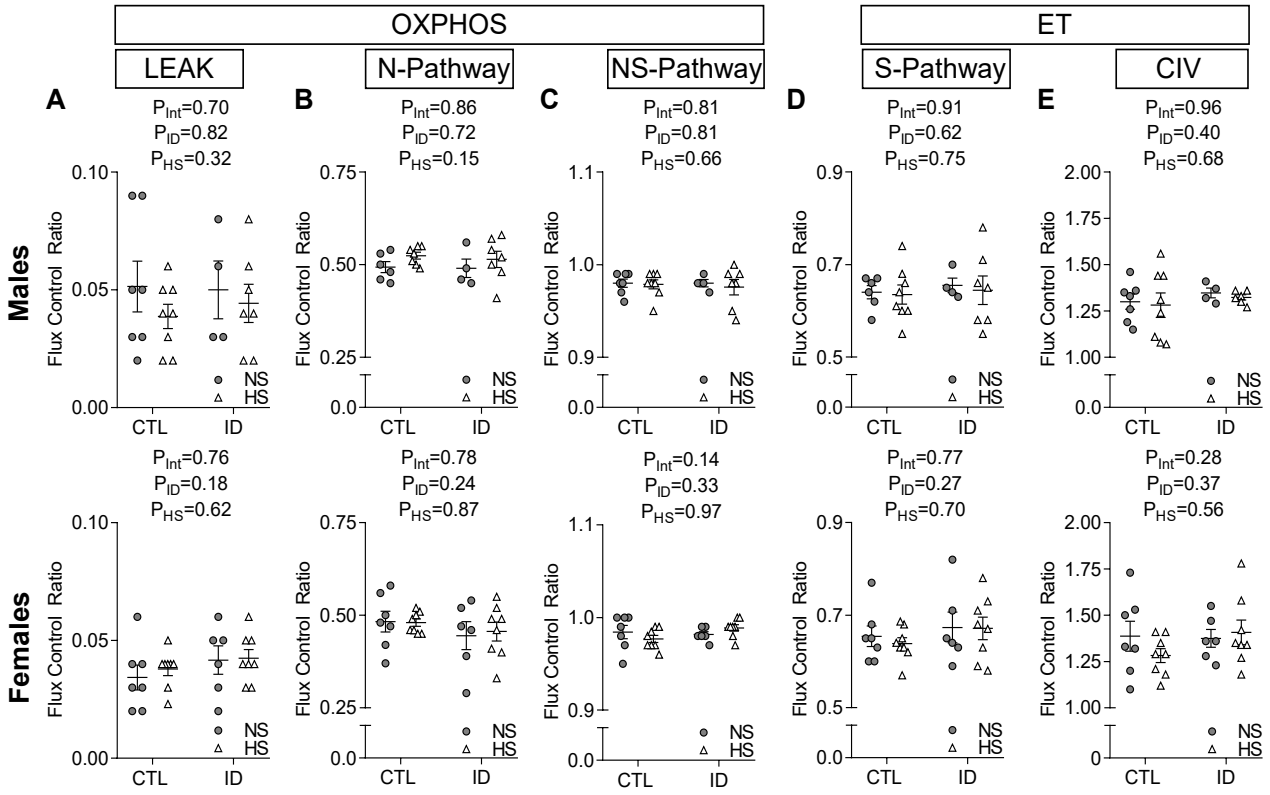

Figure 6.3: Kidney medullary mitochondrial flux control ratios (FCR). Renal medullary respirometry data expressed as FCR from 6-month-old offspring challenged with a normal salt (NS) or high salt (HS) diet for 6 weeks, born from iron deficient (ID) or control (CTL) dams. (**A**) LEAK (respiration in the absence of ADP), (**B**) NADH (N-) pathway oxidative phosphorylation (OXPHOS), (**C**) N- and Succinate (S-) pathway OXPHOS,

(**D**) S-pathway electron transfer (ET), and (**E**) complex IV activity. In the male ID-NS group n=4, and n=6-8 in all others. Data are analyzed by two-way ANOVA and Sidak's *post hoc* test.

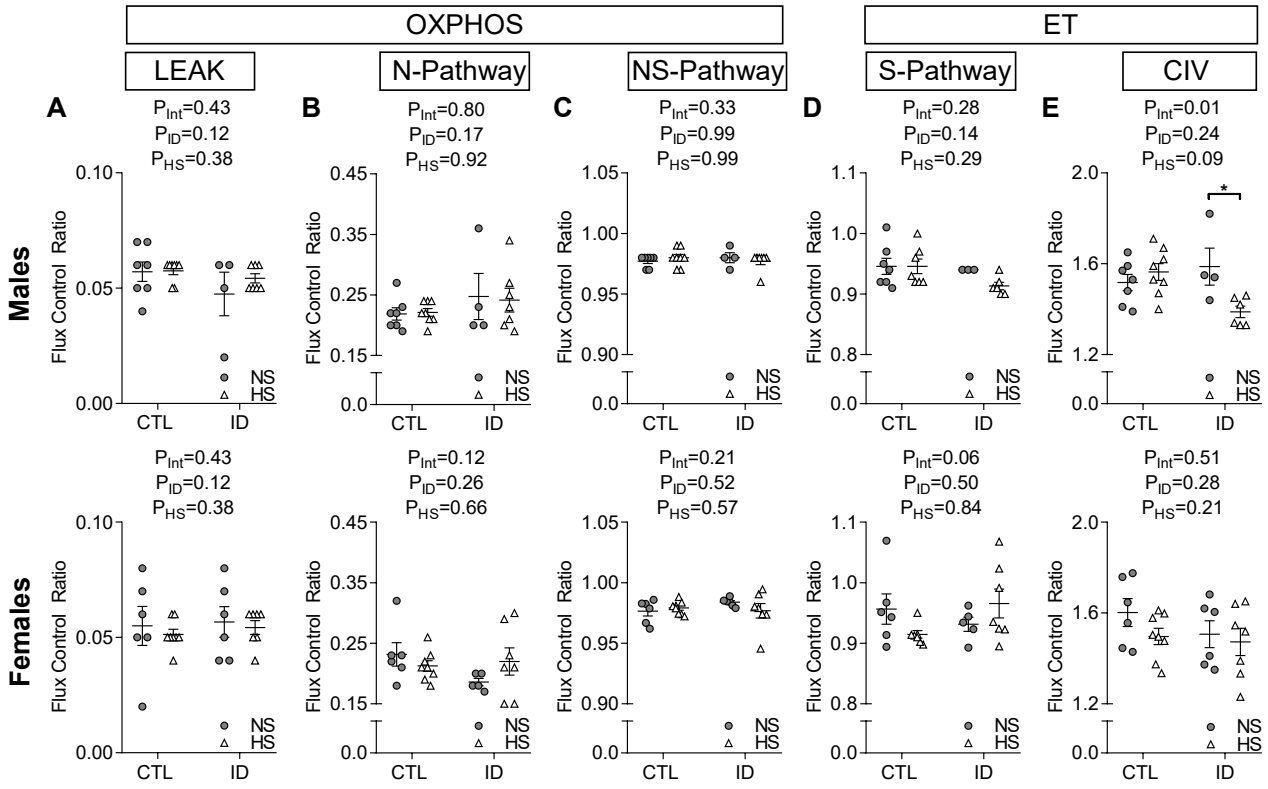

Figure 6.4: Kidney cortical mitochondrial flux control ratios (FCR). Renal cortical respirometry data expressed as FCR from 6-month-old offspring challenged with a normal salt (NS) or high salt (HS) diet for 6 weeks, born from iron deficient (ID) or control (CTL) dams. (**A**) LEAK (respiration in the absence of ADP), (**B**) NADH (N-) pathway oxidative phosphorylation (OXPHOS), (**C**) N- and Succinate (S-) pathway OXPHOS,

(**D**) S-pathway electron transfer (ET), and (**E**) complex IV activity. In the male ID-NS group n=4, and n=6-8 in all others. Data are analyzed by two-way ANOVA and Sidak's *post hoc* test where * denotes P<0.05 vs. NS.

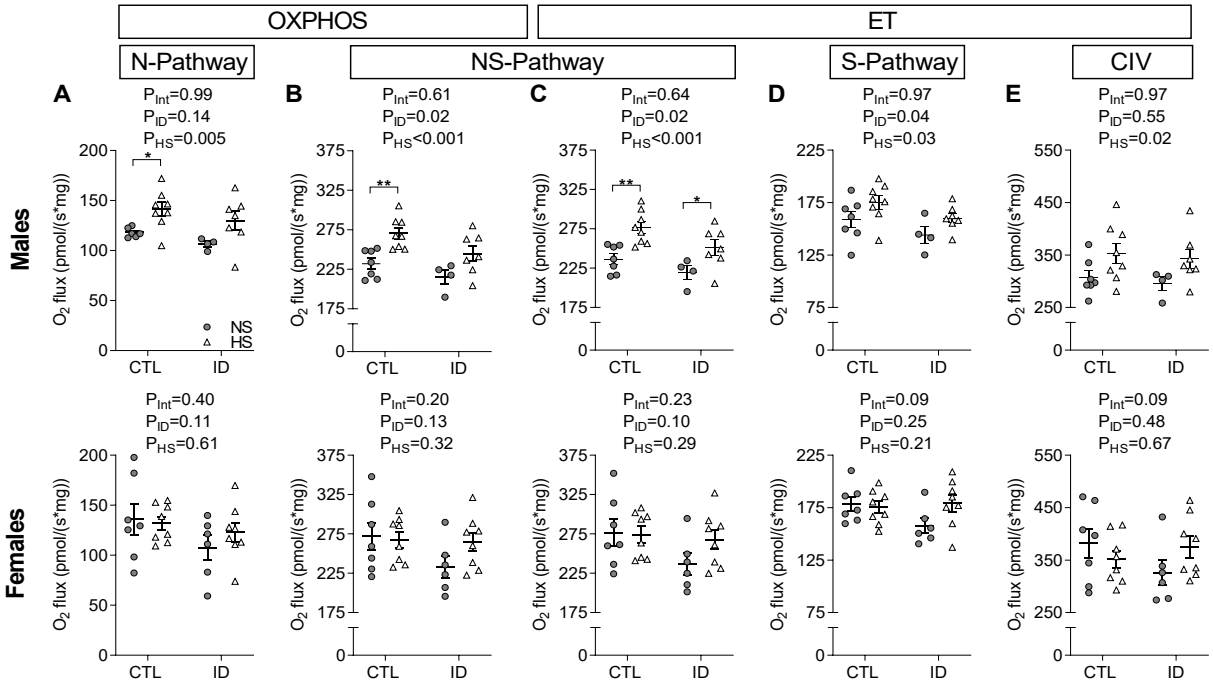

Figure 6.5: Kidney medullary mitochondrial flux per unit mass. Renal medullary respirometry data expressed as flux per unit mass of tissue from 6-month-old offspring fed a normal salt (NS) or high salt (HS) diet, born from iron deficient (ID) or control (CTL) dams. Measurement of function is made under two states, oxidative phosphorylation capacity (OXPHOS; coupled to ATP production) and electron transfer capacity (ET; uncoupled). (**A**) NADH (N-) pathway OXPHOS, (**B**) N- and Succinate (S-) pathway OXPHOS, (**C**) NS-pathway ET (**D**) S-pathway ET, and (**E**)

complex IV activity. Males n=4 in ID-NS, 6-8 in all others; Females n=6-8 in all groups. Data analyzed by two-way ANOVA with *Sidak's post hoc test* where * and ** denote P<0.05 and P<0.01 vs. NS, respectively.

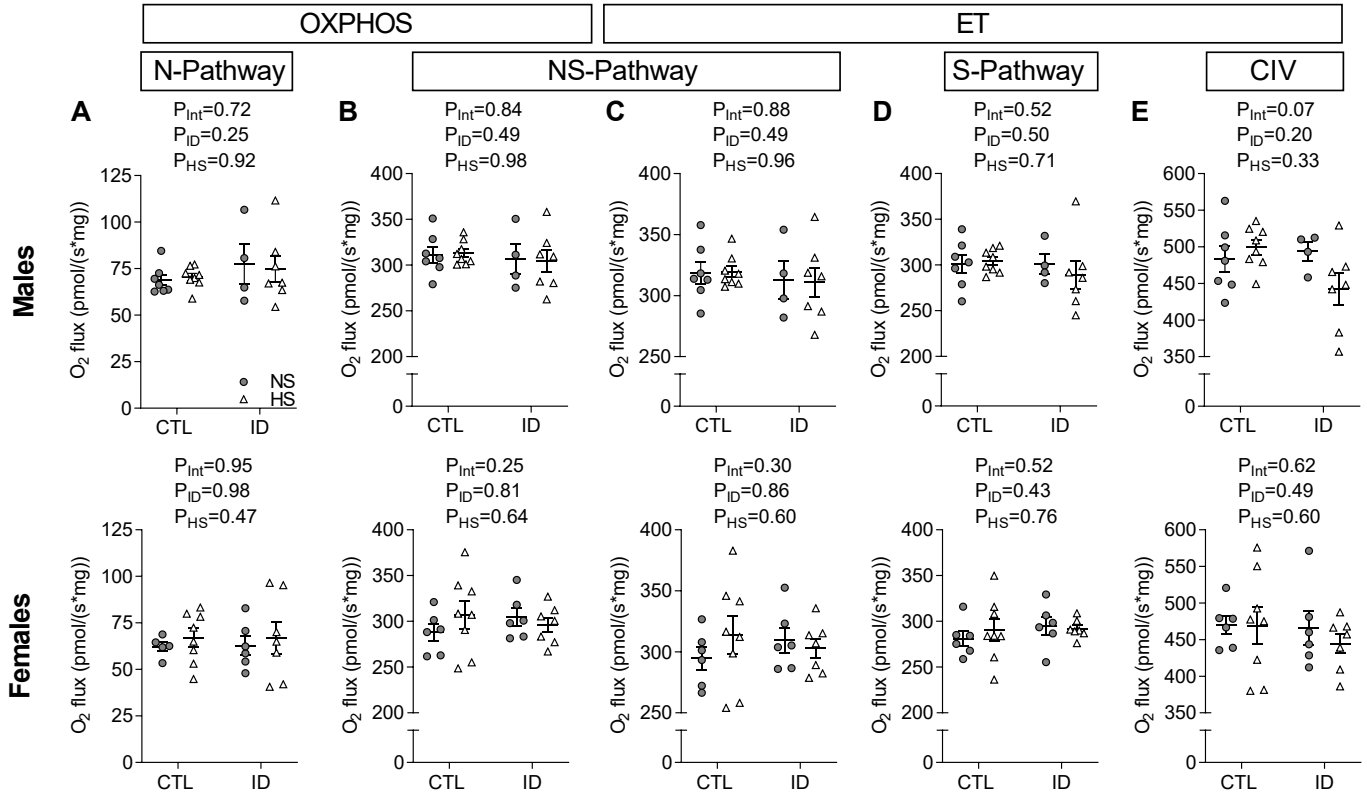

Figure 6.6: Kidney cortical mitochondrial flux per unit mass. Renal cortical respirometry data expressed as flux per unit mass of tissue from 6-month-old offspring fed a normal salt (NS) or high salt (HS) diet, born from iron deficient (ID) or control (CTL) dams. Measurement of function is

made under two states, oxidative phosphorylation capacity (OXPHOS; coupled to ATP production) and electron transfer capacity (ET; uncoupled). (**A**) NADH (N-) pathway OXPHOS, (**B**) N- and Succinate (S-) pathway OXPHOS, (**C**) NS-pathway ET (**D**) S-pathway ET, and (**E**) complex IV activity. Males n=4 in ID-NS, 6-8 in all others; Females n=6-8 in all groups. Data analyzed by two-way ANOVA with *Sidak's post hoc test.*

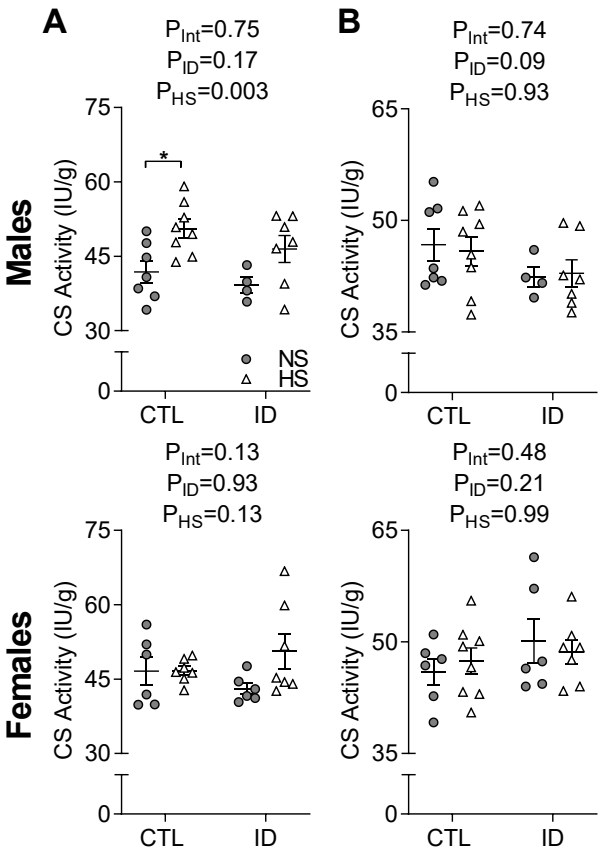

Figure 6.7. Kidney citrate synthase (CS) activity. (**A**) medulla and (**B**) cortex homogenates from six-month-old offspring fed a normal salt (NS) or high salt (HS) diet, born from iron deficient (ID) or control (CTL) dams. Males n=4 in ID-NS, 6-8 in all others; Females n=6-8 in all groups. Data analyzed by two-way ANOVA with *Sidak's post hoc test* where * denotes P<0.05 vs. NS.

6.4.4 Kidney Superoxide and NO Levels

In male offspring, there was an overall effect of HS on mitochondrial superoxide within the medulla (**Figure 6.8A**), but there was no effect of either ID or HS within the cortex (**Figure 6.8A** & **6.8D**). Perinatal ID caused an increase in cytosolic superoxide levels in both the renal medulla (**Figure 6.8B**) and cortex (**Figure 6.8E**) in adult male offspring, and HS caused a further increase within the cortex (**Figure 6.8E**). NO bioavailability in the medulla and cortex of male offspring was reduced by ID, with a trend for further decreases by HS in the medulla (P=0.08; **Figure 6.8C** & **6.8F**). In female offspring, mitochondrial superoxide was not altered by perinatal ID or HS within either the cortex or medulla of the kidney (**Figure 6.8A** & **6.8D**). Females exhibited a subtle but significant interaction effect for cytosolic superoxide levels due to perinatal ID and HS within the medulla and cortex (**Figure 6.8B** & **6.8E**). No reductions in NO levels were seen in females due to perinatal ID in either the medulla or cortex, and there was a trend for decreased NO in the cortex due to HS (P=0.06; **Figure 6.8C** & **6.8F**). Representative fluorescence images are shown in **Figures 6.9** & **6.10**.

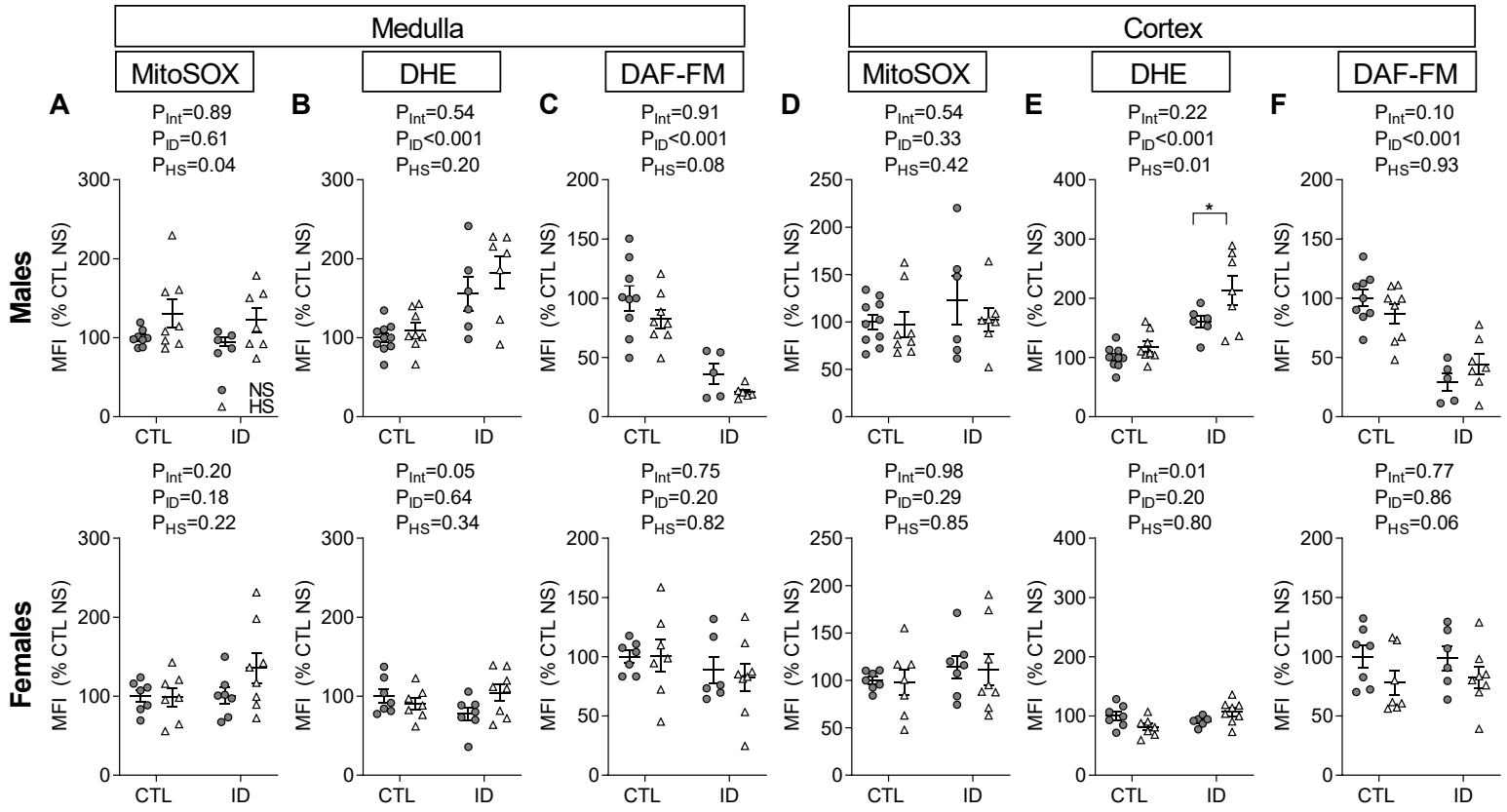

Figure 6.8: Kidney reactive species. Mitochondrial superoxide (MitoSOX), cytosolic superoxide (DHE) and cytosolic NO (DAF-FM) mean fluorescent intensities (MFI) in six-month-old offspring fed a normal salt (NS) or high salt (HS) diet, born from iron deficient (ID) or control (CTL) dams. (**A**) Medulla MitoSOX, (**B**) Medulla DHE, (**C**) medulla DAF-FM, (**D**) cortex MitoSOX, (**E**) cortex DHE, and (**F**) cortex DAF-FM. Males n=5-10; Females n=6-8 in all groups. Data analyzed by two-way ANOVA with *Sidak's post hoc test* where * denotes P<0.05 vs. NS.

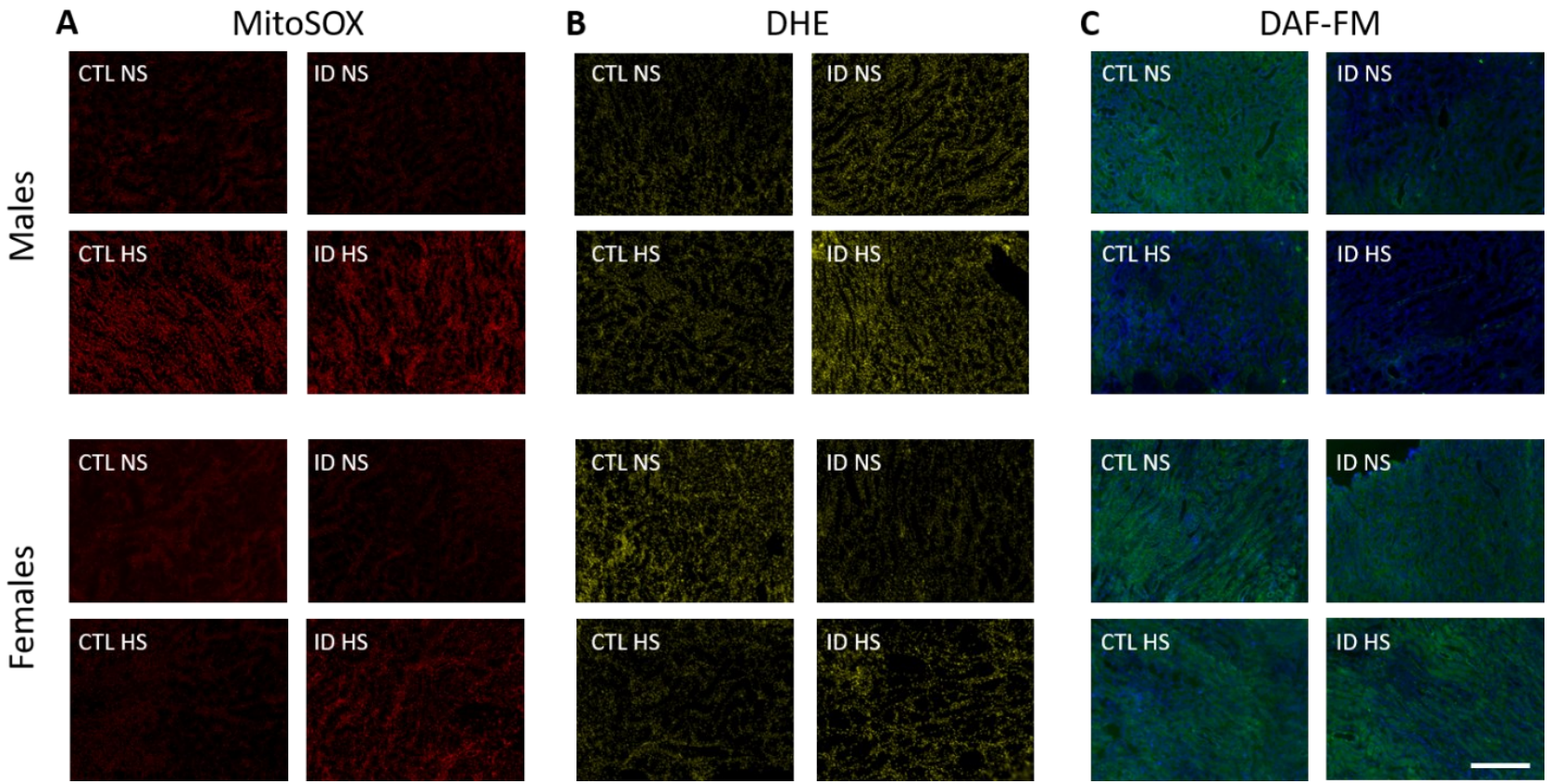

Figure 6.9: Renal medullary reactive species representative images. (**A**) MitoSOX in red, (**B**) DHE in yellow and (**C**) DAF-FM in green (with a DAPI blue nuclear counterstain) from 6-month-old offspring challenged with a normal salt (NS) or high salt (HS) diets for 6 weeks, born from control (CTL) or iron deficient (ID) dams. See summary data in **Figure 6.8A-C**. White scale bar represents 240 μm, which is the same in all images.

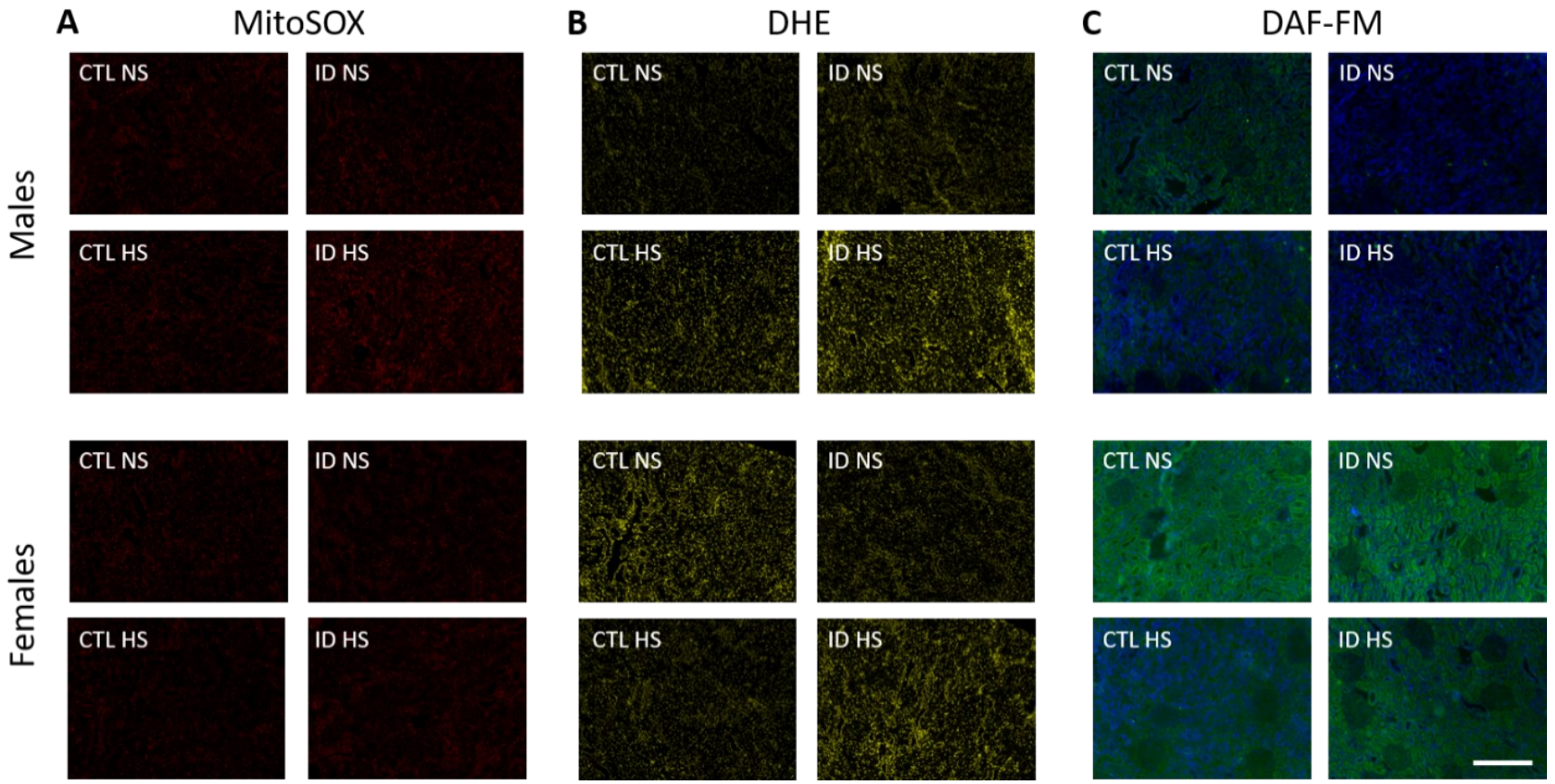

Figure 6.10: Renal cortex representative images. (**A**) MitoSOX in red, (**B**) DHE in yellow and (**C**) DAF-FM in green (with a DAPI blue nuclear counterstain) from 6-month-old offspring challenged with a normal salt (NS) or high salt (HS) diets for 6 weeks, born from control (CTL) or iron deficient (ID) dams. See summary data in **Figure 6.8D-F**. White scale bar represents 240 μm, which is the same in all images.

6.4.5 Renal Morphology

In male offspring, GBM thickness was increased by both perinatal ID and HS (**Figure 6.11A**). Maximal glomerular cross-sectional area in male offspring was increased by the combination of perinatal ID and HS, but not by either factor alone (**Figure 6.11B**). Finally, interstitial and glomerular collagen deposition in male offspring was increased by both perinatal ID and HS (**Figure 6.11C**). In contrast, female offspring exhibit no alterations in GBM thickness, maximal glomerular cross-sectional area, or collagen deposition due to either perinatal ID or HS (**Figure 6.11A-C**). Representative histological images are shown in **Figure 6.12**.

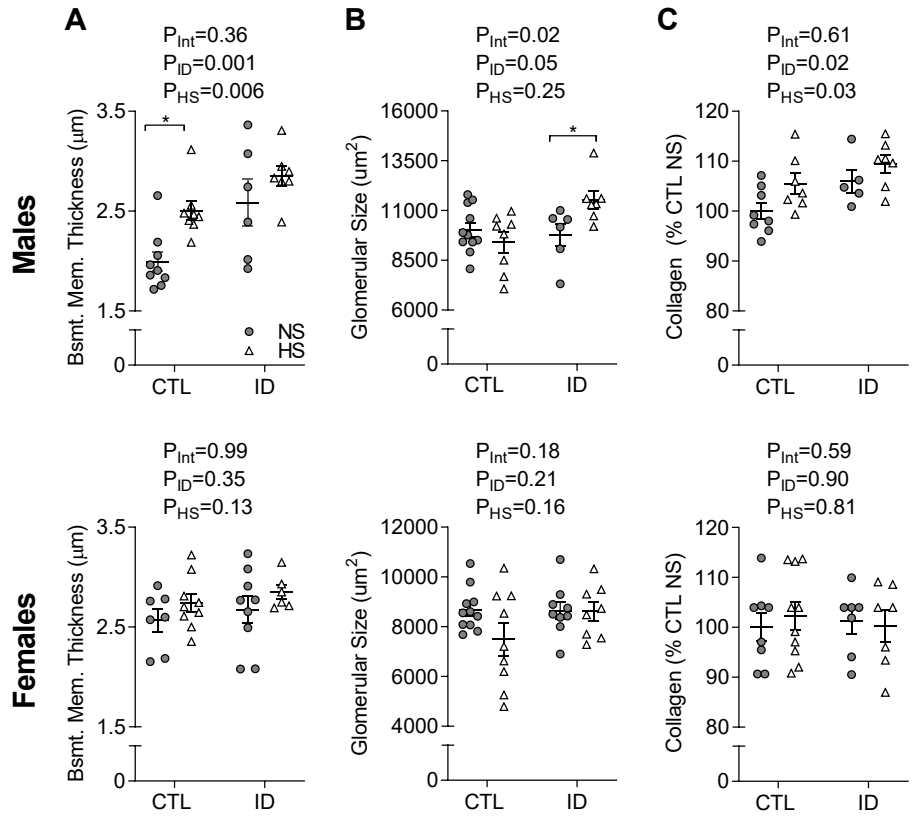

Figure 6.11: Renal injury and morphology. Renal morphological parameters in six-month-old offspring fed a normal salt (NS) or high salt (HS) diet, born from iron deficient (ID) or control (CTL) dams. (**A**) glomerular basement membrane thickness, (**B**) maximum glomerular cross-sectional area, and (**C**) interstitial & glomerular collagen deposition. Male n=5-8; female n=6-10. Data analyzed by two-way ANOVA with *Sidak's post hoc test* where * denotes P<0.05 vs. NS.

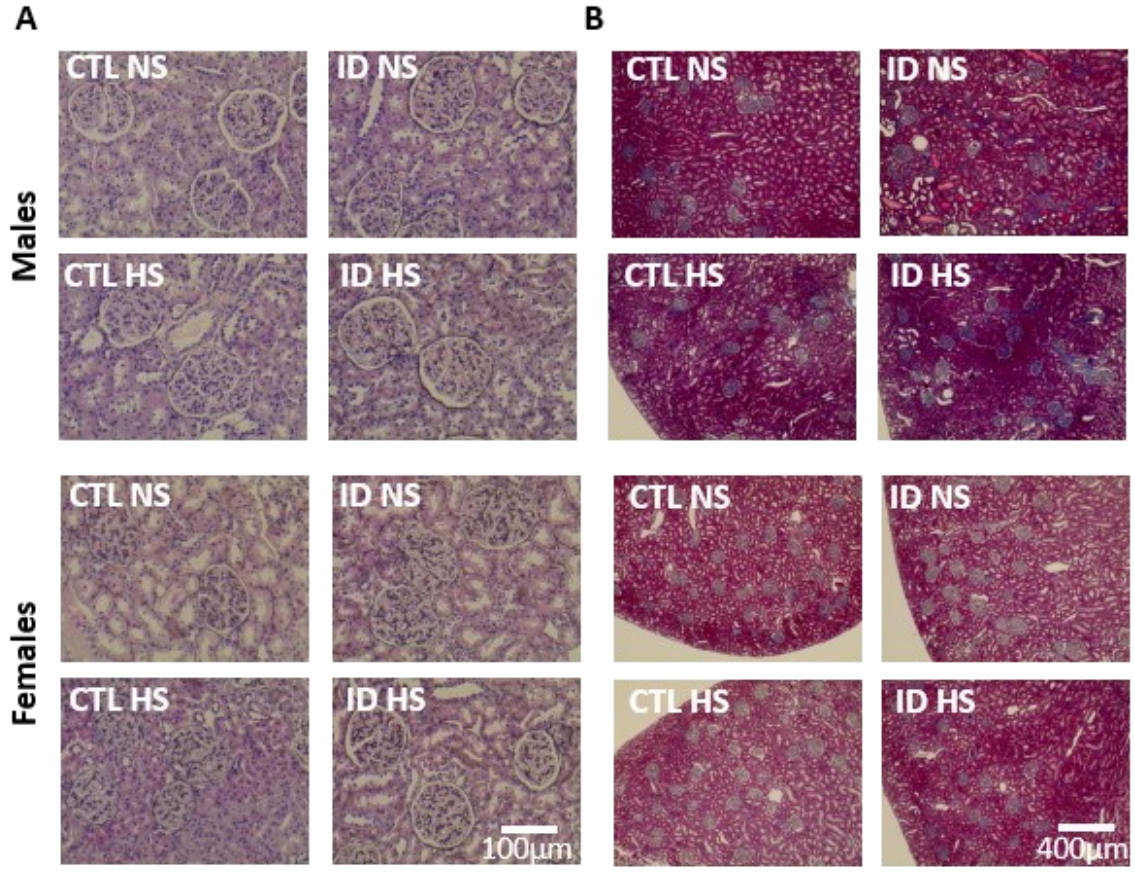

Figure 6.12: Renal morphology representative images. (**A**) Jones silver stain and (**B**) Masson's trichrome stained kidney sections for assessment of glomerular basement membrane thickness (stained black) and collagen deposition (stained blue), respectively. 6-month-old offspring were challenged with a normal salt (NS) or high salt (HS) diets for 6 weeks, born from control (CTL) or iron deficient (ID) dams. See summary data in **Figure 6.11**.

6.5 Discussion

Here, we show that perinatal ID and a HS diet in adulthood cause sex-specific alterations in haemodynamics, and kidney morphology and metabolic function. Specifically, adult male perinatal ID offspring exhibit increased BP concomitant with renal structural changes, alterations in medullary mitochondrial function in flux per mass, and dysregulation of ROS and NO levels, whereas female offspring are largely unaffected. In addition, male offspring exhibit an interaction effect for reduced complex IV activity in the cortex with the combination of both perinatal ID and HS. Taken together, these findings suggest that the developing kidney is susceptible to long-term programming by perinatal ID, and female offspring are protected from these long-term effects.

Maternal iron restriction during pregnancy caused anaemia in the dams and offspring at birth, as well as reduced weight gain in the dams during pregnancy, which is consistent with smaller litters and fetal growth restriction. Notably, male and female offspring exhibited similar levels of anaemia and growth restriction at birth, suggesting the degree of insult on the offspring was similar in both sexes. Although all rats were fed iron replete diets after giving birth, offspring born to iron restricted dams exhibit reduced Hb levels until shortly after weaning.[159,170,253] This exposure therefore reflects a 'perinatal' rather than exclusively 'prenatal' insult which encompasses the entire window of kidney development in the rat.[175] By six months, an age which corresponds to approximately 18-25 years in humans,[371] male perinatal ID offspring remained growth restricted (based on body weights, lengths and abdominal girth) compared to their control counterparts, yet differences were no longer evident in female offspring. Thus, based on growth patterns alone, male and female offspring exhibit different susceptibilities to the effects of perinatal ID.

The observation that perinatal ID resulted in elevated BP in adult male offspring is consistent with previous findings from our group[159,160,170] and others.[215,230–232,254] The introduction of a HS diet to the adult offspring was intended to mimic the excess consumption of dietary sodium, a modifiable risk factor for hypertension and CVD.[115]

Approximately 89% of the US population[372] and 58% of the Canadian population[373] exceed daily recommended salt intake, which can negatively impact both renal and vascular function.[115] In the present study, HS diet induced a greater than two-fold increase in water intake (without affecting food intake), thus imposing stress to the cardiovascular system by increasing renal filtration and pressure natriuresis, as reflected in increased SBP in both CTL and perinatal ID male offspring. However, the interaction between the perinatal ID and HS treatments was not significant in male offspring, suggesting the salt-sensitivity of BP was not more pronounced in programmed offspring, in contrast to our previous reports.[159,160,170] The explanation for this may reside in the fact that BP assessments in the present study were done entirely under isoflurane anaesthesia, which can blunt sympathetic outflow[374] and thus attenuate underlying salt-sensitivity.[375]

Renal injury was observed in male offspring due to both perinatal ID and HS. GBM thickness and collagen deposition were increased due to both perinatal ID and HS diet, which were likely secondary to increased BP. Furthermore, the combination of perinatal ID and HS resulted in enlargement of glomerular cross-sectional area, which may indicate compensatory hypertrophy to maintain GFR with a reduced nephron complement.[215] Elevations in LVS mass occur secondary to increased BP,[376] which may supports the patterns of cardiac hypertrophy observed in the HS-treated offspring. In contrast, the effect of perinatal ID on LVS size did not reach statistical significance, despite these offspring being hypertensive and exhibiting renal injury, which may indicate that the study was not powered to detect this difference. Alternatively, it may be that LV effects will become manifest as the hypertension progresses with age; indeed, Rueda-Clausen *et al.* reported that LV weights in offspring exposed to prenatal hypoxia, which shares a common etiology to perinatal ID,[164] showed no overt differences in LV size at 4 months of age, but pronounced effects at 12 months of age[377] when hypertension becomes apparent in this model.[239] RV hypertrophy was also noted in adult male perinatal ID offspring, potentially reflecting increased resistance within the pulmonary circulation.[378] Although this remains to be investigated, adult offspring exposed to

prenatal hypoxia develop signs of pulmonary hypertension in rat models,[377] drawing further parallels between these models of developmental stress.

In our first study focusing on BP outcomes in programmed female offspring, we found that there was no effect of perinatal ID on BP. For reasons unclear to us, BPs assessed under anesthesia even in control female offspring were higher than anticipated, which could arguably mask an elevated BP in the programmed females. However, left ventricular weights and histological assessments of renal morphology were similar in all groups, suggesting no overt cardiovascular phenotype in female perinatal ID offspring. Although reports utilizing tail cuff plethysmography have shown perinatal ID increases BP in offspring of both sexes, the effects are less pronounced in females.[215,230,232,254] HS also had little effect on BP in female offspring, consistent with a lack of effect of perinatal ID and HS on LVS weights. Interestingly, the effect of perinatal ID approached significance in RV weights, suggesting the increased pulmonary resistance occurring in offspring is not sex-dependent. These patterns are consistent with those in adult offspring exposed to prenatal hypoxia, in which males exhibited a greater propensity for systemic hypertension (in later life),[239] whereas both males and females are susceptible to pulmonary hypertension.[377]

The BP effects in male offspring attributed to perinatal ID and HS occur concomitantly with marked alterations in renal mitochondrial function, ROS generation, and ultimately NO-signaling. Mitochondrial dysfunction within the kidney has been implicated in chronic kidney disease,[379] and has been observed in models characterized by renal dysfunction[380] and sensitivity to HS diet,[237] suggesting proper kidney function relies on a delicate balance of cellular energy metabolism. While perinatal ID had no effect on mitochondrial content, the medullae of male offspring exhibited reductions in oxygen flux per mass through the succinate-dependent pathway. In contrast, HS caused marked increases in medullary mitochondrial content in male offspring (irrespective of perinatal exposure), despite having little impact on mitochondrial content or function within the cortex. This is consistent with previous reports describing mitochondrial biogenesis in the wake of increased medullary osmolality and Na^+ concentrations.[381] Our

results show that the medulla is highly sensitive to both perinatal stressors and a chronic HS diet. Interestingly, in female offspring, neither perinatal ID nor HS diet caused alterations in mitochondrial content or function in the medulla or cortex, which suggests fundamental differences in the way males and females respond to excess sodium intake.[382]

The mitochondrial function data described above are supported by the patterns of renal superoxide in adult offspring. Male perinatal ID offspring exhibit increased cytosolic superoxide within the medulla and cortex, consistent with dysfunction in complexes II and IV,[297,383] respectively. Within the medulla, HS caused an increase in mitochondrial content roughly proportional to increased mitochondrial superoxide levels. In contrast, female offspring had no alterations in mitochondrial content or function, coincident with minimal alterations in mitochondrial and cytosolic superoxide levels due to ID or HS. Although a significant interaction between perinatal ID and HS was observed in DHE staining in both medulla and cortex of female offspring, the magnitude of differences were small, and therefore the physiological relevance is likely minor. Vieyra-Reyes *et al*. have shown adult female perinatal ID offspring exhibit increased antioxidant enzyme activity,[85] which could explain why perinatal ID females are less prone to oxidative stress, including from major non-mitochondrial sources such as NADPH oxidases.[384]

Oxidant status within the kidney plays a direct role in the bioavailability of NO, which is known to regulate sodium and fluid homeostasis.[103] We report that male perinatal ID offspring exhibit >50% reductions in NO levels within both the medulla and cortex, in agreement with elevated superoxide levels scavenging NO.[103] Low levels of NO may contribute to the hypertension in male offspring by promoting salt-retention, either via direct actions on tubular sodium reuptake,[103] or via reducing medullary blood flow.[103,385] Indeed, L-NAME treatment ultimately normalized BP levels in male offspring, suggesting loss of NO may underlie the baseline differences between control and perinatal ID offspring. Although NO can modulate medullary blood flow, tubuloglomerular feedback and natriuresis,[103,385] contributing to hypertension[386] and salt

sensitivity,[387] we cannot discount intrinsic differences in systemic vascular NO signaling that contribute to programming of BP regulation in perinatal ID offspring. Therefore, the programming of vascular function in perinatal ID male offspring treated with a HS diet should be studied. Investigations in female offspring may also provide important insights, and may uncover clues as to why oxidant status and NO signalling remain largely unaffected. Increased antioxidant capacity and actions of sex-hormones are potential mechanisms by which female offspring exposed to perinatal ID maintain normal oxidant status, NO signaling, and normal cardiovascular and renal function.

This study has limitations. First, as discussed above, the use of anaesthesia may have influenced haemodynamic assessments, particularly if programmed offspring have altered responsiveness to the blood pressure lowering effect of isoflurane.[388] Because of this potential confounder, BP data was complemented with measures of ventricular mass and renal morphology, which exhibit pathophysiological changes secondary to hypertension.[389] Second, certain aspects of the rat model used in this study limit the extrapolation of results to humans. For example, as an altricial species, rats are born immature and undergo comparatively greater growth and development in the immediate postnatal period compared to humans. The extent to which iron supply and demand are mismatched dictate the severity of iron deficiency, and whether this is similar in rats and humans during periods of kidney development is not clear. Nevertheless, the rat model of perinatal ID employed herein has notable strengths (e.g. development of maternal anemia mirrors that in humans, shared hemochorial placentation), and provides a platform to study the impact of maternal effects (e.g. liver hypoxia[164] and altered lipid metabolism[390]) versus offspring effects (e.g. renal hypoxia[164] and mitochondrial dysfunction[165]) in the long-term programming of offspring health. Finally, while not a limitation *per se*, the present study characterizes renal pathology in adult offspring but it does not mechanistically link these effects to previously observed fetal kidney hypoxia,[164] oxidative stress and mitochondrial dysfunction[165]. It is possible that the mitochondrial dysfunction and oxidative stress observed in fetuses persist into adulthood and contribute to renal dysfunction in later life. The alternative is that alterations in fetal energy

metabolism may cause persistent renal structural and functional changes, which in turn promote *de novo* cellular stress in adulthood. More studies are needed to assess the link between fetal and adult kidney oxidative stress and mitochondrial dysfunction in perinatal ID offspring.

In summary, the results presented herein show that perinatal ID causes long-term alterations in mitochondrial function and oxidative stress in the kidneys, which have been implicated in hypertension and cardiovascular dysfunction. Together with our previous findings in the fetal kidney,[164,165] these results suggest that the developing male kidney is particularly vulnerable to hypoxia-like insults.[218] Though beyond the scope of the current study, the involvement of mitochondrial dysfunction and increased ROS levels points to the use of mitochondrial targeted therapeutics to improve energetics in the developing and adult kidney. Irrespective of the mechanism, these findings speak to the importance of early interventions to prevent the programming of cardiovascular and renal function in adulthood and improve long-term outcomes.

Sources of Funding

This work was supported by grants from the Canadian Institutes of Health Research (CIHR; MOP142396) and the Women and Children's Health Research Institute (both to S.L.B.), and a Discovery Grant from the National Sciences and Engineering Research Council (RGPIN 402636; to H.L.). A.G.W. is a Vanier Scholar (CIHR) and receives additional support from an Alberta Innovates Graduate Studentship. S.L.B. holds a CIHR New Investigator Salary Award.

Acknowledgements

The authors acknowledge the University of Alberta Cardiovascular Research Centre for the use of their confocal microscope.

Conflicts of Interest/Disclosures

None declared.

Chapter 7

Perinatal Iron Deficiency Combined with a High Salt Diet in Adulthood Causes Sex-Dependent Vascular Dysfunction in Rats

Andrew G. Woodman[a,b,c], Ronan M.N. Noble[a,b,d], Sareh Panahi[a,b,e], Ferrante S. Gragasin[a,b,e], Stephane L. Bourque[a,b,c,d,e]

[a]Women and Children's Health Research Institute, University of Alberta, Edmonton, Canada [b]Cardiovascular Research Centre, University of Alberta, Edmonton, Canada
[c]Department of Pharmacology, University of Alberta, Edmonton, Canada
[d]Department of Pediatrics, University of Alberta, Edmonton, Canada
[e]Department of Anesthesiology and Pain Medicine, University of Alberta, Edmonton, Canada

PUBLISHED:
Woodman *et al. Journal of Physiology* 2019. 597(18):4715-4728

7.1 Abstract

Pre- and immediate postnatal stressors, such as iron deficiency, can alter developmental trajectories and predispose offspring to long-term cardiovascular dysfunction. Here, we investigated the impact of perinatal iron deficiency on vascular function in the adult offspring, and whether these long-term effects were exacerbated by prolonged consumption of a high salt diet in adulthood. Female Sprague Dawley rats were fed either an iron-restricted or -replete diet prior to and throughout pregnancy. Six weeks prior to experimentation at six months of age, adult offspring were fed either a normal or high-salt diet. Mesenteric artery responses to vasodilators and vasoconstrictors were assessed *ex vivo* by wire myography. Male perinatal iron deficient offspring exhibited decreased reliance on nitric oxide with methacholine-induced vasodilation (interaction P=0.03), coincident with increased superoxide levels when fed the high salt diet (P=0.01). Male perinatal iron deficient offspring exhibit enhanced big endothelin-1 conversion to active endothelin-1 (P=0.02) concomitant with decreased nitric oxide levels (P=0.005). Female offspring vascular function was unaffected by perinatal iron deficiency, albeit high salt diet was associated with impaired vasodilation and decreased nitric oxide production (P=0.02), particularly in the perinatal iron deficient offspring. These findings implicate vascular dysfunction in the sex-specific programming of cardiovascular dysfunction in the offspring by perinatal iron deficiency.

7.2 Introduction

Cardiovascular disease is a leading cause of global mortality, responsible for approximately a third of all deaths worldwide [93]. Historically, the aetiology of cardiovascular disease has focused on genetic and environmental factors, in which the former dictated the relative predisposition, and the latter the onset and severity. The developmental origins of health and disease (DOHaD) concept, first articulated by the late Professor David Barker, provided a new paradigm of chronic disease susceptibility. The DOHaD hypothesis posits that relative risk is dictated, at least in part, by the quality of the early developmental environment [140]. In the ensuing decades since its proposal, a large body of evidence has amassed in support of the DOHaD hypothesis, showing that various stressors during development, such as macro- and micronutrient deficiencies, contribute to long-term chronic disease risk in later life [139].

Iron-deficiency (ID) is the most common nutritional deficiency worldwide, and is highly prevalent in pregnant women and young children [21]. Increased iron demands due to rapid growth rates, coupled with inadequate iron uptake, are largely responsible for the depletion of tissue iron stores and eventual reduction of circulating haemoglobin (Hb) levels in these subpopulations [4]. Globally, an estimated 39% of pregnant women develop anaemia [21], and the estimated prevalence of latent ID, in which there is depletion of iron stores without manifestation of anaemia, is undoubtedly higher. Despite the seeming simplicity of the problem (i.e. inadequate iron uptake), the solution to ID in pregnancy is deceptively complex. Issues with poor iron absorption, patient compliance, and potential toxicity to the mother and foetus constitute notable challenges—a point which is underscored by the high rates of ID in pregnancy despite widespread supplementation and fortification efforts [21]. Moreover, while iron supplementation strategies have been shown to improve maternal anaemia, whether they also improve pregnancy outcomes in tandem is unclear [44,45]. These complexities emphasize the need better understand the immediate and long-term implications of perinatal ID for offspring health.

In addition to increasing the risk of foetal death, preterm birth, and intrauterine growth restriction [366,367], perinatal ID has been shown to cause long-term cardiovascular

complications, which include hypertension, salt sensitivity, and susceptibility to renal injury [170,215,230,231,309]. However, the impact of perinatal ID on vascular function has not been investigated. Changes in vascular function have been implicated in numerous models of developmental programming, such as prenatal hypoxia [154], which shares a common aetiology with perinatal ID [164]. Prenatal hypoxia has been shown to cause persistent alterations in vasoregulatory mechanisms, including reductions in nitric oxide (NO) bioavailability and dysregulation of vasoactive signalling in adult offspring in both rodent [233,239,391] and sheep models [249,392,393]. We hypothesized that perinatal ID would also result in altered reactivity to vasoactive compounds, which would be mediated by a loss in NO signalling and an increase in oxidative stress within the mesenteric arteries. Furthermore, we sought to determine whether these outcomes would be exacerbated by chronic consumption of a high salt diet.

7.3 Methods

7.3.1 Ethical Approval

The protocols described herein were approved by the University of Alberta Animal Care Committee in accordance with guidelines established by the Canadian Council of Animal Care. The authors confirm that experiments herein comply with the policies and regulations of *The Journal of Physiology* [394].

7.3.2 Animals and Treatments

The experiments carried out in this study were conducted using a cohort of offspring which were also used to study renal mitochondrial function [309]. Briefly, thirty experimentally naïve and nulliparous female Sprague-Dawley rats (initially 6 weeks of age) were purchased from Charles River (Saint-Constant, QC, Canada) and housed at the University of Alberta animal care facility under a 12-h light/dark cycle and ambient temperature of 23ºC. Rats were housed in conventional wire-top cages fitted with filter tops and enriched with wooden blocks and shredded paper pucks. All rats had *ad libitum* access to food and water throughout the study.

Female rats were fed purified diets based on the AIN-93G rodent diet (Research Diets Inc. New Brunswick, NJ). All diets are identical in composition, except for the amount of added ferric citrate. Two weeks prior to pregnancy, female rats were randomly assigned to the iron-restricted group, in which they were fed a diet low in iron (3 mg/kg iron; D03072501); the remaining females were allocated to the control group, in which they received a purified control diet (37 mg/kg iron diet; D10012G). After 2 weeks on their respective diets, female rats were bred by co-housing overnight with age-matched males fed a standard rodent chow (5L0D; PicoLab, St. Louis, MO, USA). Pregnancy was confirmed by the presence of sperm in a vaginal smear the following morning [defined as gestational day (GD)0]. Pregnant dams were single-housed thereafter, and those in the control group were maintained on the control diet throughout pregnancy, whereas the iron-restricted dams were fed a diet moderately low in iron (10 mg/kg iron; D15092501) for the duration of pregnancy. Maternal parameters such as Hb levels, body weight gain, and food consumption were recorded weekly. Within 12 hours of giving birth, all dams were fed the standard rodent chow, and litters were standardized to 8 offspring (four males and four females). Offspring were weaned from their mothers on postnatal day 21 and maintained on the rodent chow.

At four and a half months of age (six weeks prior experimentation), male and female offspring from each litter were allocated to receive either a normal salt diet (NS, 0.27% NaCl *w/w*; D06041501DW) or high salt diet (HS, 5.0% NaCl *w/w*; D17053103DW) for six weeks; these diets were also based on the AIN93G diet, and were identical in composition with the exception of added NaCl. Body weights, food intake and water consumption were monitored weekly for the duration of the salt treatment [309]. At 6 months of age (after 6 weeks of salt treatment), offspring were anesthetized with isoflurane (5% in medical grade oxygen) and euthanized by exsanguination and excision of the heart. Mesenteric blood vessels were collected for ex vivo assessments of vascular function in this study. Additional tissues (e.g. kidneys, hearts) were collected from these offspring for a parallel study, and haemodynamic assessments were performed in littermates; these data have been published [309].

7.3.3 Wire Myography

Vascular function was assessed in mesenteric resistance arteries of offspring according to established procedures at 37ºC [239]. The mesentery was rapidly excised and placed in ice-cold HEPES-buffered physiological saline solution (PSS; 142mM NaCl, 4.7mM KCl, 1.17mM $MgSO_4$, 4.7mM $CaCl_2$, 1.18mM KH_2PO_4, 10mM HEPES, and 5.5mM glucose, pH 7.4). Mesenteric arteries with internal diameters ranging 150-250µm were isolated from the surrounding adipose tissue using a binocular microscope, cut into 2mm segments, and mounted in an isometric myograph system (DMT, Copenhagen, Denmark) using 40µm tungsten wire. After a normalization protocol using stepwise increases in diameter to achieve optimal resting tension, vessels were rinsed and allowed to equilibrate for 15 minutes. Vessels were then tested for viability by assessing contractile responses to high-potassium PSS buffer (containing 123.7mM KCl and 24mM NaCl; otherwise identical to PSS buffer), then twice with a high dose of phenylephrine (PE; 10µM) (with multiple washes in between); endothelial integrity was confirmed by adequate vasodilation with the addition of methacholine (MCh; 1µM) following the second PE-induced constriction. Vessels with <50% vasodilation in response to 1µM MCh were excluded from analysis.

After viability testing, vessels were washed with PSS, then treated with either vehicle (PSS) or the nitric oxide synthase inhibitor L-N^G-Nitroarginine methyl ester (L-NAME; 100µM) for 30 min. Following pre-incubation, cumulative concentration response curves to PE (10nM-10µM; Sigma Aldrich), endothelin-1 (Et-1, 1-100nM; Calbiochem), or big Et-1 (bET-1, 10-310nM; Anaspec) were generated. For MCh (1nM - 5µM; Sigma Aldrich) and SNP (1nM - 5µM; Sigma Aldrich) responses, vessels were pre-constricted to 80% of maximal constriction with PE and given 5 min to stabilize before administration of vasodilators. For vasoconstriction data, all vessel constriction values are normalized to their response to the second PE dose obtained during the viability testing procedures described above. Vasodilation data are plotted as percent vasodilation, as measured from the state of constriction prior to MCh or SNP administration to resting baseline tension following drug washout (defined as 100% vasodilation).

7.3.4 Fluorescence Microscopy

During the preparation of vessels for myography (see section 2.2), an additional length of mesenteric artery was cryopreserved in OCT embedding medium for fluorescence assessments. Dihydroethidium (DHE) and 4-amino-5-methylamino-2`,71-difluorofluorescein diacetate (DAF-FM) were purchased from Thermo Fisher Scientific (Waltham, MA, USA), and used to assess cytosolic superoxide and NO production, respectively, as previously described [165,309]. Isolated mesenteric arteries (see section 2.2) were embedded in optimal cutting temperature compound (OCT, Tissue Tek, Sakura Inc.) and sectioned (10 µm thickness) at -20ºC by cryostat onto SuperFrost Plus microscope slides (Fisher Scientific), and then stored at -80ºC. Sections were thawed and washed 3 times with Hanks Buffered Salt Solution (HBSS), and warmed to 37ºC in a humidified chamber for 10min. Slides were washed again with HBSS and then incubated with either DHE (20µmol/L for 30min) or DAF-FM (20µmol/L for 30min). After incubation, slides were washed (2 min) three times with HBSS and subsequently mounted in HBSS (for DHE) or Vectashield Antifade Mounting Medium with DAPI (Vector Laboratories, Burlingame, CA). Fluorescence images were captured using an Olympus IX81 fluorescent microscope (Tokyo, Japan), and mean fluorescence intensity was quantified using Photoshop Elements 13 (Adobe Inc., San Jose, CA). Fluorescence of the internal elastic lamina was excluded from quantification.

7.3.5 Statistical Analyses

Data obtained from the same litter were averaged and treated as a single value; thus, n values reflect the number of litters (i.e. treated dams). A total of 63 adult offspring from a total of 30 litters were used in the current study; as noted above, these data represent a subset of offspring from which haemodynamics and renal mitochondrial function were studied [309]. Data were analysed by mixed-model or two-way ANOVA for the effects of perinatal ID and HS diet with Sidak's *post hoc* test; data sets were paired for vehicle and L-NAME treatments in the vessels harvested from the same rat. All male and female offspring data were analysed separately. For concentration response curves, area under

the curve (AUC) or area over the curve (AOC) were calculated; EC_{50} values were derived by fitting data to the Hill equation when dose response curves were sigmoidal. Grubbs test was performed following completion of analysis, and statistical outliers were removed from all analyses. Data are presented as mean±SD unless otherwise stated. $P<0.05$ was considered significant. All statistical analyses were conducted using GraphPad Prism 8.1 software. Investigators were not blinded for any analyses.

7.4 Results

7.4.1 Pregnancy Outcomes and Offspring Characteristics

Pregnancy outcomes for this cohort have been reported [309], and are reproduced herein with permission (**Table 7.1**). Iron-restricted dams had ~31% reductions in Hb levels compared to controls by gestational day 21. At birth, neonates born to iron-restricted dams had ~41% reductions in Hb values compared to controls. Litters from iron-restricted dams were ~20% smaller than controls, and offspring birth weights were ~10% lower than controls at birth, coinciding with ~14% lower maternal weight gain in pregnancy in the iron restricted dams.

Adult offspring characteristics (**Table 7.2**) represent a subgroup of the study cohort previously described in Woodman *et al.* (2019). In 6 month old male offspring, perinatal ID caused decreased bodyweight, crown rump length, and abdominal girth (all $P<0.05$), whereas HS diet had no overall effect. Female offspring growth at 6 months was not altered by perinatal ID or HS diet. Left ventricle and septum (LVS) mass, when normalized to body weight, was increased by HS diet in male offspring, but there was no effect of perinatal ID. A trend for increased relative right ventricular mass was observed for both perinatal ID and HS diet in male offspring (both $P=0.08$). Relative ventricular mass in female offspring was not altered by either perinatal ID or HS diet.

Table 7.1. Pregnancy and neonatal outcomes.

Parameter		Treatment		P Value
		CTL	ID	
Maternal Weight Gain GD0-GD21 (g)		227.2 ± 26.9	195.5 ± 32.5	0.01
Litter Size (No. pups)		18.1 ± 2.3	14.6 ± 1.8	0.003
Maternal Hb (g/dL)	GD0	15.3 ± 0.6	11.8 ± 2.2	<0.001
	GD7	14.7 ± 0.8	11.7 ± 1.7	<0.001
	GD14	14.0 ± 0.7	10.7 ± 1.9	<0.001
	GD21	12.5 ± 1.3	8.3 ± 1.4	<0.001
PD1 Hb (g/dL)	Males	11.2 ± 1.2	6.8 ± 1.3	<0.001
	Females	11.0 ± 0.7	6.3 ± 1.4	<0.001
PD1 Body Weight (g)	Males	6.49 ± 0.37	5.76 ± 0.46	0.004
	Females	6.13 ± 0.48	5.54 ± 0.43	0.02

All groups n=8-11 offspring from separate litters Data are expressed as mean ± SD and analysed by unpaired *t*-test. CTL, control; GD, gestational day; Hb, haemoglobin; ID, perinatal iron deficient group; PD, postnatal day. Reproduced with permission [309].

Table 7.2. Body measurements and cardiac ventricular weights of 6-month old offspring.

Parameter		Treatment				P-Value		
		CTL		ID		ID	HS	INT.
		NS	HS	NS	HS			
M	Body Wt. (g)	738.4±84.3	681.6±66.1	626.2±103.1#	637.7±43.6	**0.01**	0.43	0.24
	CR Length (cm)	21.2±0.6	21.0±0.6	20.0±1.4#	20.1±0.4	**0.001**	0.79	0.52
	Ab. Girth (cm)	25.5±1.4	24.2±1.3	23.6±1.7#	23.6±1.5	**0.03**	0.25	0.22
	LVS (mg/g)	1.64±0.11	1.79±0.18	1.69±0.21	1.90±0.19	0.19	**0.009**	0.64
	RV (mg/g)	0.39±0.03	0.47±0.08	0.47±0.11	0.49±0.06	0.08	0.08	0.36
F	Body Wt. (g)	409.2±77.4	408.2±49.9	405.9±59.8	434.0±70.0	0.62	0.55	0.52
	CR Length (cm)	17.1±0.9	17.1±0.7	17.0±1.2	17.4±0.9	0.16	0.98	0.51
	Ab. Girth (cm)	20.2±1.9	19.9±1.2	19.8±1.4	20.6±2.0	0.84	0.71	0.33
	LVS (mg/g)	1.90±0.22	2.03±0.20	1.91±0.23	1.87±0.21	0.32	0.59	0.27
	RV (mg/g)	0.49±0.09	0.48±0.07	0.50±0.09	0.49±0.10	0.72	0.84	0.97

Male offspring n=6-9, females n=7-9 offspring from different litters. Data are expressed as mean ± SD and are analysed by two-way ANOVA with *Sidak's post hoc test*; #P<0.05 vs. CTL of the same salt diet group. Ab, abdominal; CR, crown-rump; CTL, control; F, female; HS, high salt diet; ID, perinatal iron deficiency group; int, interaction; LVS, left ventricle-septum; M, male; NS, normal salt diet; RV, right ventricle. Results describe outcomes that pertain to offspring used in this study, and represent a subset of data previously published [309].

7.4.2 Ex-Vivo Vascular Function

Myography experiments were performed on isolated third order mesenteric arteries from 6-month-old offspring. Responses to high-potassium PSS buffer yielded similar levels of vasoconstriction in all male (CTL NS= 9.8±0.5 mN/mm, CTL HS= 8.6±0.5 mN/mm, ID NS=8.9±0.5 mN/mm, ID HS=8.4±0.6 mN/mm; P_{ID}=0.36, P_{HS}=0.15, $P_{interaction}$=0.50) and female offspring (CTL NS=7.8±0.5 mN/mm, CTL HS=7.3±0.4 mN/mm, ID NS=7.4±0.2 mN/mm, ID HS=7.2±0.3 mN/mm; P_{ID}=0.54, P_{HS}=0.41, $P_{interaction}$=0.75). Similarly, vasoconstriction profiles generated by PE were not affected by perinatal ID or HS diet, albeit L-NAME treatment potentiated PE-induced vasoconstriction in both male and female offspring (**Table 7.3**). When analysed as AUC, there were no effects of perinatal ID or HS diet on PE-induced vasoconstriction (data not shown).

Table 7.3. Mesenteric artery responses to phenylephrine (PE) administration.

		NS Group				**P-Value**		
		Vehicle		L-NAME				
		CTL (n=10)	ID (n=6)	CTL (n=10)	ID (n=6)	ID	L-NAME	INT
Males	EC_{50} (x10^{-6} M)	2.58±1.16	2.32±0.10	1.17±0.44 ***	0.96±0.25 **	0.42	**<0.001**	0.81
	Emax (%)	113.2±5.2	115.0±9.9	125.1±8.8 ***	126.3±9.7 **	0.69	**<0.001**	0.88
		HS Group				P-Value		
		Vehicle		L-NAME				
		CTL (n=8)	ID (n=7)	CTL (n=8)	ID (n=7)	ID	L-NAME	INT
	EC_{50} (x10^{-6} M)	2.05±0.94	2.28±1.2	1.25±0.45 *	0.91±0.51 **	0.84	**<0.001**	0.25
	Emax (%)	111.3±9.0	111.8±5.9	122.9±5.7 ***	122.1±5.0 **	0.96	**<0.001**	0.72
		NS Group				P-Value		
		Vehicle		L-NAME				
		CTL (n=8)	ID (n=8)	CTL (n=8)	ID (n=8)	ID	L-NAME	INT
Females	EC_{50} (x10^{-6} M)	1.74±0.42	2.89±1.90	1.18±0.40	1.07±0.37 **	0.19	**0.005**	0.10
	Emax (%)	108.9±7.9	106.8±12.4	117.2±4.2 *	119.7±9.8 ***	0.78	**<0.001**	0.28
		HS Group				P-Value		
		Vehicle		L-NAME				
		CTL (n=7)	ID (n=7)	CTL (n=7)	ID (n=7)	ID	L-NAME	INT
	EC_{50} (x10^{-6} M)	1.93±0.75	1.86±0.66	1.04±0.47 **	1.02±0.34 **	0.87	**<0.001**	0.85
	Emax (%)	107.3±5.9	109.6±6.6	116.3±4.4 **	121.1±3.6 ***	0.16	**<0.001**	0.39

Data are expressed as mean ±SD and are analysed by two-way ANOVA with *Sidak's post hoc test;* *P<0.05, **P<0.01, and ***P<0.001 vs. vehicle from the same perinatal treatment group. Shifts in EC_{50} due to the administration of L-NAME were not altered by perinatal ID or HS diet (data not shown). CTL; control; HS, high salt; ID, perinatal iron deficient; INT, interaction; L-NAME, L-N^G-Nitroarginine methyl ester; NS, normal salt.

Next, responses to the endothelial-dependent vasodilator MCh were tested in vessels pre-constricted with PE. In male offspring fed a NS diet, L-NAME reduced vascular responsiveness to MCh ($P<0.001$), and there was no effect of perinatal ID ($P=0.17$; **Figure 7.1A & D**). In HS diet-fed offspring, L-NAME attenuated responses to MCh ($P=0.003$), albeit this effect was blunted in the perinatal ID offspring (interaction $P=0.04$, **Figure 7.1B & E**); thus, the L-NAME-induced shift in MCh EC_{50} (ΔEC_{50}) was smaller in HS-fed perinatal ID offspring compared to HS-fed controls (interaction $P=0.03$, **Figure 7.1F**). No differences in maximal vasodilation (E_{max}) values for MCh-mediated vasodilation were observed due to either perinatal ID or HS diet in male offspring (data not shown). Despite differences in EC_{50} values for MCh, the relative contribution of NO-dependent and NO-independent vasodilatory mechanisms, calculated by AOC, were not different between groups (**Figure 7.1C**). In females, vascular responses to MCh were attenuated by L-NAME administration in both NS and HS-fed groups, and there was no effect of perinatal ID on these outcomes (**Figure 7.1G-L**). Accordingly, the L-NAME-induced shift in MCh EC_{50} was not altered by either perinatal ID or HS diet (**Figure 7.1L**), nor were E_{max} values (data not shown). Interestingly, the NO-independent component of the MCh-mediated vasodilation was impaired by HS diet ($P=0.04$; **Figure 7.1I**).

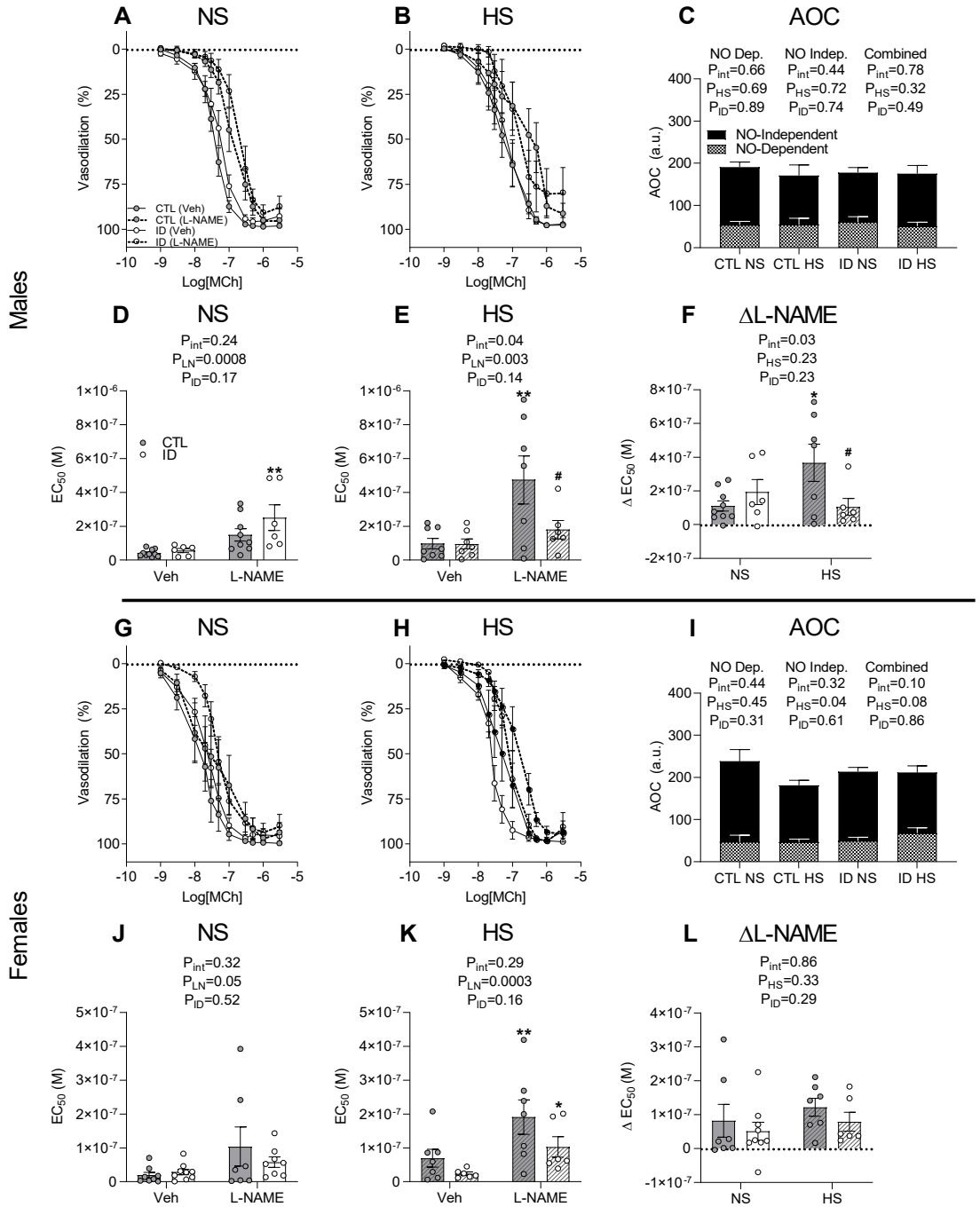

Figure 7.1: Endothelium-dependent vasodilation. Responses to MCh in mesenteric arteries from CTL or perinatal ID male (**A-F**) and female (**G-L**) offspring fed a NS or HS diet. Dose response curves (**A, B, G, H**) and corresponding EC_{50} values (**D, E, J, K**) are shown. The

magnitude of shift in EC_{50} attributed to L-NAME is shown (**F, L**). Finally, summarized vascular responses attributed to NO-dependent, NO-independent and combined (NO-dependent + NO-independent) components (calculated as absolute AOC) are also shown (**C, I**). Data are presented ±SEM (n=6-10) and analysed by mixed-model or two-way ANOVA as appropriate with *Sidak's* post hoc test; *P<0.05, **P<0.01, and ***P<0.001 versus veh or NS in the same perinatal diet group; #P<0.05 compared to CTL in the same L-NAME or salt diet group. AOC; area over the curve; CTL, control; HS, high salt; ID, perinatal iron deficient; L-NAME, L-N^G-Nitroarginine methyl ester; MCh, methacholine; NS, normal salt; veh, vehicle.

Similar experiments were conducted with the endothelial-independent vasodilator SNP (an NO-donor) to further interrogate downstream vasodilatory pathways. Perinatal ID had no overall effect on vascular reactivity to SNP in NS or HS fed male offspring (**Figure 7.2A-E**). In all groups, L-NAME pre-treatment caused increased vascular sensitivity to SNP (**Figure 7.2A-E**), corresponding to similar L-NAME-induced shifts in SNP EC_{50} in male offspring (**Figure 7.2F**). No differences in E_{max} in response to SNP were observed due to either perinatal ID or HS diet in male offspring (data not shown), nor in NO-dependent and -independent contributions (**Figure 7.2C**). In female offspring, perinatal ID has no overall effect on SNP vascular responses (**Figure 7.2G-L**). L-NAME similarly enhanced SNP-mediated vasodilation in all groups, corresponding to a similar L-NAME-induced shift in SNP EC_{50}, albeit a trend for a greater shift due to HS diet was observed (P=0.06; **Figure 7.2L**). AOC revealed enhanced SNP-mediated vasodilation in female vessels due to HS diet, which was largely attributed to an increase in NO-independent pathways (P=0.07; **Figure 7.2I**). No differences in E_{max} in response to SNP were observed due to either perinatal ID or HS diet in female offspring (data not shown).

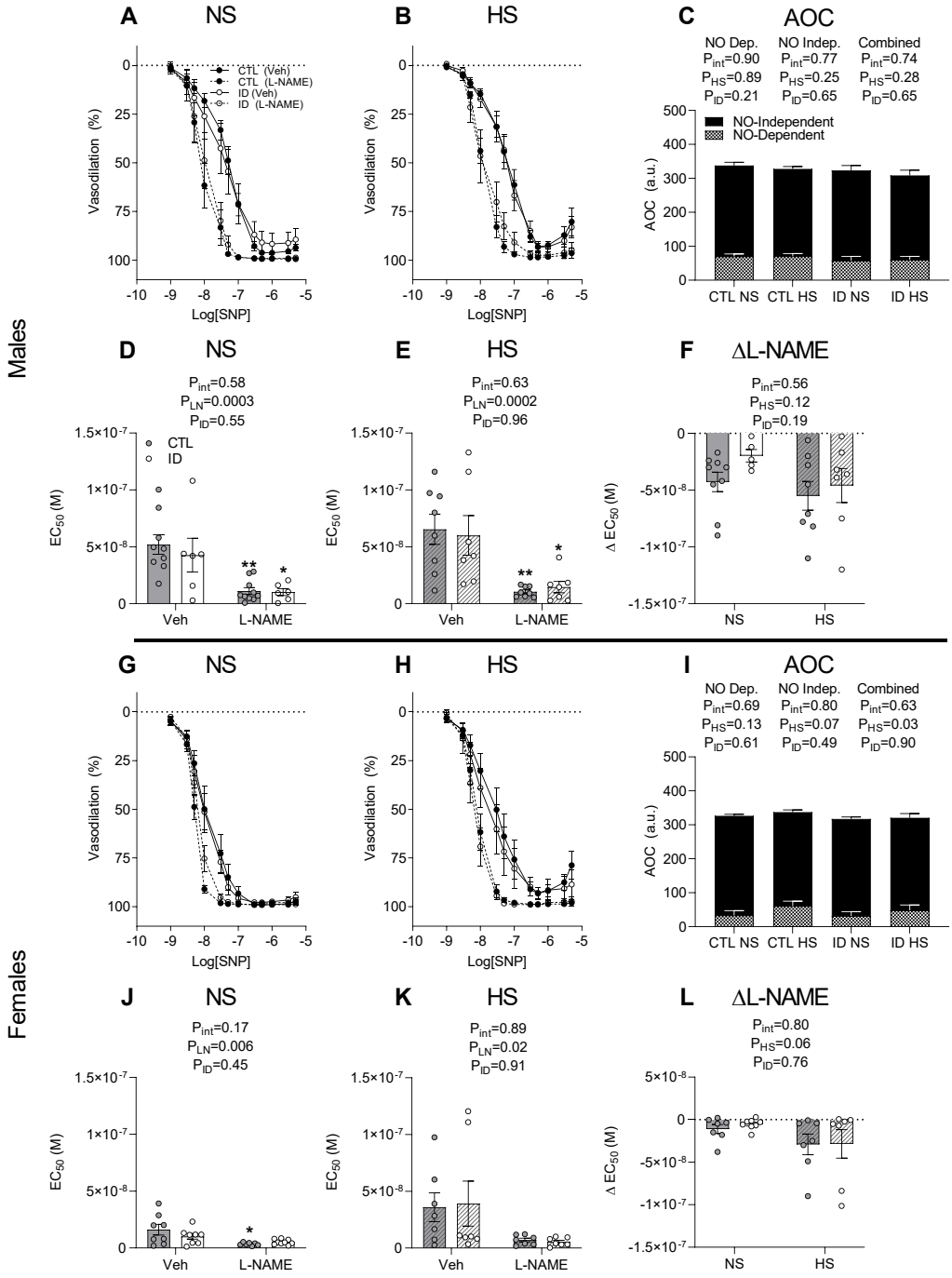

Figure 7.2: Endothelium-independent vasodilation. Responses to SNP in mesenteric arteries from CTL or perinatal ID male (**A-F**) and female (**G-L**) offspring fed a NS or HS diet. Dose response curves (**A, B, G, H**) and corresponding EC_{50} values (**D, E, J, K**) are shown. The

magnitude of shift in EC_{50} attributed to L-NAME is shown (**F, L**). Finally, summarized vascular responses attributed to NO-dependent, NO-independent and combined (NO-dependent + NO-independent) components (calculated as absolute AOC) are also shown (**C, I**). Data are presented ±SEM (n=5-10) and analysed by mixed-model or two-way ANOVA as appropriate with *Sidak's* post hoc test; *P<0.05, **P<0.01, and ***P<0.001 versus veh or NS in the same perinatal diet group; #P<0.05 compared to CTL in the same L-NAME or salt diet group. AOC; area over the curve; CTL, control; HS, high salt; ID, perinatal iron deficient; L-NAME, L-N^G-Nitroarginine methyl ester; NS, normal salt; SNP, sodium nitroprusside; veh, vehicle.

Given the intimate relationship between NO and bEt-1/Et-1, we subsequently studied vascular responses to the inactive precursor bEt-1 and vasoactive Et-1. In male offspring fed a NS diet, vascular responses to bEt-1 were enhanced by perinatal ID (P=0.02; **Figure 7.3A & 7.3D**), albeit this effect was not seen in offspring fed a HS diet (**Figure 7.3B & 7.3E**). L-NAME administration enhanced response to bEt-1 in all groups (P<0.0001), corresponding to similar increases in bEt-1 AUC (data not shown). Vascular responses to Et-1, in the form of either EC_{50} or E_{max} (data not shown), was not affected by either perinatal ID or HS diet in male offspring (**Figure 7.3C & 7.3F**). In female offspring, responses to bEt-1 were not altered by perinatal ID in either NS or HS-fed offspring (**Figure 7.3G, 7.3H, 7.3J, 7.3K**). L-NAME enhanced bEt-1-mediated vasoconstriction (P<0.0001), corresponding to similar increases in bEt-1 AUC in all groups (data not shown). Interestingly, in female offspring HS diet caused a trend for an increased vascular response to active Et-1 (P=0.06; **Figure 7.3I & 7.3L**), albeit no differences in E_{max} were observed (data not shown).

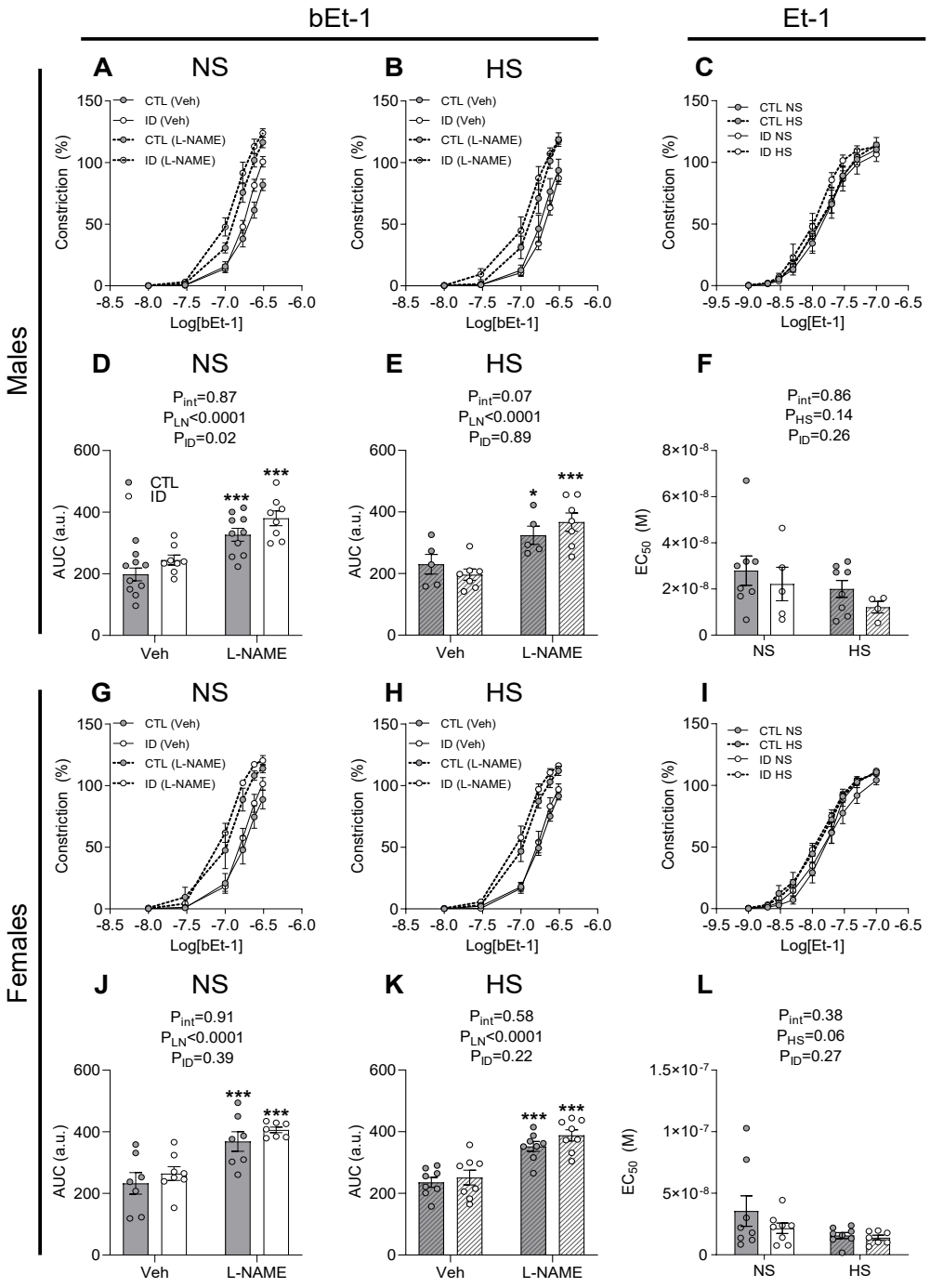

Figure 7.3: Endothelin mediated vasoconstriction. Responses to bEt-1 (**A, B, D, E, G, H, J, K**) and Et-1 (**C, F, I, L**) in mesenteric arteries of male (**A-F**) and female (**G-L**) perinatal ID and CTL offspring fed a NS or HS diet. Data are presented ±SEM (n=4-10) and analysed by mixed-

model or two-way ANOVA as appropriate with *Sidak's* post hoc test; *P<0.05, **P<0.01, and ***P<0.001 versus veh or NS in the same perinatal diet group; #P<0.05 compared to CTL in the same L-NAME treatment or salt diet group. AUC, area under the curve; bEt-1, big endothelin-1; CTL, control; Et-1, endothelin-1; HS, high salt; ID, perinatal iron deficient; L-NAME, L-N^G-Nitroarginine methyl ester; NS, normal salt; veh, vehicle.

7.4.3 Vascular Superoxide and Nitric Oxide

Next, we performed fluorescence microscopy to assess NO and superoxide levels in mesenteric artery sections. In male offspring, mesenteric artery superoxide levels were increased by consumption of a HS diet (P=0.01), and this effect was driven predominantly by the perinatal ID offspring (*post hoc* P=0.03; **Figure 7.4C**). Reductions in NO levels in males were observed due to perinatal ID (P=0.005), predominantly in offspring fed a HS diet (*post hoc* P=0.02), albeit no overall effect of HS diet was observed (P=0.10; **Figure 7.4D**). In females, no significant alterations in superoxide levels were observed due to either perinatal ID or HS diet (**Figure 7.4E**). Interestingly, a significant reduction in NO was caused by HS diet in females (P=0.02), which was driven largely by the reduction in perinatal ID offspring (*post hoc* P=0.049; **Figure 7.4F**).

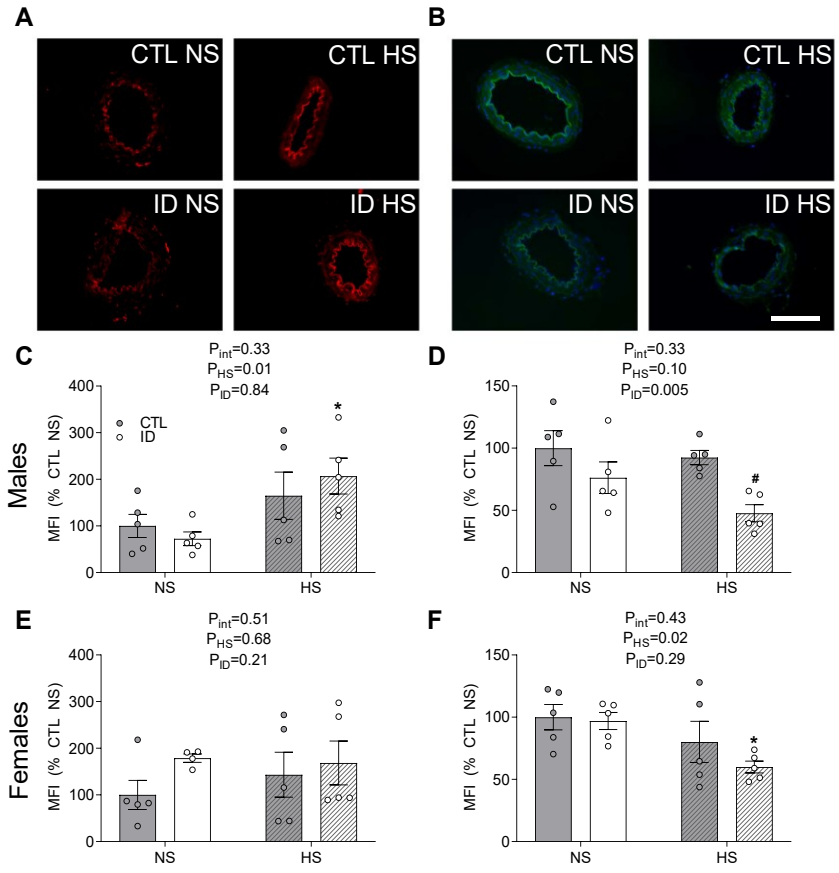

Figure 7.4: Vascular reactive species. Fluorescence staining in mesenteric arteries from male (**A-D**) and female (**E, F**) perinatal ID and CTL offspring for superoxide (**A, C, E**) and NO (**B, D, F**). Data are presented ±SEM (n=4-5) and are analysed by two-way ANOVA with *Sidak's* post hoc test; *P<0.05 versus NS in the same perinatal treatment group; #P<0.05 compared to CTL in the same salt diet group. Representative fluorescence staining images from male offspring show DHE (red), DAF-FM (green), and DAPI (blue). Scale bar represents 225μm. CTL, control; DAF-FM, 4-Amino-5-methylamino-2',7'-difluorofluorescein diacetate; DAPI, 4',6-diamidino-2-phenylindole; DHE, dihydroethidium; HS, high salt; ID, perinatal iron deficient; MFI, mean fluorescent intensity; NS, normal salt.

7.5 Discussion

ID is a common pregnancy complication, which can have severe impact on pregnancy outcomes and perinatal health of the offspring. Using a model of maternal iron restriction during pregnancy, offspring develop ID anaemia by the end of gestation [165,309], which persists for several weeks after birth despite maternal iron replenishment [159,170]. Work from our laboratory and others show that perinatal ID can impact long-term cardio-metabolic function [159,170,309], including blood pressure regulation, and renal function. Here, we investigated the impact of perinatal ID on vascular function in male and female offspring. We tested the hypothesis that vascular function is altered by perinatal ID in 6-month-old offspring, and these effects are exacerbated by consumption of a HS diet. The main findings can be summarized as follows: adult male perinatal ID offspring exhibited (i) attenuated NO-dependence in MCh induced vasodilation following consumption of a HS diet; (ii) enhanced response to bEt-1, but not Et-1; and (iii) increased vascular superoxide levels following consumption of a HS diet, concomitant with decreased vascular NO levels. Finally, in adult female offspring, (iv) perinatal ID was associated with no changes in vascular function, albeit reductions in vascular NO levels due to HS were seen. Together, these results suggest that male offspring are susceptible to the vascular programming effects of perinatal ID, which is exacerbated by a HS diet, whereas females appear more resistant to these alterations.

Our study included the integration of a HS diet during adulthood, which is a highly prevalent dietary issue. It is estimated that 89% of adults in the US consume excess dietary salt [372]. HS intake is a known risk factor for the development of hypertension, renal dysfunction, and impaired vascular function [381], and may otherwise exacerbate underlying cardiovascular dysfunction. In the context of developmental stressors, cardiovascular programming effects may be subtle, and the imposition of a secondary stress such as chronic consumption of HS in adulthood could accelerate decline and precipitate cardiovascular events earlier in life [395]. Experimentally, imposition of a HS diet provides a useful approach to interrogate underlying mechanisms of developmental programming. Indeed, evidence of altered endothelial function

programmed by perinatal ID in male offspring did not become apparent until the imposition of a HS diet. In the presence of a HS diet, control male offspring exhibit an increased reliance on NO-mediated signalling in response to MCh, consistent with reports that NO production *in vivo* enhances sodium excretion and prevents excessive increases in blood pressure [396]. Interestingly, whereas L-NAME caused marked shifts in EC_{50} to MCh in CTL male offspring fed HS, the effect of HS on NO bioavailability in perinatal ID offspring vasculature was blunted substantially. We have previously shown that perinatal ID offspring exhibit sensitivity to high salt intake [159,170], resulting in increased BP after prolonged high salt intake [309]. In this regard, whether the reduced NO bioavailability in mesenteric arteries reflects a systemic consequence of altered sodium handling, and hence driven by increased blood pressure [170,309], is not clear. It may be that systemic and renal resistance arteries are similarly affected by perinatal ID, and the systemic vascular dysfunction reflects an independent risk factor for hypertension and cardiovascular dysfunction. These possibilities require further investigation.

The lack of differences in vascular responses to the endothelial-independent vasodilator SNP suggests that differences in MCh responses are due to differences in endothelial function, and not alterations in vascular smooth muscle signalling. One interpretation of these findings is that male perinatal ID offspring have intrinsically low levels of vascular NO production, and when challenged by a cardiovascular stress such as a HS diet, these vessels depend on alternative vasodilator mechanisms to regulate vascular tone. Indeed, in littermates of the offspring studied herein, baseline haemodynamics of perinatal ID offspring were elevated in NS and HS conditions, and infusion of L-NAME caused proportionally lower blood pressure increases [309], suggesting a reduced reliance on NO signalling. Other groups have also shown that adult offspring exposed to prenatal hypoxia exhibit reduced NO-dependence with endothelial-dependent vasodilators, whereas NO-independent mechanisms (e.g. endothelial derived hyperpolarization, EDH) remain intact and compensate for reduced NO-signalling [121,162,233,391,397]. Furthermore, HS intake has also been shown to enhance EDH mediated

vasodilation [398,399], consistent with the possibility of compensatory increases occurring in perinatal ID males.

Under baseline conditions, bEt-1 responses were enhanced in male perinatal ID offspring compared to controls. The findings that Et-1 was not altered by either perinatal ID or HS suggests the enhanced responses to bEt-1 are due to enhanced conversion of bEt-1 to active Et-1. We have previously shown that alterations in NO bioavailability can impact other vasoregulatory mechanisms, such as bEt-1/ Et-1 signalling [239,400,401]. Here, vascular pre-treatment with L-NAME potentiated bEt-1 induced constriction in all groups, providing further evidence NO regulation of bEt-1 conversion, since NO synthase inhibition has no effect on Et-1-mediated vasoconstriction [400]. Similarly, enhanced response to bEt-1, but not Et-1, was reported in mesenteric arteries in 14-month old in male offspring born from prenatal hypoxia [239].

Consistent with the evidence of reduced NO bioavailability in male perinatal ID offspring fed a HS diet, we observed significant increases in superoxide levels concomitant with decreases in NO. The patterns of increased superoxide and reduced NO levels in mesenteric vessels of male perinatal ID offspring are in agreement with the patterns found in the kidneys of these same offspring [309]. Upregulation of reactive oxygen species have been previously observed in the mesenteric arteries of prenatal hypoxia exposed males at 7 months of age, wherein superoxide dismutase treatment enhanced responses to MCh in hypoxic, but not control offspring [233]. These reports suggest that excess ROS generation may be an important etiological factor in the vascular dysfunction observed, and therapeutic strategies focused on reducing oxidative stress may be useful in several models of perinatal stress.

In female offspring, no alterations in mesenteric artery responses to vasodilators or vasoconstrictors were observed due to perinatal ID. Our findings from this same cohort of offspring showed that adult females do not exhibit the same hypertension, renal injury, or increased ROS generation due to perinatal ID and a HS diet as their male counterparts despite nearly identical severities of anaemia and patterns of asymmetric growth restriction at birth [165,309]. Whether these outcomes are causally linked (i.e. vascular

dysfunction only occurs secondary to overt hypertension), or whether male and female offspring exhibit inherent differences in susceptibility to vascular dysfunction independent of blood pressure, is not presently clear. It is possible that a more prolonged HS diet treatment would exacerbate the comparatively subtle vascular dysfunction in the female offspring [224]; indeed, HS diet caused early signs of vasodilatory impairment in female offspring in both perinatal treatment groups, and this may become more pronounced with advanced age. In rodent models of prenatal hypoxia, male offspring over 4 months of age consistently develop overt vascular dysfunction, whereas female offspring develop dysfunction at later ages (12-14 months of age), albeit with less consistency [162,224,233,239,391,397]. This variability in outcomes may reflect, at least in part, the influence of sex hormones. For example, oestrogen signalling promotes vascular health, and can induce vasorelaxation through both NO-dependent and independent pathways [402]. Ovariectomy of female offspring exposed to developmental stressors exacerbates the vascular and cardiac dysfunction compared to their intact littermates [97].

When fed a HS diet, female perinatal ID offspring had reduced NO levels, which is consistent with the previously reported attenuated rise in blood pressure when administered L-NAME [309]. Interestingly, these changes did not occur in tandem with increased DHE staining, suggesting the reduced NO bioavailability is attributed to factors other than scavenging by excess superoxide. The notable lack of excess superoxide levels may reflect intrinsically greater antioxidant capacity in females [403], which may mitigate the oxidative stress in adulthood. This greater antioxidant capacity in females may also be an important mechanism mitigating the programming effects caused by ID during development, which are mediated, at least in part by excess reactive oxygen species in foetuses [165]. Consistent with this, maternal vitamin C treatment was shown to attenuate reductions in NO dependent vasodilation in a model of prenatal hypoxia [391].

In conclusion, we have shown that male and female offspring exhibit different outcomes in the programming of vascular dysfunction by perinatal ID, and the effects of high salt intake in adulthood. The current study emphasizes the importance of resistance artery endothelial function and health. Isolated mesenteric arteries were used herein due

to their importance in dictating total peripheral resistance, however the impact of perinatal ID on other vascular beds must be considered. If reduced NO bioavailability is pervasive in the circulation, the implications for long-term cardiovascular health could be profound. Loss of NO is considered to be an initial step in the progression of vascular dysfunction, and as such, lower bioavailability of NO due to perinatal stressors could be an important aetiological factor in accelerated age-related cardiovascular disease. While the data presented herein cannot be directly extrapolated to humans, this work and other preclinical studies provide a rationale for clinical studies investigating altered NO and oxidant status as mechanisms underlying the vascular dysfunction in subjects born to complicated pregnancies. Finally, the results from this study and others should serve as an impetus for agencies and health care providers to consider and educate the public on the importance of pre- and perinatal health, including maternal and foetal iron status, on susceptibility to long-term chronic disease.

Competing Interests

The authors have no conflicts to disclose.

Author Contributions

Experiments were performed in the laboratory of S.L.B. at the University of Alberta. A.G.W., F.S.G., and S.L.B. conceived the study. A.G.W., R.M.N.N., S.P., and S.L.B. conducted the experiments. A.G.W. analysed the data. All authors contributed to the drafting of the work and/or revising the manuscript for intellectual content. The authors, defined as all those who qualify for authorship by *The Journal of Physiology*, each approved the final version of the manuscript and agree to be accountable for all aspects of the work.

Funding

This work is supported by grants from the Women and Children's Health Research Institute and the Canadian Institutes of Health Research (CIHR; MOP142396). A.G.W. is supported

by a Vanier Canada Graduate Scholarship (CIHR) and Alberta Innovates Health Solutions Graduate Studentship. S.L.B. was a CIHR New Investigator during the course of this study, and is currently a CIHR Canada Research Chair (Tier 2) in Developmental and Integrative Cardiovascular Pharmacology.

Acknowledgements

The authors wish to thank the Cardiovascular Research Centre at the University of Alberta for the use of their fluorescent microscope.

Chapter 8
Summary and Conclusions

8.1 Perinatal ID and the Global Burden of Cardiovascular Disease

Despite the control of anemia being declared a global health priority by the WHO [23], ID anemia remains an epidemic. ID is the most common nutritional deficiency worldwide, affecting between 1-3 billion people, and is the number one cause of anemia in reproductive age women [22,23]. ID anemia is the leading cause of years lived with disability among women in 35 countries, and is in the top five causes of disability among all populations globally [23]. Additionally, ID anemia is more common in populations of lower socioeconomic status or from marginalized groups, highlighting the importance developing accessible treatment strategies for all [23]. The high incidence of ID anemia in reproductive age women places both potential mothers and fetuses at risk of pregnancy complications [32]. Perinatal ID is associated with enhanced maternal and neonatal mortality, in addition to increasing risk of pre-term birth and intrauterine growth restriction [39,47]. When further considering the propensity for perinatal ID to cause long-term cardiovascular [170,230,232], metabolic [159,160,390], and cognitive dysfunction [41,63,252], the true risks associated with this preventable condition are far greater than previously realized.

The work presented herein, in addition to previous literature [170,215,216,227,230], has shown that perinatal ID increases susceptibility for offspring to develop cardiovascular disease and chronic kidney disease in later life through risk factors such as hypertension. Cardiovascular disease is the leading cause of death worldwide, estimated to be responsible for over 30% of all deaths annually[93]. Chronic kidney disease was the 12th leading cause of death in 2017, with global mortality rates increasing over 40% since 1990 [95]. Hypertension is one of the most important risk factors for both cardiovascular disease and chronic kidney disease [94,95]. Although hypertension prevention has precipitated a decline in prevalence in developed nations since the 1970s, low and middle income countries are seeing dramatic increases [94]. Importantly, perinatal ID also

contributes to other independent risk factors for related conditions, such as cardiometabolic syndrome, through increased propensity for fat deposition [159,160]. Due to the long-term programming effects evident from perinatal ID, it likely contributes greatly to the global burden of cardiovascular and chronic kidney disease, especially in lower and middle income countries where ID is most prevalent [40,94,95].

8.2 Mechanisms of Cardiovascular Programming by Perinatal ID

Two studies (**Chapters 2 & 3**) were completed in fetal offspring to assess the acute health impacts of prenatal ID. The results from **Chapter 2** are critical to substantiate long-held assumptions that prenatal ID results in fetal hypoxia secondary to reductions in oxygen carrying capacity caused by anemia. Importantly, we showed that patterns of hypoxia were organ-specific, such that "vital" organs (i.e. brain) remained normoxic during gestation at the expense of others (i.e. liver and kidney; **Figure 8.1**). Moreover, these patterns were observed even when the degree of iron restriction was modest, resulting in minimal decreases in maternal iron status (i.e. no change in serum ferritin or transferrin) and no gross alterations in relative fetal organ weights. In contrast to previous studies completed in sheep, where fetal or maternal anemia was induced by blood loss [52,260,273,404], this was the first study to assess how dietary ID impacts such outcomes. This distinction is important, as a recent study in fetal hearts exposed to either prenatal hypoxia or ID emphasizes the differential response to each stressor. Transcriptomic analysis comparing changes in gene expression from ID and hypoxia show fewer than 10% of the >500 genes whose expression is perturbed by each stressor are shared between them [227]. As such, it is foreseeable that fetal organs may adapt to each stressor differently, potentially leading to differences in patterns of hypoxia *in utero*.

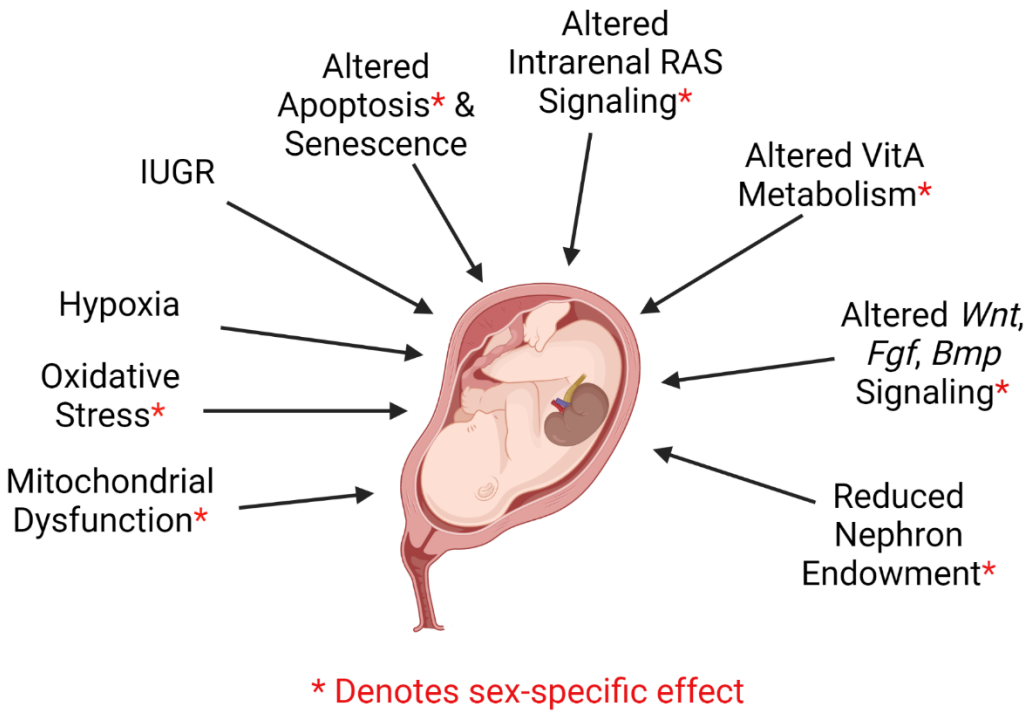

Figure 8.1: Gestational and early postnatal effects of perinatal iron deficiency on renal development. The effects of hypoxia, IUGR, and altered cellular senescence were observed in male and female perinatal ID offspring. The remaining effects were sex-specific such that perinatal ID exposed males exhibited the most prominent alterations compared to females, with the exception of intrarenal RAS mediator expression. Bone morphogenetic protein, Bmp; Fibroblast growth factor, Fgf; Intrauterine growth restriction, IUGR; Renin angiotensin system, RAS; Vitamin A, VitA; Wingless-related integration site, Wnt. Image created under license with Biorender.com.

The results reported in **Chapter 3** (see **Figure 8.1**) provide insights as to why nephron endowment is reduced by perinatal ID in male but not female offspring. First, male fetal kidneys exhibit enhanced oxidative stress and mitochondrial dysfunction due to perinatal ID, whereas female offspring do not. Additionally, the results highlight the relative susceptibility of the developing kidney to developmental stressors. Despite both the fetal kidney and liver becoming hypoxic secondary to perinatal ID during gestation, the kidney exhibits a greater degree of dysfunction. These findings are critical for several

reasons: (1) male kidneys exposed to perinatal ID are likely to exhibit poor renal growth potential and functional capacity due to reductions in energy production, (2) enhanced ROS generation due to perinatal ID in male kidneys predispose the organ to damage and induction of cellular stress responses (i.e. elevations in apoptosis), and (3) sex differences *in utero* may contribute to feed-forward dysfunction in male but not female offspring.

Our work has uncovered several mechanisms acting in a sex-specific fashion, which may explain why male but not female offspring exposed to perinatal ID exhibit long-term cardiovascular dysfunction. A summary of acute mechanisms studied herein which contribute to sex differences in offspring exposed to perinatal ID are summarized in **Figure 8.1**. Despite seemingly similar exposure to perinatal ID in each sex, as indicated by similar fetal and neonatal Hb levels and fetal growth restriction, it is possible that the exposure is mitigated in female offspring. A recent study reported that perinatal ID has a larger effect on gene expression profiles in male versus female placentae [405], consistent with a previous meta-analysis showing poorer placental development and function in males due a plethora of stressors [240]. While our work demonstrates substantial differences in how male and female offspring respond to the effects of perinatal ID in the developing kidney, the potential contribution of differential exposure to perinatal ID (i.e. due to placental or maternal factors) [240] should be considered.

Differential cellular stress responses to perinatal ID within the fetal kidney may precipitate further dysfunction through transitioning to the postnatal environment. The relatively hyperoxic postnatal environment, combined with the increased reliance on renal function *ex utero*, may further exacerbate dysfunction in male perinatal ID offspring. For instance, mitochondrial ROS production increases with availability of O_2, a phenomenon which may be further exacerbated by the presence of pre-existing oxidative stress [198,406]. Furthermore, mitochondrial dysfunction reduces ATP production, potentially limiting growth and maturation of the kidney through a variety of cellular proliferation cascades [171,209], as well as limiting functional capacity of the kidney acutely. Indeed, efficiency of energy production within the kidney is of paramount importance, as increases in renal blood flow are matched with commensurate increases in metabolic

demand due to the filtration functions of the kidney [206]. As such, it is unsurprising that the developing kidney is highly susceptible to dysfunction following perinatal stressors [151,171,209].

In **Chapter 4**, perturbations cellular health and their role in postnatal kidney development were studied. These results highlight the importance of cellular patterning in renal development, which can be represented in part by the balance of developmental senescence and apoptosis which occurs (**Figure 8.1**). In contrast to models of gestational cigarette smoke exposure and postnatal overfeeding [304,407], to our knowledge we are the first to report reductions rather than increases in renal senescence secondary to a developmental stressor in the immediate postnatal period. Notwithstanding, disruptions in cellular senescence may be an understudied mechanism through which renal development is altered, leading to long-term functional perturbations. Additionally, Male but not female offspring exposed to perinatal ID exhibit enhanced apoptosis on PD1, presumably in response to enhanced oxidative stress and mitochondrial dysfunction.

In **Chapter 5**, some mechanisms through which perinatal ID may reduce nephron endowment were explored. Importantly, we recapitulated the finding that perinatal ID results in reductions in nephron endowment [214,215], and this outcome was observed only in male offspring (**Figure 8.1**). Previously, Lisle *et al* reported that perinatal ID affect nephron endowment in both male and female offspring [215], but there are several explanations that may account for this discrepancy. First, in the latter study, glomerular number was assessed at 18 months of age, and as such the reduced nephron count observed in female offspring could reflect age-related nephron loss rather than congenital effects [151]. Second, Lisle *et al.* quantified glomeruli using a non-stereological technique, which may introduce bias [370], whereas the study presented herein utilized a comprehensive approach shown to be comparable to MRI based stereological methods [337]. Our results showing sex-differences in nephron endowment are consistent with those of many developmental models, including prenatal hypoxia and maternal macronutrient restriction, in which glomerular number is reduced primarily in male offspring [97].

The results from **Chapter 5** are also the first to implicate dysregulated vitamin A metabolism in altered renal development due to perinatal ID. Our findings are consistent with previous studies have shown that perinatal ID perturbs vitamin A metabolism in other fetal organs, such as the liver and heart [225,227]. Additionally, dysregulation of vitamin A metabolism may represent a common pathway through which nephron endowment is reduced by developmental stressors. For instance, alterations in RA/RAR signaling have been observed in the kidneys of male mice exposed to prenatal hypoxia [208]. Furthermore, supplementation of RA in pregnancy reverses reductions in nephron endowment in offspring caused by a maternal low protein diet [221]. Moreover, we have also shown that perinatal ID impacts various signaling pathways which are crucial for proper patterning of the ureteric bud and metanephric mesenchyme, including the WNT, FGF, and BMP pathways (**Figure 8.1**).

Finally, **Chapters 6 & 7** describe the long-term cardiovascular outcomes associated with perinatal ID **(Figure 8.2**). We recapitulated previous findings of hypertension in perinatal ID exposed offspring [170,230,232], albeit the dysfunction was largely evident only in male offspring. Moreover, we identified systemic NO deficiency contributes to hypertension observed in perinatal ID male offspring, which is further reduced by a high-salt diet. Similarly, we showed that renal NO levels are also decreased by perinatal ID in males, which may be due in part to mitochondrial dysfunction induced ROS generation. Consistent with these findings, morphological indicators that the kidneys of male perinatal ID offspring struggle to compensate when a high salt diet is introduced were identified, including glomerular hypertrophy and injury. The additional findings in **Chapter 7** highlight that decreases in vascular NO levels may also play a role in the systemic NO deficiency observed in male perinatal ID offspring. Deficiencies in resistance artery NO bioavailability may contribute to the potentiation of the activation of endothelin, as well as decreased endothelial mediated vasodilation observed in male perinatal ID offspring.

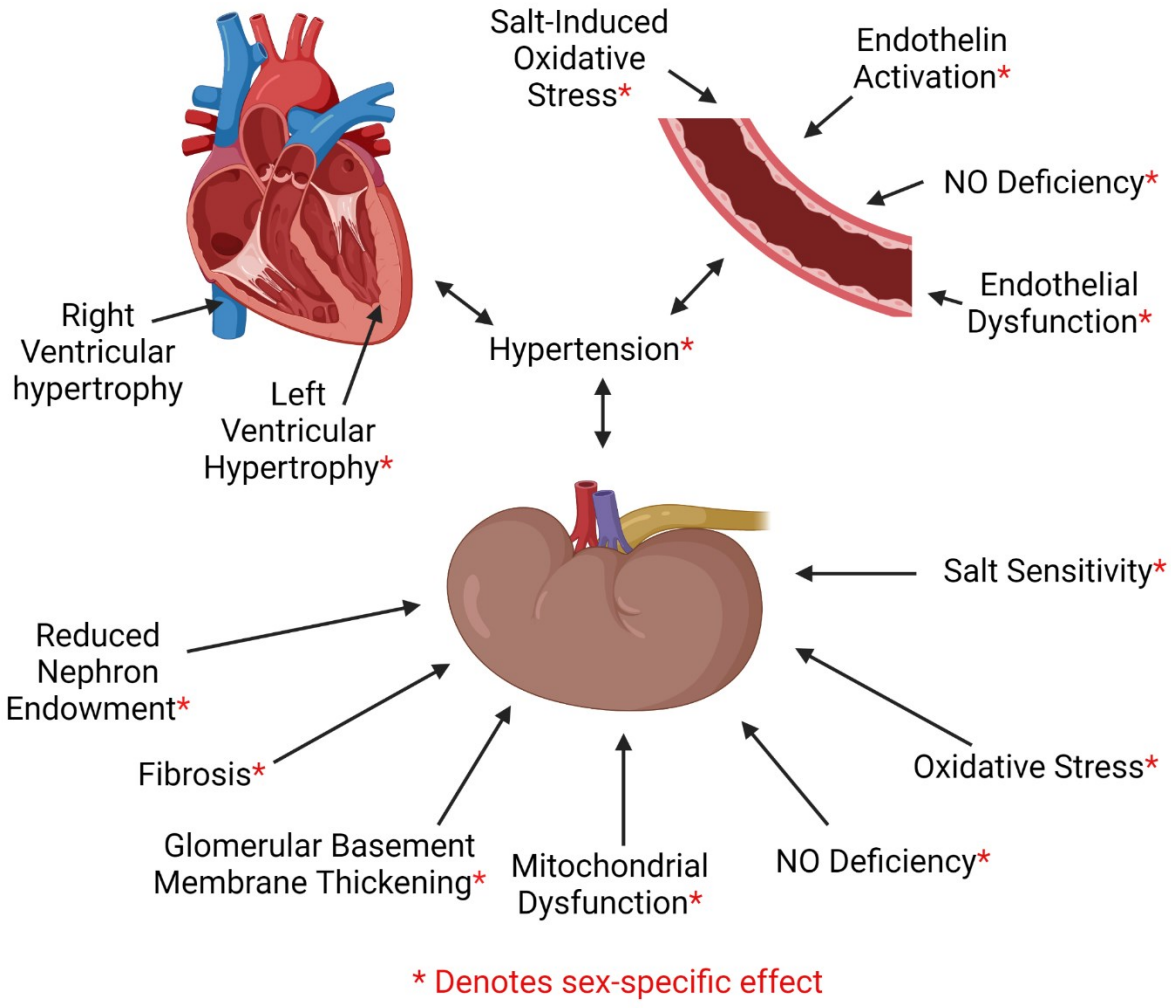

Figure 8.2: Outcomes associated with perinatal iron deficiency in rats at 6 months of age. Notably, apart from right ventricular hypertrophy, all effects observed herein occurred in male but not female offspring. Nitric oxide, NO. Image created under license with Biorender.com.

8.3 Controversies and Remaining Questions

Perhaps not surprisingly, elucidating how developmental stressors affect kidney development and long-term function is challenging. Mechanistically linking developmental changes to long-term adverse health outcomes is notoriously difficult because overt functional deficits often only develop in later life. Moreover, fetal responses to stressors tend to be systemic in nature, and therefore implicate multiple organ systems; that is, separating the programming effects on renal developmental *per se*, from the influences of other programmed systems, like the heart, vasculature, and endocrine function, is deceptively complex. Even within the kidney, the study of one parameter is complicated by the need to consider the breadth of changes that accompany it.

A case in point is the role of reduced nephron endowment in the long-term programming of hypertension and chronic kidney disease. Since nephrons do not proliferate beyond late gestation in humans, or within the first weeks of life in rats, fewer nephrons at this stage effectively means a lower complement throughout life [171]. The Brenner hypothesis posits that reductions in congenital nephron endowment are associated with hypertension and increased risk of developing chronic kidney disease later in life [153]. With time and increased functional demands (i.e. high-sodium diet), the increased filtration load on each nephron leads to glomerulosclerosis and tubular dysfunction, culminating in kidney disease [153,212]. The results presented herein are consistent with this hypothesis, which can be used as a framework to exemplify how the observed short and long-term outcomes are interconnected in perinatal ID offspring (**Figure 8.3**). Although a reduction in nephron endowment alone would be sufficient to satisfy the central tenet of the Brenner hypothesis *per se*, the additional perturbations in renal development likely contributed further to the dysfunction observed in adult perinatal ID offspring. The potential role of alterations in renal health and function beyond nephron endowment, and how they impact long-term health, will be discussed further below.

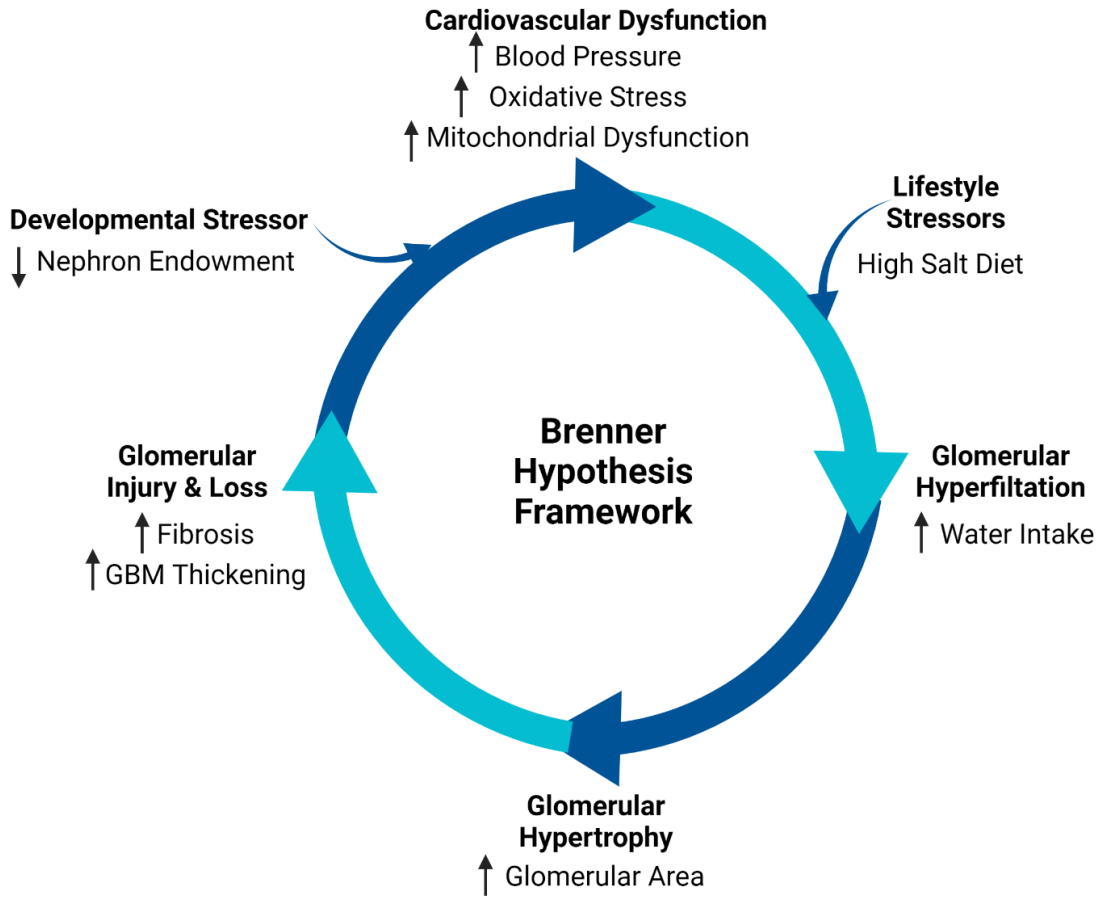

Figure 8.3: The Brenner hypothesis as a framework to explore long-term renal outcomes in perinatal ID offspring. Male perinatal ID offspring exhibit congenital reductions in nephron endowment, which can be exacerbated by introduction of a lifestyle stressor (i.e. a high salt diet). Male perinatal ID offspring exhibit greater than two-fold increases in water intake and further increases in blood pressure following consumption of a high salt diet, contributing further to glomerular hyperfiltration. Signs of glomerular hypertrophy and injury were observed, likely accelerating age-related loss of nephrons and predisposing offspring to further kidney dysfunction (i.e. as indicated by enhanced renal oxidative stress and mitochondrial dysfunction). Critically, female perinatal ID offspring, which did not exhibit reductions in nephron endowment, exhibited no alterations in blood pressure, nor glomerular hypertrophy or injury. Glomerular basement membrane, GBM. Figure is adapted from Didion, 2017 [408], and created under license with Biorender.com.

Since being published in 1988, several criticisms of the Brenner hypothesis have emerged. For instance, offspring with a reduced nephron endowment do not invariably develop hypertension and renal disease. What's more, the Brenner Hypothesis doesn't explain the marked variability in nephron endowment between seemingly healthy individuals, which can vary by more than 10-fold [150]. Thus, nephron endowment must be considered in the context of concomitant developmental changes, as well as traditional genetic and environmental risk factors which predispose an individual to chronic disease. As a corollary to DOHaD programming of renal function, patterns of hypertension in kidney donors serve as an informative exemplar of the importance of genetic and environmental risk factors.

Living kidney donors have been studied extensively to identify the role of nephron endowment in the pathogenesis of hypertension, eliminating the confounding factors involved in development. Interestingly, undergoing a unilateral nephrectomy for the purposes of donation, effectively reducing nephron endowment by a larger degree than seen in DOHaD models, is not in itself a considered a risk factor for the development of hypertension [409]. Notwithstanding, long-term follow-ups on kidney donors reveal modest elevations in mean arterial pressure versus non-donor controls, with hypertension occurring in approximately one third of donors [410]. However, the incidence of hypertension among donors did not exceed that which would be otherwise expected in a control population with similar characteristics, suggesting that reductions in nephron number alone may be insufficient for the development of hypertension [409,410]. Furthermore, the development of hypertension post-donation was strongly associated with older age, obesity, a family history of hypertension, and hyperlipidemia at the time of donation [410]. As such, comorbidities and other factors likely contribute substantially to cardiovascular dysfunction attributed to reductions in nephron endowment. The apparent importance of the timing for the reduction in nephron endowment may also suggest plasticity plays an important role in enhancing risk. Indeed, although the plastic developing kidney may have superior capacity to adapt to a congenital loss of nephrons via compensation, these changes likely contribute to greater risk of injury later in life [143].

Similarly, many preclinical DOHaD studies also suggest that factors beyond a reduction in nephron endowment may contribute to the long-term effects articulated by the Brenner hypothesis [171,411]. Congenital reductions in nephron number may best be described as a marker of poor renal development, rather than the degree of reduction in functional capacity of an otherwise healthy kidney. In other words, the physiologic reserve of a kidney exposed to a developmental stressor is likely diminished to a greater extent than could be explained by a reduction in nephron number alone. For instance, Walton *et al*. have shown that prenatal hypoxia exposure results in abnormal collecting duct structure and function, in addition to reductions in nephron endowment, in male offspring [208,218]. Moreover, a variety of developmental programming models have reported alterations in sodium transporter expression, RAS signaling, and renal sympathetic activity [171]. Similarly, the results herein show that perturbations decreased renal mitochondrial function, enhanced ROS, and decreased NO contribute to renal dysfunction. However, the complexity of biological systems makes it difficult to interpret how these mechanisms are interconnected. Many of these changes could arguably be viewed as compensatory, and therefore secondary to reductions in nephron number. Alternatively, the chronic nature of these observed structural and functional changes may suggest that they further contribute to renal pathogenesis. When taken together with data from kidney donors however, the evidence would suggest that they increase susceptibility for kidney dysfunction, regardless or whether they are truly independent of glomerular number.

Under the Guytonian view of the long-term regulation of blood pressure, renal function is of paramount importance. Consistent with this view, our results highlight mechanisms through which decreases in kidney function occur beyond reductions in nephron endowment and directly influence pressure natriuresis. Male perinatal ID offspring exhibit a systemic NO deficiency, which was also observed within both the kidney, and may be a chief mechanism through which perinatal ID impairs renal function (**Figure 8.3**). Deficiencies in NO signaling within the kidney are implicated in a variety of disorders which reduce renal function [104]. Importantly, NO acts within the kidney to

decrease tubular Na reabsorption and tubuloglomerular feedback, in addition to decreasing myogenic responses and enhancing GFR [104]. Furthermore, NO deficiency and excessive ROS formation are known to attenuate the slope of the natriuretic response to increased arterial pressure, consistent with our previous findings in male offspring [170]. Thus, deficiency of NO in fetal and adult male perinatal ID offspring, possibly due to increased ROS generation, is likely to limit functional capacity of the kidney.

Importantly, although male perinatal ID offspring did exhibit salt-sensitivity in the current study, the response was less exaggerated than expected based on previous studies [170]. Indeed, in non-anesthetized male rats exposed to perinatal ID, changes in dietary salt intake coincided with large blood pressure responses when compared to controls, as measured by radiotelemetry [170]. However, in the current studies, blood pressure appears to increase similarly in male control and perinatal ID offspring when fed a high salt diet. One possible mechanism which may account for this difference is the use of anesthesia during hemodynamics assessments in the present study, which is known to reduce sympathetic outflow to both the mesentery and the kidney, thereby decreasing vascular resistance [412]. Therefore, the discrepancy in our current findings may provide indirect evidence of a role of sympathetic nervous activity in the pathogenesis of perinatal ID-induced hypertension. Indeed, increased sympathetic activity is observed in small for gestational age individuals that develop hypertension, as well as in preclinical models of developmental stressors [209,413,414]. These data provide an impetus to further investigate the role of enhanced sympathetic responses in the pathogenesis of perinatal ID induced cardiovascular dysfunction.

Finally, considerable attention has been paid to extra-renal factors which are implicated in the control of long-term blood pressure in recent years. Similar to the criticisms of the reductionist views of the Brenner hypothesis, many recent publications have begun to question underlying assumptions of the Guytonian view of long-term blood pressure regulation [102,105,106]. For instance, sympathetic nervous activity is known to contribute to hypertension as described above. Interestingly, renal denervation results in sustained reductions arterial pressure in patients with refractory hypertension one year

[415]; highly suggestive that external inputs which may modulate pressure natriuresis can be the root cause of the abnormal pressure natriuresis described by Guyton, rather than the kidney itself [102]. The extent to which sympathetic nervous activity may contribute to long-term arterial pressure warrants further consideration.

Furthermore, considerable evidence exists that changes in TPR induced by the vasculature are sufficient to alter long-term blood pressure. For instance, transgenic models which raise TPR via manipulation of mineralocorticoid exposure, which do not alter sodium excretion, induce sustained elevations in blood pressure [102]. Additionally, genetic manipulation of cGMP-dependent protein kinase I, activated by NO via cGMP, also results in sustained hypertension [118]. Moreover, many preclinical and clinical studies have shown that alterations in vascular function, which have the potential to raise TPR, often precede the development of hypertension [139,172,344]. As such, a potential role for altered TPR may be more important in the pathogenesis of blood pressure dysregulation than originally considered within the Guytonian framework.

Despite their limitations, the models produced by Guyton and Brenner have tremendous value in linking observed pathologies with physiologic mechanisms. Importantly, emerging evidence within the field of DOHaD challenges these paradigms through the variety of mechanisms discussed above. The numerous identified, and yet to be identified, mechanisms through which renal development is impacted by perinatal stressors such as ID likely act synergistically to induce dysfunction in later life. As such, the importance of identifying novel mechanisms through which developmental stressors impact the integrated systems of blood pressure control and renal function in offspring cannot be understated. Broadening our understanding of how developmental stressors result in increased blood pressure set point, is our best chance to develop therapeutics which effectively treat future patients.

8.4 Concluding Remarks

Perinatal ID, like many other developmental stressors, has a profound impact on long-term cardiovascular function in offspring. By virtue of the prevalence of ID in reproductive age women, it undoubtedly contributes to the global burden of chronic disease through its effects as a developmental stressor. However, unlike other developmental stressors, such as prenatal hypoxia, uteroplacental insufficiency, pre-eclampsia, and others, perinatal ID is arguably entirely preventable. Importantly, this is recognized by organizations such as the WHO, which committed in 2012 to reduce the burden of anemia in reproductive age women by 50% by 2025 [23]. However, such a reduction will be insufficient to reduce the burden of perinatal ID induced chronic disease, for a variety of reasons.

Iron supplementation during pregnancy does not appear to be sufficient to reduce perinatal morbidity and mortality associated with ID, which are likely the best indicators of chronic disease risk. This may seem counterintuitive, as many studies highlight the efficacy of iron supplementation in pregnancy for a variety of formulations [416]. However, the definition of efficacy most widely used, namely the improvement in maternal hematologic or iron status indices [416], but do not consider that such interventions do not improve fetal/neonatal hematological indices or biomarkers of iron status [44,45]. Indeed, our group has also shown that maternal and neonatal hematologic and iron status indices correlate poorly [19], and therefore a greater emphasis on neonatal and birth outcomes in supplementation studies is needed. Moreover, the use of maternal indices to identify fetuses at risk of perinatal ID during gestation also remains a challenge, with an urgent need for identification of biomarkers which better reflect fetal iron status to allow for timely interventions [19,32].

Currently, evidence suggests that optimization of iron status prior to pregnancy is the most effective method to reduce the deleterious impacts of perinatal ID on offspring [32,41]. Further study of the mechanisms by which perinatal ID predisposes offspring for poor health outcomes, in conjunction with clinical studies corroborating the long-term findings within the pre-clinical literature, will help emphasize the importance of ID

prevention. Further investment into organizations such as the WHO to supply screening and treatment options for those with ID in nations where it is most common, such as south Asia and central and western Africa, appear to be most critical [21].

Finally, preclinical DOHaD studies show significant promise for the targeting of dysfunction secondary to developmental stressors [171]. However, the stringent regulatory oversights surrounding therapeutics intended for use in pregnancy likely mean that any therapeutic interventions currently under development are decades away from widespread use. As such, a multifaceted approach must be undertaken to minimize the chronic disease associated with perinatal ID. Continued focus on the prevention of perinatal ID, in conjunction with the development of efficacious therapeutic interventions targeting dysfunction in offspring, may be the best path forward to optimizing offspring health.

Bibliography

1. Wang J, Pantopoulos K. Regulation of cellular iron metabolism. *Biochem J*. 2011;434(3):365-381.

2. Andrews NC. Disorders of iron metabolism. *N Engl J Med*. 1999;341(26):1986-1995.

3. Benson CS, Shah A, Stanworth SJ, et al. The effect of iron deficiency and anaemia on women's health. *Anaesthesia*. 2021;76(S4):84-95.

4. Allen LH. Anemia and iron deficiency: effects on pregnancy outcome. *Am J Clin Nutr*. 2000;71(5 Suppl):1280S-4S.

5. Sebastiani G, Wilkinson N, Pantopoulos K. Pharmacological targeting of the hepcidin/ferroportin axis. *Front Pharmacol*. 2016;7:160.

6. Cerami C. Iron Nutriture of the Fetus, Neonate, Infant, and Child. *Ann Nutr Metab*. 2017;71(3):8-14.

7. Institute of Medicine (US) Panel on Micronutrients. Iron. In: *Dietary Reference Intakes for Vitamin A, Vitamin K, Arsenic, Boron, Chromium, Copper, Iodine, Iron, Manganese, Molybdenum, Nickel, Silicon, Vanadium, and Zinc.* National Academies Press (US); 2001.

8. Prättälä R, Paalanen L, Grinberga D, Helasoja V, Kasmel A, Petkeviciene J. Gender differences in the consumption of meat, fruit and vegetables are similar in Finland and the Baltic countries. *Eur J Public Health*. 2007;17(5):520-525.

9. Saboor M, Zehra A, Hamali HA, Mobarki AA. Revisiting iron metabolism, iron homeostasis and iron deficiency anemia. *Clin Lab*. 2021;67(3):660-666.

10. Afsar RE, Kanbay M, Ibis A, Afsar B. In-depth review: is hepcidin a marker for the heart and the kidney? *Mol Cell Biochem*. 2021;E-Pub:doi:10.1007/s11010-021-04168-4.

11. Lopez A, Cacoub P, Macdougall IC, Peyrin-Biroulet L. Iron deficiency anaemia. *Lancet*. 2015;387(10021):907-916.

12. Sangkhae V, Nemeth E. Regulation of the iron homeostatic hormone hepcidin. *Adv Nutr*. 2017;8(1):126-136.

13. Yiannikourides A, Latunde-Dada G. A Short Review of Iron Metabolism and Pathophysiology of Iron Disorders. *Medicines*. 2019;6(3):85.

14. Kowdley K V., Gochanour EM, Sundaram V, Shah RA, Handa P. Hepcidin Signaling in Health and Disease: Ironing Out the Details. *Hepatol Commun*. 2021;5(5):723-735.

15. Lynch S, Pfeiffer CM, Georgieff MK, et al. Biomarkers of Nutrition for Development (BOND)-Iron review. *J Nutr*. 2018;148(suppl_1):1001S-1067S.

16. Ems T, St Lucia K, Huecker MR. *Biochemistry, Iron Absorption*. StatPearls Publishing; 2021.

17. Wang W, Knovich MA, Coffman LG, Torti FM, Torti S V. Serum ferritin: Past, present and future. *Biochim Biophys Acta - Gen Subj*. 2010;1800(8):760-769.

18. Garcia-Casal MN, Peña-Rosas JP, Pasricha S-R. Rethinking ferritin cutoffs for iron deficiency and overload. *Lancet Haematol*. 2014;1(3):e92-4.

19. Sanni OB, Chambers T, Li JH, et al. A systematic review and meta-analysis of the correlation between maternal and neonatal iron status and haematologic indices. *EClinicalMedicine*. 2020;27.

20. Winn NC, Volk KM, Hasty AH. Regulation of tissue iron homeostasis: The macrophage "ferrostat." *JCI Insight*. 2020;5(2):132964.

21. Stevens GA, Finucane MM, De-Regil LM, et al. Global, regional, and national trends in haemoglobin concentration and prevalence of total and severe anaemia in children and pregnant and non-pregnant women for 1995-2011: a systematic analysis of population-representative data. *Lancet Glob Heal*. 2013;1(1):e16-25.

22. Kassebaum NJ. The Global Burden of Anemia. *Hematol Oncol Clin North Am*. 2016;30(2):247-308.

23. Pasricha SR, Tye-Din J, Muckenthaler MU, Swinkels DW. Iron deficiency. *Lancet*. 2021;397(10270):233-248.

24. US Preventative Services Task Force. *Screening for Iron Deficiency Anemia and Iron Supplementation in Pregnant Women to Improve Maternal Health and Birth Outcomes: Recommendation Statement*. Vol 93.; 2016.

25. Garcia-Casal MN, Pasricha SR, Martinez RX, Lopez-Perez L, Peña-Rosas JP. Are Current Serum and Plasma Ferritin Cut-offs for Iron Deficiency and Overload

Accurate and Reflecting Iron Status? A Systematic Review. *Arch Med Res*. 2018;49(6):405-417.

26. Suchdev PS, Williams AM, Mei Z, et al. Assessment of iron status in settings of inflammation: Challenges and potential approaches. *Am J Clin Nutr*. 2017;106(Suppl 6):1626S-1633S.

27. Mei Z, Namaste SM, Serdula M, et al. Adjusting total body iron for inflammation: Biomarkers Reflecting Inflammation and Nutritional Determinants of Anemia (BRINDA) project. *Am J Clin Nutr*. 2017;106:383S-389S.

28. Soppi ET. Iron deficiency without anemia – a clinical challenge. *Clin Case Reports*. 2018;6(6):1082-1086.

29. Daru J, Allotey J, Peña-Rosas JP, Khan KS. Serum ferritin thresholds for the diagnosis of iron deficiency in pregnancy: a systematic review. *Transfus Med*. 2017;27(3):167-174.

30. Milman N. Iron and pregnancy--a delicate balance. *Ann Hematol*. 2006;85(9):559-565.

31. Miller EM. The reproductive ecology of iron in women. *Am J Phys Anthropol*. 2016;159(Suppl 61):S172-95.

32. Breymann C, Auerbach M. Iron deficiency in gynecology and obstetrics: Clinical implications and management. *Hematology*. 2017;2017(1):152-159.

33. McLean E, Cogswell M, Egli I, Wojdyla D, de Benoist B. Worldwide prevalence

of anaemia, WHO Vitamin and Mineral Nutrition Information System, 1993-2005. *Public Health Nutr*. 2009;12(4):444-454.

34. World Health Organization Department of Nutrition for Health and Development. *Iron Deficiency Anaemia: Assessment, Prevention and Control: A Guide for Programme Managers*. Geneva: World Health Organization; 2001.

35. Suominen P, Punnonen K, Rajamäki A, Irjala K. Serum Transferrin Receptor and Transferrin Receptor-Ferritin Index Identify Healthy Subjects With Subclinical Iron Deficits. *Blood*. 1998;92(8):2934-2939.

36. Garcia-Casal MN, Pasricha S-R, Martinez RX, Lopez-Perez L, Peña-Rosas JP. Serum or plasma ferritin concentration as an index of iron deficiency and overload. *Cochrane Database Syst Rev*. 2021;5(5):CD011817.

37. Achebe MM, Gafter-Gvili A. How I treat anemia in pregnancy: Iron, cobalamin, and folate. *Blood*. 2017;129(8):940-949.

38. Gragasin FS, Ospina MB, Serrano-Lomelin J, et al. Maternal and Cord Blood Hemoglobin as Determinants of Placental Weight: A Cross-Sectional Study. *J Clin Med*. 2021;10(5):997.

39. Breymann C. Iron Deficiency Anemia in Pregnancy. *Semin Hematol*. 2015;52(4):339-347.

40. Zimmermann MB. Global look at nutritional and functional iron deficiency in infancy. *Hematol (United States)*. 2020;20(1):471-477.

41. Georgieff MK. Iron deficiency in pregnancy. *Am J Obstet Gynecol*. 2020;223(4):516-524.

42. Roberts H, Bourque SL, Renaud SJ. Maternal iron homeostasis: Effect on placental development and function. *Reproduction*. 2020;160(4):R65-R78.

43. Dewey KG, Oaks BM. U-shaped curve for risk associated with maternal hemoglobin, iron status, or iron supplementation. *Am J Clin Nutr*. 2017;106(Suppl 6):1694S-1702S.

44. Peña-Rosas JP, De-Regil LM, Garcia-Casal MN, Dowswell T. Daily oral iron supplementation during pregnancy. *Cochrane Database Syst Rev*. 2015;(7):CD004736.

45. Peña-Rosas JP, De-Regil LM, Gomez Malave H, Flores-Urrutia MC, Dowswell T. Intermittent oral iron supplementation during pregnancy. *Cochrane Database Syst Rev*. 2015;(10):CD009997.

46. Rahman MM, Abe SK, Rahman MS, et al. Maternal anemia and risk of adverse birth and health outcomes in low- and middle-income countries: Systematic review and meta-analysis. *Am J Clin Nutr*. 2016;103(2):495-504.

47. Scholl TO. Maternal iron status: relation to fetal growth, length of gestation, and iron endowment of the neonate. *Nutr Rev*. 2011;69 Suppl 1:S23-9.

48. Rao R, Georgieff MK. Iron in fetal and neonatal nutrition. *Semin Fetal Neonatal Med*. 2007;12(1):54.

49. M D. Meeting the Iron Needs of Low and Very Low Birth Weight Infants. *Ann Nutr Metab*. 2017;71 Suppl 3(3):16-23.

50. Davis L, Thornburg KL, Giraud GD. The effects of anaemia as a programming agent in the fetal heart. *J Physiol*. 2005;565(Pt 1):35-41.

51. Davis LE, Hohimer AR, Morton MJ. Myocardial blood flow and coronary reserve in chronically anemic fetal lambs. *Am J Physiol*. 1999;277(1 Pt 2):R306-13.

52. Martin C, Yu AY, Jiang BH, et al. Cardiac hypertrophy in chronically anemic fetal sheep: Increased vascularization is associated with increased myocardial expression of vascular endothelial growth factor and hypoxia-inducible factor 1. *Am J Obstet Gynecol*. 1998;178(3):527-534.

53. Allison BJ, Brain KL, Niu Y, et al. Fetal in vivo continuous cardiovascular function during chronic hypoxia. *J Physiol*. 2016;594(5):1247-1264.

54. Giussani DA. The fetal brain sparing response to hypoxia: physiological mechanisms. *J Physiol*. 2016;594(5):1215-1230.

55. Finer LB, Zolna MR. Declines in Unintended Pregnancy in the United States, 2008–2011. *N Engl J Med*. 2016;374(9):843-852.

56. Pasricha S-R, Drakesmith H. Iron Deficiency Anemia: Problems in Diagnosis and Prevention at the Population Level. *Hematol Oncol Clin North Am*. 2016;30(2):309-325.

57. Cockell KA, Miller DC, Lowell H. Application of the dietary reference intakes in

developing a recommendation for pregnancy iron supplements in Canada. *Am J Clin Nutr*. 2009;90(4):1023-1028.

58. Georgieff MK, Krebs NF, Cusick SE. The Benefits and Risks of Iron Supplementation in Pregnancy and Childhood. *Annu Rev Nutr*. 2019;39:121.

59. Sun CF, Liu H, Hao YH, et al. Association between gestational anemia in different trimesters and neonatal outcomes: a retrospective longitudinal cohort study. *World J Pediatr*. 2021;17(2):197-204.

60. Govindappagari S, Burwick RM. Treatment of Iron Deficiency Anemia in Pregnancy with Intravenous versus Oral Iron: Systematic Review and Meta-Analysis. *Am J Perinatol*. 2019;36(4):366-376.

61. Bresgen N, Eckl PM. Oxidative stress and the homeodynamics of iron metabolism. *Biomolecules*. 2015;5(2):808-847.

62. Thomas CE, Morehouse LA, Aust SD. Ferritin and superoxide-dependent lipid peroxidation. *J Biol Chem*. 1985;260(6):3275-3280.

63. Bastian TW, Rao R, Tran P V., Georgieff MK. The Effects of Early-Life Iron Deficiency on Brain Energy Metabolism. *Neurosci Insights*. 2020;15:1-12.

64. Lin E, Graziano JH, Freyer GA. Regulation of the 75-kDa Subunit of Mitochondrial Complex I by Iron. *J Biol Chem*. 2001;276(29):27685-27692.

65. Gray NK, Pantopoulos K, Dandekar T, Ackrell BAC, Hentze MW. Translational regulation of mammalian and Drosophila citric acid cycle enzymes via iron-

responsive elements. *Proc Natl Acad Sci U S A*. 1996;93(10):4925-4930.

66. Higashida K, Inoue S, Nakai N. Iron deficiency attenuates protein synthesis stimulated by branched-chain amino acids and insulin in myotubes. *Biochem Biophys Res Commun*. 2020;531(2):112-117.

67. Walter PB, Knutson MD, Paler-Martinez A, et al. Iron deficiency and iron excess damage mitochondria and mitochondrial DNA in rats. *Proc Natl Acad Sci U S A*. 2002;99(4):2264-2269.

68. Rineau E, Gueguen N, Procaccio V, et al. Iron deficiency without anemia decreases physical endurance and mitochondrial complex i activity of oxidative skeletal muscle in the mouse. *Nutrients*. 2021;13(4):1056.

69. Tajes M, Díez-López C, Enjuanes C, et al. Neurohormonal activation induces intracellular iron deficiency and mitochondrial dysfunction in cardiac cells. *Cell Biosci*. 2021;11(1):89.

70. Simcox JA, McClain DA. Iron and diabetes risk. *Cell Metab*. 2013;17(3):329-341.

71. Peña-Montes DJ, Huerta-Cervantes M, Ríos-Silva M, et al. Effects of dietary iron restriction on kidney mitochondria function and oxidative stress in streptozotocin-diabetic rats. *Mitochondrion*. 2020;54:41-48.

72. Chance B, Sies H, Boveris A. Hydroperoxide metabolism in mammalian organs. *Physiol Rev*. 1979;59(3):527-605.

73. Zorov DB, Juhaszova M, Sollott SJ. Mitochondrial reactive oxygen species (ROS)

and ROS-induced ROS release. *Physiol Rev*. 2014;94(3):909-950.

74. Yoo J-H, Maeng H-Y, Sun Y-K, et al. Oxidative status in iron-deficiency anemia. *J Clin Lab Anal*. 2009;23(5):319-323.

75. Zhao G, Arosio P, Chasteen ND. Iron(II) and hydrogen peroxide detoxification by human H-chain ferritin. An EPR spin-trapping study. *Biochemistry*. 2006;45(10):3429-3436.

76. Arosio P, Levi S. Ferritin, iron homeostasis, and oxidative damage. *Free Radic Biol Med*. 2002;33(4):457-463.

77. Tran TN, Eubanks SK, Schaffer KJ, Zhou CYJ, Linder MC. Secretion of ferritin by rat hepatoma cells and its regulation by inflammatory cytokines and iron. *Blood*. 1997;90(12):4979-4986.

78. Rogers JT, Bridges KR, Durmowicz GP, Glass J, Auron PE, Munro HN. Translational control during the acute phase response. Ferritin synthesis in response to interleukin-1. *J Biol Chem*. 1990;265(24):14572-14578.

79. Pham CG, Bubici C, Zazzeroni F, et al. Ferritin heavy chain upregulation by NF-κB inhibits TNFα-induced apoptosis by suppressing reactive oxygen species. *Cell*. 2004;119(4):529-542.

80. Miller LL, Miller SC, Torti S V., Tsuji Y, Torti FM. Iron-independent induction of ferritin H chain by tumor necrosis factor. *Proc Natl Acad Sci U S A*. 1991;88(11):4946-4950.

81. Qi Y, Dawson G. Hypoxia specifically and reversibly induces the synthesis of ferritin in oligodendrocytes and human oligodendrogliomas. *J Neurochem*. 1994;63(4):1485-1490.

82. Hintze KJ, Theil EC. Cellular regulation and molecular interactions of the ferritins. *Cell Mol Life Sci*. 2006;63(5):591-600.

83. Kurtoglu E, Ugur A, Baltaci AK, Undar L. Effect of iron supplementation on oxidative stress and antioxidant status in iron-deficiency anemia. *Biol Trace Elem Res*. 2003;96(1-3):117-123.

84. Toblli JE, Cao G, Oliveri L, Angerosa M. Effects of iron deficiency anemia and its treatment with iron polymaltose complex in pregnant rats, their fetuses and placentas: Oxidative stress markers and pregnancy outcome. *Placenta*. 2012;33(2):81-87.

85. Vieyra-Reyes P, Millán-Aldaco D, Palomero-Rivero M, Jiménez-Garcés C, Hernández-González M, Caballero-Villarraso J. An iron-deficient diet during development induces oxidative stress in relation to age and gender in Wistar rats. *J Physiol Biochem*. 2017;73(1):99-110.

86. Tiwari AKM, Mahdi AA, Zahra F, et al. Evaluation of oxidative stress and antioxidant status in pregnant anemic women. *Indian J Clin Biochem*. 2010;25(4):411-418.

87. Aslaner H, Dündar MA, Arslan A, Karakükcü Ç, Altuner Torun Y. Reduced antioxidant capacity in children with iron deficiency and iron-deficiency anemia.

Minerva Pediatr. 2021;E-Pub:doi: 10.23736/S2724-5276.21.06193-4.

88. Altun D, Kurekci AE, Gursel O, et al. Malondialdehyde, Antioxidant Enzymes, and Renal Tubular Functions in Children with Iron Deficiency or Iron-Deficiency Anemia. *Biol Trace Elem Res*. 2014;161(1):48-56.

89. Kumar C, Igbaria A, D'Autreaux B, et al. Glutathione revisited: A vital function in iron metabolism and ancillary role in thiol-redox control. *EMBO J*. 2011;30(10):2044-2056.

90. Berndt C, Lillig CH. Glutathione, Glutaredoxins, and Iron. *Antioxidants Redox Signal*. 2017;27(15):1235-1251.

91. Haase VH. Hypoxic regulation of erythropoiesis and iron metabolism. *Am J Physiol Renal Physiol*. 2010;299(1):F1-F13.

92. Woo KJ, Lee T-J, Park J-W, Kwon TK. Desferrioxamine, an iron chelator, enhances HIF-1α accumulation via cyclooxygenase-2 signaling pathway. *Biochem Biophys Res Commun*. 2006;343(1):8-14.

93. GBD 2013 Mortality and Causes of Death Collaborators. Global, regional, and national age-sex specific all-cause and cause-specific mortality for 240 causes of death, 1990-2013: a systematic analysis for the Global Burden of Disease Study 2013. *Lancet (London, England)*. 2015;385(9963):117-171.

94. Zhou B, Perel P, Mensah GA, Ezzati M. Global epidemiology, health burden and effective interventions for elevated blood pressure and hypertension. *Nat Rev*

Cardiol. 2021;E-Pub:doi: 10.1038/s41569-021-00559-8.

95. Cockwell P, Fisher LA. The global burden of chronic kidney disease. *Lancet*. 2020;395(10225):662-664.

96. Maranon R, Reckelhoff JF. Sex and gender differences in control of blood pressure. *Clin Sci (Lond)*. 2013;125(7):311-318.

97. Loria AS, Goulopoulou S, Bourque SL, Davidge ST. Sex Differences in Developmental Origins of Cardiovascular Disease. *Sex Differ Cardiovasc Physiol Pathophysiol*. Published online January 1, 2019:253-289.

98. Bourque SL, Davidge ST. Developmental programming of cardiovascular function: A translational perspective. *Clin Sci*. 2020;134(22):3023-3046.

99. Thornburg KL. The programming of cardiovascular disease. *J Dev Orig Health Dis*. 2015;6(5):366-376.

100. Guyton AC, Coleman TG, Young DB, Lohmeier TE, DeClue JW. Salt Balance and Long-Term Blood Pressure Control. *Annu Rev Med*. 1980;31(1):15-27.

101. Guyton AC, Lohmeier TE, Hall JE, Smith MJ, Kastner PR. The Infinite Gain Principle for Arterial Pressure Control by the Kidney-Volume-Pressure System. In: Springer, Dordrecht; 1984:35-61.

102. Pao AC. Update on the Guytonian view of hypertension. *Curr Opin Nephrol Hypertens*. 2014;23(4):391-398.

103. Mount PF, Power DA. Nitric oxide in the kidney: functions and regulation of

synthesis. *Acta Physiol*. 2006;187(4):433-446.

104. Carlström M. Nitric oxide signalling in kidney regulation and cardiometabolic health. *Nat Rev Nephrol*. 2021;E-Pub:doi: 10.1038/s41581-021-00429-z.

105. Evans RG, Bie P. Role of the kidney in the pathogenesis of hypertension: time for a neo-Guytonian paradigm or a paradigm shift? *Am J Physiol Regul Integr Comp Physiol*. 2016;310(3):R217-29.

106. Kurtz TW, DiCarlo SE, Morris RC. Logical issues with the pressure natriuresis theory of chronic hypertension. *Am J Hypertens*. 2016;29(12):1325-1331.

107. Mishra S, Ingole S, Jain R. Salt sensitivity and its implication in clinical practice. *Indian Heart J*. 2018;70(4):556-564.

108. Granger JP, Alexander BT, Llinas M. Mechanisms of pressure natriuresis. *Curr Hypertens Rep*. 2002;4(2):152-159.

109. Kawarazaki W, Fujita T. Kidney and epigenetic mechanisms of salt-sensitive hypertension. *Nat Rev Nephrol*. 2021;17(5):350-363.

110. Skarlatos S, Brand PH, Metting PJ, Britton SL. Spontaneous changes in arterial blood pressure and renal interstitial hydrostatic pressure in conscious rats. *J Physiol*. 1994;481 (Pt 3):743-752.

111. Choi HY, Park HC, Ha SK. Salt Sensitivity and Hypertension: A Paradigm Shift from Kidney Malfunction to Vascular Endothelial Dysfunction. *Electrolytes Blood Press E BP*. 2015;13(1):7.

112. Charkoudian N, Rabbitts JA. Sympathetic neural mechanisms in human cardiovascular health and disease. *Mayo Clin Proc*. 2009;84(9):822-830.

113. Gardner RT, Ripplinger CM, Myles RC, Habecker BA. Molecular Mechanisms of Sympathetic Remodeling and Arrhythmias. *Circ Arrhythmia Electrophysiol*. 2016;9(2):e001359.

114. Kurtz A. Control of renin synthesis and secretion. *Am J Hypertens*. 2012;25(8):839-847.

115. Majid DSA, Prieto MC, Navar LG. Salt-Sensitive Hypertension: Perspectives on Intrarenal Mechanisms. *Curr Hypertens Rev*. 2015;11(1):38-48.

116. Falkner B. Cardiac output versus total peripheral resistance a wrinkle in time. *Hypertension*. 2018;72(5):1093-1094.

117. Park C, Fraser A, Howe LD, et al. Elevated blood pressure in adolescence is attributable to a combination of elevated cardiac output and total peripheral resistance evidence against a hyperkinetic State. *Hypertension*. 2018;72(5):1103-1108.

118. Michael SK, Surks HK, Wang Y, et al. High blood pressure arising from a defect in vascular function. *Proc Natl Acad Sci U S A*. 2008;105(18):6702-6707.

119. MK P, R T. The vascular system. An overview of structure and function. *J Pharmacol Toxicol Methods*. 2000;44(2):333-340.

120. Stauss HM. Identification of blood pressure control mechanisms by power spectral

analysis. *Clin Exp Pharmacol Physiol*. 2007;34(4):362-368.

121. Hemmings DG, Williams SJ, Davidge ST. Increased myogenic tone in 7-month-old adult male but not female offspring from rat dams exposed to hypoxia during pregnancy. *Am J Physiol Circ Physiol*. 2005;289(2):H674-H682.

122. Christensen KL, Mulvany MJ. Location of resistance arteries. *J Vasc Res*. 2001;38(1):1-12.

123. Sandoo A, van Zanten JJCSV, Metsios GS, Carroll D, Kitas GD. The endothelium and its role in regulating vascular tone. *Open Cardiovasc Med J*. 2010;4:302-312.

124. C F. Mechanisms of vasoconstriction. *Am Heart J*. 1991;121(3 Pt 1):958-960.

125. Zelis R. Mechanisms of vasodilation. *Am J Med*. 1983;74(6):3-12.

126. Gilani M, Kaiser DR, Bratteli CW, et al. Role of nitric oxide deficiency and its detection as a risk factor in pre-hypertension. *J Am Soc Hypertens*. 2007;1(1):45-55.

127. Rook W, Johnson CD, Coney AM, Marshall JM. Prenatal hypoxia leads to increased muscle sympathetic nerve activity, sympathetic hyperinnervation, premature blunting of neuropeptide Y signaling, and hypertension in adult life. *Hypertension*. 2014;64(6):1321-1327.

128. PI K. The phenotypic patterns of essential hypertension are the key to identifying "high blood pressure" genes. *Physiol Res*. 2010;59(6):841-857.

129. Rodrigo R, González J, Paoletto F. The role of oxidative stress in the

pathophysiology of hypertension. *Hypertens Res 2011 344*. 2011;34(4):431-440.

130. Moriya J, Minamino T. Angiogenesis, Cancer, and Vascular Aging. *Front Cardiovasc Med*. 2017;4:65.

131. Kim Y-W, Byzova T V. Oxidative stress in angiogenesis and vascular disease. *Blood*. 2014;123(5):625-631.

132. Pugh CW, Ratcliffe PJ. Regulation of angiogenesis by hypoxia: Role of the HIF system. *Nat Med*. 2003;9(6):677-684.

133. Brown IAM, Diederich L, Good ME, et al. Vascular smooth muscle remodeling in conductive and resistance arteries in hypertension. *Arterioscler Thromb Vasc Biol*. 2018;38(9):1969-1985.

134. Varik BJ van, Rennenberg RJMW, Reutelingsperger CP, Kroon AA, Leeuw PW de, Schurgers LJ. Mechanisms of arterial remodeling: lessons from genetic diseases. *Front Genet*. 2012;3:290.

135. Barker DJP. The origins of the developmental origins theory. In: *Journal of Internal Medicine*. Vol 261. J Intern Med; 2007:412-417.

136. Barker DJ, Osmond C. Infant mortality, childhood nutrition, and ischaemic heart disease in England and Wales. *Lancet (London, England)*. 1986;1(8489):1077-1081.

137. Barker DJ, Osmond C. Low birth weight and hypertension. *BMJ*. 1988;297(6641):134-135.

138. Barker DJ, Winter PD, Osmond C, Margetts B, Simmonds SJ. Weight in infancy and death from ischaemic heart disease. *Lancet (London, England)*. 1989;2(8663):577-580.

139. Morton JS, Cooke C-L, Davidge ST. In Utero Origins of Hypertension: Mechanisms and Targets for Therapy. *Physiol Rev*. 2016;96(2):549-603.

140. Barker DJP. The developmental origins of adult disease. *J Am Coll Nutr*. 2004;23(6 Suppl):588S-595S.

141. Ho SM, Cheong A, To S, Janakiram V, Tarapore P, Leung YK. Cancer and Developmental Origins of Health and Disease-Epigenetic Reprogramming as a Mediator. In: *The Epigenome and Developmental Origins of Health and Disease*. Elsevier Inc.; 2015:315-336.

142. Ho SM, Cheong A, Adgent MA, et al. Environmental factors, epigenetics, and developmental origin of reproductive disorders. *Reprod Toxicol*. 2017;68:85-104.

143. Hanson MA, Gluckman PD. Early Developmental Conditioning of Later Health and Disease: Physiology or Pathophysiology? *Physiol Rev*. 2014;94(4):1027-1076.

144. Goldstein JA, Norris SA, Aronoff DM. DOHaD at the intersection of maternal immune activation and maternal metabolic stress: A scoping review. *J Dev Orig Health Dis*. 2017;8(3):273-283.

145. Chehade H, Simeoni U, Guignard J-P, Boubred F. Preterm Birth: Long Term Cardiovascular and Renal Consequences. *Curr Pediatr Rev*. 2018;14(4):219-226.

146. Lammertink F, Vinkers CH, Tataranno ML, Benders MJNL. Premature Birth and Developmental Programming: Mechanisms of Resilience and Vulnerability. *Front Psychiatry*. 2021;11:531571.

147. Peleg D, Kennedy CM, Hunter SK. Intrauterine Growth Restriction: Identification and Management. *Am Fam Physician*. 1998;58(2):453.

148. Zeve D, Regelmann MO, Holzman IR, Rapaport R. Small at Birth, but How Small? the Definition of SGA Revisited. *Horm Res Paediatr*. 2016;86(5):357-360.

149. Gilbert JS, Cox LA, Mitchell G, Nijland MJ. Nutrient-restricted fetus and the cardio-renal connection in hypertensive offspring. *Expert Rev Cardiovasc Ther*. 2006;4(2):227-238.

150. Bertram JF, Douglas-Denton RN, Diouf B, Hughson MD, Hoy WE. Human nephron number: implications for health and disease. *Pediatr Nephrol*. 2011;26(9):1529-1533.

151. Low Birth Weight and Nephron Number Working Group. The Impact of Kidney Development on the Life Course: A Consensus Document for Action. *Nephron*. 2017;136(1):3-49.

152. Sutton EF, Gilmore LA, Dunger DB, et al. Developmental programming: State-of-the-science and future directions-Summary from a Pennington Biomedical symposium. *Obesity*. 2016;24(5):1018-1026.

153. Gurusinghe S, Tambay A, Sethna CB. Developmental origins and nephron

endowment in hypertension. *Front Pediatr*. 2017;5:151.

154. Giussani DA, Davidge ST. Developmental programming of cardiovascular disease by prenatal hypoxia. *J Dev Orig Health Dis*. 2013;4(5):328-337.

155. Ozanne SE, Hales CN. Catch-up growth and obesity in male mice. *Nature*. 2004;427(6973):411-412.

156. Jimenez-Chillaron JC, Hernandez-Valencia M, Lightner A, et al. Reductions in caloric intake and early postnatal growth prevent glucose intolerance and obesity associated with low birthweight. *Diabetologia*. 2006;49(8):1974-1984.

157. Tarry-Adkins JL, Chen JH, Smith NS, Jones RH, Cherif H, Ozanne SE. Poor maternal nutrition followed by accelerated postnatal growth leads to telomere shortening and increased markers of cell senescence in rat islets. *FASEB J*. 2009;23(5):1521-1528.

158. Kesavan K, Devaskar SU. Intrauterine Growth Restriction: Postnatal Monitoring and Outcomes. *Pediatr Clin North Am*. 2019;66(2):403-423.

159. Bourque SL, Komolova M, McCabe K, Adams MA, Nakatsu K. Perinatal iron deficiency combined with a high-fat diet causes obesity and cardiovascular dysregulation. *Endocrinology*. 2012;153(3):1174-1182.

160. Komolova M, Bourque SL, Nakatsu K, Adams MA. Sedentariness and increased visceral adiposity in adult perinatally iron-deficient rats. *Int J Obes (Lond)*. 2008;32(9):1441-1444.

161. Rueda-Clausen CF, Morton JS, Oudit GY, Kassiri Z, Jiang Y, Davidge ST. Effects of hypoxia-induced intrauterine growth restriction on cardiac siderosis and oxidative stress. *J Dev Orig Health Dis*. 2012;3(5):350-357.

162. Morton JS, Rueda-Clausen CF, Davidge ST. Flow-mediated vasodilation is impaired in adult rat offspring exposed to prenatal hypoxia. *J Appl Physiol*. 2011;110(4):1073-1082.

163. Moritz KM, Mazzuca MQ, Siebel AL, et al. Uteroplacental insufficiency causes a nephron deficit, modest renal insufficiency but no hypertension with ageing in female rats. *J Physiol*. 2009;587(Pt 11):2635-2646.

164. Woodman AG, Care AS, Mansour Y, et al. Modest and Severe Maternal Iron Deficiency in Pregnancy are Associated with Fetal Anaemia and Organ-Specific Hypoxia in Rats. *Sci Rep*. 2017;7:46573.

165. Woodman AG, Mah R, Keddie D, et al. Prenatal iron deficiency causes sex-dependent mitochondrial dysfunction and oxidative stress in fetal rat kidneys and liver. *FASEB J*. 2018;32(6):3254-4263.

166. Lee Y, Collins C, Gordon A, Rae K, Pringle K. The Relationship between Maternal Nutrition during Pregnancy and Offspring Kidney Structure and Function in Humans: A Systematic Review. *Nutrients*. 2018;10(2):241.

167. Talbot CPJ, Dolinsky VW. Sex differences in the developmental origins of cardiometabolic disease following exposure to maternal obesity and gestational diabetes. *Appl Physiol Nutr Metab*. 2019;44(7):687-695.

168. Brawerman GM, Kereliuk SM, Brar N, et al. Maternal resveratrol administration protects against gestational diabetes-induced glucose intolerance and islet dysfunction in the rat offspring. *J Physiol*. 2019;597(16):4175-4192.

169. Hieronimus B, Ensenauer R. Influence of maternal and paternal pre-conception overweight/obesity on offspring outcomes and strategies for prevention. *Eur J Clin Nutr*. 2021;E-Pub:doi: 10.1038/s41430-021-00920-7.

170. Bourque SL, Komolova M, Nakatsu K, Adams MA. Long-term circulatory consequences of perinatal iron deficiency in male wistar rats. *Hypertension*. 2008;51(1):154-159.

171. Tain YL, Hsu CN. Developmental origins of chronic kidney disease: Should we focus on early life? *Int J Mol Sci*. 2017;18(2).

172. Hsu C-N, Tain Y-L. Animal Models for DOHaD Research: Focus on Hypertension of Developmental Origins. *Biomedicines*. 2021;9(6):623.

173. Hsu C-N, Tain Y-L. Targeting the Renin–Angiotensin–Aldosterone System to Prevent Hypertension and Kidney Disease of Developmental Origins. *Int J Mol Sci*. 2021;22(5):2298.

174. McGill HC, McMahan CA, Gidding SS. Preventing heart disease in the 21st century: implications of the Pathobiological Determinants of Atherosclerosis in Youth (PDAY) study. *Circulation*. 2008;117(9):1216-1227.

175. Rookmaaker MB, Joles JA. The nephron number counts--from womb to tomb.

Nephrol Dial Transplant. 2013;28(6):1325-1328.

176. Ryan D, Sutherland MR, Flores TJ, et al. Development of the Human Fetal Kidney from Mid to Late Gestation in Male and Female Infants. *EBioMedicine*. 2018;27:275-283.

177. McMahon AP. Development of the Mammalian Kidney. In: *Current Topics in Developmental Biology*. Vol 117. Curr Top Dev Biol; 2016:31-64.

178. Wang Y, Stokes A, Duan Z, et al. LDL receptor-related protein 6 modulates ret proto-oncogene signaling in renal development and cystic dysplasia. *J Am Soc Nephrol*. 2016;27(2):417-427.

179. Wang Y, Zhou CJ, Liu Y. Wnt Signaling in Kidney Development and Disease. In: *Progress in Molecular Biology and Translational Science*. Vol 153. Prog Mol Biol Transl Sci; 2018:181-207.

180. Costantini F. GDNF/Ret signaling and renal branching morphogenesis: From mesenchymal signals to epithelial cell behaviors. *Organogenesis*. 2010;6(4):252-262.

181. Ide S, Finer G, Maezawa Y, et al. Transcription factor 21 is required for branching morphogenesis and regulates the Gdnf-Axis in kidney development. *J Am Soc Nephrol*. 2018;29(12):2795-2808.

182. Bates CM. Role of fibroblast growth factor receptor signaling in kidney development. *Am J Physiol - Ren Physiol*. 2011;301(2):F245.

183. Nishinakamura R, Sakaguchi M. BMP signaling and its modifiers in kidney development. In: *Pediatric Nephrology*. Vol 29. Pediatr Nephrol; 2014:681-686.

184. Kreidberg JA. WT1 and kidney progenitor cells. *Organogenesis*. 2010;6(2):61-70.

185. Muñoz-Espín D, Cañamero M, Maraver A, et al. Programmed cell senescence during mammalian embryonic development. *Cell*. 2013;155(5):1104-1118.

186. Storer M, Mas A, Robert-Moreno A, et al. Senescence Is a Developmental Mechanism that Contributes to Embryonic Growth and Patterning. *Cell*. 2013;155(5):1119-1130.

187. Banito A, Lowe SW. A new development in senescence. *Cell*. 2013;155(5):977.

188. Childs BG, Baker DJ, Kirkland JL, Campisi J, Deursen JM. Senescence and apoptosis: dueling or complementary cell fates? *EMBO Rep*. 2014;15(11):1139-1153.

189. Fisher DJ, Heymann MA, Rudolph AM. Regional myocardial blood flow and oxygen delivery in fetal, newborn, and adult sheep. *Am J Physiol*. 1982;243(5):H729-31.

190. Harris AP, Sendak MJ, Donham RT. Changes in arterial oxygen saturation immediately after birth in the human neonate. *J Pediatr*. 1986;109(1):117-119.

191. Itskovitz J, Goetzman BW, Roman C, Rudolph AM. Effects of fetal-maternal exchange transfusion on fetal oxygenation and blood flow distribution. *Am J Physiol*. 1984;247(4 Pt 2):H655-60.

192. Carter AM. Placental Gas Exchange and the Oxygen Supply to the Fetus. In: *Comprehensive Physiology*. Vol 5. John Wiley & Sons, Inc.; 2015:1381-1403.

193. Wispe JR, Bell EF, Roberts RJ. Assessment of lipid peroxidation in newborn infants and rabbits by measurements of expired ethane and pentane: influence of parenteral lipid infusion. *Pediatr Res*. 1985;19(4):374-379.

194. Wispé JR, Knight M, Roberts RJ. Lipid peroxidation in newborn rabbits: effects of oxygen, lipid emulsion, and vitamin E. *Pediatr Res*. 1986;20(6):505-510.

195. Yoshioka T, Motoyama H, Yamasaki F, Noma J. Lipid peroxidation and its protective mechanism during developmental stage in rat. *Nihon Sanka Fujinka Gakkai Zasshi*. 1982;34(7):966-970.

196. McCarthy K, Bhogal M, Nardi M, Hart D. Pathogenic factors in bronchopulmonary dysplasia. *Pediatr Res*. 1984;18(5):483-488.

197. Phaniendra A, Jestadi DB, Periyasamy L. Free radicals: properties, sources, targets, and their implication in various diseases. *Indian J Clin Biochem*. 2015;30(1):11-26.

198. Turrens JF, Freeman BA, Levitt JG, Crapo JD. The effect of hyperoxia on superoxide production by lung submitochondrial particles. *Arch Biochem Biophys*. 1982;217(2):401-410.

199. Boveris A. Mitochondrial Production of Superoxide Radical and Hydrogen Peroxide. In: *Advances in Experimental Medicine and Biology*. Vol 78. ; 1977:67-

82.

200. Vlessis AA, Mela-Riker L. Perinatal Development of Heart, Kidney, and Liver Mitochondrial Antioxidant Defense. *Pediatr Res*. 1989;26(3):220-226.

201. Sosenko IR, Frank L. Guinea pig lung development: antioxidant enzymes and premature survival in high O2. *Am J Physiol*. 1987;252(4 Pt 2):R693-8.

202. Yam J, Frank L, Roberts RJ. Oxygen toxicity: comparison of lung biochemical responses in neonatal and adult rats. *Pediatr Res*. 1978;12(2):115-119.

203. Mavelli I, Rigo A, Federico R, Ciriolo MR, Rotilio G. Superoxide dismutase, glutathione peroxidase and catalase in developing rat brain. *Biochem J*. 1982;204(2):535-540.

204. Wang Z, Ying Z, Bosy-Westphal A, et al. Specific metabolic rates of major organs and tissues across adulthood: evaluation by mechanistic model of resting energy expenditure. *Am J Clin Nutr*. 2010;92(6):1369-1377.

205. Pagliarini DJ, Calvo SE, Chang B, et al. A mitochondrial protein compendium elucidates complex I disease biology. *Cell*. 2008;134(1):112-123.

206. O'Connor PM. Renal oxygen delivery: matching delivery to metabolic demand. *Clin Exp Pharmacol Physiol*. 2006;33(10):961-967.

207. Dennery PA. Oxidative stress in development: nature or nurture? *Free Radic Biol Med*. 2010;49(7):1147-1151.

208. Walton SL, Singh RR, Little MH, Bowles J, Li J, Moritz KM. Prolonged prenatal

hypoxia selectively disrupts collecting duct patterning and postnatal function in male mouse offspring. *J Physiol*. 2018;596(23):5873-5889.

209. Baum M. Role of the kidney in the prenatal and early postnatal programming of hypertension. *AJP Ren Physiol*. 2010;298(2):F235-F247.

210. Marlier A, Cantley LG. An Overview of Renal Development. In: *Genetic Diseases of the Kidney*. Elsevier Inc.; 2009:365-392.

211. Stritzke A, Thomas S, Amin H, Fusch C, Lodha A. Renal consequences of preterm birth. *Mol Cell Pediatr*. 2017;4(1):2.

212. Brenner BM, Garcia DL, Anderson S. Glomeruli and blood pressure less of one, more the other? *Am J Hypertens*. 1988;1(4):335-347.

213. Keller G, Zimmer G, Mall G, Ritz E, Amann K. Nephron number in patients with primary hypertension. *N Engl J Med*. 2003;348(2):101-108.

214. Drake KA, Sauerbry MJ, Blohowiak SE, Repyak KS, Kling PJ. Iron Deficiency and Renal Development in the Newborn Rat. *Pediatr Res*. 2009;66(6):619-624.

215. Lisle SJM, Lewis RM, Petry CJ, Ozanne SE, Hales CN, Forhead AJ. Effect of maternal iron restriction during pregnancy on renal morphology in the adult rat offspring. *Br J Nutr*. 2003;90(1):33-39.

216. Sun MY, Woolley JC, Blohowiak SE, et al. Dietary-induced gestational iron deficiency inhibits postnatal tissue iron delivery and postpones the cessation of active nephrogenesis in rats. *Reprod Fertil Dev*. 2017;29(5):855-866.

217. Wilkinson LJ, Neal CS, Singh RR, et al. Renal developmental defects resulting from in utero hypoxia are associated with suppression of ureteric β-catenin signaling. *Kidney Int*. 2015;87(5):975-983.

218. Walton SL, Bielefeldt-Ohmann H, Singh RR, et al. Prenatal hypoxia leads to hypertension, renal renin-angiotensin system activation and exacerbates salt-induced pathology in a sex-specific manner. *Sci Rep*. 2017;7(1):8241.

219. Lelièvre-Pégorier M, Vilar J, Ferrier ML, et al. Mild vitamin A deficiency leads to inborn nephron deficit in the rat. *Kidney Int*. 1998;54(5):1455-1462.

220. Gilbert JS, Lang AL, Grant AR, Nijland MJ. Maternal nutrient restriction in sheep: Hypertension and decreased nephron number in offspring at 9 months of age. *J Physiol*. 2005;565(1):137-147.

221. Makrakis J, Zimanyi MA, Black MJ. Retinoic acid enhances nephron endowment in rats exposed to maternal protein restriction. *Pediatr Nephrol*. 2007;22(11):1861-1867.

222. Bhat P V, Manolescu D-C. Role of vitamin A in determining nephron mass and possible relationship to hypertension. *J Nutr*. 2008;138(8):1407-1410.

223. Gilbert T. Vitamin A and kidney development. *Nephrol Dial Transplant*. 2002;17 Suppl 9:78-80.

224. Walton SL, Singh RR, Tan T, Paravicini TM, Moritz KM. Late gestational hypoxia and a postnatal high salt diet programs endothelial dysfunction and

arterial stiffness in adult mouse offspring. *J Physiol*. 2016;594(5):1451-1463.

225. Cottin SC, Gambling L, Hayes HE, Stevens VJ, McArdle HJ. Pregnancy and maternal iron deficiency stimulate hepatic CRBPII expression in rats. *J Nutr Biochem*. 2016;32:55-63.

226. Li Y, Wei CH, Green MH, Ross AC. Dietary Iron Repletion Stimulates Hepatic Mobilization of Vitamin A in Previously Iron-Deficient Rats as Determined by Model-Based Compartmental Analysis. *J Nutr*. 2020;150(7):1982-1988.

227. Kalisch-Smith JI, Ved N, Szumska D, et al. Maternal iron deficiency perturbs embryonic cardiovascular development in mice. *Nat Commun*. 2021;12(1):3447.

228. Chen JH, Tarry-Adkins JL, Matharu K, Yeo GSH, Ozanne SE. Maternal protein restriction affects gene expression profiles in the kidney at weaning with implications for the regulation of renal function and lifespan. *Clin Sci*. 2010;119(9):373-384.

229. Grigore D, Ojeda NB, Robertson EB, et al. Placental insufficiency results in temporal alterations in the renin angiotensin system in male hypertensive growth restricted offspring. *Am J Physiol - Regul Integr Comp Physiol*. 2007;293(2):R804-811.

230. Gambling L, Dunford S, Wallace DI, et al. Iron deficiency during pregnancy affects postnatal blood pressure in the rat. *J Physiol*. 2003;552(Pt 2):603-610.

231. Crowe C, Dandekar P, Fox M, Dhingra K, Bennet L, Hanson MA. The effects of

anaemia on heart, placenta and body weight, and blood pressure in fetal and neonatal rats. *J Physiol*. 1995;488(2):515-519.

232. Lewis RM, Petry CJ, Ozanne SE, Hales CN. Effects of maternal iron restriction in the rat on blood pressure, glucose tolerance, and serum lipids in the 3-month-old offspring. *Metabolism*. 2001;50(5):562-567.

233. Williams SJ, Hemmings DG, Mitchell JM, McMillen IC, Davidge ST. Effects of maternal hypoxia or nutrient restriction during pregnancy on endothelial function in adult male rat offspring. *J Physiol*. 2005;565(Pt 1):125-135.

234. Kane AD, Herrera EA, Camm EJ, Giussani DA. Vitamin C prevents intrauterine programming of in vivo cardiovascular dysfunction in the rat. *Circ J*. 2013;77(10):2604-2611.

235. Herrera EA, Verkerk MM, Derks JB, Giussani DA. Antioxidant Treatment Alters Peripheral Vascular Dysfunction Induced by Postnatal Glucocorticoid Therapy in Rats. Federici M, ed. *PLoS One*. 2010;5(2):e9250.

236. Lee H, Abe Y, Lee I, et al. Increased mitochondrial activity in renal proximal tubule cells from young spontaneously hypertensive rats. *Kidney Int*. 2014;85(3):561-569.

237. Wang Z, Sun Q, Sun N, Liang M, Tian Z. Mitochondrial Dysfunction and Altered Renal Metabolism in Dahl Salt-Sensitive Rats. *Kidney Blood Press Res*. 2017;42(3):587-597.

238. Herrera EA, Riquelme RA, Ebensperger G, et al. Long-term exposure to high-altitude chronic hypoxia during gestation induces neonatal pulmonary hypertension at sea level. *Am J Physiol Integr Comp Physiol*. 2010;299(6):R1676-R1684.

239. Bourque SL, Gragasin FS, Quon AL, Mansour Y, Morton JS, Davidge ST. Prenatal hypoxia causes long-term alterations in vascular endothelin-1 function in aged male, but not female, offspring. *Hypertension*. 2013;62(4):753-758.

240. Buckberry S, Bianco-Miotto T, Bent SJ, Dekker GA, Roberts CT. Integrative transcriptome metaanalysis reveals widespread sex-biased gene expression at the human fetal-maternal interface. *Mol Hum Reprod*. 2014;20(8):810-819.

241. Al-Qaraghouli M, Fang YMV. effect of fetal sex on maternal and obstetric outcomes. *Front Pediatr*. 2017;5:144.

242. Habert R, Picon R. Testosterone, dihydrotestosterone and estradiol-17 beta levels in maternal and fetal plasma and in fetal testes in the rat. *J Steroid Biochem*. 1984;21(2):193-198.

243. Arnold AP, Cassis LA, Eghbali M, Reue K, Sandberg K. Sex hormones and sex chromosomes cause sex differences in the development of cardiovascular diseases. *Arterioscler Thromb Vasc Biol*. 2017;37(5):746-756.

244. Menazza S, Murphy E. The expanding complexity of estrogen receptor signaling in the cardiovascular system. *Circ Res*. 2016;118(6):994-1007.

245. Iorga A, Cunningham CM, Moazeni S, Ruffenach G, Umar S, Eghbali M. The protective role of estrogen and estrogen receptors in cardiovascular disease and the controversial use of estrogen therapy. *Biol Sex Differ*. 2017;8(1):33.

246. Zeh JA, Zeh DW. Maternal inheritance, sexual conflict and the maladapted male. *Trends Genet*. 2005;21(5):281-286.

247. Ventura-Clapier R, Moulin M, Piquereau J, et al. Mitochondria: a central target for sex differences in pathologies. *Clin Sci*. 2017;131(9):803-822.

248. Innocenti P, Morrow EH, Dowling DK. Experimental evidence supports a sex-specific selective sieve in mitochondrial genome evolution. *Science*. 2011;332(6031):845-848.

249. Brain KL, Allison BJ, Niu Y, et al. Intervention against hypertension in the next generation programmed by developmental hypoxia. Lo C, ed. *PLoS Biol*. 2019;17(1):e2006552.

250. Minghetti L, Greco A, Zanardo V, Suppiej A. Early-life sex-dependent vulnerability to oxidative stress: the natural twining model. *J Matern Neonatal Med*. 2013;26(3):259-262.

251. Kassebaum NJ, Jasrasaria R, Naghavi M, et al. A systematic analysis of global anemia burden from 1990 to 2010. *Blood*. 2013;123(5):615-624.

252. Doom JR, Georgieff MK. Striking while the iron is hot: Understanding the biological and neurodevelopmental effects of iron deficiency to optimize

intervention in early childhood. *Curr Pediatr Rep*. 2014;2(4):291-298.

253. Bourque SL, Iqbal U, Reynolds JN, Adams MA, Nakatsu K. Perinatal iron deficiency affects locomotor behavior and water maze performance in adult male and female rats. *J Nutr*. 2008;138(5):931-937.

254. Lewis RM, Forhead AJ, Petry CJ, Ozanne SE, Hales CN. Long-term programming of blood pressure by maternal dietary iron restriction in the rat. *Br J Nutr*. 2002;88(3):283-290.

255. Andersen HS, Gambling L, Holtrop G, McArdle HJ. Maternal iron deficiency identifies critical windows for growth and cardiovascular development in the rat postimplantation embryo. *J Nutr*. 2006;136(5):1171-1177.

256. Grandone A, Marzuillo P, Perrone L, Del Giudice EM. Iron Metabolism Dysregulation and Cognitive Dysfunction in Pediatric Obesity: Is There a Connection? *Nutrients*. 2015;7(11):9163-9170.

257. Pasricha S-R, Hayes E, Kalumba K, Biggs B-A. Effect of daily iron supplementation on health in children aged 4-23 months: a systematic review and meta-analysis of randomised controlled trials. *Lancet Glob Heal*. 2013;1(2):e77-86.

258. Chapler CK, Cain SM. The physiologic reserve in oxygen carrying capacity: studies in experimental hemodilution. *Can J Physiol Pharmacol*. 1986;64(1):7-12.

259. Pereira AA, Sarnak MJ. Anemia as a risk factor for cardiovascular disease. *Kidney*

Int Suppl. 2003;(87):S32-9.

260. Davis LE, Hohimer AR. Hemodynamics and organ blood flow in fetal sheep subjected to chronic anemia. *Am J Physiol*. 1991;261(6 Pt 2):R1542-8.

261. Darby MJ, Edelstone DI, Bass K, Miller K. Effects of fetal anemia on PO2 difference between uterine venous and umbilical venous blood. *Am J Physiol*. 1991;260(1 Pt 2):H276-81.

262. Mascio CE, Olison AK, Ralphe JC, Tomanek RJ, Scholz TD, Segar JL. Myocardial vascular and metabolic adaptations in chronically anemic fetal sheep. *Am J Physiol Regul Integr Comp Physiol*. 2005;289(6):R1736-45.

263. Bishop T, Ratcliffe PJ. HIF Hydroxylase Pathways in Cardiovascular Physiology and Medicine. *Circ Res*. 2015;117(1):65-79.

264. Reeves PG, Nielsen FH, Fahey GC. AIN-93 purified diets for laboratory rodents: final report of the American Institute of Nutrition ad hoc writing committee on the reformulation of the AIN-76A rodent diet. *J Nutr*. 1993;123(11):1939-1951.

265. Care AS, Sung MM, Panahi S, et al. Perinatal Resveratrol Supplementation to Spontaneously Hypertensive Rat Dams Mitigates the Development of Hypertension in Adult Offspring. *Hypertension*. 2016;67(5):1038-1044.

266. Fischer AH, Jacobson KA, Rose J, Zeller R. Paraffin embedding tissue samples for sectioning. *CSH Protoc*. 2008;E-Pub:doi: 10.1101/pdb.prot4989.

267. Blumfield ML, Hure AJ, Macdonald-Wicks L, Smith R, Collins CE. A systematic

review and meta-analysis of micronutrient intakes during pregnancy in developed countries. *Nutr Rev*. 2013;71(2):118-132.

268. Bothwell TH. Iron requirements in pregnancy and strategies to meet them. *Am J Clin Nutr*. 2000;72(1 Suppl):257S-264S.

269. Mihaila C, Schramm J, Strathmann FG, et al. Identifying a window of vulnerability during fetal development in a maternal iron restriction model. Burne T, ed. *PLoS One*. 2011;6(3):e17483.

270. Jankovic B, Aquino-Parsons C, Raleigh JA, et al. Comparison between pimonidazole binding, oxygen electrode measurements, and expression of endogenous hypoxia markers in cancer of the uterine cervix. *Cytometry B Clin Cytom*. 2006;70(2):45-55.

271. Chou S-C, Azuma Y, Varia MA, Raleigh JA. Evidence that involucrin, a marker for differentiation, is oxygen regulated in human squamous cell carcinomas. *Br J Cancer*. 2004;90(3):728-735.

272. Raleigh JA, Chou SC, Arteel GE, Horsman MR. Comparisons among pimonidazole binding, oxygen electrode measurements, and radiation response in C3H mouse tumors. *Radiat Res*. 1999;151(5):580-589.

273. Mostello D, Chalk C, Khoury J, Mack CE, Siddiqi TA, Clark KE. Chronic anemia in pregnant ewes: maternal and fetal effects. *Am J Physiol*. 1991;261(5 Pt 2):R1075-83.

274. Fumia FD, Edelstone DI, Holzman IR. Blood flow and oxygen delivery to fetal organs as functions of fetal hematocrit. *Am J Obs Gynecol*. 1984;150(3):274-282.

275. Bastian TW, Santarriaga S, Nguyen TA, Prohaska JR, Georgieff MK, Anderson GW. Fetal and neonatal iron deficiency but not copper deficiency increases vascular complexity in the developing rat brain. *Nutr Neurosci*. 2015;18(8):365-375.

276. Hébert PC, Van der Linden P, Biro G, Hu LQ. Physiologic aspects of anemia. *Crit Care Clin*. 2004;20(2):187-212.

277. Ritchie H, Oakes D, Hung T, Hegedus E, Sood S, Webster W. The Effect of Dofetilide on the Heart Rate of GD11 and GD13 Rat Embryos, in vivo, Using Ultrasound. *Birth Defects Res B Dev Reprod Toxicol*. 2015;104(5):196-203.

278. Lewis RM, Doherty CB, James LA, Burton GJ, Hales CN. Effects of maternal iron restriction on placental vascularization in the rat. *Placenta*. 2001;22(6):534-539.

279. Youdim MB, Green AR, Bloomfield MR, Mitchell BD, Heal DJ, Grahame-Smith DG. The effects of iron deficiency on brain biogenic monoamine biochemistry and function in rats. *Neuropharmacology*. 1980;19(3):259-267.

280. Unger EL, Hurst AR, Georgieff MK, et al. Behavior and monoamine deficits in prenatal and perinatal iron deficiency are not corrected by early postnatal moderate-iron or high-iron diets in rats. *J Nutr*. 2012;142(11):2040-2049.

281. Gambling L, Charania Z, Hannah L, Antipatis C, Lea RG, McArdle HJ. Effect of

iron deficiency on placental cytokine expression and fetal growth in the pregnant rat. *Biol Reprod*. 2002;66(2):516-523.

282. Lewis RM, James LA, Zhang J, Byrne CD, Hales CN. Effects of maternal iron restriction in the rat on hypoxia-induced gene expression and fetal metabolite levels. *Br J Nutr*. 2001;85(2):193-201.

283. Schoch HJ, Fischer S, Marti HH. Hypoxia-induced vascular endothelial growth factor expression causes vascular leakage in the brain. *Brain*. 2002;125(Pt 11):2549-2557.

284. Almutairi MM, Gong C, Xu YG, Chang Y, Shi H. Factors controlling permeability of the blood-brain barrier. *Cell Mol Life Sci*. 2016;73(1):57-77.

285. Maduwegedera D, Kett MM, Flower RL, et al. Sex differences in postnatal growth and renal development in offspring of rabbit mothers with chronic secondary hypertension. *Am J Physiol Regul Integr Comp Physiol*. 2007;292(2):R706-14.

286. Ortiz LA, Quan A, Zarzar F, Weinberg A, Baum M. Prenatal dexamethasone programs hypertension and renal injury in the rat. *Hypertens (Dallas, Tex 1979)*. 2003;41(2):328-334.

287. Mackler B, Grace R, Person R, Shepard TH, Finch CA. Iron deficiency in the rat: biochemical studies of fetal metabolism. *Teratology*. 1983;28(1):103-107.

288. Dallman PR. Biochemical Basis for the Manifestations of Iron Deficiency. *Annu Rev Nutr*. 1986;6(1):13-40.

289. Gnaiger E. *Mitochondrial Pathways and Respiratory Control: An Introduction to OXPHOS Analysis*. 4th ed. MiPNet Publications; 2014.

290. Srere PA. Citrate synthase. *Methods Enzymol*. 1969;13:3-11.

291. Pesta D, Hoppel F, Macek C, et al. Similar qualitative and quantitative changes of mitochondrial respiration following strength and endurance training in normoxia and hypoxia in sedentary humans. *Am J Physiol Regul Integr Comp Physiol*. 2011;301(4):R1078-87.

292. Gnaiger E. Capacity of oxidative phosphorylation in human skeletal muscle. *Int J Biochem Cell Biol*. 2009;41(10):1837-1845.

293. Paddenberg R, Ishaq B, Goldenberg A, et al. Essential role of complex II of the respiratory chain in hypoxia-induced ROS generation in the pulmonary vasculature. *Am J Physiol Lung Cell Mol Physiol*. 2003;284(5):L710-9.

294. Iverson TM, Maklashina E, Cecchini G. Structural basis for malfunction in complex II. *J Biol Chem*. 2012;287(42):35430-35438.

295. Ralph SJ, Moreno-Sánchez R, Neuzil J, Rodríguez-Enríquez S. Inhibitors of succinate: quinone reductase/Complex II regulate production of mitochondrial reactive oxygen species and protect normal cells from ischemic damage but induce specific cancer cell death. *Pharm Res*. 2011;28(11):2695-2730.

296. Luo S, Lei H, Qin H, Xia Y. Molecular mechanisms of endothelial NO synthase uncoupling. *Curr Pharm Des*. 2014;20(22):3548-3553.

297. Srinivasan S, Avadhani NG. Cytochrome c oxidase dysfunction in oxidative stress. *Free Radic Biol Med*. 2012;53(6):1252-1263.

298. Gnaiger E, Lassnig B, Kuznetsov A, Rieger G, Margreiter R. Mitochondrial oxygen affinity, respiratory flux control and excess capacity of cytochrome c oxidase. *J Exp Biol*. 1998;201(Pt 8):1129-1139.

299. Tower J. Sex-specific regulation of aging and apoptosis. *Mech Ageing Dev*. 2006;127(9):705-718.

300. Weisz J, Ward IL. Plasma testosterone and progesterone titers of pregnant rats, their male and female fetuses, and neonatal offspring. *Endocrinology*. 1980;106(1):306-316.

301. Rensvold JW, Krautkramer KA, Dowell JA, Denu JM, Pagliarini DJ. Iron Deprivation Induces Transcriptional Regulation of Mitochondrial Biogenesis. *J Biol Chem*. 2016;291(40):20827-20837.

302. Rensvold JW, Ong S-E, Jeevananthan A, Carr SA, Mootha VK, Pagliarini DJ. Complementary RNA and protein profiling identifies iron as a key regulator of mitochondrial biogenesis. *Cell Rep*. 2013;3(1):237-245.

303. Ozçay F, Derbent M, Aldemir D, et al. Effect of iron deficiency anemia on renal tubular function in childhood. *Pediatr Nephrol*. 2003;18(3):254-256.

304. Stangenberg S, Nguyen LT, Chen H, et al. Oxidative stress, mitochondrial perturbations and fetal programming of renal disease induced by maternal

smoking. *Int J Biochem Cell Biol*. 2015;64:81-90.

305. Pereira SP, Oliveira PJ, Tavares LC, et al. Effects of moderate global maternal nutrient reduction on fetal baboon renal mitochondrial gene expression at 0.9 gestation. *Am J Physiol Renal Physiol*. 2015;308(11):F1217-28.

306. Gjerde A, Lillås BS, Marti HP, Reisæter AV, Vikse BE. Intrauterine growth restriction, preterm birth and risk of end-stage renal disease during the first 50 years of life. *Nephrol Dial Transplant*. 2020;35(7):1157-1163.

307. Gjerde A, Reisæter AV, Skrunes R, Marti H-P, Vikse BE. Intrauterine Growth Restriction and Risk of Diverse Forms of Kidney Disease during the First 50 Years of Life. *Clin J Am Soc Nephrol*. Published online August 17, 2020:CJN.04080320.

308. Woodman AG, Noble RMN, Panahi S, Gragasin FS, Bourque SL. Perinatal iron deficiency combined with a high salt diet in adulthood causes sex-dependent vascular dysfunction in rats. *J Physiol*. 2019;597(18):4715-4728.

309. Woodman AG, Mah R, Keddie DL, et al. Perinatal iron deficiency and a high salt diet cause long-term kidney mitochondrial dysfunction and oxidative stress. *Cardiovasc Res*. 2020;116(1):183-192.

310. Muñoz-Espín D, Serrano M. Cellular senescence: from physiology to pathology. *Nat Rev Mol Cell Biol*. 2014;15(7):482-496.

311. Pfaffl MW. A new mathematical model for relative quantification in real-time RT-PCR. *Nucleic Acids Res*. 2001;29(9):e45.

312. Miller DM, Spear NH, Aust SD. Effects of deferrioxamine on iron-catalyzed lipid peroxidation. *Arch Biochem Biophys*. 1992;295(2):240-246.

313. Patt A, Horesh IR, Berger EM, Harken AH, Repine JE. Iron depletion or chelation reduces ischemia/reperfusion-induced edema in gerbil brains. *J Pediatr Surg*. 1990;25(2):224-228.

314. Chandler DB, Barton JC, Briggs DD, et al. Effect of iron deficiency on bleomycin-induced lung fibrosis in the hamster. *Am Rev Respir Dis*. 1988;137(1):85-89.

315. Knutson MD, Walter PB, Ames BN, Viteri FE. Both iron deficiency and daily iron supplements increase lipid peroxidation in rats. *J Nutr*. 2000;130(3):621-628.

316. Sperotto RA, Boff T, Duarte GL, Fett JP. Increased senescence-associated gene expression and lipid peroxidation induced by iron deficiency in rice roots. *Plant Cell Rep*. 2008;27(1):183-195.

317. Dabbagh AJ, Shwaery GT, Keaney JF, Frei B. Effect of iron overload and iron deficiency on atherosclerosis in the hypercholesterolemic rabbit. *Arterioscler Thromb Vasc Biol*. 1997;17(11):2638-2645.

318. Díaz-Castro J, Alférez MJM, López-Aliaga I, et al. Influence of nutritional iron deficiency anemia on DNA stability and lipid peroxidation in rats. *Nutrition*. 2008;24(11-12):1167-1173.

319. Chatterjee N, Walker GC. Mechanisms of DNA damage, repair, and mutagenesis. *Environ Mol Mutagen*. 2017;58(5):235-263.

320. Malhotra KM, Murthy RC, Srivastava RS, Chandra S V. Concurrent exposure of lead and manganese to iron-deficient rats: effect on lipid peroxidation and contents of some metals in the brain. *J Appl Toxicol*. 1984;4(1):22-25.

321. Redza-Dutordoir M, Averill-Bates DA. Activation of apoptosis signalling pathways by reactive oxygen species. *Biochim Biophys Acta - Mol Cell Res*. 2016;1863(12):2977-2992.

322. Scherz-Shouval R, Elazar Z. Regulation of autophagy by ROS: physiology and pathology. *Trends Biochem Sci*. 2011;36(1):30-38.

323. Hamanaka RB, Chandel NS. Mitochondrial reactive oxygen species regulate cellular signaling and dictate biological outcomes. *Trends Biochem Sci*. 2010;35(9):505-513.

324. Lorente-Pozo S, Parra-Llorca A, Torres B, et al. Influence of Sex on Gestational Complications, Fetal-to-Neonatal Transition, and Postnatal Adaptation. *Front Pediatr*. 2018;6:63.

325. Vina J, Gambini J, Lopez-Grueso R, Abdelaziz KM, Jove M, Borras C. Females live longer than males: role of oxidative stress. *Curr Pharm Des*. 2011;17(36):3959-3965.

326. Hamad M, Bajbouj K, Taneera J. The Case for an Estrogen-iron Axis in Health and Disease. *Exp Clin Endocrinol Diabetes*. 2020;128(4):270-277.

327. Seno K, Tanikawa N, Takahashi H, et al. Oxygen concentration modulates cellular

senescence and autophagy in human trophoblast cells. *Am J Reprod Immunol*. 2018;79(6):e12826.

328. Welford SM, Giaccia AJ. Hypoxia and senescence: The impact of oxygenation on tumor suppression. *Mol Cancer Res*. 2011;9(5):538-544.

329. Polettini J, Richardson LS, Menon R. Oxidative stress induces senescence and sterile inflammation in murine amniotic cavity. *Placenta*. 2018;63:26-31.

330. Masaldan S, Clatworthy SAS, Gamell C, et al. Iron accumulation in senescent cells is coupled with impaired ferritinophagy and inhibition of ferroptosis. *Redox Biol*. 2018;14:100-115.

331. Verschuren MTC, Morton JS, Abdalvand A, et al. The effect of hypoxia-induced intrauterine growth restriction on renal artery function. *J Dev Orig Health Dis*. 2012;3(5):333-341.

332. Reisman D, Takahashi P, Polson A, Boggs K. Transcriptional regulation of the p53 tumor suppressor gene in S-phase of the cell-cycle and the cellular response to DNA damage. *Biochem Res Int*. 2012;2012:808934.

333. Prá D, Franke SIR, Henriques JAP, Fenech M. Iron and genome stability: an update. *Mutat Res*. 2012;733(1-2):92-99.

334. Pra D, Rech Franke SI, Pegas Henriques JA, Fenech M. A possible link between iron deficiency and gastrointestinal carcinogenesis. *Nutr Cancer*. 2009;61(4):415-426.

335. Schreuder MF. Safety in Glomerular Numbers. *Pediatr Nephrol*. 2012;27(10):1881-1887.

336. Yosypiv I V., El-Dahr SS. Role of the renin-angiotensin system in the development of the ureteric bud and renal collecting system. *Pediatr Nephrol*. 2005;20(9):1219-1229.

337. Peterson SM, Wang X, Johnson AC, Coate ID, Garrett MR, Didion SP. Estimation of nephron number in whole kidney using the acid maceration method. *J Vis Exp*. 2019;(147):e58599.

338. Rocke AW, Clarke TG, Dalmer TRA, McCluskey SA, Rivas JFG, Clugston RD. Low maternal vitamin A intake increases the incidence of teratogen induced congenital diaphragmatic hernia in mice. *Pediatr Res*. 2021;E-Pub:doi: 10.1038/s41390-021-01409-6.

339. JX Y, JM M. Quantitative Immunohistochemistry of the Cellular Microenvironment in Patient Glioblastoma Resections. *J Vis Exp*. 2017;(125):56025.

340. Chambon P. A decade of molecular biology of retinoic acid receptors. *FASEB J*. 1996;10(9):940-954.

341. Marlier A, Gilbert T. Expression of retinoic acid-synthesizing and -metabolizing enzymes during nephrogenesis in the rat. *Gene Expr Patterns*. 2004;5(2):179-185.

342. Hawkesworth S, Wagatsuma Y, Kahn AI, et al. Combined food and micronutrient

supplements during pregnancy have limited impact on child blood pressure and kidney function in rural Bangladesh. *J Nutr*. 2013;143(5):728-734.

343. Sorokina I V., Myroshnychenko MS, Kapustnyk N V., Simachova A V., Ivanova AA. Morphometrical evaluation of fetuses and newborns kidneys status developing under maternal iron deficiency anemaia conditions. *Wiad Lek*. 2018;71(7):1222-1230.

344. Gilbert JS, Nijland MJ. Sex differences in the developmental origins of hypertension and cardiorenal disease. *AJP Regul Integr Comp Physiol*. 2008;295(6):R1941-R1952.

345. Gilbert T, Merlet-Bénichou C. Retinoids and nephron mass control. *Pediatr Nephrol*. 2000;14(12):1137-1144.

346. Li Y, Wei CH, Xiao X, Green MH, Ross AC. Perturbed Vitamin A Status Induced by Iron Deficiency Is Corrected by Iron Repletion in Rats with Pre-Existing Iron Deficiency. *J Nutr*. 2020;150(7):1989-1995.

347. Li Y, Wang L, Ai W, et al. Regulation of retinoic acid synthetic enzymes by WT1 and HDAC inhibitors in 293 cells. *Int J Mol Med*. 2017;40(3):661-672.

348. Rosselot C, Spraggon L, Chia I, et al. Non-cell-autonomous retinoid signaling is crucial for renal development. *Development*. 2010;137(2):283-292.

349. Michos O, Cebrian C, Hyink D, et al. Kidney development in the absence of Gdnf and Spry1 requires Fgf10. *PLoS Genet*. 2010;6(1):e1000809.

350. Majumdar A, Vainio S, Kispert A, McMahon J, McMahon AP. Wnt11 and Ret/Gdnf pathways cooperate in regulating ureteric branching during metanephric kidney development. *Development*. 2003;130(14):3175-3185.

351. Li H, Kurtzeborn K, Kupari J, et al. Postnatal prolongation of mammalian nephrogenesis by excess fetal GDNF. *Development*. 2021;148(10):dev197475.

352. Lee LMY, Leung C-Y, Tang WWC, et al. A paradoxical teratogenic mechanism for retinoic acid. *Proc Natl Acad Sci*. 2012;109(34):13668-13673.

353. Mazzei L, Manucha W. Growing evidence suggests WT1 effects in the kidney development are modulated by Hsp70/NO interaction. *J Nephrol*. 2017;30(1):11-18.

354. Kreidberg JA. WT1 and kidney progenitor cells. *Organogenesis*. 2010;6(2):61-70.

355. Dressler GR. Transcription factors in renal development: The WT1 and Pax-2 story. *Semin Nephrol*. 1995;15(4):263-271.

356. McConnell MJ, Cunliffe HE, Chua LJ, Ward TA, Eccles MR. Differential regulation of the human Wilms tumour suppressor gene (WT1) promoter by two isoforms of PAX2. *Oncogene*. 1997;14(22):2689-2700.

357. Motamedi FJ, Badro DA, Clarkson M, et al. WT1 controls antagonistic FGF and BMP-pSMAD pathways in early renal progenitors. *Nat Commun*. 2014;5(9):1-14.

358. Ohmori T, Tanigawa S, Kaku Y, Fujimura S, Nishinakamura R. Sall1 in renal stromal progenitors non-cell autonomously restricts the excessive expansion of

nephron progenitors. *Sci Rep*. 2015;5:15676.

359. Karner CM, Das A, Ma Z, et al. Canonical Wnt9b signaling balances progenitor cell expansion and differentiation during kidney development. *Development*. 2011;138(7):1247-1257.

360. Halt K, Vainio S. Coordination of kidney organogenesis by Wnt signaling. In: *Pediatric Nephrology*. Vol 29. Pediatr Nephrol; 2014:737-744.

361. Schley G, Scholz H, Kraus A, et al. Hypoxia inhibits nephrogenesis through paracrine Vegfa despite the ability to enhance tubulogenesis. *Kidney Int*. 2015;88(6):1283-1292.

362. Naito Y, Tsujino T, Matsumoto M, Sakoda T, Ohyanagi M, Masuyama T. Adaptive response of the heart to long-term anemia induced by iron deficiency. *Am J Physiol Heart Circ Physiol*. 2009;296(3):H585-93.

363. Ichihara A, Kobori H, Nishiyama A, Gabriel Navar L. Renal renin-angiotensin system. *Contrib Nephrol*. 2004;143:117-130.

364. Li H, He P, Lin T, et al. Association between plasma retinol levels and the risk of all-cause mortality in general hypertensive patients: A nested case-control study. *J Clin Hypertens*. 2020;22(5):906-913.

365. Chen A, Liu Y, Lu Y, Lee K, He JC. Disparate roles of retinoid acid signaling molecules in kidney disease. *Am J Physiol - Ren Physiol*. 2021;320(5):F683-F692.

366. Alwan NA, Cade JE, McArdle HJ, Greenwood DC, Hayes HE, Simpson NAB.

Maternal iron status in early pregnancy and birth outcomes: insights from the Baby's Vascular health and Iron in Pregnancy study. *Br J Nutr*. 2015;113(12):1985-1992.

367. Abioye AI, Aboud S, Premji Z, et al. Iron Supplementation Affects Hematologic Biomarker Concentrations and Pregnancy Outcomes among Iron-Deficient Tanzanian Women. *J Nutr*. 2016;146(6):1162-1171.

368. Danson MJ, Hough DW. Citrate synthase from hyperthermophilic Archaea. *Methods Enzymol*. 2001;331:3-12.

369. Chen Y, Yu Q, Xu CB. A convenient method for quantifying collagen fibers in atherosclerotic lesions by imagej software. *Int J Clin Exp Med*. 2017;10(10):14904-14910.

370. Puelles VG, Bertram JF. Counting glomeruli and podocytes: rationale and methodologies. *Curr Opin Nephrol Hypertens*. 2015;24(3):224-230.

371. Sengupta P. The Laboratory Rat: Relating Its Age With Human's. *Int J Prev Med*. 2013;4(6):624-630.

372. Jackson SL, King SMC, Zhao L, Cogswell ME. Prevalence of Excess Sodium Intake in the United States — NHANES, 2009–2012. *MMWR Morb Mortal Wkly Rep*. 2016;64(52):1393-1397.

373. Health Canada. *Sodium Intake of Canadians in 2017*.; 2018.

374. Skovsted P, Sapthavichaikul S. The effects of isoflurane on arterial pressure, pulse

rate, autonomic nervous activity, and barostatic reflexes. *Can Anaesth Soc J*. 1977;24(3):304-314.

375. Fujita T. Mechanism of salt-sensitive hypertension: focus on adrenal and sympathetic nervous systems. *J Am Soc Nephrol*. 2014;25(6):1148-1155.

376. Burnier M, Phan O, Wang Q. High salt intake: a cause of blood pressure-independent left ventricular hypertrophy? *Nephrol Dial Transplant*. 2007;22(9):2426-2429.

377. Rueda-Clausen CF, Morton JS, Davidge ST. Effects of hypoxia-induced intrauterine growth restriction on cardiopulmonary structure and function during adulthood. *Cardiovasc Res*. 2009;81(4):713-722.

378. Thenappan T, Ormiston ML, Ryan JJ, Archer SL. Pulmonary arterial hypertension: pathogenesis and clinical management. *BMJ*. 2018;360:j5492.

379. Granata S, Dalla Gassa A, Tomei P, Lupo A, Zaza G. Mitochondria: a new therapeutic target in chronic kidney disease. *Nutr Metab (Lond)*. 2015;12(1):49.

380. He X, Liu Y, Usa K, Tian Z, Cowley AW, Liang M. Ultrastructure of mitochondria and the endoplasmic reticulum in renal tubules of Dahl salt-sensitive rats. *Am J Physiol Physiol*. 2014;306(10):F1190-F1197.

381. Catena C, Colussi G, Sechi LA. Aldosterone, organ damage and dietary salt. *Clin Exp Pharmacol Physiol*. 2013;40(12):922-928.

382. Xue B, Badaue-Passos D, Guo F, Gomez-Sanchez CE, Hay M, Johnson AK. Sex

differences and central protective effect of 17beta-estradiol in the development of aldosterone/NaCl-induced hypertension. *Am J Physiol Heart Circ Physiol*. 2009;296(5):H1577-85.

383. Zhang L, Kang PT, Chen C-L, Green KB, Chen Y-R. Oxidative Modifications of Mitochondria Complex II. In: *Methods in Molecular Biology (Clifton, N.J.)*. Vol 1005. ; 2013:143-156.

384. Zou AP, Li N, Cowley AW. Production and actions of superoxide in the renal medulla. *Hypertens (Dallas, Tex 1979)*. 2001;37(2 Pt 2):547-553.

385. Baylis C, Qiu C. Importance of nitric oxide in the control of renal hemodynamics. *Kidney Int*. 1996;49(6):1727-1731.

386. Mattson DL, Lu S, Nakanishi K, Papanek PE, Cowley AW. Effect of chronic renal medullary nitric oxide inhibition on blood pressure. *Am J Physiol Circ Physiol*. 1994;266(5):H1918-H1926.

387. Nakanishi K, Hara N, Nagai Y. Salt-sensitive hypertension in conscious rats induced by chronic nitric oxide blockade. *Am J Hypertens*. 2002;15(2 Pt 1):150-156.

388. Intapad S, Tull FL, Brown AD, et al. Renal denervation abolishes the age-dependent increase in blood pressure in female intrauterine growth-restricted rats at 12 months of age. *Hypertens (Dallas, Tex 1979)*. 2013;61(4):828-834.

389. Kenchaiah S, Pfeffer MA. Cardiac remodeling in systemic hypertension. *Med Clin*

North Am. 2004;88(1):115-130.

390. Hay SM, McArdle HJ, Hayes HE, Stevens VJ, Rees WD. The effect of iron deficiency on the temporal changes in the expression of genes associated with fat metabolism in the pregnant rat. *Physiol Rep*. 2016;4(21):e12908.

391. Giussani DA, Camm EJ, Niu Y, et al. Developmental Programming of Cardiovascular Dysfunction by Prenatal Hypoxia and Oxidative Stress. Calbet JAL, ed. *PLoS One*. 2012;7(2):e31017.

392. Herrera EA, Riquelme RA, Ebensperger G, et al. Long-term exposure to high-altitude chronic hypoxia during gestation induces neonatal pulmonary hypertension at sea level. *Am J Physiol Integr Comp Physiol*. 2010;299(6):R1676-R1684.

393. Jellyman JK, Gardner DS, Edwards CMB, Fowden AL, Giussani DA. Fetal cardiovascular, metabolic and endocrine responses to acute hypoxaemia during and following maternal treatment with dexamethasone in sheep. *J Physiol*. 2005;567(2):673-688.

394. Grundy D. Principles and standards for reporting animal experiments in The Journal of Physiology and Experimental Physiology. *J Physiol*. 2015;593(12):2547-2549.

395. O'Donnell M, Mente A, Rangarajan S, et al. Joint association of urinary sodium and potassium excretion with cardiovascular events and mortality: prospective cohort study. *BMJ*. 2019;364:l772.

396. Shultz PJ, Tolins JP. Adaptation to increased dietary salt intake in the rat. Role of endogenous nitric oxide. *J Clin Invest*. 1993;91(2):642-650.

397. Morton JS, Rueda-Clausen CF, Davidge ST. Mechanisms of endothelium-dependent vasodilation in male and female, young and aged offspring born growth restricted. *Am J Physiol Integr Comp Physiol*. 2010;298(4):R930-R938.

398. Sendão Oliveira AP, Bendhack LM. Relaxation induced by acetylcholine involves endothelium-derived hyperpolarizing factor in 2-kidney 1-clip hypertensive rat carotid arteries. *Pharmacology*. 2004;72(4):231-239.

399. Sofola OA, Knill A, Hainsworth R, Drinkhill M. Change in endothelial function in mesenteric arteries of Sprague-Dawley rats fed a high salt diet. *J Physiol*. 2002;543(Pt 1):255-260.

400. Bourque SL, Whittingham HA, Brien SE, Davidge ST, Adams MA. Role of endothelin-1 in the hyper-responsiveness to nitrovasodilators following acute NOS inhibition. *Br J Pharmacol*. 2012;165(6):1992-1999.

401. Bourque SL, Davidge ST, Adams MA. The interaction between endothelin-1 and nitric oxide in the vasculature: new perspectives. *Am J Physiol Regul Integr Comp Physiol*. 2011;300(6):R1288-R1295.

402. Usselman CW, Stachenfeld NS, Bender JR. The molecular actions of oestrogen in the regulation of vascular health. *Exp Physiol*. 2016;101(3):356-361.

403. Kander MC, Cui Y, Liu Z. Gender difference in oxidative stress: a new look at the

mechanisms for cardiovascular diseases.Kander MC, Cui Y & Liu Z (2017). Gender difference in oxidative stress: a new look at the mechanisms for cardiovascular diseases. J Cell Mol Med 21, 1024–1032. *J Cell Mol Med*. 2017;21(5):1024-1032.

404. Davis LE, Hohimer AR, Giraud GD, Reller MD, Morton MJ. Right ventricular function in chronically anemic fetal lambs. *Am J Obstet Gynecol*. 1996;174(4):1289-1294.

405. Cao C, Prado MA, Sun L, et al. Maternal Iron Deficiency Modulates Placental Transcriptome and Proteome in Mid-Gestation of Mouse Pregnancy. *J Nutr*. 2021;151(5):1073-1083.

406. Waypa GB, Smith KA, Schumacker PT. O2 sensing, mitochondria and ROS signaling: The fog is lifting. *Mol Aspects Med*. 2016;47-48:76-89.

407. Juvet C, Siddeek B, Yzydorczyk C, et al. Renal Programming by Transient Postnatal Overfeeding: The Role of Senescence Pathways. *Front Physiol*. 2020;11:511.

408. Didion SP. A novel genetic model to explore the Brenner hypothesis: Linking nephron endowment and number with hypertension. *Med Hypotheses*. 2017;106:6-9.

409. Rastogi A, Yuan S, Arman F, et al. Blood Pressure and Living Kidney Donors: A Clinical Perspective. *Transplant Direct*. 2019;5(10):e488.

410. Sanchez OA, Ferrara LK, Rein S, Berglund D, Matas AJ, Ibrahim HN. Hypertension after kidney donation: Incidence, predictors, and correlates. *Am J Transplant*. 2018;18(10):2534-2543.

411. Woodman AG, Bourque SL. Developmental programming of renal function: nephron endowment and beyond. *J Physiol*. 2018;596(23):5495-5496.

412. Aneman A, Ponten J, Fandriks L, Eisenhofer G, Friberg P, Biber B. Splanchnic and renal sympathetic activity in relation to hemodynamics during isoflurane administration in pigs. *Anesth Analg*. 1995;80(1):135-142.

413. Mizuno M, Siddique K, Baum M, Smith SA. Prenatal programming of hypertension induces sympathetic overactivity in response to physical stress. *Hypertension*. 2013;61(1):180-186.

414. Ojeda NB. Prenatal programming of hypertension: Role of sympathetic response to physical stress. *Hypertension*. 2013;61(1):16-17.

415. Esler MD, Krum H, Sobotka PA, et al. Renal sympathetic denervation in patients with treatment-resistant hypertension (The Symplicity HTN-2 Trial): A randomised controlled trial. *Lancet*. 2010;376(9756):1903-1909.

416. Rogozińska E, Daru J, Nicolaides M, et al. Iron preparations for women of reproductive age with iron deficiency anaemia in pregnancy (FRIDA): a systematic review and network meta-analysis. *Lancet Haematol*. 2021;8(7):e503-e512.